NRC Nuclear Regulatory Commission

NUREG-2272

Validation of a Computational Fluid Dynamics Method Using Advanced Drying Cycle Simulator Data

Office of Nuclear Regulatory Research

AVAILABILITY OF REFERENCE MATERIALS IN NRC PUBLICATIONS

NRC Reference Material

As of November 1999, you may electronically access NUREG-series publications and other NRC records at the NRC's Library at www.nrc.gov/reading-rm.html. Publicly released records include, to name a few, NUREG-series publications; *Federal Register* notices; applicant, licensee, and vendor documents and correspondence; NRC correspondence and internal memoranda; bulletins and information notices; inspection and investigative reports; licensee event reports; and Commission papers and their attachments.

NRC publications in the NUREG series, NRC regulations, and Title 10, "Energy," in the *Code of Federal Regulations* may also be purchased from one of these two sources:

1. **The Superintendent of Documents**
   U.S. Government Publishing Office
   Washington, DC 20402-0001
   Internet: https://bookstore.gpo.gov/
   Telephone: (202) 512-1800
   Fax: (202) 512-2104

2. **The National Technical Information Service**
   5301 Shawnee Road
   Alexandria, VA 22312-0002
   Internet: https://www.ntis.gov/
   1-800-553-6847 or, locally, (703) 605-6000

A single copy of each NRC draft report for comment is available free, to the extent of supply, upon written request as follows:

Address: **U.S. Nuclear Regulatory Commission**
Office of the Chief Information Officer
Communication, Collaboration and
Workspace Branch
Washington, DC 20555-0001
E-mail: Reproduction.Resource@nrc.gov
Facsimile: (301) 415-2289

Some publications in the NUREG series that are posted at the NRC's Web site address www.nrc.gov/reading-rm/doc-collections/nuregs are updated periodically and may differ from the last printed version. Although references to material found on a Web site bear the date the material was accessed, the material available on the date cited may subsequently be removed from the site.

Non-NRC Reference Material

Documents available from public and special technical libraries include all open literature items, such as books, journal articles, transactions, *Federal Register* notices, Federal and State legislation, and congressional reports. Such documents as theses, dissertations, foreign reports and translations, and non-NRC conference proceedings may be purchased from their sponsoring organization.

Copies of industry codes and standards used in a substantive manner in the NRC regulatory process are maintained at—

The NRC Technical Library
Two White Flint North
11545 Rockville Pike
Rockville, MD 20852-2738

These standards are available in the library for reference use by the public. Codes and standards are usually copyrighted and may be purchased from the originating organization or, if they are American National Standards, from—

American National Standards Institute
11 West 42nd Street
New York, NY 10036-8002
Internet: https://www.ansi.org/
(212) 642-4900

Legally binding regulatory requirements are stated only in laws; NRC regulations; licenses, including technical specifications; or orders, not in NUREG-series publications. The views expressed in contractor prepared publications in this series are not necessarily those of the NRC.

The NUREG series comprises (1) technical and administrative reports and books prepared by the staff (NUREG–XXXX) or agency contractors (NUREG/CR–XXXX), (2) proceedings of conferences (NUREG/CP–XXXX), (3) reports resulting from international agreements (NUREG/IA–XXXX),(4) brochures (NUREG/BR–XXXX), and (5) compilations of legal decisions and orders of the Commission and the Atomic and Safety Licensing Boards and of Directors' decisions under Section 2.206 of the NRC's regulations (NUREG-0750), (6) Knowledge Management prepared by NRC staff or agency contractors (NUREG/KM-XXXX).

DISCLAIMER: This report was prepared as an account of work sponsored by an agency of the U.S. Government. Neither the U.S. Government nor any agency thereof, nor any employee, makes any warranty, expressed or implied, or assumes any legal liability or responsibility for any third party's use, or the results of such use, of any information, apparatus, product, or process disclosed in this publication, or represents that its use by such third party would not infringe privately owned rights.

NUREG-2272

Validation of a Computational Fluid Dynamics Method Using Advanced Drying Cycle Simulator Data

Manuscript Completed: March 2026
Date Published: October 2026

Prepared by:
A. Zigh
J. Coury

Office of Nuclear Regulatory Research

ABSTRACT

Applicants submit dry storage cask designs for spent nuclear fuel to the U.S. Nuclear Regulatory Commission (NRC) for certification under Title 10 of the *Code of Federal Regulations* (10 CFR Part 72), "Licensing Requirements for the Independent Storage of Spent Nuclear Fuel, High-Level Radioactive Waste, and Reactor-Related Greater than Class C Waste". The NRC staff performs its technical review of these designs in accordance with 10 CFR Part 72 and NUREG-2215, "Standard Review Plan for Spent Fuel Dry Storage Systems and Facilities," issued April 2020. To ensure the cask and fuel material temperatures of the dry cask storage system remain within the allowable limits or criteria for normal, off-normal, and accident conditions, the NRC staff performs a thermal review as part of the technical review.

Recent applications have increasingly used thermal-hydraulic analyses using computational fluid dynamics (CFD) codes (e.g., Ansys Fluent) to demonstrate the adequacy of the thermal design. The applicants are also seeking to license casks with decay heat close to 70 kilowatts (kW), resulting in a peak cladding temperature (PCT) close to the temperature limit of 400 degrees Celsius (°C) (752 degrees Fahrenheit (°F)) suggested in Interim Staff Guidance-11, "Cladding Considerations for the Transportation and Storage of Spent Fuel," issued November 2003. It is part of CFD best practice guidelines in NUREG-2152, "Computational Fluid Dynamics Best Practice Guidelines for Dry Cask Applications," issued March 2013, to present CFD predictions for the PCT or any other target variable supported by an uncertainty quantification (UQ) to provide assurance and confidence that the obtained margin is adequate.

The NRC recognizes that finite-volume-based CFD is one of the methods applicants use to perform dry cask thermal modeling and to demonstrate adequate margins with the temperature limits suggested in NUREG-2215. Additionally, when demonstrating the thermal margins, it is valuable to quantify the uncertainty in the simulation result as a function of the computational mesh and simulation inputs. When finite-volume-based CFD is applied carefully through the use of CFD best practice guidelines in NUREG-2152, and UQ is performed, there will be confidence and certainty in the obtained margins.

The numerical modeling validation study was based on data collected at Sandia National Laboratories (SNL) in an experiment sponsored by the U.S. Department of Energy on an Advanced Drying Cycle Simulator (ADCS) documented in report SAND2022-12078R, SAND2023-01454R, SAND2023-09746R, and SAND2024. The ADCS simulates one prototypic 17x17 pressurized-water reactor (PWR) fuel assembly, which uses electrical resistance heaters to simulate the decay heat. The ADCS testing program included two test series. The first is referred to as the dry test series with three decay heats of 1, 2, and 3 kW; four helium fill pressures of 1,200 kPa (12 bar), 800 kPa (8 bar), 220 kPa (2.2 bar), 101 kPa (1 atm); and six vacuum pressure levels of 51 kPa (383 Torr), 10.1 kPa (75.8 Torr), 3.33 kPa (25 Torr), 1.33 kPa (10 Torr), 0.133 kPa (1 Torr), and 0.0133 kPa (0.1 Torr). This first test series was planned to include the range of decay heat values and pressure levels expected in the second (i.e., wet) test series. For each test in the dry test series, the ADCS used constant helium fill-pressure and decay heat and reached steady-state conditions. In the wet test series, the ADCS simulated all the transient processes involved in a commercial dry cask drying cycle, as shown in Table ES-1, Figure ES-1, and Figure ES-2.

The ADCS experiment included extensive temperature measurements that were made throughout the cask, including throughout the axial length of the fuel assembly and on different wall surfaces of the ADCS, inside and outside the pressure vessel representing the dry cask canister. The measurements included peak guide tube temperature (PGTT, analogous and effectively identical to the PCT), canister pressure, and water vapor molar fraction. The ADCS experiment included

two types of boundary conditions on the external wall of the flanges, as seen in Figure 1-8. One boundary condition involved keeping a constant temperature using heat-trace cable around the flanges and insulation on the horizontal surfaces of the flanges. The alternate boundary condition was to abandon the heat trace completely and let the flanges exchange heat with the surroundings. To avoid the uncertainty on this boundary, data from the latter were used to verify and validate the CFD method, including uncertainty quantification. The verification, validation, and uncertainty quantification (VVUQ) of the steady cases included the data for 3 kW corresponding to canister pressures of 12 bar, 1 atm, 25 Torr, 10 Torr, 1 Torr, and 0.1 Torr. For the transient wet testing case, the VVUQ was performed for a case with constant power of 1.483 kW, with pressure varying depending on the process, as shown in Figure ES-1 and Table ES-1. As the last step, several sensitivities were performed using the base case model for the transient vacuum drying using different assumptions about the fluids inside the canister. Some of these assumptions about the fluid choice inside the canister are used by dry cask applicants. This report investigates these sensitivities to show the conservatism of the model or lack thereof.

This report discusses the validation and UQ of the ADCS CFD model using SNL's experimental data. The CFD model used both the porous media representation (used as the base model) and the explicit geometry representation of the fuel rod region without any simplifications. Uncertainty quantification was performed and evaluated for the base case porous model, following the procedures outlined in American Society of Mechanical Engineers (ASME) Verification and Validation (V&V) 20-2009, "Standard for Verification and Validation in Computational Fluid Dynamics and Heat Transfer".

The sources of uncertainty examined in the analysis of the steady-state dry test series and the transient case wet test series include iterative uncertainty, spatial discretization, experimental uncertainty, and uncertainty due to modeling input parameters. Input parameter uncertainties included uncertainties in outer wall heat transfer coefficient, decay heat, ambient temperature, emissivity values, fuel region porous media hydraulic resistance (i.e., a porous media model was used to model the fuel region), and the fuel axial power profile correlation. For the wet transient test series, water vapor molar fraction was also among the input parameter uncertainties. SNL recognized that air ingress was an issue for the experiment at very low pressure. Therefore, for the 1 Torr steady-state experiment, air ingress (i.e., air molar fraction) was considered in the uncertainty quantification to reconcile the discrepancy found between the experimental data and the CFD predictions. This report documents the ADCS CFD model validation exercise, and is not intended to be used for regulatory guidance.

The CFD predictions using the porous media model and NUREG-2152 best practice guidelines were very favorable when compared to the experimental data. The CFD predictions showed that the base case porous media and the explicit geometry representation of fuel rod region models agreed very favorably in the prediction of the temperature profile in the fuel region and the external wall of the cask. Additionally, the CFD results of the base case model and experimental data for PCT, location of PCT, and temperature profiles in the fuel region, and on the external wall, agreed very favorably for all the collected cases, falling within the calculated validation uncertainty band.

The validation uncertainty was calculated using best estimate CFD analysis that includes the most likely scenario supplemented by UQ. The uncertainty in the power profile correlation and the external heat transfer coefficient in steady-state case runs were found to be the principal sources of uncertainty in the ADCS experiment. The PCT validation uncertainty for the dry steady-state cases varied 22–25°C. For the transient wet test vacuum drying case, the decay heat power profile and the water vapor molar fraction were the input variables that contributed the most to the validation uncertainty. The PCT validation uncertainty for the wet transient vacuum drying case was 21°C.

This report also shows that when proper CFD analysis is performed using NUREG-2152 guidelines and applicants' assumptions for a single running fluid depending on the vacuum drying processes, a conservative PCT prediction is obtained. Additionally, the VVUQ of the CFD model showed that the thermal conductivity of helium in the low vacuum pressure range of 0.1 to 25 Torr did not change with pressure. In that pressure range, the VVUQ showed that helium thermal conductivity is only temperature dependent. As such, it was concluded that helium is not in a rarefied regime in that pressure range of vacuum drying processes. Additionally, sensitivity analyses for the transient vacuum drying case using different fluids showed that when helium or combinations of helium and steam were used in draining and blowdown stages, with pure steam throughout the vacuum steps, then pure helium for the initial backfill, final vacuum, and final backfill steps, conservative results are obtained.

The results show that an Ansys Fluent thermal model using NUREG-2152 CFD best practice guidelines, including simulating the fuel assembly using a porous media approach, can demonstrate the safety of the storage of spent nuclear fuel by accurately predicting the PCT with accurate model inputs. This report also looks at the quality of the data collected in the ADCS experiment documents SAND2022-12078R, SAND2023-01454R, SAND2023-09746R, and SAND2024 using the calculated validation uncertainty. The ADCS experiment was designed to minimize validation uncertainty, the key factor and the basis for thermal model validation. Consequently, a well-validated thermal model will enable thermal reviewers to have confidence in the predictions, even with decreased margins.

TABLE OF CONTENTS

ABSTRACT ..... **iii**

LIST OF FIGURES ..... **ix**

LIST OF TABLES ..... **xiii**

EXECUTIVE SUMMARY ..... **xvii**

ABBREVIATIONS ..... **xxvii**

1 INTRODUCTION **1-1**
1.1 Objective 1-3
1.2 Description of the Advanced Drying Cycle Simulator Experiment 1-3
1.2.1 Test Plan… 1-14
1.3 Uncertainty Quantification 1-16
1.3.1 Computational Fluid Dynamics-Grade Experiment 1-18

2 COMPUTATIONAL FLUID DYNAMICS MODEL **2-1**
2.1 ADCS Computational Fluid Dynamics Model 2-1
2.2 Models, Geometry, Mesh, Solver Settings, and Boundary Conditions 2-3
2.3 Porous Media Radial and Axial Thermal Conductivity 2-11
2.4 Porous Media Equivalent Density, Specific Heat, and Frictional Coefficients 2-15
2.5 Decay Heat 2-16
2.6 Comparison of Porous Media with the Explicitly Represented Geometry Model 2-17
2.7 Baseline Simulation Results 2-27
2.7.1 Validation Metrics 2-28
2.8 Consistency Checks 2-29
2.9 Heat Profile Sensitivity 2-30

3 VERIFICATION, VALIDATION, AND UNCERTAINTY QUANTIFICATION **3-1**
3.1 Numerical Uncertainty 3-1
3.1.1 Iterative Uncertainty 3-1
3.1.2 Discretization Uncertainty 3-3
3.1.3 Overall Numerical Uncertainty 3-4
3.2 Input Uncertainty 3-5
3.3 Simulation Uncertainty Quantification 3-9
3.4 Experimental Uncertainty 3-10
3.5 Validation Uncertainty Quantification 3-11

4 RESULTS AND DISCUSSIONS **4-1**
4.1 Steady-State Computational Fluid Dynamics Model Validation Results 4-1
4.2 Transient Vacuum Drying Validation 4-20
4.3 Transient Vacuum Drying Sensitivity Results 4-25

5 CONCLUSIONS **5-1**

6 REFERENCES **6-1**

APPENDIX A DETAILED VERIFICATION, VALIDATION, AND UNCERTAINTY QUANTIFICATION FOR ALL CASES..... A-1

LIST OF FIGURES

Figure ES-1 Vacuum Drying Test Steps: Pressure and Power as Functions of Time xxi
Figure ES-2 Peak Cladding Temperature (PCT) as Function of Time for the Experiment, Base Case CFD Porous Media Model, and Base Case Explicit Geometry CFD Model xxiii
Figure 1-1 Major Components of the ADCS 1-5
Figure 1-2 The ADCS Inside the CYBL Facility 1-6
Figure 1-3 Photo of the 17x17 PWR Skeleton Taken During TC Installation 1-7
Figure 1-4 Photos of (a) Basket, (b) a Mouse Hole Cut in the Bottom of the Assembly Basket, (c) the ADCS Pressure Vessel with Uninsulated and Non-Heat-Traced Flanges, and (d) ADCS Pressure Vessel with Insulated and Heat-traced flanges 1-8
Figure 1-5 (a) Sight Glass in the Bottom Flange of the ADCS and (b) View from Below the Lower Pressure Vessel with the Bottom Flange Removed, Showing the Standoff, Support, Assembly, and Basket Inside the ADCS 1-9
Figure 1-6 Diagram of Heater Assembly TC Locations 1-10
Figure 1-7 Visualization of Heater Assembly Quadrants and TC Placement on Guide Tubes and Heater Rods 1-11
Figure 1-8 Heat-Trace Cables and Fiberglass Pipe Insulation on Top and Bottom Flanges 1-12
Figure 1-9 Diagram of Basket TC Locations 1-13
Figure 1-10 Diagram of ADCS Pressure Vessel TC Locations 1-14
Figure 2-1 Half-Symmetry CFD Models for (a) the Explicit-Geometry Model (b) the Porous Media Model 2-1
Figure 2-2 Surfaces Outlining the One-Eighth Symmetry CFD Models for (a) the Explicit-Geometry Model (b) the Porous Media Model 2-2
Figure 2-3 One-Eighth Symmetry Explicit-Geometry CFD Model for (a) Bottom of the Model Geometry (b) Top of the Model Geometry 2-2
Figure 2-4 Porous Geometry Model Mesh (Outside Pressure Vessel View): (a) Full, (b) Top, and (c) Bottom 2-4
Figure 2-5 Porous Geometry Model Mesh (Fuel Side View): (a) Full, (b) Top, and (c) Bottom 2-5
Figure 2-6 Explicit Geometry Model Mesh (Pressure Vessel Side View): (a) Bottom, (b) Top 2-6
Figure 2-7 Explicit Geometry Model Mesh (Fuel Side View): (a) Full, (b) Top, and (c) Bottom 2-7
Figure 2-8 (a) Explicit Geometry and (b) Porous Geometry Model Contours of Temperature (K) at z = 0.91 m and z = 3.66 m with View of Mesh for the 3 kW, 10 Torr, Helium Fill Steady Case 2-8
Figure 2-9 CFD Base Case Power Profile Shape 2-17
Figure 2-10 Maximum (a) Fuel and (b) Pressure Vessel External Wall Temperature Profiles Comparison Using the Explicit Geometry and Porous CFD Models for 3 kW and 12 Bar Steady-State Case 2-19
Figure 2-11 Maximum (a) Fuel and (b) Pressure Vessel External Wall Temperature Profiles Comparison Using the Explicit Geometry and Porous CFD Models for 3 kW and 1 atm Steady-State Case 2-20
Figure 2-12 Maximum (a) Fuel and (b) Pressure Vessel External Wall Temperature Profiles Comparison Using the Explicit Geometry and Porous CFD Models for 3 kW and 25 Torr Steady-State Case 2-21

Figure 2-13 Maximum (a) Fuel and (b) Pressure Vessel External Wall Temperature Profiles Comparison Using the Explicit Geometry and Porous CFD Models for 3 kW and 10 Torr Steady-State Case 2-22
Figure 2-14 Maximum (a) Fuel and (b) Pressure Vessel External Wall Temperature Profiles Comparison Using the Explicit Geometry and Porous CFD Models for 3 kW and 1 Torr Steady-State Case 2-23
Figure 2-15 Maximum (a) Fuel and (b) Pressure Vessel External Wall Temperature Profiles Comparison Using the Explicit Geometry and Porous CFD Models for 3 kW and 0.1 Torr Steady-State Case 2-24
Figure 2-16 Maximum (a) Fuel and (b) Pressure Vessel External Wall Temperature Profiles Comparison Using the Explicit Geometry and Porous CFD Models for the Transient Vacuum Drying Case for 1.483 kW at Regulatory Hold Point 2-25
Figure 2-17 Maximum Fuel Temperature Profile Comparison Using the Explicit Geometry and Porous CFD Models for the Vacuum Drying Transient Wet Case; Base Case Plotted for All Transient Steps and VOF Multiphase Model Plotted Only for the Hold After Water-Fill Step 2-26
Figure 2-18 Fuel Rod Layout—Axial Measurements at Guide Tube J9 2-28
Figure 2-19 Maximum (a) Fuel and (b) Pressure Vessel External Wall Temperature Profiles Comparison Using Base Case with the Base Linear and Uniform Heat Profiles for 3 kW and 12 Bar Steady-State Case 2-31
Figure 2-20 Maximum (a) Fuel and (b) Pressure Vessel External Wall Temperature Profiles Comparison Using Base Case with the Base Linear and Uniform Heat Profile for 3 kW and 1 atm Steady-State Case 2-32
Figure 2-21 Maximum (a) Fuel and (b) Pressure Vessel External Wall Temperature Profiles Comparison Using Base Case with the Base Linear and Uniform Heat Profile for 3 kW and 25 Torr Steady-State Case 2-33
Figure 3-1 Iterative Convergence of PCT for the 12 Bar, 3 kW Steady-State Case 3-2
Figure 3-2 Normal Distribution and PCT Iterative Convergence for the 12 Bar, 3 kW Steady-State Case 3-2
Figure 3-3 Power Profile Shapes Used for Input Uncertainties 3-7
Figure 3-4 Log-Log Plot of the Power Law Fit of the Raw Water Content Measurements, along with the 95 Percent Confidence and Prediction Intervals (SAND2023-0976R) 3-8
Figure 4-1 PCT Prediction (K) for Steady-State Cases 4-2
Figure 4-2 PCT Location Prediction (m) for Steady-State Cases 4-3
Figure 4-3 3 kW, 12 Bar, Helium, Steady-State Case Profiles of (a) Maximum (i.e., Centerline) Fuel Temperature and (b) Pressure Vessel Temperature, with Validation Uncertainty Bars at Selected Locations 4-4
Figure 4-4 3 kW, 1 atm, Helium, Steady-State Case Profiles of (a) Maximum (i.e., Centerline) Fuel Temperature and (b) Pressure Vessel Temperature, with Validation Uncertainty Bars at Selected Locations 4-5
Figure 4-5 3 kW, 25 Torr, Helium, Steady-State Case Profiles of (a) Maximum (i.e., Centerline) Fuel Temperature and (b) Pressure Vessel Temperature, with Validation Uncertainty Bars at Selected Locations 4-6
Figure 4-6 3 kW, 10 Torr, Helium, Steady-State Case Profiles of (a) Maximum Fuel Temperature and (b) Pressure Vessel Temperature, with Validation Uncertainty Bars at Selected Locations 4-7

Figure 4-7 3 kW, 1 Torr, Helium, Steady-State Case Profiles of (a) Maximum Fuel Temperature and (b) Pressure Vessel Temperature, with Validation Uncertainty Bars (Using Air Ingress Molar Fraction of 10 Percent as an Input Uncertainty) 4-9
Figure 4-8 3 kW, 0.1 Torr, Helium, Steady-State Case Profiles of (a) Maximum Fuel Temperature and (b) Pressure Vessel Temperature, with Validation Uncertainty Bars (Experimental Data from the Insulated, Heat-Traced Flanges Case) 4-10
Figure 4-9 3 kW, 1 Torr, Helium without Air Ingress, Steady-State Case Profiles of (a) Maximum Fuel Temperature and (b) Pressure Vessel Temperature, with Validation Uncertainty Bars 4-14
Figure 4-10 Fuel Max Temperature Profiles (a) With Air Ingress Molar Fraction of 5 Percent and (b) With Air Ingress Molar Fraction of 40 Percent for the 3 kW, 1 Torr, Helium, Steady-State Case, with Validation Uncertainty Bars 4-15
Figure 4-11 3 kW, 1 Torr Sensitivity Predictions for Fuel Max Temperature Profiles Using Porous Media Base Case 4-16
Figure 4-12 Comparison Between CFD and Experiment for Insulated, Heat-Traced Flanges and without (3 kW, 12 bar) 4-17
Figure 4-13 Comparison Between CFD and Experiment for Insulated, Heat-Traced Flanges and without (3 kW, 1 atm) 4-17
Figure 4-14 Comparison Between CFD and Experiment for Insulated, Heat-Traced Flanges and without (3 kW, 10 Torr) 4-18
Figure 4-15 Comparison Between CFD and Experiment for Insulated, Heat-Traced Flanges and without (3 kW, 1 Torr) 4-18
Figure 4-16 Comparison Between CFD and Experiment for Insulated, Heat-Traced Flanges and without (3 kW, 0.1 Torr) 4-19
Figure 4-17 Thermal Conductivity (W/(m.k) of Helium Versus Pressure (Torr) from Figure 7 in Ganta et al., 2011 4-19
Figure 4-18 PCT as a Function of Time for the 1.483 kW Transient Vacuum Drying Case, Including 30 Percent Water Vapor Molar Fraction Input Uncertainty 4-20
Figure 4-19 PCT as a Function of Time for the 1.483 kW Transient Vacuum Drying Case, without Including Any Uncertainty on the Water Vapor Molar Fraction 4-21
Figure 4-20 (a) Fuel Maximum Axial Temperature and (b) Pressure Vessel Axial Temperature Profile for the 1.483 kW Transient, at Regulatory Hold Point, with Validation Uncertainty Bars Including 30 Percent Water Vapor Molar Fraction Input Uncertainty 4-22
Figure 4-21 PCT Prediction (K) for Transient Vacuum Drying Case at Regulatory Hold Step 4-23
Figure 4-22 PCT Location Prediction (m) for the Transient Vacuum Drying Case at the Regulatory Hold Step 4-23
Figure 4-23 Transient Fuel Axial Max Temperature Profile for the 1.483 kW for Sensitivities 1, 2, 3, and 4 4-45
Figure 4-24 Transient Fuel Axial Max Temperature Profile for the 1.483 kW for Sensitivities 1, 2, 5, and 6 4-46
Figure 4-25 Transient Fuel Axial Max Temperature Profile for the 1.483 kW for Sensitivities 1, 2, 7, 8, and 9 4-47
Figure 4-26 Transient Fuel Axial Max Temperature Profile for the 1.483 kW for Sensitivities 1, 2, 10, and 11 4-48
Figure 4-27 Transient Fuel Axial Max Temperature Profile for the 1.483 kW for Sensitivities 1, 2, 12, 13, 14, and 15 4-49

Figure 4-28 Transient Fuel Axial Max Temperature Profile for the 1.483 kW for Sensitivities 1, 2, 16, and 17 4-50
Figure 4-29 Transient Fuel Axial Max Temperature Profile for the 1.483 kW for Sensitivities 1, 2, 18, 19, and 20 4-51
Figure A-1 PCT Results for Steady-State Cases and Transient Vacuum Drying Case at Regulatory Hold A-7
Figure A-2 PCT Locations Results for Steady-State Cases and Transient Vacuum Drying Case at Regulatory Hold A-8
Figure A-3 Fuel Assembly Temperature Results for Steady-State Cases and Transient Vacuum Drying Case at Regulatory Hold at 0.36 m A-9
Figure A-4 Fuel Assembly Temperature Results for Steady-State Cases and Transient Vacuum Drying Case at Regulatory Hold at 0.91 m A-10
Figure A-5 Fuel Assembly Temperature Results for Steady-State Cases and Transient Vacuum Drying Case at Regulatory Hold at 1.83 m A-11
Figure A-6 Fuel Assembly Temperature Results for Steady-State Cases and Transient Vacuum Drying Case at Regulatory Hold at 2.44 m A-12
Figure A-7 Fuel Assembly Temperature Results for Steady-State Cases and Transient Vacuum Drying Case at Regulatory Hold at 3.01 m A-13
Figure A-8 Fuel Assembly Temperature Results for Steady-State Cases and Transient Vacuum Drying Case at Regulatory Hold at 3.66 m A-14
Figure A-9 Fuel Assembly Temperature Results for Steady-State Cases and Transient Vacuum Drying Case at Regulatory Hold at 3.78 m A-15
Figure A-10 Pressure Vessel External Wall Temperature Results for Steady-State Cases and Transient Vacuum Drying Case at Regulatory Hold at 0.56 m A-16
Figure A-11 Pressure Vessel External Wall Temperature Results for Steady-State Cases and Transient Vacuum Drying Case at Regulatory Hold at 0.91 m A-17
Figure A-12 Pressure Vessel External Wall Temperature Results for Steady-State Cases and Transient Vacuum Drying Case at Regulatory Hold at 1.83 m A-18
Figure A-13 Pressure Vessel External Wall Temperature Results for Steady-State Cases and Transient Vacuum Drying Case at Regulatory Hold at 2.44 m A-19
Figure A-14 Pressure Vessel External Wall Temperature Results for Steady-State Cases and Transient Vacuum Drying Case at Regulatory Hold at 3.01 m A-20
Figure A-15 Pressure Vessel External Wall Temperature Results for Steady-State Cases and Transient Vacuum Drying Case at Regulatory Hold at 3.66 m A-21
Figure A-16 Pressure Vessel External Wall Temperature Results for Steady-State Cases and Transient Vacuum Drying Case at Regulatory Hold at 4.01 m A-22

LIST OF TABLES

Table ES-1 Transient Vacuum Drying Steps for 1.483 kW Test xxi
Table 2-1 CFD Solver Settings 2-9
Table 2-2 BCs for Each Configuration 2-10
Table 2-3 Radiation Model Settings 2-10
Table 2-4 PWR-17x17 Fuel Region Porous Model—Radial k_{eff} (Helium) 2-11
Table 2-5 PWR-17x17 Fuel Region Porous Model—Axial k_{eff} (Helium) 2-11
Table 2-6 PWR Fuel Region Porous Model—Radial k_{eff} (Water Vapor) 2-11
Table 2-7 PWR Fuel Region Porous Model—Axial k_{eff} (Water Vapor) 2-12
Table 2-8 PWR 17x17 Fuel Region Porous Model—Radial k_{eff} (Water Liquid) 2-12
Table 2-9 PWR 17x17 Fuel Region Porous Model—Axial k_{eff} (Water Liquid) 2-12
Table 2-10 PWR 17x17 Fuel Region Porous Model—Radial k_{eff} (Dry Air) 2-12
Table 2-11 PWR Fuel Region Porous Model—Axial k_{eff} (Dry Air) 2-13
Table 2-12 PWR 17x17 Fuel Region Porous Model—Radial k_{eff} (Saturated Air) 2-13
Table 2-13 PWR Fuel Region Porous Model—Axial k_{eff} (Saturated Air) 2-13
Table 2-14 PWR 17x17 Fuel Region Porous Model—Radial k_{eff} (mix0 = 90 Percent Helium, 10 Percent Water Vapor) 2-13
Table 2-15 PWR Fuel Region Porous Model—Axial k_{eff} (mix0 = 90 Percent Helium, 10 Percent Water Vapor) 2-14
Table 2-16 PWR 17x17 Fuel Region Porous Model—Radial k_{eff} (mix1 = 83.2 Percent Helium, 16.8 Percent Water Vapor) 2-14
Table 2-17 PWR Fuel Region Porous Model—Axial k_{eff} (mix1 = 83.2 Percent Helium, 16.8 Percent Water Vapor) 2-14
Table 2-18 PWR 17x17 Fuel Region Porous Model—Radial k_{eff} (mix2 = 52.6 Percent Helium, 47.4 Percent Water Vapor) 2-14
Table 2-19 PWR Fuel Region Porous Model—Axial k_{eff} (mix2 = 52.6 Percent Helium, 47.4 Percent Water Vapor) 2-15
Table 2-20 Fuel Region Porous Media Equivalent Density 2-15
Table 2-21 Assembly Fuel Region Porous Media Equivalent Specific Heat Capacity (J/kg*K) for Different Fill Fluids as Function of Temperature (K) 2-15
Table 2-22 Assembly Fuel Region Porous Media Equivalent Specific Heat Capacity (J/kg*K) for Liquid Water as Function of Temperature (K) 2-16
Table 2-23 Assembly Fuel Region Porous Media Equivalent Specific Heat Capacity (J/kg*K) for Saturated Air at 84 kPa as Function of Temperature (K) 2-16
Table 2-24 Porous and Explicit CFD Model PCT 2-18
Table 2-25 Energy Balance Consistency Check for 10 Torr Steady-State Case 2-30
Table 2-26 PCT and PCT Location Using Base Case and Uniform Heat Profile 2-30
Table 3-1 GCI Mesh Sizes 3-3
Table 3-2 GCI Values for PCT for the (10 Torr, 3 kW) Steady-State Case 3-4
Table 3-3 Overall Numerical Uncertainty for PCT for the (10 Torr, 3 kW) Steady-State Case 3-5
Table 3-4 Input Uncertainty for the (10 Torr, 3 kW) Steady-State Case 3-9
Table 3-5 Simulation Uncertainty for PCT for the (10 Torr, 3 kW) Steady-State Case 3-10
Table 3-6 Summary of the Expanded Uncertainty Determined for Each Measurement 3-11
Table 3-7 Total Validation Uncertainty for PCT for the (10 Torr, 3 kW) Steady-State Case 3-11
Table 3-8 Validation Uncertainty for PCT Location for the (10 Torr, 3 kW) Steady-State Case 3-12
Table 4-1 PCT for Steady-State Cases 4-1

Table 4-2 PCT Location Prediction (m) 4-2
Table 4-3 Test Results for 3 kW, 10 Torr, Helium, Steady-State Case 4-8
Table 4-4 Experimental Data and CFD PCT for Steady-State Cases Using Two Types of Boundary Conditions at the Flanges 4-16
Table 4-5 Transient Test Results at Regulatory Hold Point (1.483 kW, 0.045 kPa, Steam) 4-24
Table 4-6 Transient Vacuum Drying Case Steps, Fill Fluid, and Characteristics for Base Case 4-29
Table 4-7 Description of Transient Vacuum Drying Case Sensitivities 1–7 for Steps 1–3 4-30
Table 4-8 Description of Transient Vacuum Drying Case Sensitivities 1–7 for Steps 4–6 4-31
Table 4-9 Description of Transient Vacuum Drying Case Sensitivities 1–7 for Steps 7–9 4-32
Table 4-10 Description of Transient Vacuum Drying Case Sensitivities 1–7 for Steps 10–12 4-33
Table 4-11 Description of Transient Vacuum Drying Case Sensitivities 1–7 for Steps 13–15 4-34
Table 4-12 Description of Transient Vacuum Drying Case Sensitivities 8–14 for Steps 1–3 4-35
Table 4-13 Description of Transient Vacuum Drying Case Sensitivities 8–14 for Steps 4–6 4-36
Table 4-14 Description of Transient Vacuum Drying Case Sensitivities 8–14 for Steps 7–9 4-37
Table 4-15 Description of Transient Vacuum Drying Case Sensitivities 8–14 for Steps 10–12 4-38
Table 4-16 Description of Transient Vacuum Drying Case Sensitivities 8–14 for Steps 12–15 4-39
Table 4-17 Description of Transient Vacuum Drying Case Sensitivities 15–20 for Steps 1–3 4-40
Table 4-18 Description of Transient Vacuum Drying Case Sensitivities 15–20 for Steps 4–6 4-41
Table 4-19 Description of Transient Vacuum Drying Case Sensitivities 15–20 for Steps 7–9 4-42
Table 4-20 Description of Transient Vacuum Drying Case Sensitivities 15–20 for Steps 10–12 4-43
Table 4-21 Description of Transient Vacuum Drying Case Sensitivities 15–20 for Steps 13–15 4-44
Table A-1 Steady-State Test Results for 3 kW, 1,200 kPa, Helium A-2
Table A-2 Steady-State Test Results for 3 kW, 1 atm, Helium A-2
Table A-3 Steady-State Test Results for 3 kW, 25 Torr, Helium A-3
Table A-4 Steady-State Test Results for 3 kW, 10 Torr, Helium A-3
Table A-5 Steady-State Test Results for 3 kW, 1 Torr, Helium A-4
Table A-6 Steady-State Test Results for 3 kW, 1 Torr, Helium, Using 10 Percent Molar Fraction Ingress in the Uncertainty Quantification A-4
Table A-7 Steady-State Test Results for 3 kW, 1 Torr, Helium, Using Insulated Heat Traced Flanges Experimental Data and Insulated Flanges CFD Predictions with Uninsulated Uncertainty A-5
Table A-8 Steady-State Test Results for 3 kW, 0.1 Torr, Helium, Using Insulated Heat Traced Flanges Experimental Data and Uninsulated Flanges CFD Predictions and Uncertainty Quantification A-5
Table A-9 Steady-State Test Results for 3 kW, 0.1 Torr, Helium, Using Insulated Heat Traced Flanges CFD and Experimental Data but Uncertainty Quantification of Uninsulated Flanges CFD Case A-6

Table A-10 Transient Test Results for 1.483 kW, at Regulatory Hold, Water Vapor A-6
Table A-11 Helium Fill Gas Steady State and Transient Vacuum Drying Case at Regulatory Hold PCT Results A-7
Table A-12 Helium Steady-State and Transient Vacuum Drying Case at Regulatory Hold PCT Location Results A-8
Table A-13 Helium Steady-State and Transient Vacuum Drying Case at Regulatory Hold Fuel Assembly Temperature Results at 0.36 m A-9
Table A-14 Helium Steady-State and Transient Vacuum Drying Case at Regulatory Hold Fuel Assembly Temperature Results at 0.91 m A-10
Table A-15 Helium Steady-State and Transient Vacuum Drying Case at Regulatory Hold Fuel Assembly Temperature Results at 1.83 m A-11
Table A-16 Helium Steady-State and Transient Vacuum Drying Case at Regulatory Hold Fuel Assembly Temperature Results at 2.44 m A-12
Table A-17 Helium Steady-State and Transient Vacuum Drying Case at Regulatory Hold Fuel Assembly Temperature Results at 3.01 m A-13
Table A-18 Helium Steady-State and Transient Vacuum Drying Case at Regulatory Hold Fuel Assembly Temperature Results at 3.66 m A-14
Table A-19 Helium Steady-State and Transient Vacuum Drying Case at Regulatory Hold Fuel Assembly Temperature Results at 3.78 m A-15
Table A-20 Helium Fill Gas Steady-State and Transient Vacuum Drying Case at Regulatory Hold Pressure Vessel External Wall Results at 0.56 m A-16
Table A-21 Helium Fill Gas Steady-State and Transient Vacuum Drying Case at Regulatory Hold Pressure Vessel External Wall Results at 0.91 m A-17
Table A-22 Helium Fill Gas Steady-State and Transient Vacuum Drying Case at Regulatory Hold Pressure Vessel External Wall Results at 1.83 m A-18
Table A-23 Helium Fill Gas Steady-State and Transient Vacuum Drying Case at Regulatory Hold Pressure Vessel External Wall Results at 2.44 m A-19
Table A-24 Helium Fill Gas Steady-State and Transient Vacuum Drying Case at Regulatory Hold Pressure Vessel External Wall Results at 3.01 m A-20
Table A-25 Helium Fill Gas Steady-State and Transient Vacuum Drying Case at Regulatory Hold Pressure Vessel External Wall Results at 3.66 m A-21
Table A-26 Helium Fill Gas Steady-State and Transient Vacuum Drying Case at Regulatory Hold Pressure Vessel External Wall Results at 4.01 m A-22

EXECUTIVE SUMMARY

The field of computational fluid dynamics (CFD) applications and technologies is expanding rapidly, with a large database of proven capabilities. The driving force for program development generally is not the nuclear community, unlike the classical thermal-hydraulic system codes. Nevertheless, many CFD capabilities overlap with those required by the nuclear industry and dry cask applications: flows in complex geometries, mixing in stratified fluids, flow separation and reattachment, turbulence, multiphase phenomena, chemical species interaction, and fire scenarios. Consequently, practitioners in areas related to dry cask applications can benefit from other industries' advances in CFD technology. To avoid errors, however, due to the complexity of modern commercial CFD packages, users must take care in selecting the inputs and equations.

Dry cask storage has an ever-increasing role in the storage of spent nuclear fuel. With no licensed repository for offsite waste storage and with spent fuel pools filling up, there is a push toward onsite dry cask storage. Additionally, the decay heat of the fuel that is placed in dry cask storage is increasing, which brings dry cask storage system temperatures closer to their regulatory limits. CFD modeling is a useful tool for demonstrating compliance with thermal performance and the temperature limit of 400 degrees Celsius (°C) (752 degrees Fahrenheit (°F)) specified for cladding in NUREG-2215, "Standard Review Plan for Spent Fuel Dry Storage Systems and Facilities" and Interim Staff Guidance-11, "Cladding Considerations for the Transportation and Storage of Spent Fuel," issued November 2003. The purpose of this work is to help ensure that cask and fuel material temperatures in the dry cask storage system remain within the allowable limits for normal, off-normal, and accident conditions.

The U.S. Nuclear Regulatory Commission (NRC) is responsible for ensuring that applicants meet compliance standards such as Title 10 of the *Code of Federal Regulations* Part 72, "Licensing Requirements for the Independent Storage of Spent Nuclear Fuel, High-Level Radioactive Waste, and Reactor-Related Greater than Class C Waste", and NUREG-2215. Increasingly, this includes reviewing the applicant's CFD analysis to demonstrate compliance. Often, applicants submit designs that have a margin of only 10–20°C (18–36 °F)—and sometimes less—between the predicted peak cladding temperature (PCT) value and the NUREG-2215-specified cladding temperature limit of 400°C (752°F). This requires demonstrating that the simulation uncertainty is less than this margin, which can be a difficult task.

The introduction of the Electric Power Research Institute's phenomena identification and ranking table for thermal modeling states that engineering simulations exist for the design and licensing of spent fuel systems, as well as other simulations for improving the state of the art in computational research. The distinction is that design and licensing simulations provide decision makers with the necessary information about a system's performance and safety, whereas state-of-the-art efforts generally aim to improve modeling and simulation codes and methods. Simulations of the first type take a "conservative" approach to model inputs. Simulations of the second type use a best estimate—a "most likely or base case plus uncertainty" approach.

The conservative approach—using an accurate model (i.e., physics modeled correctly) with conservative geometric assumptions and boundary conditions—is useful for applicants. This approach minimizes the number of sensitivity runs needed to quantify the input uncertainty. However, it is still necessary to quantify the numerical uncertainty and to use a modeling process following CFD best-practice guidelines, as outlined in NUREG-2152, "Computational Fluid Dynamics Best Practice Guidelines for Dry Cask Applications". When validated against

experimental data for problems involving the same physical processes, modeling approaches that follow CFD best-practice guidelines in NUREG-2152 have been demonstrated to exhibit low uncertainty.

For example, some applications contain CFD predictions within a margin of 10–20°C (18–36°F) or less. To demonstrate that the modeling approach is accurate to that desired margin, there must be model validation using best estimate analysis that includes a most likely base case, supplemented by uncertainty quantification that demonstrates that the modeling approach can match experimental data to within accuracy of that margin.

Looking at validation experiments for CFD application to dry cask simulation in both design and safety studies, it appears that available data often suffer from a lack of local measurements, an insufficient number of measured flow variables, a lack of well-defined initial and boundary conditions, and/or a lack of information on experimental uncertainty. A key working group on CFD application to nuclear safety—the Organization for Economic Co-operation and Development, Nuclear Energy Agency, Committee on Safety of Nuclear Installations, Working Group on the Analysis and Management of Accidents—established some requirements for CFD-grade experiments able to properly validate single-phase CFD tools (Bestion (2016) and Bestion (2019)) using existing information and American Society of Mechanical Engineers (ASME) Verification and Validation (V&V) 20-2009 or similar guidance. These reports (ASME V&V 20-2009, Bestion (2016) and Bestion (2019)) found that the quality of the experiment used for the validation was a concern because many input parameters of value to the modeler were lacking. The discussion of this topic establishes whether a particular experiment is of a CFD grade. CFD-grade experiments should be able to validate a CFD model; the main concern is to minimize the validation uncertainty on some selected figures of merit or target variables, such as PCT.

In an experimental program designed to validate a computational method, clear objectives should first be defined. The success of the validation hinges on constant collaboration between the experimentalist and the CFD specialist. This discussion should include the definition of the test section geometry, initial and boundary conditions, and the requirement for measurement uncertainty. Agreement is necessary on what to measure, where it will be measured, and with which measurement technique. Acceptance criteria may be defined for the sensitivity of the measured parameters to the process of interest, for the required accuracy of some selected physical quantity, or for both. Preliminary code simulations are necessary to define appropriate model boundaries and measurement locations, with sensitivity tests to determine the uncertainty of initial and boundary conditions and of measured field parameters. Iterations may be necessary to optimize the design.

The purpose of this investigation is to validate the CFD model built in Ansys Fluent version 24 and based on the modeling practices in NUREG-2152, using experimental data collected in the Advanced Drying Cycle Simulator (ADCS), as documented in Sandia National Laboratories (SNL) reports SAND2022-12078R, “Update on the Investigation of Commercial Drying Cycles Using the Advanced Drying Cycle Simulator,” issued September 2022; SAND2023-01454R, “Advanced Drying Cycle Simulator Thermal Response to Commercial Drying Conditions,” issued March 2023; SAND2023-09746R, “Preliminary Simulations of Commercial Drying Cycles Using the Advanced Drying Cycle Simulator,” issued September 2023; and SANS2024 report, “Summary of Spent Nuclear Fuel Thermal and Drying Research at Sandia National Laboratories”. CFD model validation included PCT, PCT location, maximum (i.e., centerline) fuel temperature profile in the assembly, and the dry cask outer wall temperature profile.

Fuel cladding temperatures are critical for evaluating the fuel cladding integrity. To produce these data sets under well-controlled boundary conditions, the ADCS was built to study the thermal-hydraulic response of fuel under a variety of heat loads and internal vessel pressures, including steady-state dry testing conditions mimicking nonventilated dry cask normal storage conditions and wet transient testing conditions analyzing prototypical vacuum drying processes.

The ADCS experiment included extensive temperature measurements made throughout the cask, including throughout the axial length of the fuel assembly and on different wall surfaces of the ADCS, inside and outside the pressure vessel representing the dry cask canister. The measurements also included peak guide tube temperature (PGTT, analogous and effectively identical to PCT), canister pressure, and water vapor molar fraction.

The ADCS experiment included two types of boundary conditions (BCs) on the external wall of the flanges. One BC involved keeping a constant temperature using heat-trace cable and insulating material around the flange, as shown in Figure 1-8. The alternate BC was to abandon the heat-trace completely and let the flanges exchange heat with the surroundings, as shown in Figure 1-4(c). To avoid the uncertainty on this BC, data from the latter were used to verify and validate the CFD method, including uncertainty quantification (UQ). The verification, validation, and uncertainty quantification (VVUQ) of the steady cases included the data for 3 kilowatts (kW), corresponding to a canister pressure of 12 bar, 1 atm, 25 Torr, 10 Torr, 1 Torr, and 0.1 Torr. For the transient wet testing case, the VVUQ was performed for a case with constant power of 1.483 kW, with pressure varying depending on the process, as shown in Table ES-1 and Figure ES-1.

As this report documents, two types of CFD models were created to simulate steady dry tests mimicking cask storage conditions and transient wet tests modeling vacuum drying steps. The first simulation used the porous media model, with the fuel region in the assembly represented by a fluid volume inside the basket with an equivalent momentum and heat sources, and equivalent axial and radial thermal conductivities to represent conduction and radiation heat transfer effects of non-represented fuel rod and grid spacer geometry. More details about the porous media model appear in NUREG-2152; NUREG-2208, “Validation of Computational Fluid Dynamics Methods Using Prototypic Light Water Reactor Spent Fuel Assembly Thermal-Hydraulic Data”; and NUREG-2174, “Impact of Variation in Environmental Conditions on the Thermal Performance of Dry Storage Casks”.

In the second model, the assembly was fully represented, including fuel rods and grid spacers inside the basket. The geometry and mesh of the second CFD model with the explicit geometry representation is more complicated and time consuming to create and run. In this validation, the explicit representation of the assembly model was feasible to create and run because the canister had only one assembly. In dry cask applications, a cask can have as many as 97 assemblies, so creating geometry and mesh can be prohibitively time consuming. Hundreds of millions of cells are needed to resolve all the assembly components in an explicit representation model of a many-assembly cask. Additionally, the solution of such a case is computationally prohibitive to run. The applicants generally use porous media for modeling dry cask applications presented to the NRC. As such, the porous media model is used as the base case in this report for the steady dry cases and the transient wet case, including validation uncertainty. In this report, the explicit geometry model is also used to look at the predictive capabilities of the porous media model and to assess the conservatism of the porous media model, if there is any.

SNL’s ADCS experiments discussed in this report provide valuable data for validation of the dry cask storage system CFD model. The model inputs, temperatures, and physical properties were

carefully measured, along with associated uncertainties, to enable a full VVUQ analysis that resulted in a reasonable level of validation uncertainty. The results of this specific study cannot justify modeling uncertainties of PCT prediction to within 10°C (18°F), especially when using air as the fill gas, but the overall accuracy of the modeling approach is demonstrated.

In the ADCS validation effort, the largest sources of uncertainty in the fuel temperature profile for the steady helium-fill cases mimicking normal storage were found to be the uncertainty in the cask external surface heat transfer coefficient and the decay heat profile correlation. For the transient wet vacuum drying case, the main sources of uncertainty in the fuel PCT (found in the last stage of vacuum drying) were the decay heat profile and the water vapor molar fraction. For the five steady dry helium cases and one transient wet vacuum drying case analyzed, all of the CFD predictions of PCT and PCT location, and most of the fuel maximum (i.e., centerline) temperature profile, were found to be within the validation uncertainty band. Overall, the dry cask modeling approach, including the use of porous media as a simplification of the detailed fuel assembly, was demonstrated to be an accurate way of simulating the heat transfer within the ADCS experiment.

The vacuum drying wet testing experiment consisted of five transient tests. Each test was conducted over multiple days. In the experiment, the top and bottom flanges acted as large heat sinks due to their large material density and volume. These flanges are required parts due to the seals formed at flange gaskets. To compensate for the heat sink effect, which would not normally be present on a welded canister lid, the first four tests used heat-trace cable and fiberglass pipe insulation on all three flanges to maintain a constant temperature. The fifth transient vacuum drying test did not use heat-trace cables or insulation. Thus, the flanges' external boundaries exchanged heat through convection and radiation to the surrounding. This report uses the fifth test to verify and validate the developed CFD method. Table ES-1 and Figure ES-1 illustrate the transient steps in this test. The first process involved bulk water fill to a level of 3.35 meters (m), measured from the top of the bottom nozzle of the assembly. Air occupied the canister volume above the liquid water. Then, heat was supplied to the pressurized-water reactor's (PWR) 17x17 fuel assembly. After a hold period, bulk water drain was initiated, followed by multiple helium blowdowns and then a hold at 109 kilopascals (kPa). Multiple vacuum steps occur next, during which pressure was reduced and briefly held at the "Vacuum #" pressures indicated in Table ES-1. Once at minimum pressure, the 30-minute regulatory hold took place, beginning 6.6 hours after the 109 kPa pre-vacuum hold ended. Following the regulatory hold, the canister was backfilled with helium, one additional vacuum was pulled, and finally, the canister was backfilled with helium and allowed to approach steady state. This report contains several ways to apply CFD to model the transient vacuum drying processes shown in Table ES-1.

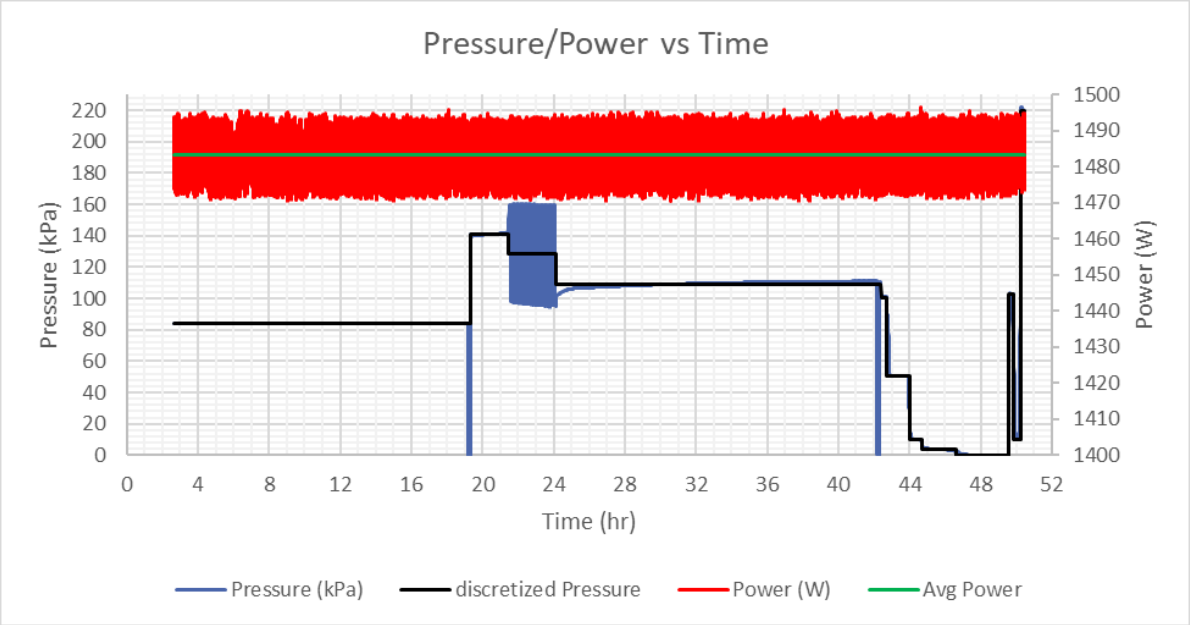


Figure ES-1 Vacuum Drying Test Steps: Pressure and Power as Functions of Time

Table ES-1 Transient Vacuum Drying Steps for 1.483 kW Test

Process	Elapsed time (hr)	Pressure (kPa)	Power (W)	Materials	H2O vapor molar fraction	He molar fraction
Water fill	2.65	84	0	H2O liquid/air	H2O liquid/air	H2O liquid/air
Hold After Water Fill	15.02	84	1,483	H2O liquid/air	H2O liquid/air	H2O liquid/air
Drain-1	1.68	84	1,483	Mixture 0	0.1	0.9
Drain-2	2.14	140.9	1,483	Mixture 0	0.1	0.9
Blowdown	2.62	128.1	1,483	Mixture 0	0.1	0.9
Hold Before Vacuum	18.3	109.3	1,483	Mixture 0	0.1	0.9
Vacuum 0	0.33	100.7	1,483	Mixture 0	0.1	0.9
Vacuum 1	1.25	50.3	1,483	Mixture 1	0.168	0.832
Vacuum 2	0.72	10	1,483	Mixture 2	0.474	0.526
Vacuum 3	1.9	3.7	1,483	Mixture 3	1	0
Vacuum 4	1.53	0.1	1,483	Mixture 4	1	0
Vacuum 5	0.89	0.045	1,483	Mixture 5	1	0
Regulatory Hold	0.57	0.045	1,483	Mixture 5	1	0
Backfill 1	0.26	102.7	1,483	Mixture 6	0.01	0.99
Final Vacuum	0.39	10	1,483	Mixture 6	0.01	0.99
Final Backfill	0.23	219.6	1,483	He	0	1

The transient analysis started when the heat was supplied in the water fill hold-time. The CFD model in the water fill hold-time period used one of two choices: (1) the Volume of Fluid (VOF) multiphase flow method or (2) single-phase CFD modeling with a physical thin wall separating the liquid water and air. In the VOF model, the interface between the liquid water and air phases was modeled without any wall between them. All the vacuum drying steps after the water fill hold-time used single-phase CFD modeling to predict the thermal behavior of the cask, as Table ES-1 shows. The running fluid and conditions shown in Table ES-1 are the best estimate conditions and assumptions obtained from the ADCS experiment.

Other sensitivity calculations were performed using different running fluids in the transient steps, using either single-component running fluids such as helium, water vapor, or combinations of the two. These sensitivities, including applicants' preferred assumptions, were used to assess the conservatism of each method compared to the base case that used the best estimate assumptions. Most applicants completely ignore the water fill step while performing CFD for the vacuum drying steps. Instead, they start their CFD predictions after the bulk water drain, using helium as the running fluid initialized at the saturation temperature of the water vapor with the pressure existing at the drain/blowdown step. After draining, blowdown, and hold-time before vacuum, water vapor is used as the running fluid until the backfill, when helium is used again.

All of the sensitivity runs are discussed in the results section of this report.

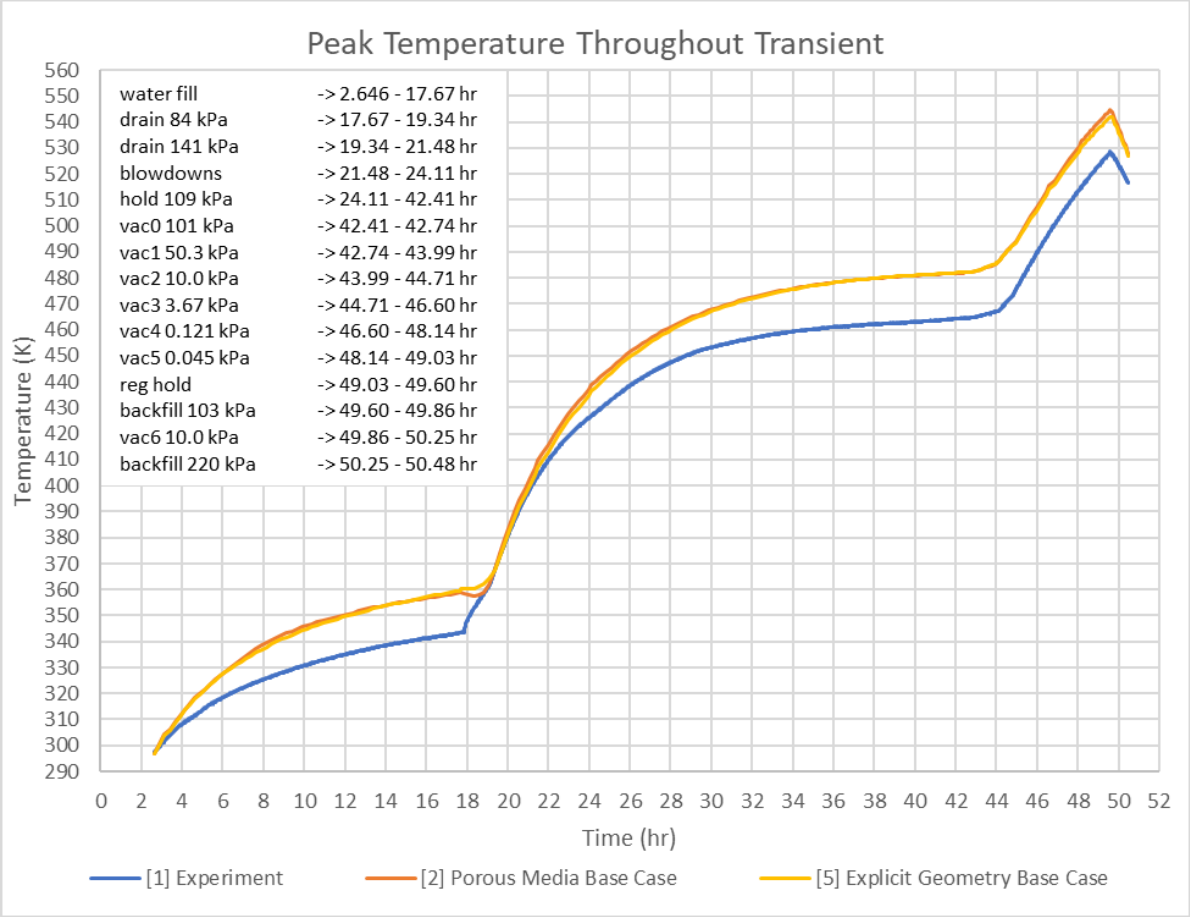


Figure ES-2 Peak Cladding Temperature (PCT) as Function of Time for the Experiment, Base Case CFD Porous Media Model, and Base Case Explicit Geometry CFD Model

During a spent fuel drying process at an observed nuclear power plant, water in the outer jacket of a cask (between the transfer cask and the canister) started to boil when the pressure inside the canister increased from low vacuum pressure (around 1–3 Torr) to high backfilling pressures above the atmospheric pressure. The explanation given was that this phenomenon is normal, because radial heat transfer during low vacuum pressure is at its minimum and will increase as canister pressure increases. Furthermore, it was claimed that this phenomenon of low heat transfer from the fuel region was due to the low thermal conductivity of helium at vacuum pressures (e.g., cask drying processes), which is tenfold or more lower than the value at atmospheric pressure and above, as shown in Figure 4-17 of the article by Ganta et al., 2011. However, data from the National Institute of Standards and Technology (NIST) Chemistry WebBook, SRD 69, Thermophysical Properties of Fluid Systems show that at low vacuum pressures (as in the vacuum drying processes), helium thermal conductivity is not dependent on pressure. At that range of low pressures, helium thermal conductivity is a function of only the temperature, just as in atmospheric pressure conditions and above.

For this report, the NRC used the VVUQ of the CFD method using the ADCS data to investigate this claim of low helium thermal conductivity at low pressure, like those present during the last stage of vacuum drying (i.e., ranging between 0.1 Torr and 10 Torr). The VVUQ of the ADCS data

at low pressures in this report showed that the claim of low helium thermal conductivity, as documented in Ganta et al., is not supported and is misleading.

UQ was performed using ASME V&V 20-2009, "Standard for Verification and Validation in Computational Fluid Dynamics and Heat Transfer", for the target variables of interest, including PCT, PCT location, fuel maximum axial temperature, and external temperature profiles. Sources of uncertainty examined in the analysis include numerical errors (as tabulated in section 3.1), simulation inputs (section 3.2), and experimental errors (section 3.4).

The CFD results and experimental data for PCT, PCT location, fuel temperature, and external dry cask wall temperature profiles agreed very favorably with the calculated validation uncertainty, as illustrated in chapter 4, for all cases. The validation uncertainty includes the combination of simulation and experimental uncertainty. The simulation uncertainty includes simulation input and numerical uncertainties. The results demonstrate that an Ansys Fluent thermal model that was developed based on CFD best practice guidelines, as documented in NUREG-2152, can be used to demonstrate the safety of dry cask storage system designs. While this work did not examine other CFD codes, it is expected that thermal models developed based on NUREG-2152 guidance but using an alternate, similarly capable, and well-validated commercial CFD code (e.g., Siemens STAR-CCM+, OpenFOAM, etc.) would be similarly useful in demonstrating the safety of dry cask storage system designs.

The NRC uses ASME V&V 20-2009 methods to evaluate uncertainties in CFD. As found in NUREG/CR-7260, "CFD Validation of Dry Cask Storage Systems":

> UQ starts by clearly identifying the various sources of uncertainties using a phenomena identification and ranking table (PIRT). The deficiencies or inaccuracies of CFD simulations can be attributed to a wide number of errors and uncertainties. These errors and uncertainties consist of two main broad categories. The first category is related to modeling physics, while the second is concerned with the numerical aspect of the solution. The first category includes simplification of physical complexity, boundary and initial conditions, and physical boundary conditions. The second category includes computer programming, round-off, spatial discretization, temporal discretization, and iterative convergence. When performing validation simulations, it is mandatory to quantify and reduce the different errors and uncertainties originating from these sources. Despite all these errors and inaccuracies, CFD still remains a reliable method to simulate dry cask thermal response accurately with low margins when best practice guidelines are used. Best practice guidelines, such as those in NUREG-2152 and ASME V&V 20-2009, are an excellent source for the CFD user to avoid errors and quantify uncertainties.

In the current validation, the geometry was well prescribed; consequently, geometrical input was not the main source of the validation error (i.e., fluid gaps), as found in NUREG/CR-7260.

ASME V&V 20-2009 clearly states that the scope of V&V is quantification of the accuracy of a simulation, for a specified validation variable at a specified validation point, for cases in which the conditions of the actual experiment are simulated. As reported in Bestion et al., 2019, practically, ASME V&V 20-2009 affirms that, "The ultimate goal of V&V is to determine the degree to which a model is an accurate representation of the real world." This standard is based strongly on the use of experimental data for V&V, and consequently for UQ. With this approach, the ASME standard puts a strong link between V&V and UQ.

Also, as reported in Bestion et al., 2016—

> The ASME standard methodology for uncertainty analysis underlines the role of V&V in the process of evaluating confidence in CFD results. Uncertainties must be evaluated step by step, using clearly defined numerical aspects of the model such as time and space discretization (time step and mesh convergence) or physical models (turbulence models, physical assumptions) with associated evaluation of error.

The ASME standard conforms to NRC regulatory practices, procedures, and methods for licensing dry cask systems, as embodied in Title 10 of the *Code of Federal Regulations* and other pertinent documents, such as Regulatory Guide 1.203, "Transient and Accident Analysis Methods", and NUREG-0800, "NRC Standard Review Plan for the Review of Safety Analysis Reports for Nuclear Power Plants: LWR Edition".

In this experimental program, the collaboration between SNL experimentalists and NRC CFD specialists was successful. The program used CFD to perform similarity analysis and adequately choose the decay heat powers through many iterations to properly scale the model to match the conditions and thermal performance of a prototypic dry cask. Additionally, CFD predictions were used to check the initial shakedown tests for all of the configurations. Consequently, the experimental data collected in this program were geared to obtain a CFD-grade experiment.

The main objective of this experiment was to minimize the validation uncertainty and thus improve the CFD thermal model. When a thermal model is well validated, the dry cask applicants and thermal reviewers have confidence in the predicted margins, even when minimized, without exceeding the set limit. This report shows that a well-crafted, best estimate thermal model uses the design basis following CFD best practice guidelines and complemented by UQ. Such a model will have enough information for dry cask applicants and thermal reviewers about the margins that can be considered safe for applications and certifications.

ABBREVIATIONS

2D	two-dimensional
3D	three-dimensional
ADCS	Advanced Drying Cycle Simulator
ASME	American Society of Mechanical Engineers
atm	atmosphere
BC	boundary condition
C	Celsius
CFD	computational fluid dynamics
CFR	*Code of Federal Regulations*
CYBL	Cylindrical Boiling Facility
F	Fahrenheit
GCI	grid convergence index
H2O	water
He	helium
hr	hour
in.	inch
ISG	interim staff guidance
K	Kelvin
k_{eff}	effective thermal conductivity
kg	kilogram
Kn	Knudsen
kPa	kilopascal
kW	kilowatt
m	meter
MgO	magnesium oxide
mm Hg	millimeter mercury (pressure unit)
NRC	U.S. Nuclear Regulatory Commission
Pa	pascal
PCT	peak cladding temperature
PGTT	peak guide tube temperature
ppmv	parts per million by volume
PIRT	phenomena identification and ranking table
psi	pounds per square inch
PWR	pressurized-water reactor
RMS	root mean square
s	second
SIMPLEC	Semi-Implicit Method for Pressure-Linked Equations-Consistent
SNL	Sandia National Laboratories
TC	thermocouple
UQ	uncertainty quantification
V&V	verification and validation
VOF	Volume of Fluid

VVUQ	verification, validation, and uncertainty quantification
W	watt
1 atm	= 101,325 Pa = 760 mm Hg = 14.7 psi (atmospheric average pressure at sea level)
1 bar	= 105 Pa = 14.5 psi
1 Torr	= 1 mm Hg = 1 atm / 760 = 101,325 / 760 = 133.322 Pa = 0.0193 psi

1 INTRODUCTION

The thermal performance of commercial spent nuclear fuel dry storage casks is evaluated through detailed analytical modeling using computational fluid dynamics (CFD). The vendor undertakes these modeling efforts to demonstrate performance and regulatory compliance, which are independently verified by the U.S. Nuclear Regulatory Commission (NRC). The confidence of CFD methods used for dry cask applications is based on verification and validation (V&V) of the models. To strengthen confidence in these models, uncertainty quantification (UQ) also needs to be performed in the V&V of the CFD methods. It is part of CFD best practice guidelines to present CFD predictions for the peak cladding temperature (PCT), or any other target variable supported by UQ, to provide confidence that the obtained margin is adequate. For this reason, the NRC Office of Nuclear Material Safety and Safeguards asked the NRC Office of Nuclear Regulatory Research to participate in a dry cask storage system numerical modeling validation study to assist it in making regulatory decisions to ensure adequate protection for storage and transportation casks. Verification, validation and uncertainty quantification (VVUQ) of the CFD method builds thermal reviewers' confidence in the adequacy of the thermal design being evaluated.

This report documents CFD validation of a series of simulated commercial drying cycle tests conducted on a single, simulated pressurized-water reactor (PWR) assembly with prototypic geometry in a simplified vessel with well-controlled boundary conditions (BCs), known as the Advanced Drying Cycle Simulator (ADCS). The ADCS was built to study the thermal-hydraulic response of fuel under a variety of heat loads and internal vessel pressures, including steady-state dry testing conditions mimicking nonventilated dry cask normal storage conditions and wet transient testing conditions analyzing prototypical vacuum drying processes. The purpose of this investigation is to validate the Ansys Fluent CFD code using the experimental data collected in the ADCS experiments documented in Sandia National Laboratories (SNL) reports SAND2022-12078R, "Update on the Investigation of Commercial Drying Cycles Using the Advanced Drying Cycle Simulator," issued September 2022; SAND2023-01454R, "Advanced Drying Cycle Simulator Thermal Response to Commercial Drying Conditions," issued March 2023; SAND2023-09746R, "Preliminary Simulations of Commercial Drying Cycles Using the Advanced Drying Cycle Simulator," issued September 2023; and SAND2024 report "Summary of Spent Nuclear Fuel Thermal and Drying Research at Sandia National Laboratories," issued September 2024.

This report discusses how the base case CFD model, using porous media to represent the fuel assembly, compares with an explicit geometry CFD model in which the true fuel assembly geometry—with its fuel rods, guide tubes, and grid spacers—is represented. CFD model validation included guide tube temperatures (which are effectively equal to fuel cladding temperatures) and the axial profiles of maximum fuel temperature and the dry cask outer wall temperature. To produce these data sets under well-controlled boundary conditions, the ADCS was built to study the thermal-hydraulic response of fuel under a variety of heat loads and internal vessel pressures, including steady-state dry testing conditions mimicking nonventilated dry cask normal storage condition, and wet transient testing condition analyzing prototypical vacuum drying processes.

UQ starts by clearly identifying the various sources of uncertainties. The deficiencies or inaccuracies of CFD simulations can be attributed to many kinds of errors and uncertainties, but consist of two main categories, one related to modeling physics, and the second concerned with numerical aspects of the solution. The first category includes simplification of physical complexity, boundary and initial conditions, and physical BCs. The second category includes computer programming, round-off, spatial discretization, temporal discretization, and iterative convergence.

American Society of Mechanical Engineers (ASME) V&V 20-2009, "Standard for Verification and Validation in Computational Fluid Dynamics and Heat Transfer", clearly states that the scope of V&V is quantification of the accuracy of a simulation, for a specified validation variable at a specified validation point, for cases in which the conditions of the actual experiment are simulated. Practically, ASME V&V 20-2009 affirms that "The ultimate goal of V&V is to determine the degree to which a model is an accurate representation of the real world." This standard is based strongly on the use of experimental data for V&V, and consequently for UQ. With this approach, the ASME standard strongly links V&V and UQ.

The standard methodology for uncertainty analysis in ASME V&V 20-2009 underlines the role of V&V in evaluating confidence in CFD results. Uncertainties must be evaluated step by step, using clearly defined numerical aspects of the model such as time and space discretization (time step and mesh convergence) or physical models (turbulence models, physical assumptions), with associated evaluation of error. Furthermore, the ASME V&V 20-2009 standard conforms to NRC regulatory practices, procedures, and methods for licensing dry cask systems, as embodied in Title 10 of the *Code of Federal Regulations* (10 CFR) and other pertinent documents, such as Regulatory Guide 1.203, "Transient and Accident Analysis Methods", and NUREG-0800, "Standard Review Plan for the Review of Safety Analysis Reports for Nuclear Power Plants: LWR Edition," issued March 2017.

When a gas molecule's mean free path (i.e., the average distance it travels between collisions) is significant compared to the characteristic size of its container, the gas is rarefied and not in continuum. Low pressure leads to low gas density, which increases the mean free path, eventually leading to a rarefied state. Thermophysical properties, such as thermal conductivity of the gas, will decrease when rarefied. In the ADCS experiment, helium gas pressures as low as 1 Torr and 0.1 Torr were reached. Figure 4-17 in Ganta, et al., 2011, shows that helium will be in a rarefied state with thermal conductivity 10 times less than if it were in continuum. In the present report, VVUQ was used to check whether the helium was in a rarefied state.

The ADCS simulates one prototypic 17x17 PWR fuel assembly, using electrical resistance heaters to simulate the decay heat. The ADCS testing program included two test series. The first is referred to as the dry test series, with three decay heats of 1, 2 and 3 kilowatts (kW), four helium fill pressures of 1,200 kilopascals (kPa) (12 bar), 800 kPa (8 bar), 220 kPa (2.2 bar), 101 kPa (1 atmosphere (atm)) and six vacuum pressure levels of 51 kPa (383 Torr), 10.1 kPa (75.8 Torr), 3.33 kPa (25 Torr), 1.33 kPa (10 Torr), 0.133 kPa (1 Torr) and 0.0133 kPa (0.1 Torr). This first test series was planned to include the range of decay heat values and pressure levels expected in the second (i.e., wet) test series. For each test in the dry test series, the ADCS operated at constant helium fill pressure and decay heat and reached the steady-state conditions. In the wet test series, the ADCS simulated all of the transient processes involved in a commercial dry cask drying cycle.

The ADCS experiment included extensive temperature measurements throughout the cask, including throughout the axial length of the fuel assembly and on different wall surfaces of the ADCS, inside and outside the pressure vessel representing the dry cask canister. The measurements included peak guide tube temperature (PGTT, analogous and effectively identical to PCT), canister pressure, and water vapor molar fraction. The ADCS experiment included two types of BCs on the external wall of the flanges, as seen in Figure 1-8. One BC involved keeping a constant temperature using insulation and heat-trace cable around the flange. The alternate BC was to abandon the heat-trace completely and let the flanges exchange heat with the surroundings. To avoid the uncertainty on this BC, data from the latter were used to verify and validate the CFD method, including UQ. The VVUQ of the steady-state cases included the data

for the 3 kW heater power at canister pressures of 12 bar, 1 atm, 25 Torr, 10 Torr, 1 Torr, and 0.1 Torr. For the transient (i.e., wet) testing case, the VVUQ was performed for a case with a constant power of 1.483 kW, with pressure varying depending on the process, as shown in Figure ES-1 and Table ES-1.

The following sections of this report outline the ADCS experiment, the different CFD models, and assumptions used to simulate it. This report also provides a detailed description of the model VVUQ using target variables such as peak fuel temperature, maximum (i.e., centerline) fuel temperature profile, and the dry cask external wall temperature profile.

1.1 Objective

The purpose of this investigation was to validate the CFD model built in Ansys Fluent version 24 against data obtained from an ADCS program that had been built to mimic the thermal-hydraulic response of fuel under a variety of heat loads and internal vessel pressures, with an initial focus on steady-state conditions replicating normal storage conditions. The next step was to validate the same CFD model by simulating transient vacuum drying processes. The validation of both cases involves the use and development of UQ analysis using ASME V&V 20-2009.

1.2 Description of the Advanced Drying Cycle Simulator Experiment

The Sandia National Laboratories (SNL) Advanced Drying Cycle Simulator (ADCS) experimental setup was used for this CFD validation effort. The ADCS consists of one prototypic 17x17 pressurized water reactor (PWR) fuel assembly with electrically powered fuel rods, guide tubes, top and bottom nozzles, grid spacers, and a siphon tube. The electrically powered fuel rods are waterproofed and housed inside a painted steel basket surrounded by a painted steel cylindrical pressure vessel, as illustrated in Figure 1-1. The ADCS was built inside the Cylindrical Boiling (CYBL) facility at SNL, as shown in Figure 1-2.

The SNL reports SAND2022-12078R, SAND2023-01454R, SAND2023-09746R, and SAND2024 contain details of the ADCS geometry and design. The ADCS system, from the center to the periphery, consists of the following:

- An existing, electrically heated prototypic 17x17 PWR assembly that has 264 fuel rods, 24 guide tubes, and 1 instrument tube in the center of the assembly, 11 grid spacers, bottom tie plate and top tie plate (Figure 1-3). The guide tubes were instrumented with type T-thermocouples (TCs) along and across the fuel assembly (Figure 1-6 and Figure 1-7). As shown in Figure 1-6 and Figure 1-7, a reference coordinate system was defined with an origin ($z = 0$) at the top of the bottom nozzle on the assembly. The z-coordinate runs along the assembly axial length. Also as shown in Figure 1-6 and Figure 1-7, an alphanumerical grid is used to identify guide tube TCs. The fuel assembly cross-section plan view is identified by four quadrants (Figure 1-7).

- In the system, 264 fuel rods were made of stainless steel cladding and filled with compacted magnesium oxide (MgO) powder to mimic the fuel pellets. Nichrome wire running through the middle of the MgO powder was used to supply a linearly decreasing electrical heat source along the length of the fuel rods. MgO powder and nichrome wire properties were chosen to match the thermal properties of the fuel pellet in a nuclear fuel rod.

- Twenty-four guide tubes and one central instrument tube were made of zircalloy. TCs were attached to both the guide tubes and the instrument tube (Figure 1-6 and Figure 1-7).
- The storage basket is made of painted stainless steel and surrounds the fuel rod skeleton, instrumented with TCs along the length of the basket (Figure 1-9). Three mouse holes are cut in the bottom of the basket, as shown in Figure 1-4(b).
- The pressure vessel is made of 10-inch, Schedule 40 painted stainless steel pipe with an inside diameter of 254.5 millimeters (10.02 inches) and a maximum allowable working pressure of 2,400 kPa at 400 degrees Celsius (°C) (752 degrees Fahrenheit (°F)). The pressure vessel is instrumented with TCs, as shown in Figure 2-10, along its length. It surrounds the storage basket (Figure 1-1).
- The complete ADCS pressure vessel is shown in Figure 1-4(d). The pressure vessel was mounted on a stand, as shown in Figure 1-5(b), composed of fixture table components and steel framing. This stand elevated the ADCS pressure vessel off the CYBL facility floor, allowing viewing access to the sight glass on the bottom flange (Figure 1-5(a) and Figure 1-5(b)).
- Three flanges connect (lower middle) and seal (top and bottom) the pressure vessel's 10-inch, Schedule 40 pipe.
- In some of the experimental data, the flanges were kept isothermal using heat-trace cable and fiberglass pipe insulation, as shown in Figure 1-4(d) and Figure 1-8.
- Other experimental data did not use heat-trace cables or insulation on the flanges. The flanges exchanged heat through convection and radiation with the surroundings, as shown in Figure 1-1 and Figure 1-4(c)
- A mass spectrometer was used to measure the water vapor mass fraction in the vacuum stages of the vacuum drying process.

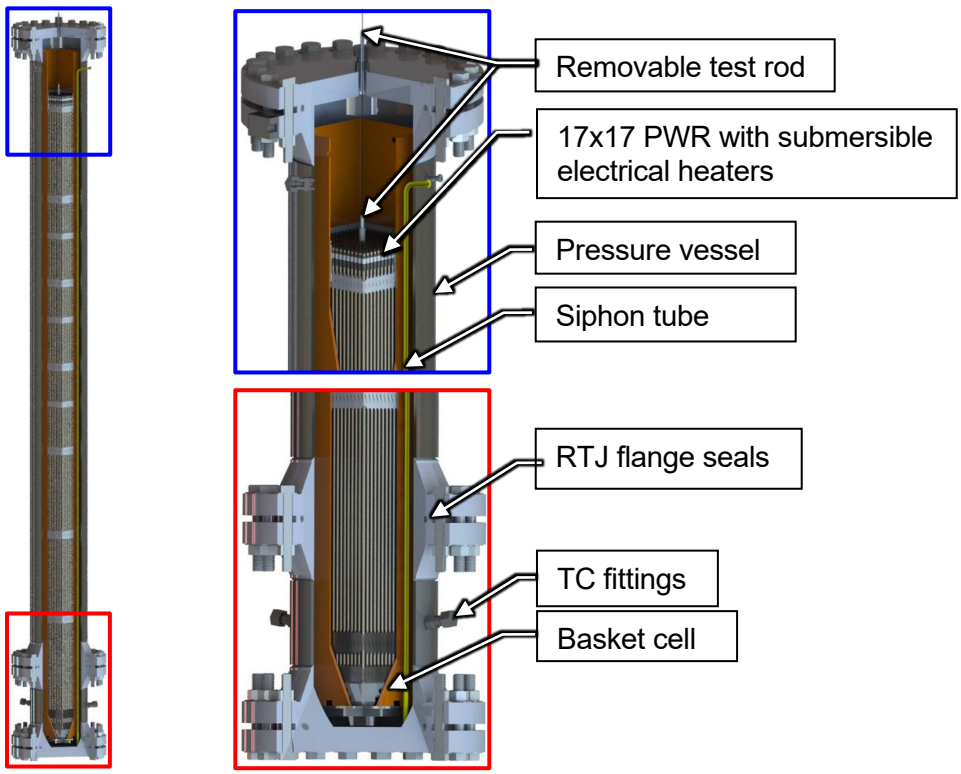


Figure 1-1 Major Components of the ADCS

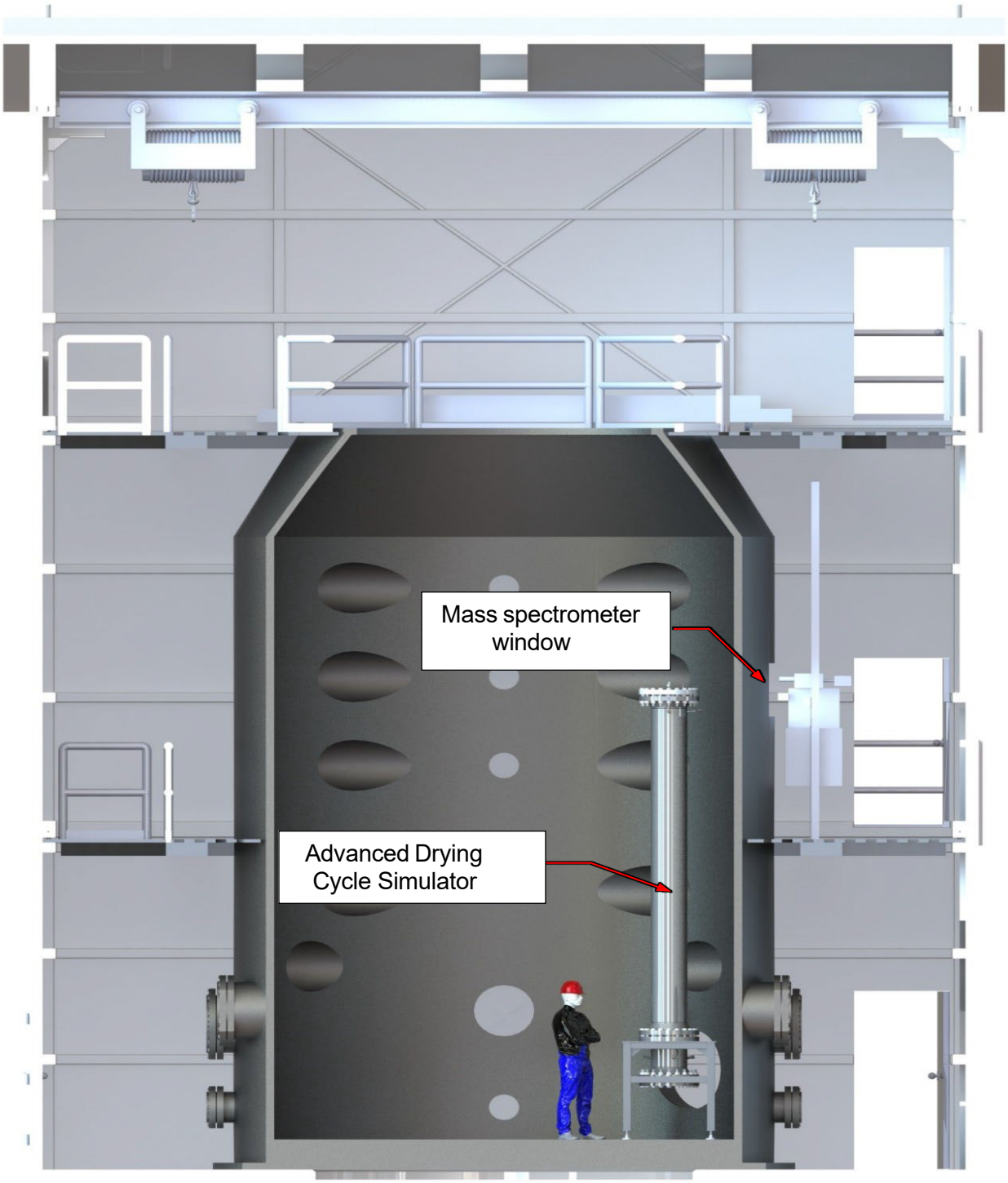


Figure 1-2 The ADCS Inside the CYBL Facility

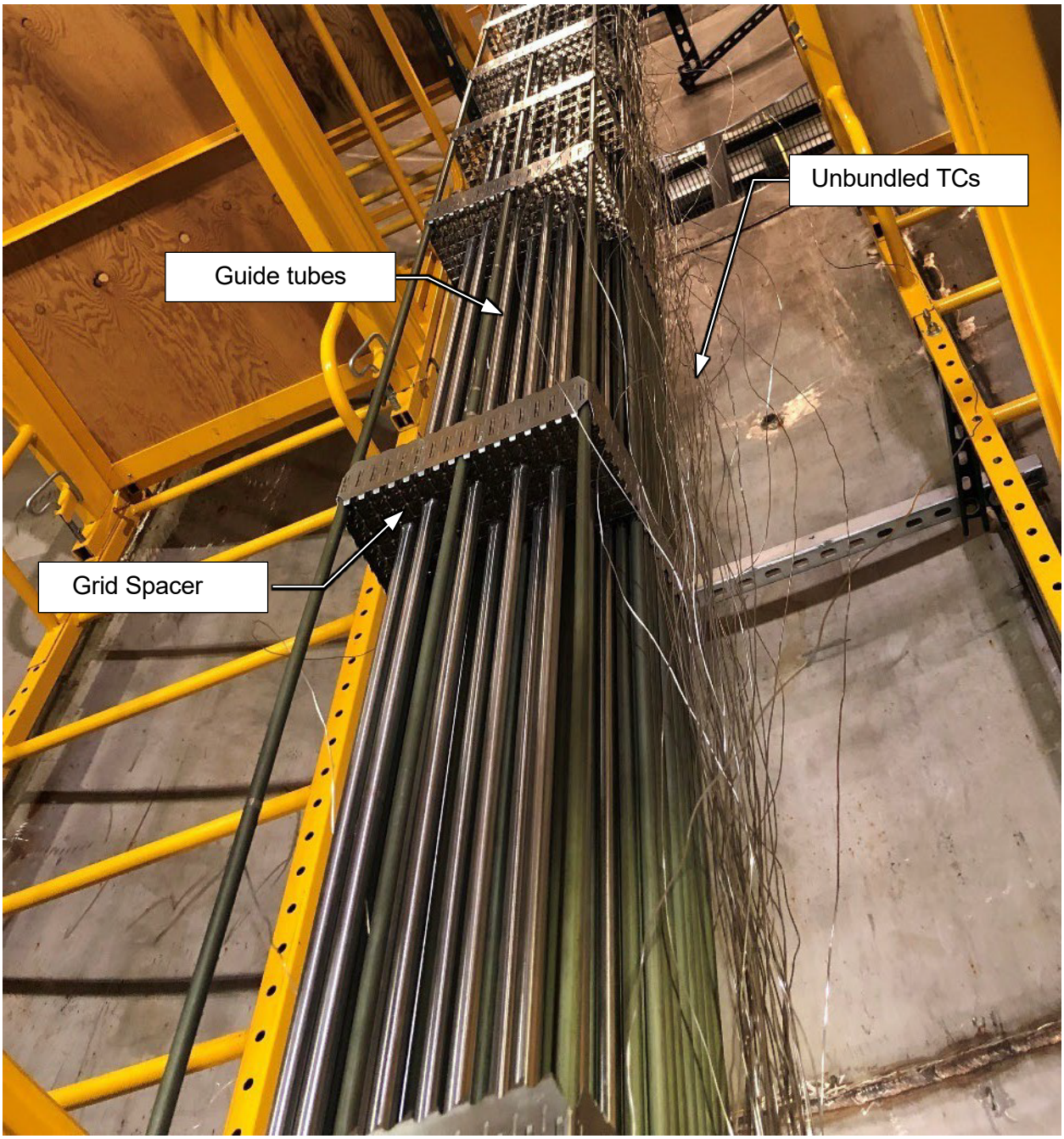


Figure 1-3 Photo of the 17x17 PWR Skeleton Taken During TC Installation

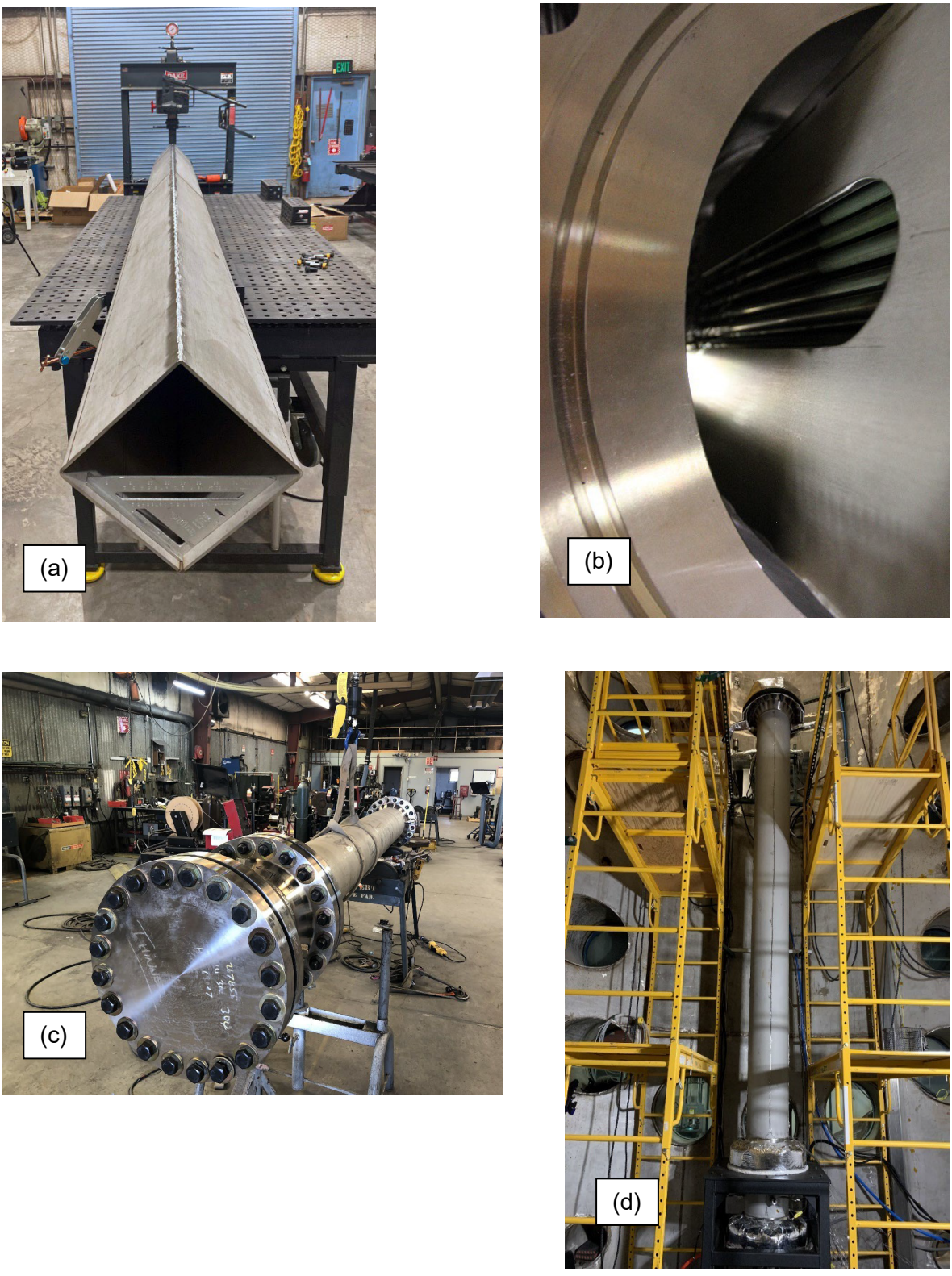


Figure 1-4 **Photos of (a) Basket, (b) a Mouse Hole Cut in the Bottom of the Assembly Basket, (c) the ADCS Pressure Vessel with Uninsulated and Non-Heat-Traced Flanges, and (d) ADCS Pressure Vessel with Insulated and Heat-traced flanges**

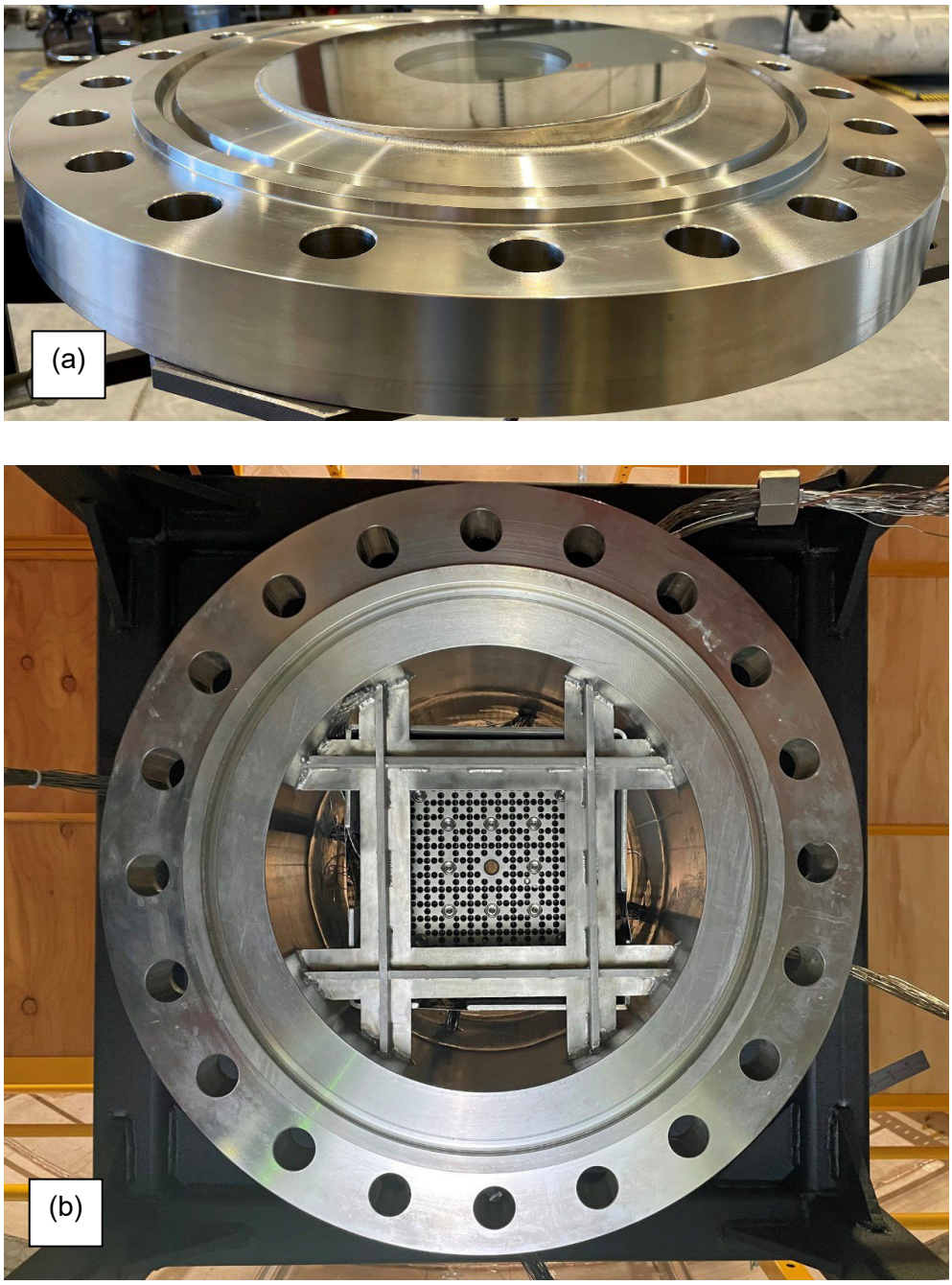


Figure 1-5 **(a) Sight Glass in the Bottom Flange of the ADCS and (b) View from Below the Lower Pressure Vessel with the Bottom Flange Removed, Showing the Standoff, Support, Assembly, and Basket Inside the ADCS**

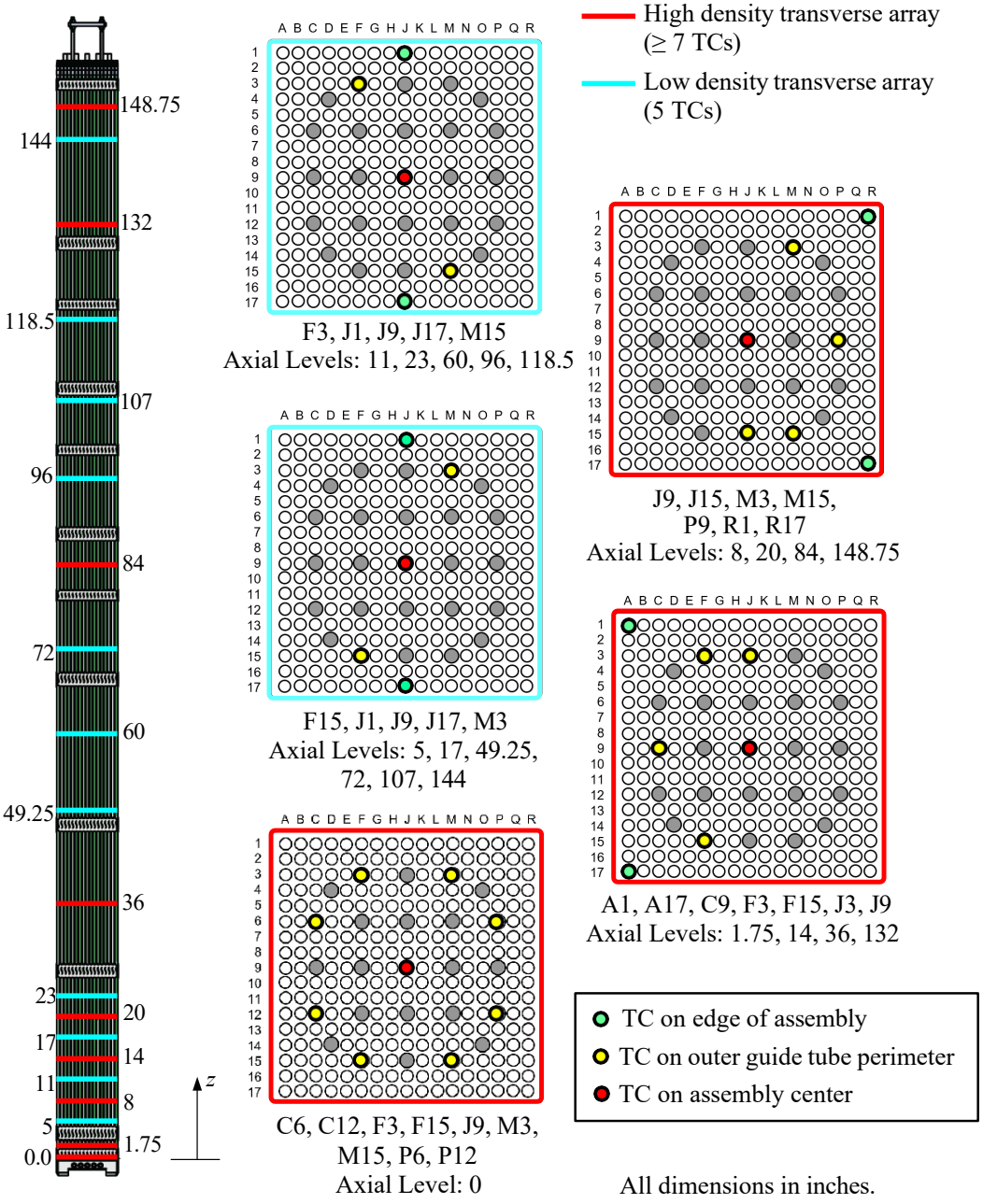


Figure 1-6 Diagram of Heater Assembly TC Locations

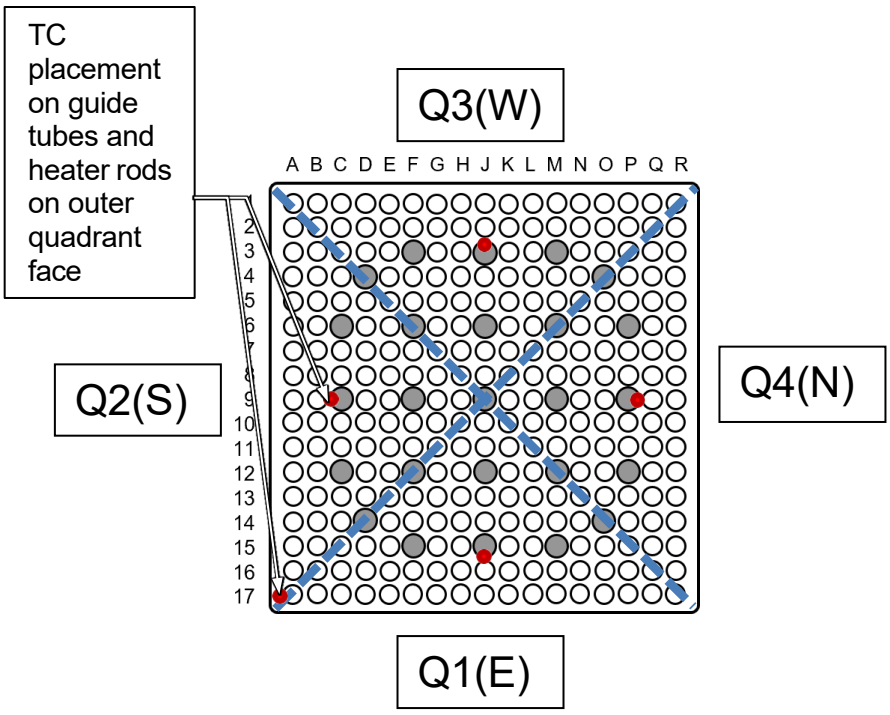


Figure 1-7 Visualization of Heater Assembly Quadrants and TC Placement on Guide Tubes and Heater Rods

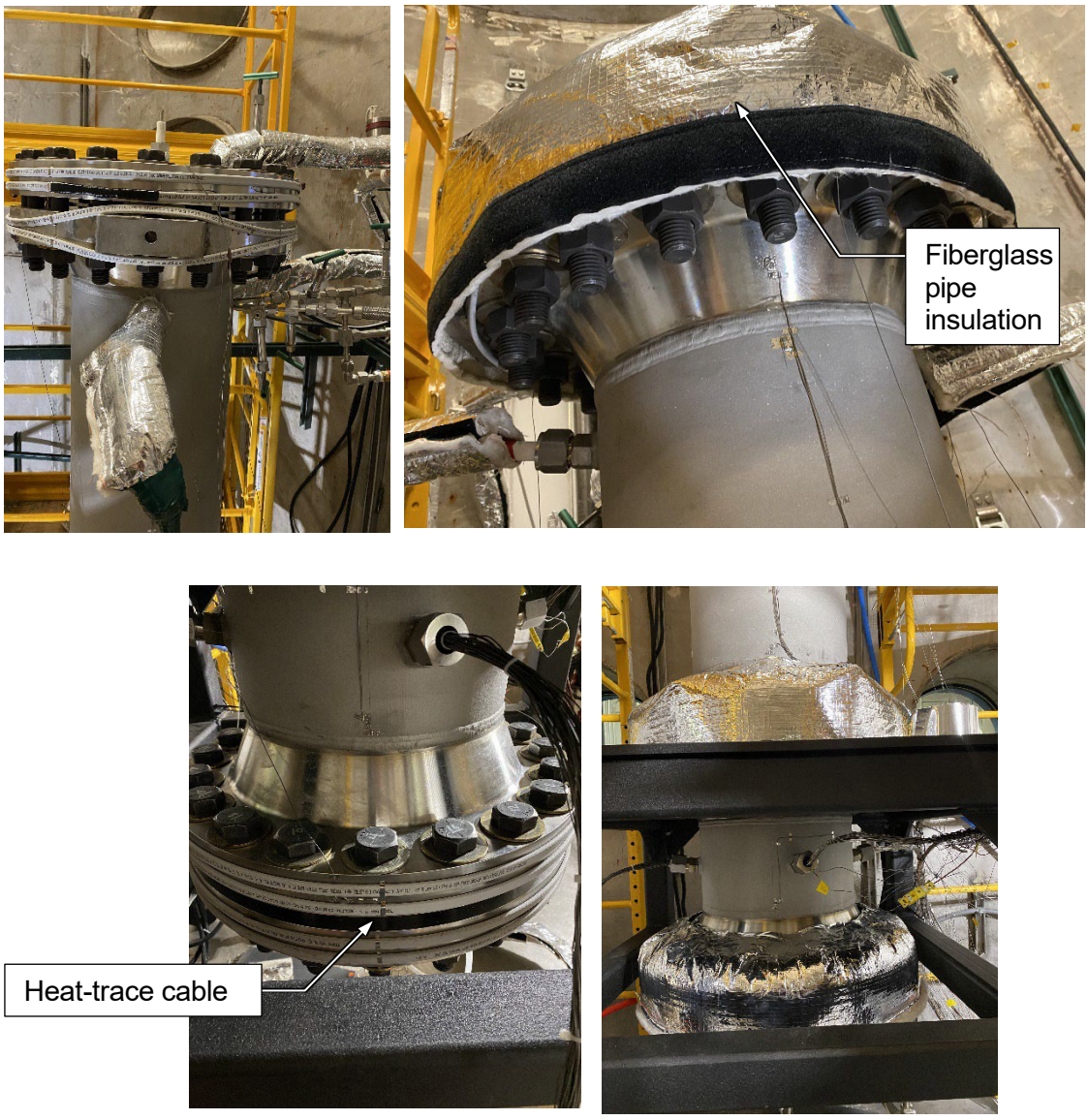


Figure 1-8 Heat-Trace Cables and Fiberglass Pipe Insulation on Top and Bottom Flanges

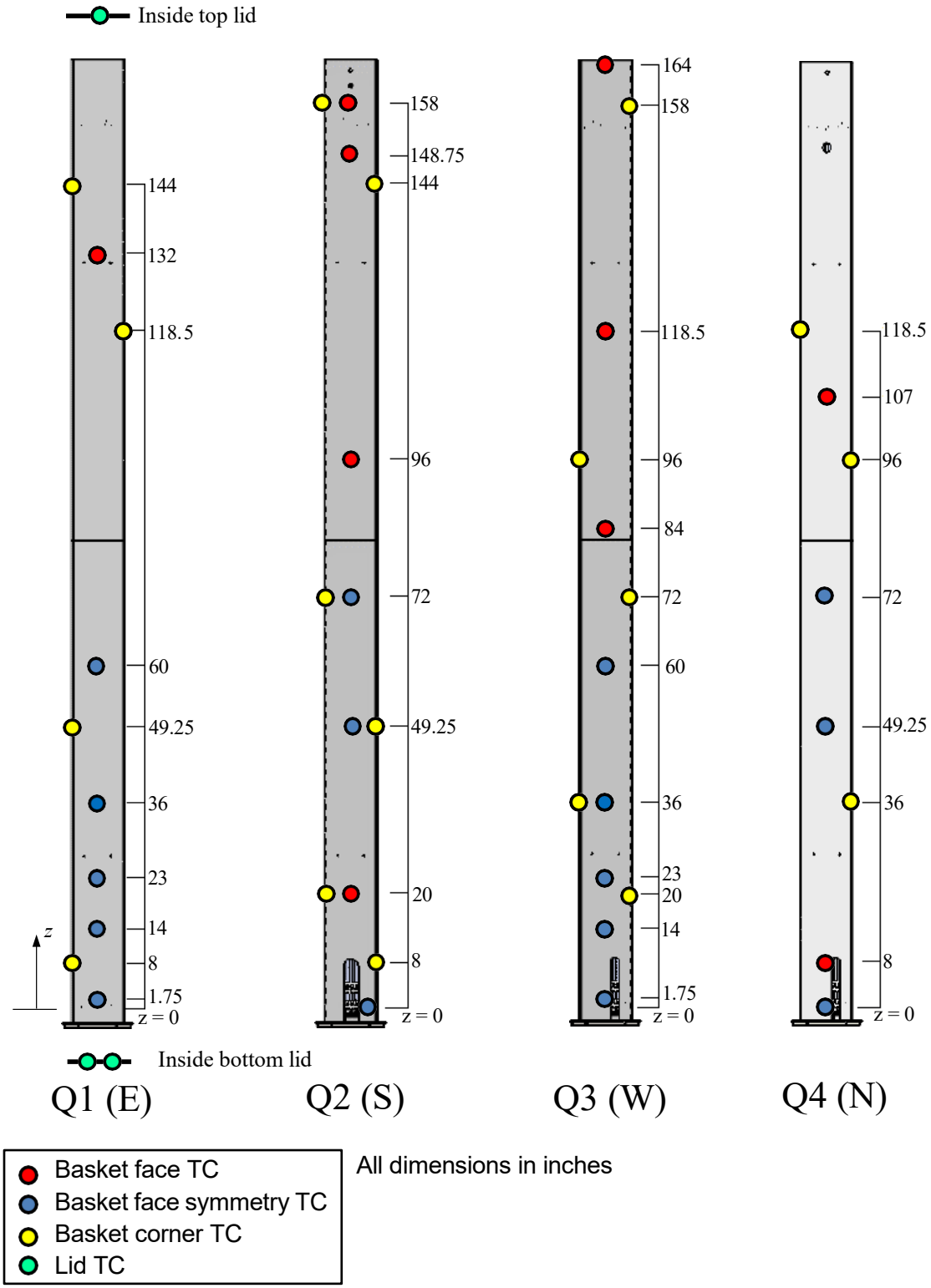
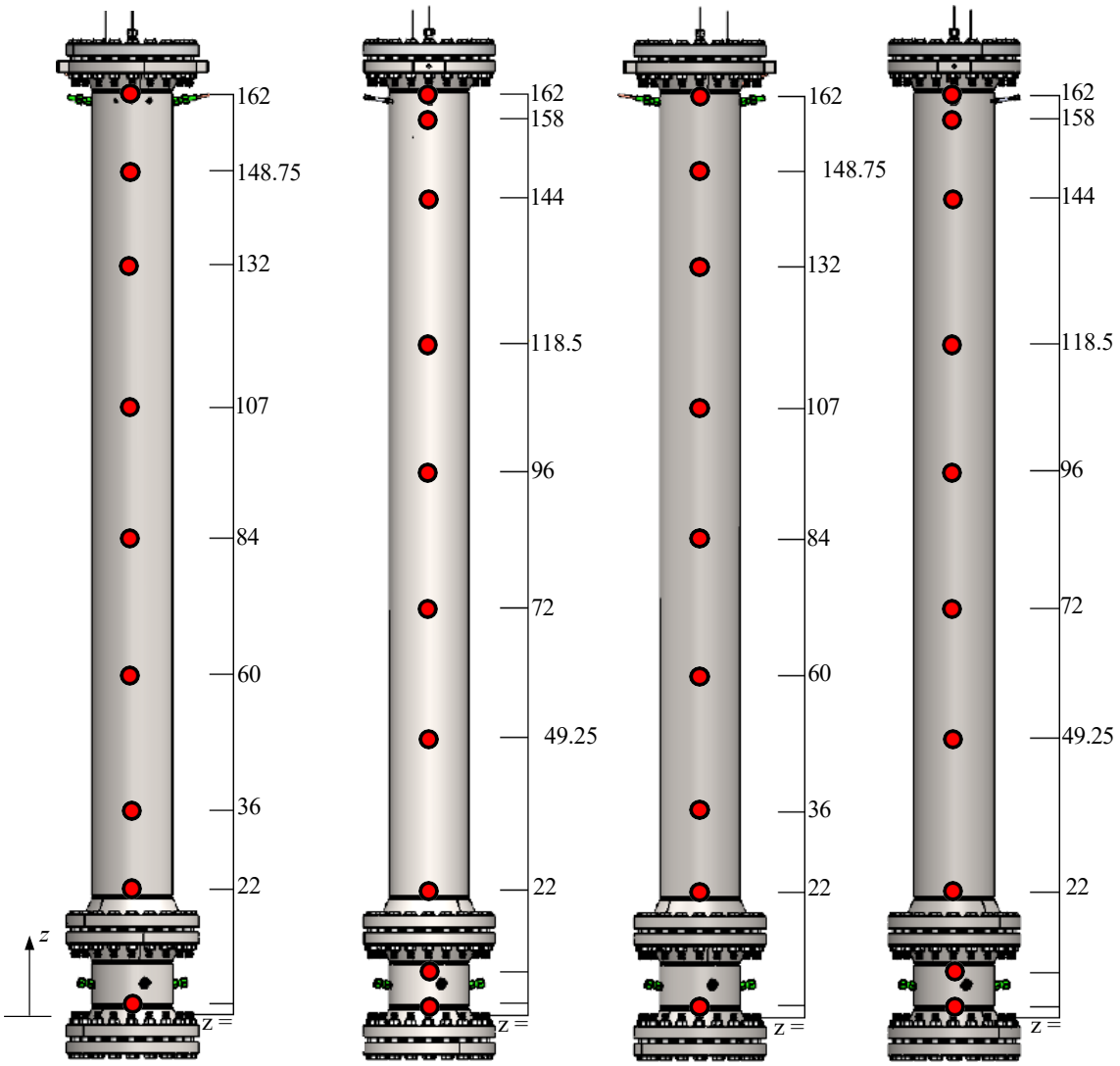


Figure 1-9 Diagram of Basket TC Locations



All dimensions in inches

Figure 1-10 Diagram of ADCS Pressure Vessel TC Locations

1.2.1 Test Plan

The cask was tested indoors in the CYBL test facility at SNL. Multiple dry steady-state tests modeled the normal dry cask storage, covering helium fill pressures from 0.1 Torr to 12 bar and decay heats of 1 kW, 2 kW, and 3 kW. The steady-state tests used two types of BCs on the flanges. In one, the flanges' vertical surfaces were kept isothermal using heat-trace cable and fiberglass pipe insulation, as shown in Figure 1-8. In the second, the boundaries of the flanges were kept uninsulated, without any heat supplied, and allowed to exchange heat with the surroundings, as shown in Figure 1-4(c). To model vacuum drying operation of dry casks, five wet transient tests were performed. SNL reports SAND2022-12078R, SAND2023-01454R, SAND2023-09746R, and SAND2024 give details on the ADCS experiment.

The steady-state tests consisted of a “thermal soak” in which the cask was allowed to reach steady-state temperatures over a period of time. The steady state was considered reached when the first derivatives of all TCs’ temperature measurements were less than or equal to 0.3 Kelvin (K) per hour (hr). Once steady state was reached, transverse and axial temperature profiles in the fuel region, basket, and pressure vessel were recorded. PGTT was measured for a wide range of input heating levels and canister pressures using backfills of helium.

The vacuum drying wet testing experiment consisted of five transient tests, with each test conducted over multiple days. Due to the large material density and volume of the top and bottom flanges, which are required parts due to the seals formed at the flange gaskets, the flanges serve as large heat sinks. To compensate for this effect, which would not normally be present on a welded canister lid, the first four tests used heat-trace cable and fiberglass pipe insulation on all three flanges to maintain a constant temperature. The fifth test did not use heat-trace cables or insulation; rather, the flanges’ external boundaries exchanged heat through convection and radiation to the surrounding. The fifth test is used in this report to verify and validate the developed CFD method. The transient steps in this fifth test are shown in Table ES-1. The first process involved bulk water fill to a level of 3.35 meters (m), measured from the top of the bottom nozzle of the assembly. Air occupied the canister volume above the liquid water. Then, heat was supplied to the PWR 17x17 fuel assembly. After a hold period, bulk water drain was initiated, followed by multiple helium blowdowns and then a hold at 109 kPa. Multiple vacuum steps then occurred, during which pressure was reduced and briefly held at the “Vacuum #” pressures indicated in Table ES-1. Once at minimum pressure, the 30-minute regulatory hold took place, beginning 6.6 hours after the 109 kPa pre-vacuum hold ended. Following the regulatory hold, the canister was backfilled with helium, one additional vacuum was pulled, and then the canister was backfilled with helium and allowed to approach steady state.

This report contains several ways to apply CFD to model transient vacuum drying processes, shown in Table ES-1. The transient analysis started when the heat was supplied in the water fill hold-time. The CFD model in the water fill hold-time period used one of two choices: (1) using Volume of Fluid (VOF) multiphase flow method as described in Ansys Fluent and (2) using single-phase CFD modeling with a physical thin wall separating the liquid water and air. In the VOF model, the interface between the liquid water and air phases was modeled without any wall between them. All the vacuum drying steps after the water fill hold-time used single-phase CFD modeling to predict the thermal behavior of the cask, as shown in Table ES-1. The running fluid and conditions in Table ES-1 are the best estimate conditions and assumptions that were obtained from the ADCS experiment. Other sensitivity calculations were performed using different running fluids in the transient steps, using either single-component running fluids such as helium, water vapor, or a combination of the two.

These sensitivities, including applicants’ preferred assumptions, were used to assess the conservatism of each method compared to the base case that used the best estimate assumptions. Some applicants completely ignore the water fill step while performing CFD for the vacuum drying steps. Instead, they start their CFD predictions after the bulk water drain, using helium as the running fluid initialized at the saturation temperature of the water vapor with the pressure existing at the drain/blowdown step. After draining, blowdown, and the hold-time before vacuum, water vapor is used as the running fluid until the backfill, when helium is used again.

The sensitivity runs are discussed in the results section.

Data collected at six pressure levels between 0.1 Torr and 12 bar were used to validate the steady-state cases. The power levels tested were 1.0 kW, 2.0 kW, and 3.0 kW. The vessel

pressures tested were 0.1 Torr, 1 Torr, 10 Torr, 25 Torr, 1 atm, and 1,200 kPa (12 bar). For the steady-state tests, two types of BCs were used. The first type involved using heat-trace cables and insulation around the flanges, as shown in Figure 1-8, to obtain isothermal conditions in the range of 55°C to 65°C. The second type did not use heat trance cables or insulation, leaving the flange external surfaces to freely exchange heat with the surroundings through radiation and convection.

To avoid the uncertainty introduced by the type 1 BCs, this report uses only the data from steady-state tests with type 2 BCs to validate the CFD method. Also, for validation of the steady-state cases, only the 3.0 kW heat source is used. For the transient vacuum drying case, five tests were conducted with varied power and pressure values. Four tests used the type 1 isothermal BCs on the flange and variable heater power, while the fifth test used type 2 BCs and a constant heater power of 1.483 kW. Similarly to the steady-state case, to avoid the uncertainty in the type 1 BCs, only the fifth test was used for validation. Table ES-1 provides the conditions for the transient vacuum drying case used in the validation.

1.3 Uncertainty Quantification

UQ was performed for the analyzed cases using the techniques outlined in ASME V&V 20-2009, which establishes steps to assess the degree of accuracy of computational simulations. The method's accuracy is obtained by comparing the experimental and simulation values of a local or global variable. From the validation process provided in ASME V&V 20-2009, the criteria for a CFD-grade experiment can be established. A CFD-grade experiment should be able to validate a CFD model by minimizing the validation uncertainty on some selected figures of merit variable. Interim Staff Guidance (ISG)-11, "Cladding Considerations for the Transportation and Storage of Spent Fuel", used PCT as a criterion to assess the safety of a dry cask; therefore, this report also adopts it as the figure of merit (i.e., the target variable) to assess the validation uncertainty. In turn, the validation uncertainty will be used to determine whether the experiment qualifies as CFD grade.

The derivations and text below are taken from ASME V&V 20-2009; NUREG-2238, "Validation of a Computational Fluid Dynamics Method Using Vertical Dry Cask Simulator Data"; and Bestion et al., 2019.

As found in NUREG-2238—

> The validation comparison error E in any validation process is defined as the difference between the solution denoted by S, and the experimental data denoted by D:
>
> $$E = S - D$$
>
> If T represents the true solution, then the errors in the solution and experiment are:
>
> $$\delta_S = S - T$$
>
> $$\delta_D = D - T$$
>
> Then E can be written as:
>
> $$E = (S - T) - (D - T) = \delta_S - \delta_D$$

The simulation error $\boldsymbol{\delta_S}$ consists of three categories, including the modeling error $\boldsymbol{\delta_{model}}$ due to physical modeling input, with approximations and assumptions; the numerical solution error $\boldsymbol{\delta_{num}}$ stemming from the numerical algorithm and the discrete mesh used to solve the partial differential equations; and the input data errors δ_{input} resulting from the simulation input parameters (e.g., initial and boundary conditions, properties). E is thus the overall result of all the errors coming from the experimental data and the simulation.

$$\mathrm{E} = \delta_{\mathrm{model}} + \delta_{\mathrm{input}} + \delta_{\mathrm{num}} - \delta_{\mathrm{D}}$$

The unknown error $\boldsymbol{\delta_{model}}$ produced by the modeling is isolated:

$$\delta_{\mathrm{model}} = \mathrm{E} - (\delta_{\mathrm{input}} + \delta_{\mathrm{num}} - \delta_{\mathrm{D}})$$

The corresponding standard uncertainties for the input, numerical, and experimental errors are $\boldsymbol{u_{input}}$, $\boldsymbol{u_{num}}$ and $\boldsymbol{u_D}$.

The validation standard deviation of the combination error $\boldsymbol{\delta_{input}} + \boldsymbol{\delta_{num}} - \boldsymbol{\delta_D}$ is denoted as $\boldsymbol{u_{val}}$ and if the three errors are mutually independent then:

$$\mathrm{u_{val}} = \sqrt{\mathrm{u_{input}^2} + \mathrm{u_{num}^2} + \mathrm{u_D^2}}$$

$$\delta_{\mathrm{model}} = \mathrm{E} \pm \mathrm{u_{val}}$$

If also $\boldsymbol{\delta_{model}}$ is considered independent, then:

$$\mathrm{u_E} = \sqrt{\mathrm{u_{model}^2} + \mathrm{u_{input}^2} + \mathrm{u_{num}^2} + \mathrm{u_D^2}}$$

The ASME standard gives solutions to evaluate every term of the comparison error (E) and the validation uncertainty ($\boldsymbol{u_{val}}$). The validation comparison error E sign and its magnitude are known once the validation comparison is made. The validation uncertainty can be estimated through the determination of the simulation uncertainty $\boldsymbol{u_{simulation}}$ and the experimental uncertainty $\boldsymbol{u_D}$. The simulation uncertainty consists of the numerical simulation uncertainty u_{num} and the input uncertainty $\boldsymbol{u_{input}}$. However, there is no established method to estimate the physical modeling uncertainty $\boldsymbol{u_{model}}$.

Propagation methods are mainly used to evaluate code result uncertainties coming from input parameters. Uncertainties of numerical solutions are given by the solution verification step or grid convergence index (GCI) method based on the Richardson extrapolation method. The standard indicates how to use the E and $\boldsymbol{u_{val}}$. These quantities give the accuracy of the model used through:

$$\mathrm{u_{model}} = \sqrt{\mathrm{u_E^2} - \mathrm{u_{val}^2}}$$

From these equations, the following criteria can be concluded:

- If $|\mathbf{E}| >> \boldsymbol{u_{val}}$, $\boldsymbol{u_{model}} \cong \boldsymbol{u_E}$, then u_{val} is relatively small and the modeling error is larger than the validation uncertainty. In this case, the comparison between the code

predictions and the experimental data can provide useful and precise information on the quality of the physical model. Consequently, the model can be improved or calibrated using the data from the experiment to achieve less uncertainty for the result.

- If $|\mathbf{E}| < \mathbf{u_{val}}$, the larger validation uncertainty implies that the model accuracy cannot be improved if the combination δ_{input}, δ_{num}, and δ_D cannot be reduced. In this case, the standard indicates that this does not prove that the model is of good or bad quality, but this kind of experiment will not be useful in improving the model.

- If $|\mathbf{E}| = \mathbf{u_{val}}$, the modeling error is within the noise level imposed by the input, numerical, and experimental uncertainties, and the possibility of model improvement is a challenge.

- If model uncertainty u_{model} is known or expected, then sensitivity analyses on sensitive modeling parameters can investigate the impact this model uncertainty can have on target variables such as PCT and $\mathbf{u_{val}}$.

  – If $\mathbf{u_{model}} < \mathbf{u_{val}}$, the experiment is not very informative.

  – If $\mathbf{u_{model}} > \mathbf{u_{val}}$, the experiment can show whether the expected model uncertainty is reached.

1.3.1 Computational Fluid Dynamics-Grade Experiment

A CFD-grade experiment is one that can be used to validate the physical model at a high fidelity. This means that the experiment provides a relatively low uncertainty of validation $\mathbf{u_{val}}$ and allows a good determination of the model uncertainty $\mathbf{u_{model}}$. Therefore, an experiment that minimizes both $\boldsymbol{\delta_{input}}$ and $\boldsymbol{\delta_D}$ also minimizes $\mathbf{u_{val}}$ and provides more information on the accuracy of the physical model. In parallel, the CFD user or specialist should strive to minimize the numerical error $\mathbf{u_{num}}$, or at least follow well-established methods to quantify it correctly.

However, the capability of an experiment to provide information on the uncertainty of model parameters may not be the concern of a dry cask safety analysis. The final goal is often to compare a parameter of interest, such as PCT, to a safety criterion to assess whether the dry cask is safe in the situation for which it is designed. Very often, and due to the lack of geometrical details inside the cask—as in the case of fluid gaps as described in the cask demonstration in NUREG/CR-7260—it is much more difficult to know all of the necessary boundary and initial conditions and flow field variables in the region of interest with low uncertainty or high confidence. As a result, $\mathbf{u_{input}}$ may be large. Such experiments should at least provide enough information to quantify the accuracy of CFD code predictions for the relevant parameters of interest in the safety analysis, such as some local temperatures or PCTs. In turn, this accuracy quantification can assess whether a reliable conclusion for the safety case can be made. The experiment should target a predetermined code uncertainty for the selected target variable, such as PCT, PCT location, or other variables. Thus, instead of providing data to allow for quantification of the uncertainty on some specific model parameters, the goal is the prediction of the uncertainty on the target variable of interest. This uncertainty is the result of the propagation of various sources of uncertainty from $\boldsymbol{\delta_{input}}$, $\boldsymbol{\delta_{num}}$, and $\boldsymbol{\delta_D}$. As such, minimizing these sources of error remains the objective of the V&V and UQ process.

Another important requirement is the collaboration between the experiment designer and the code user from the start of the experimental project. The collaboration should target the models in the dry cask application, as shown in NUREG-2152. Code users and safety analysts can then

reveal the goal of the experiment, in terms of model validation. Among the modeling goals that can be targeted and investigated are the turbulence model that best predicts the flow field, state laws for the fluid of interest, or porous media parameters if a porous media model is used. A list of modeling challenges, including BCs for dry cask applications, appears in NUREG-2152 and NUREG-2208, "Validation of Computational Fluid Dynamics Methods Using Prototypic Light Water Reactor Spent Fuel Assembly Thermal-Hydraulic Data". In this important initial step, CFD code users can perform pre-calculations to help define the mockup in terms of geometrical design, range of flow variables, choice of BCs, and scaling analyses. This collaboration can also be used to define the plan of the experiment. A CFD-grade experiment should first be characterized by an exchange between experimentalists and code users from the beginning of the design of the experiment to the end of the project.

The preliminary specification of fluid and solid volumes of interest and of inlet and outlet fluid surfaces is of prime importance in selecting where initial and boundary conditions must be known. A CFD-grade experiment should specify the BCs, initial conditions, and model domain in a way that they can be used as simulation input data with the required accuracy.

A general requirement may be to define a priori acceptance criteria before designing an experiment. If the only objective is to validate a CFD code on a specific flow configuration, then the acceptance criterion may be to minimize the validation uncertainty (i.e., experimental, numerical, and input uncertainties) on a specific target variable. In dry cask applications, examples may be the following:

- If the objective is to validate a CFD code for PCT, then the acceptance criterion may be that the validation uncertainty related to this PCT should not exceed a given value.

- If the objective is to predict the canister wall heat transfer in a ventilated cask, then the acceptance criterion may be that the validation uncertainty related to a predetermined temperature difference ΔT between the air inlet and outlet should not exceed a given value.

- If the objective is to predict the mass flow rate in a cask, then the acceptance criterion may be that the validation uncertainty related to a measured mass flow rate in a flow passage should not exceed a given value.

In the last few years, dry cask applicants requested licenses for cask designs with total decay heats close to 70 kW or higher. The analyses accompanying these applications presented CFD thermal analysis cases with PCT very close to the ISG-11 allowable limit of 400°C (752°F), with margins as small as 10–20°C. In this validation exercise, the calculated validation uncertainty $\mathbf{u_{val}}$ is compared to these margins to determine whether the experiment can be classified as CFD grade.

2 COMPUTATIONAL FLUID DYNAMICS MODEL

This section summarizes the different model choices, solver settings, and thermophysical properties used in the ADCS analysis.

2.1 ADCS Computational Fluid Dynamics Model

A one-eighth symmetry, three-dimensional (3D) CFD model of the ADCS apparatus was created with two symmetry planes—one on the vertical, longitudinal axis of the fuel bundle assembly and another parallel to the first but rotated 45 degrees about the vertical axis. Two 3D solid models were created. The first used an explicit representation of all the components of the assembly geometry (i.e., fuel rods, guide tubes, and grid spacers) without any simplifications, as shown in Figure 2-1(a), Figure 2-2(a), and Figure 2-3. The second model, which was the base case model in this validation, used porous media to represent the components inside the assembly; all of the components inside the assembly (i.e., fuel rods, guide tubes, and grid spacers) were substituted with a porous volume with an equivalent flow resistance coefficient (i.e., viscous and inertial) and an equivalent thermal conductivity coefficient, as shown in Figure 2-1(b) and Figure 2-2(b).

The second model was used as the base case because it is the dry cask applicants' preferred choice, as it is easy to create the model geometry and mesh. Additionally, the porous model requires less effort and computational time to run and is thus less expensive. The BCs and model inputs used in the CFD model were representative of those present during the experiment, as documented in the ADCS test description (SAND2023-01454R and SAND2023-09764R).

Ansys Fluent versions 23 and 24 were used to create a 3D CFD thermal model (illustrated in Figure 2-1, Figure 2-2, and Figure 2-3) to simulate the thermal response of the ADCS. The model's geometry and mesh were created using Gambit version 2.4.6. CFD guidelines in NUREG-2152 were followed to create the ADCS thermal model. Both the porous and explicit geometry models used one-eighth symmetry BCs to reduce case creation effort and computational expense. These models did not include the inside of the CYBL facility. Convective and radiative heat transfer BCs were applied at the external walls of the pressure vessel. A quiescent environment was assumed for the surroundings to model the heat transfer outside the cask. Although the CFD models were one-eighth symmetric, as shown in Figure 2-2 and Figure 2-3, Figure 2-1 shows half-symmetry representations of the explicit-geometry and porous media geometry models.

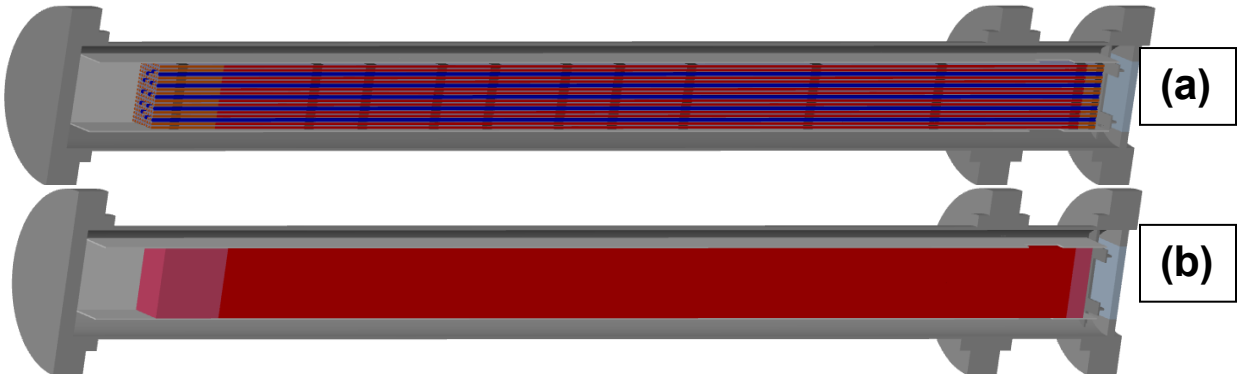


Figure 2-1 Half-Symmetry CFD Models for (a) the Explicit-Geometry Model (b) the Porous Media Model

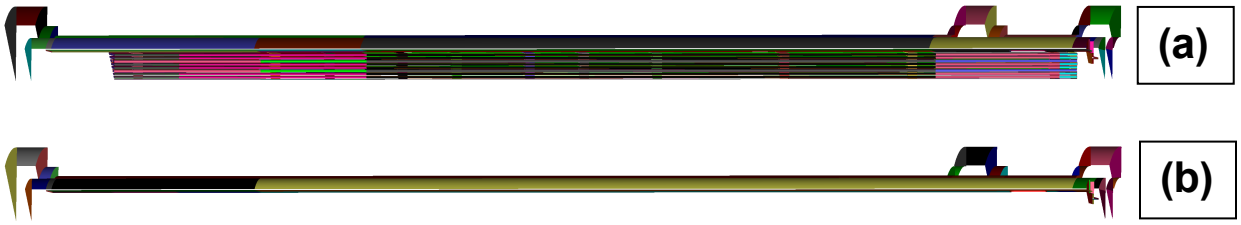


Figure 2-2 Surfaces Outlining the One-Eighth Symmetry CFD Models for (a) the Explicit-Geometry Model (b) the Porous Media Model

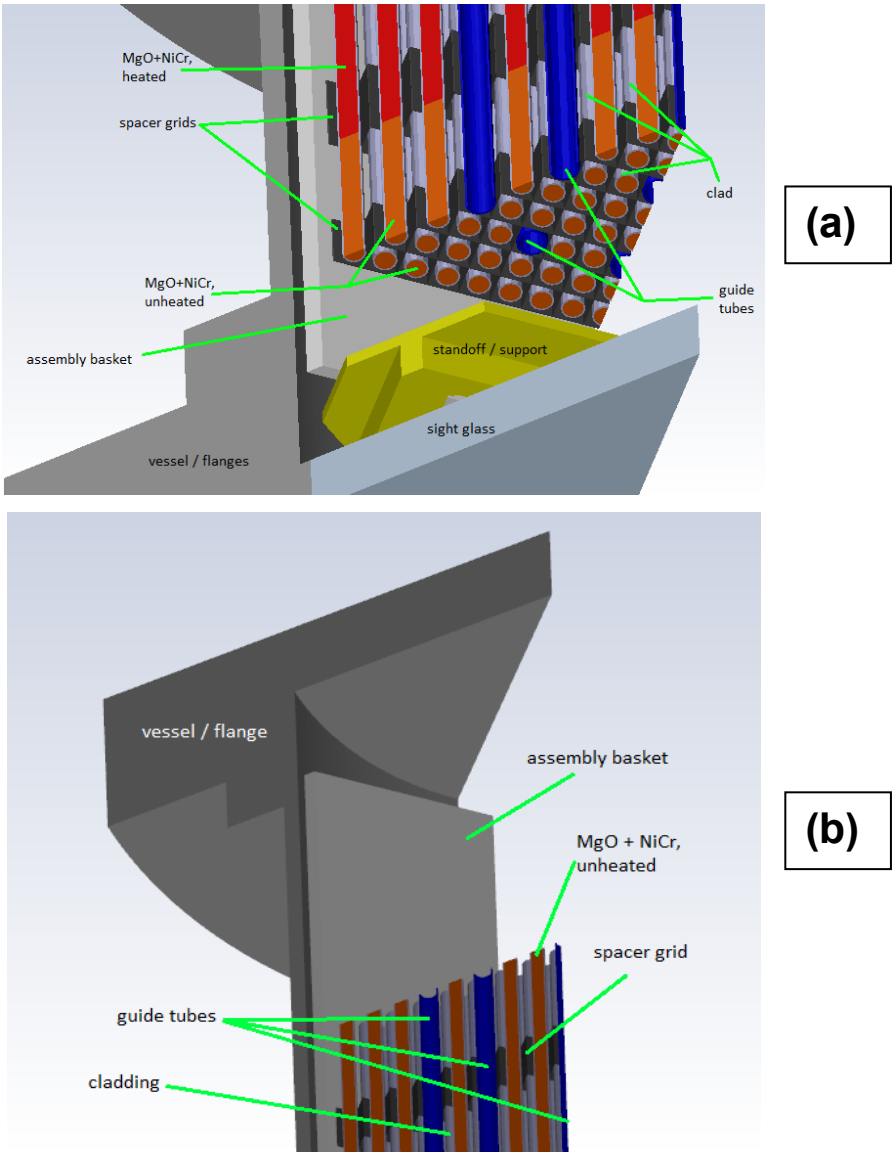


Figure 2-3 One-Eighth Symmetry Explicit-Geometry CFD Model for (a) Bottom of the Model Geometry (b) Top of the Model Geometry

2.2 Models, Geometry, Mesh, Solver Settings, and Boundary Conditions

The commercially available, finite-volume-based CFD code Ansys Fluent versions 23 and 24 were used to simulate the 3D heat and flow patterns within the ADCS. Gambit version 2.4.6 was used to generate geometry and create the mesh.

In accordance with CFD best practice guidelines (NUREG-2152), when the geometry and mesh for the explicit geometry and porous media models were generated, preference was given to the hex mesh type. In a few places, however, the wedge mesh type was used in both models to control the mesh skewness. According to NUREG-2152, a skewed mesh will lead to convergence issues in the solution of the conservation equations. The laminar regime (i.e., no turbulence model) was used to model flow in the canister because the flow Reynolds number and Raleigh number were both low, indicating that a laminar flow regime existed inside the canister used in the experiment. CFD best practice guidelines in NUREG-2152 were used for the mesh expansion ratio and mesh skewness.

As explained in section 2.1, two models were created. The first model involved the explicit representation of all of the components in the assembly geometry (i.e., fuel rods, guide tubes, and grid spacers) without any geometry simplifications, as shown in Figure 2-1(a), Figure 2-2(a), and Figure 2-3. The second model, which was the base case model in this validation, used porous media to represent the components inside the assembly; that is, all components inside the assembly were substituted with a porous volume with an equivalent flow resistance coefficient (i.e., viscous and inertial) and an equivalent thermal conductivity coefficient as shown in Figure 2-1(b) and Figure 2-2(b). The second model was chosen as the base case because it is the method preferred by dry cask applicants. The BCs and model inputs used in the CFD model were representative of those present during the experiment, as documented in the ADCS test description in SAND2023-01454R and SAND2023-09746R.

Figure 2-4, Figure 2-5, Figure 2-6, and Figure 2-7 show the meshes used for the porous and explicit geometry CFD models. Because the explicit geometry included fuel rods, guide tubes, and grid spacers, it was more complicated to create a high-quality conformal mesh. To deal with this task in the pre-processor (Gambit) the geometry was divided into three parts longitudinally, with geometrical interfaces created to connect the three parts in Ansys Fluent. For a conformal mesh, the interfaces perfectly match the nodes and element edges between the three sections of the geometry—requiring precise alignment to ensure the continuity of the mesh. The quality of the mesh was examined using the mesh skewness and aspect ratio metrics in Gambit. The porous mesh—which lacks fuel rods, guide tubes, and grid spacers—was easy to generate.

Applicants prefer the porous media model because it is easier to build and computationally less expensive than a model where all dry cask components are represented explicitly. Thus, for this report, the porous media model was used for VVUQ of the CFD model for both the steady-state dry cases mimicking the normal storage operation and the transient wet case modeling the vacuum drying process. The VVUQ of the porous model involved three mesh sizes to compute the numerical uncertainty using the GCI, as described in section 3.1.2 of this document. Figure 2-7 shows a sample of the surface mesh on the stand-off, basket, guide tubes, fuel rods, and pressure vessel for the baseline simulation. Figure 2-8 shows a cross-sectional view of the baseline mesh, along with temperature contours at the axial locations z = 0.91 m and z = 3.66 m for both the porous media CFD model and the explicit geometry CFD model.

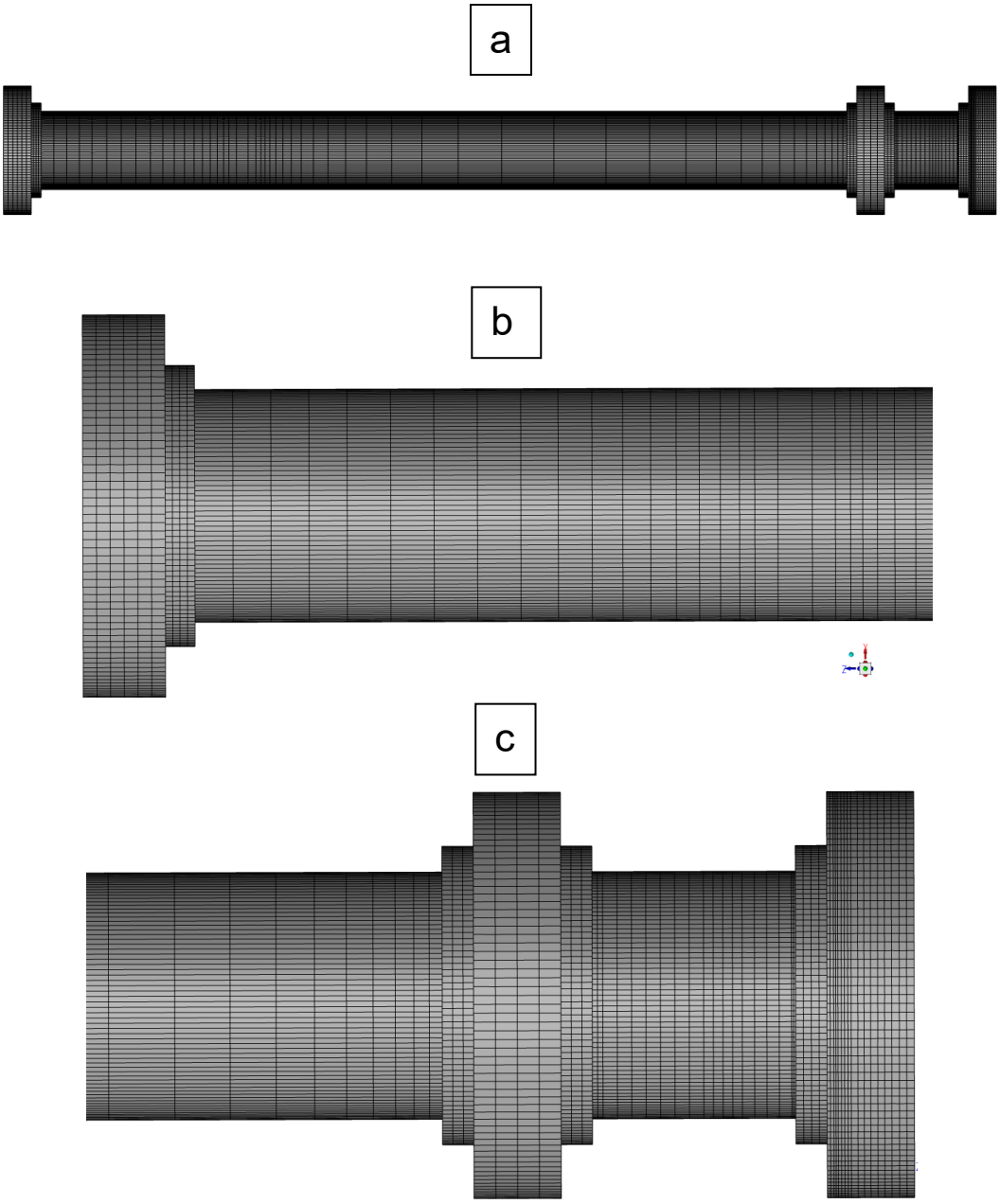


Figure 2-4 Porous Geometry Model Mesh (Outside Pressure Vessel View): (a) Full, (b) Top, and (c) Bottom

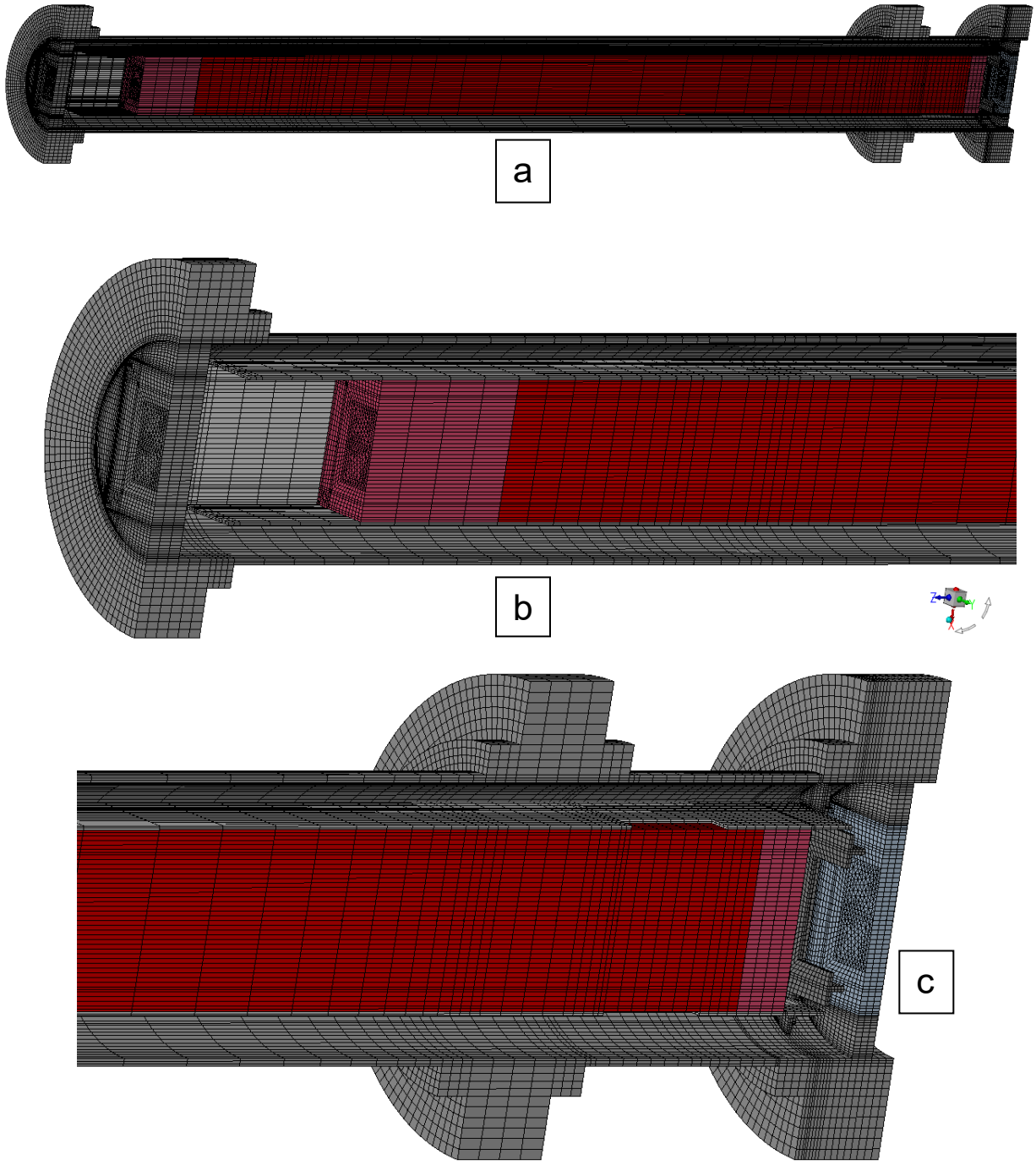


Figure 2-5 Porous Geometry Model Mesh (Fuel Side View): (a) Full, (b) Top, and (c) Bottom

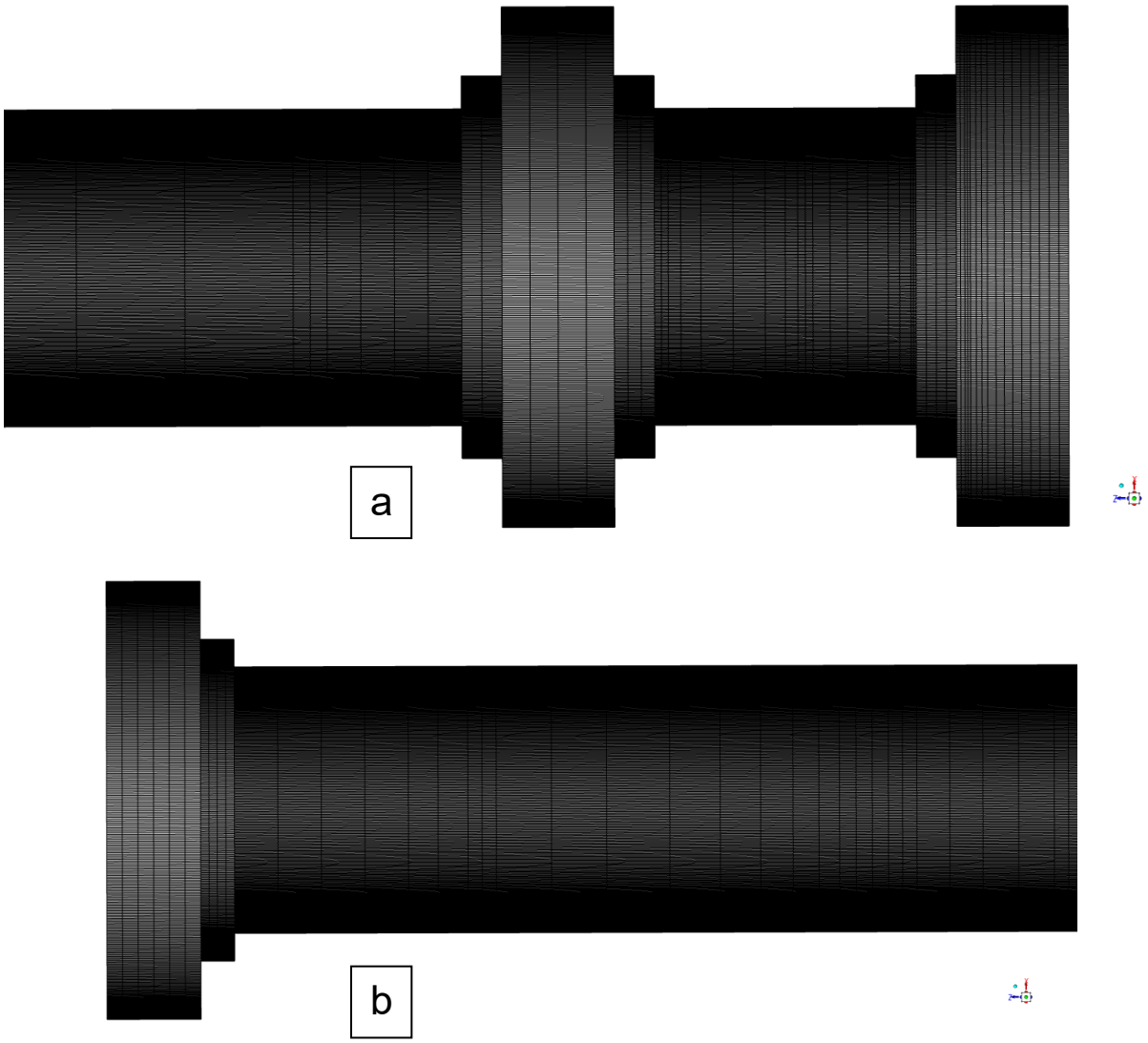


Figure 2-6 Explicit Geometry Model Mesh (Pressure Vessel Side View): (a) Bottom, (b) Top

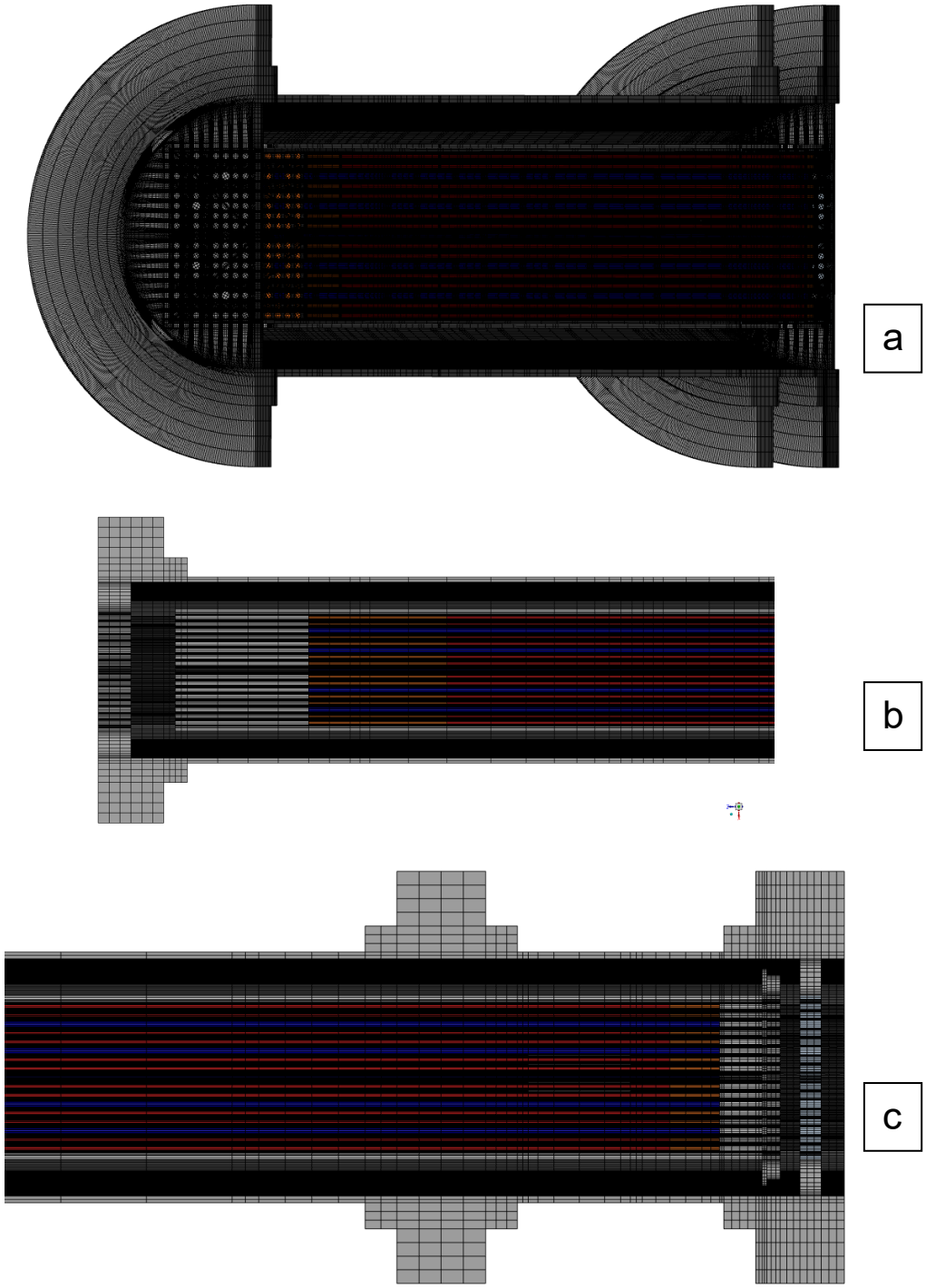


Figure 2-7 Explicit Geometry Model Mesh (Fuel Side View): (a) Full, (b) Top, and (c) Bottom

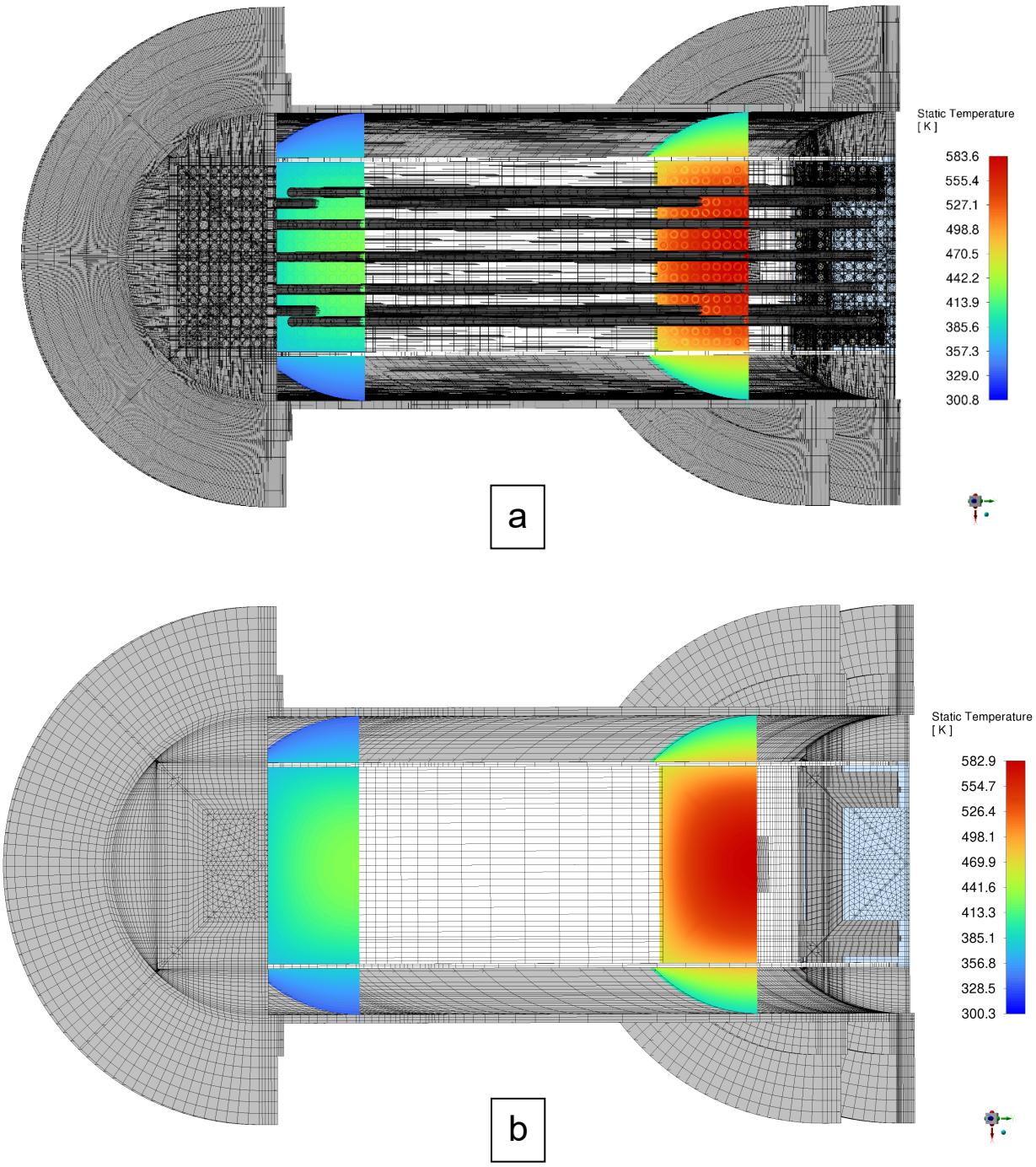


Figure 2-8 (a) Explicit Geometry and (b) Porous Geometry Model Contours of Temperature (K) at z = 0.91 m and z = 3.66 m with View of Mesh for the 3 kW, 10 Torr, Helium Fill Steady Case

Equivalent frictional and inertial losses in the porous model were calculated using existing flow area contractions and expansions. The outer surfaces bounding the control volume for both model types were allowed to interact with the surroundings using convection and radiation heat

transfer. A constant heat transfer coefficient was applied at these external surfaces obtained from natural turbulent heat transfer correlations.

The gas inside the pressure vessel was one of the following (depending on the case studied): helium, a mixture of helium and air, or a mixture helium and steam. In all cases, the flow regime inside the canister was assumed to be laminar. Calculations of Rayleigh and Reynolds numbers for helium flow inside the pressure vessel confirmed that the flow regime was, in fact, laminar. However, Rayleigh and Reynolds numbers estimated that the air flow outside the pressure vessel was in the transitional regime. Helium and air were modeled using the ideal gas law. Transient and steady solutions were both performed in this work. The model used temperature-dependent thermophysical properties for solid materials and fluids. Solid material properties—including density, thermal conductivity, specific heat, and emissivity—came from SNL reports (SAND2022-12078R, SAND2023-01454R ,and SAND2023-09746R).

All of the conservation equations used second-order upwind discretization. Radiation heat transfer was modeled using the discrete ordinates model with second-order upwind discretization. A pressure-based solver using the SIMPLEC algorithm (Semi-Implicit Method for Pressure-Linked Equations-Consistent) linked the conservation of momentum equations to the continuity equation. The least square cell-based method was used for gradient discretization. The PRESTO! (PREssure STaggering Option) scheme was used for pressure interpolation. The grid was refined until a grid-independent solution was obtained to minimize the discretization error. Table 2-1 shows the solver settings used in Ansys Fluent.

Table 2-1 CFD Solver Settings

CFD Solver Settings:	Input Value:
Solver Code	Ansys Fluent versions 23 and 24
Solver Type	Pressure-based
Viscous	Laminar
Radiation	Discrete Ordinates, Gray Model
Pressure-Velocity Coupling Scheme	SIMPLEC
Time Discretization	Steady-state, transient (second order)
Spatial Discretization:	
Gradient	Least squares cell-based
Pressure	PRESTO!
Momentum	Second-order upwind
Energy	Second-order upwind
Discrete Ordinates	Second-order upwind
Volume Fraction for Multiphase VOF Model	Implicit scheme, second order

Table 2-2 summarizes the BCs used for the ADCS CFD analysis for all the steady-state cases and the transient vacuum drying case.

Table 2-2 BCs for Each Configuration

Boundary	ADCS BCs
Bottom Flange	(Convection + Radiation) to CYBL environment
Middle Flange	(Convection + Radiation) to CYBL environment
Top Flange	(Convection + Radiation) to CYBL environment
Outside Vertical Pressure Vessel Walls	(Convection + Radiation) to CYBL environment
Bottom Walls + Bottom Viewing Glass	(Convection + Radiation) to CYBL environment
Top Wall	(Convection + Radiation) to CYBL environment

Table 2-3 gives the settings for the Discrete Ordinates (DO) radiation model. Sensitivity runs for higher radiation parameter values than in Table 2-3 showed almost unchanged results for the temperature values. The difference in the result was minimal—less than the iterative convergence uncertainty (discussed in section 3.1.1). As such, the input uncertainty analysis did not include the UQ for DO radiation parameters. The Ansys Fluent User's Guide includes detailed information about the DO radiation model.

Table 2-3 Radiation Model Settings

Discrete Ordinates, Gray Model Inputs	Input Value
Theta Divisions	4
Phi Divisions	4
Theta Pixels	2
Phi Pixels	2
Energy Iterations per Radiation Iteration	10

NUREG-2208 validated the use of porous media and showed that such an approach gave comparable results to the explicit geometry model (which included fuel rods, guide tubes, and grid spacers). Furthermore, SAND2019-6079R, "Modeling Validation Exercises Using the Dry Cask Simulator", confirmed that the porous media representation compared very favorably with the experimental data from the aboveground Dry Cask Simulator. SAND2019-6079R stated that the NRC's porous CFD model offered results that, overall, best fit the experimental data when compared with other participants' CFD models (including models that used an explicit fuel representation). Furthermore, in the CFD models submitted to the NRC for review, all dry cask applicants currently favor the use of porous media representations for fuel assemblies, because it simplifies the configuration and saves processing time.

Use of the porous media model for fuel assemblies requires the representation of assembly components with equivalent frictional and inertial hydraulic loss. An equivalent thermal conductivity (k_{eff}) representing both radiation and conduction inside the assembly, along with an equivalent density and specific heat capacity, were used to represent the fuel assemblies in the model.

To determine the appropriate k_{eff} for the porous media model, a two-dimensional CFD model representing the detailed cross-section of an assembly (i.e., explicitly showing fuel rods and guide tubes) was used to obtain k_{eff} for different cell wall temperatures. Radial and axial components of the effective conductivity were calculated as shown in TRW Environmental

Safety Systems' report, "Spent Nuclear Fuel Effective Thermal Conductivity", and used as input for the porous media model as a function of temperature.

2.3 Porous Media Radial and Axial Thermal Conductivity

The TRW report describes the k_{eff} approach in detail. In NUREG-2208, calculations in the TRW report were confirmed with two-dimensional CFD developed model using Ansys Fluent, which was then used to obtain the k_{eff} for the PWR 17x17 assembly. Table 2-4 through Table 2-19 summarize the input values for the radial and axial components of the effective thermal conductivity of the porous media assembly in this study. The radial k_{eff} values for helium, air, water vapor, and any mixture involving these three species were evaluated. Helium was used when the pressure vessel was pressurized between 100 and 1,200 kPa and air was introduced to the pressure vessel for the 1 Torr subatmospheric pressure steady-state case to quantify the uncertainty due to air ingress (i.e., leakage) into the canister. In the transient vacuum drying case, steam was present either as part of the mixture of helium and steam or fully in most of the vacuum steps with very low-pressure values.

Table 2-4 PWR-17x17 Fuel Region Porous Model—Radial k_{eff} (Helium)

Temperature (K)	k_{eff} (W/m*K)
281.0	0.364
327.1	0.414
421.1	0.527
516.9	0.659
613.5	0.819
711.0	1.011

Table 2-5 PWR-17x17 Fuel Region Porous Model—Axial k_{eff} (Helium)

Temperature (K)	k_{eff} (W/m*K)
250	8.082
400	5.868
600	5.034
800	4.870
1,000	5.006
1,200	5.177

Table 2-6 PWR Fuel Region Porous Model—Radial k_{eff} (Water Vapor)

Temperature (K)	k_{eff} (W/m*K)
277.3	0.064
402.4	0.124
467.1	0.182
544.4	0.267
630.1	0.386
721.0	0.546

Table 2-7 PWR Fuel Region Porous Model—Axial k_{eff} (Water Vapor)

Temperature (K)	k_{eff} (W/m*K)
250	8.007
400	5.768
600	4.909
800	4.725
1,000	4.844
1,200	5.001

Table 2-8 PWR 17x17 Fuel Region Porous Model—Radial k_{eff} (Water Liquid)

Temperature (K)	k_{eff} (W/m*K)
278.7	1.243
308.0	1.352
327.7	1.403
347.5	1.442
367.3	1.468

Table 2-9 PWR 17x17 Fuel Region Porous Model—Axial k_{eff} (Water Liquid)

Temperature (K)	k_{eff} (W/m*K)
250	8.336
290	7.759
310	7.479
330	7.194
350	6.905
368	6.642

Table 2-10 PWR 17x17 Fuel Region Porous Model—Radial k_{eff} (Dry Air)

Temperature (K)	k_{eff} (W/m*K)
279.6	0.082
390.8	0.136
462.6	0.191
543.4	0.271
630.3	0.382
721.6	0.530

Table 2-11 PWR Fuel Region Porous Model—Axial k_{eff} (Dry Air)

Temperature (K)	k_{eff} (W/m*K)
250	8.012
400	5.773
600	4.908
800	4.718
1,000	4.828
1,200	4.975

Table 2-12 PWR 17x17 Fuel Region Porous Model—Radial k_{eff} (Saturated Air)

Temperature (K)	k_{eff} (W/m*K)
278.1	0.081
296.3	0.127
469.0	0.174
548.8	0.243
634.2	0.341
724.2	0.477

Table 2-13 PWR Fuel Region Porous Model—Axial k_{eff} (Saturated Air)

Temperature (K)	k_{eff} (W/m*K)
273.2	7.666
313.2	7.069
333.2	6.770
353.2	6.470
373.2	6.169
393.2	5.798

Table 2-14 PWR 17x17 Fuel Region Porous Model—Radial k_{eff} (mix0 = 90 Percent Helium, 10 Percent Water Vapor)

Temperature (K)	k_{eff} (W/m*K)
272.6	0.267
335.6	0.318
427.4	0.411
521.2	0.529
616.5	0.677
713.0	0.860

Table 2-15 PWR Fuel Region Porous Model—Axial k_{eff} (mix0 = 90 Percent Helium, 10 Percent Water Vapor)

Temperature (K)	k_{eff} (W/m*K)
250	8.059
400	5.835
600	4.992
800	4.822
1,000	4.952
1,200	5.121

Table 2-16 PWR 17x17 Fuel Region Porous Model—Radial k_{eff} (mix1 = 83.2 Percent Helium, 16.8 Percent Water Vapor)

Temperature (K)	k_{eff} (W/m*K)
279.8	0.230
341.4	0.276
431.5	0.361
523.9	0.473
618.3	0.615
714.1	0.794

Table 2-17 PWR Fuel Region Porous Model—Axial k_{eff} (mix1 = 83.2 Percent Helium, 16.8 Percent Water Vapor)

Temperature (K)	k_{eff} (W/m*K)
250	8.049
400	5.820
600	4.974
800	4.801
1,000	4.929
1,200	5.095

Table 2-18 PWR 17x17 Fuel Region Porous Model—Radial k_{eff} (mix2 = 52.6 Percent Helium, 47.4 Percent Water Vapor)

Temperature (K)	k_{eff} (W/m*K)
288.0	0.135
365.8	0.180
447.2	0.248
533.5	0.344
624.1	0.473
717.7	0.641

Table 2-19 PWR Fuel Region Porous Model—Axial k_{eff} (mix2 = 52.6 Percent Helium, 47.4 Percent Water Vapor)

Temperature (K)	k_{eff} (W/m*K)
250	8.024
400	5.788
600	4.933
800	4.754
1,000	4.876
1,200	5.037

2.4 Porous Media Equivalent Density, Specific Heat, and Frictional Coefficients

Porous media equivalent density and heat capacity based on the area ratio as a function of temperature was calculated. Table 2-20 through Table 2-23 show the corresponding values. NUREG-2208 includes further details on how to calculate these values. SAND2017-13058R was also used to obtain some of the material properties used in the ADCS system.

Table 2-20 Fuel Region Porous Media Equivalent Density

Fill Gas	Porous Media Equivalent Density (kg/m^3)
Helium	1,806
Water Vapor	1,806
Water Liquid	2,404
Dry Air	1,806
Saturated Air	1,806
90% Helium, 10% Water Vapor (mix0)	1,806
83.2% Helium, 16.8% Water Vapor (mix1)	1,806
52.6% Helium, 47.4% Water Vapor (mix2)	1,806

Table 2-21 Assembly Fuel Region Porous Media Equivalent Specific Heat Capacity (J/kg*K) for Different Fill Fluids as Function of Temperature (K)

Temperature (K)	250	400	600	800
Helium	623.0	767.2	833.4	871.7
Dry Air	623.1	767.3	833.5	871.7
Mix0	623.2	767.4	833.6	871.8
Mix1	623.1	767.3	833.5	871.7
Mix2	623.0	767.2	833.4	871.7
Water Vapor	622.9	767.2	833.4	871.7

Table 2-22 Assembly Fuel Region Porous Media Equivalent Specific Heat Capacity (J/kg*K) for Liquid Water as Function of Temperature (K)

Temperature (K)	250.0	300.0	330.0	368.0
Water Liquid	1,545.1	1,552.1	1,567.1	1,586.0

Table 2-23 Assembly Fuel Region Porous Media Equivalent Specific Heat Capacity (J/kg*K) for Saturated Air at 84 kPa as Function of Temperature (K)

Temperature (K)	273.2	313.2	333.2	368.0
Saturated Air	645.3	683.8	703.0	736.6

The fuel assembly porous media equivalent frictional and inertial hydraulic losses were based on the previous analysis, documented in NUREG-2208. To accomplish this, the dry cask thermal response of a detailed explicit assembly was compared to that of a porous media assembly. The final friction coefficient, D value with units of ($1/m^2$), was obtained by comparing the mass flow rate through both the detailed and porous media fuel assemblies. The D value is an input to porous media friction in the Ansys Fluent software. The shear stress method from NUREG-2208 was used to calculate the porous media friction coefficient (D). The calculated frictional and inertial flow resistances were used to define a porous media to model the presence of the PWR 17x17 fuel assembly (i.e., fuel rods and grid spacers). An equivalent frictional D value of 1×10^6 m^{-2} was obtained. NUREG-2152 and NUREG-2208 explain the D value in detail.

2.5 Decay Heat

SNL provided the experimentally measured heat input value for each test, along with the associated uncertainty. The experimentally measured power input in watts (W) was distributed linearly along the axial heated length in the fuel rods in the explicit geometry or the axial effective heated porous region in the porous media model. The linearly varying decay heat was obtained from SNL using the measured mass of the nichrome throughout the length of the fuel rod. That heat source was entered into the Ansys Fluent CFD code as a volumetric heat generation rate in W/m^3 in the heated cell zones. Figure 2-9 illustrates the correlation obtained for this linear power profile.

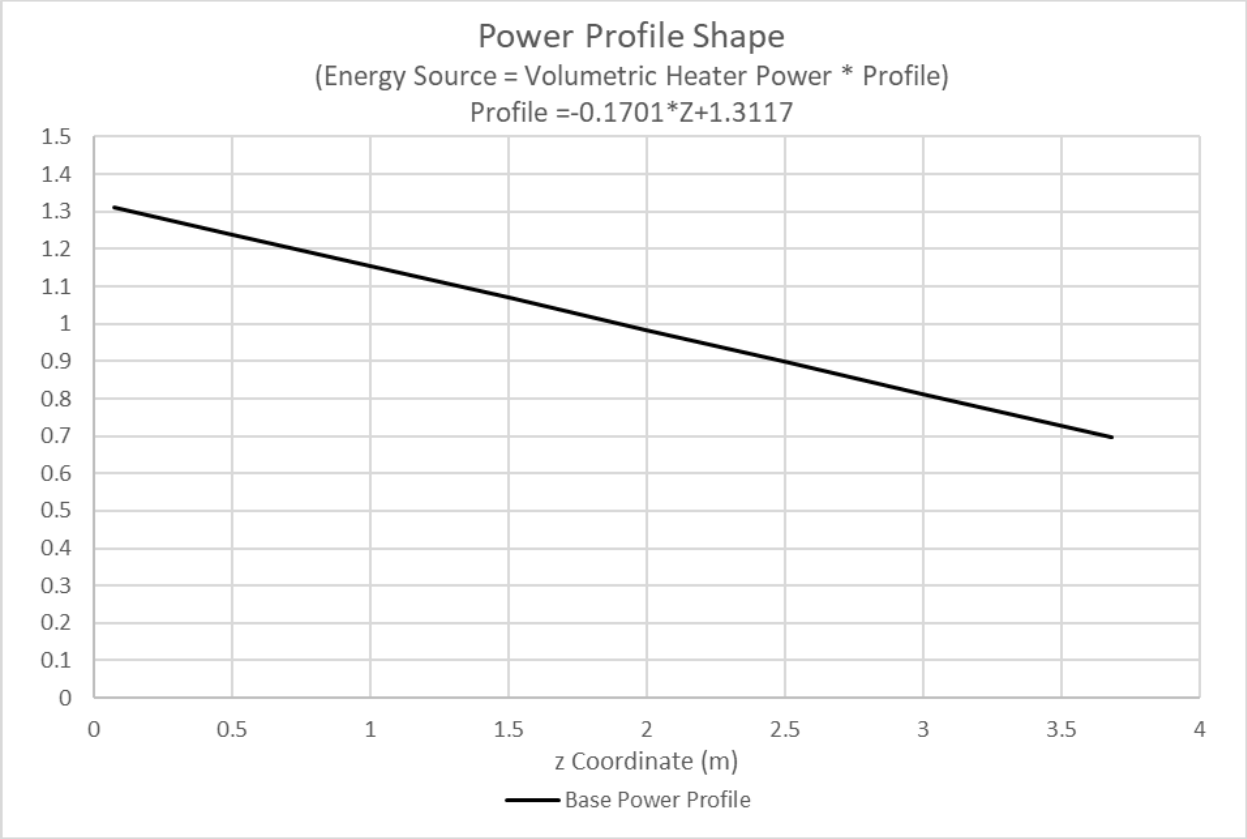


Figure 2-9 CFD Base Case Power Profile Shape

2.6 Comparison of Porous Media with the Explicitly Represented Geometry Model

As an initial validation effort, the accuracy of the porous media approach for this application was evaluated and compared to the explicitly represented geometry model for the six dry steady-state cases and the wet transient case.

The explicit case with fuel rods fully resolved had heat applied to the MgO heating elements, whereas the porous media case had heat applied to the volume inside the fuel basket with the same axial extent. In both cases, heat was applied using the following power profile:

$$Q = -0.1701 * (Z - 0.071326) + 1.3117$$

where Z is the axial distance measured from the top of the bottom nozzle and the heated length of the fuel assembly extends from Z = 0.071326 m to Z = 3.6845 m. The steady-state cases used a decay heat of 3 kW and helium pressure fills of 12 bar, 1 atm, 25 Torr, 10 Torr, 1 Torr, and 0.1 Torr. The transient case used a decay heat of 1,483 W and a canister pressure varying from vacuum pressure as low as 0.045 kPa (0.34 Torr) to 220 kPa, using different running fluids depending on the transient step, as shown in Table ES-1.

The porous and explicit geometry models were compared using axial temperature profiles along the centerline of the porous fuel assembly (i.e., the radial location of peak temperatures) and along the center guide tube (i.e., the location of the hottest TCs in the experiment), respectively, as well as along the pressure vessel external wall. Table 2-24 shows the PCT and PCT location

comparison between the 3D porous model and the 3D explicitly represented geometry model. The PCT and PCT location predictions of the two models agree very favorably.

Table 2-24 Porous and Explicit CFD Model PCT

Case	Pressure	PCT (K)	PCT location (m) and time (hr)
Steady-Porous	12 bar	467.8	3.66
Steady-Explicit	12 bar	470.3	3.64
Steady-Porous	1 atm	580.4	0.94
Steady-Explicit	1 atm	581.6	1.00
Steady-Porous	25 Torr	583.7	0.78
Steady-Explicit	25 Torr	584.7	0.88
Steady-Porous	10 Torr	583.0	0.78
Steady-Explicit	10 Torr	583.9	0.88
Steady-Porous	1 Torr	583.0	0.78
Steady-Explicit	1 Torr	583.9	0.88
Steady-Porous	0.1 Torr	583.1	0.78
Steady-Explicit	0.1 Torr	584.1	0.88
Transient-Porous at Regulatory Hold	Variable (Table ES-1)	544.5	0.94 @ 49.6 hr
Transient Using Explicit Geometry at Regulatory Hold	Variable (Table ES-1)	541.9	1.00 @ 49.6 hr

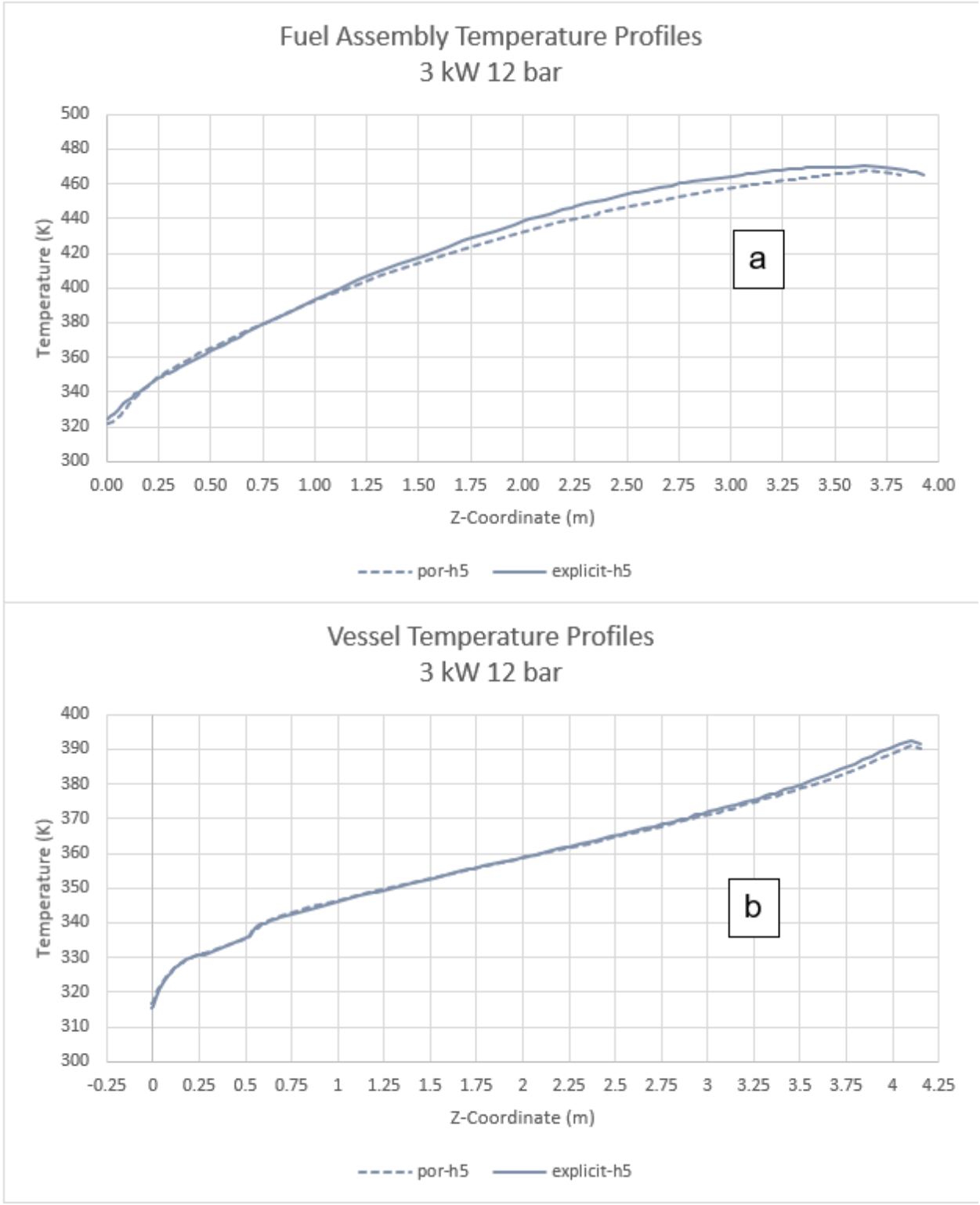


Figure 2-10 Maximum (a) Fuel and (b) Pressure Vessel External Wall Temperature Profiles Comparison Using the Explicit Geometry and Porous CFD Models for 3 kW and 12 bar Steady-State Case

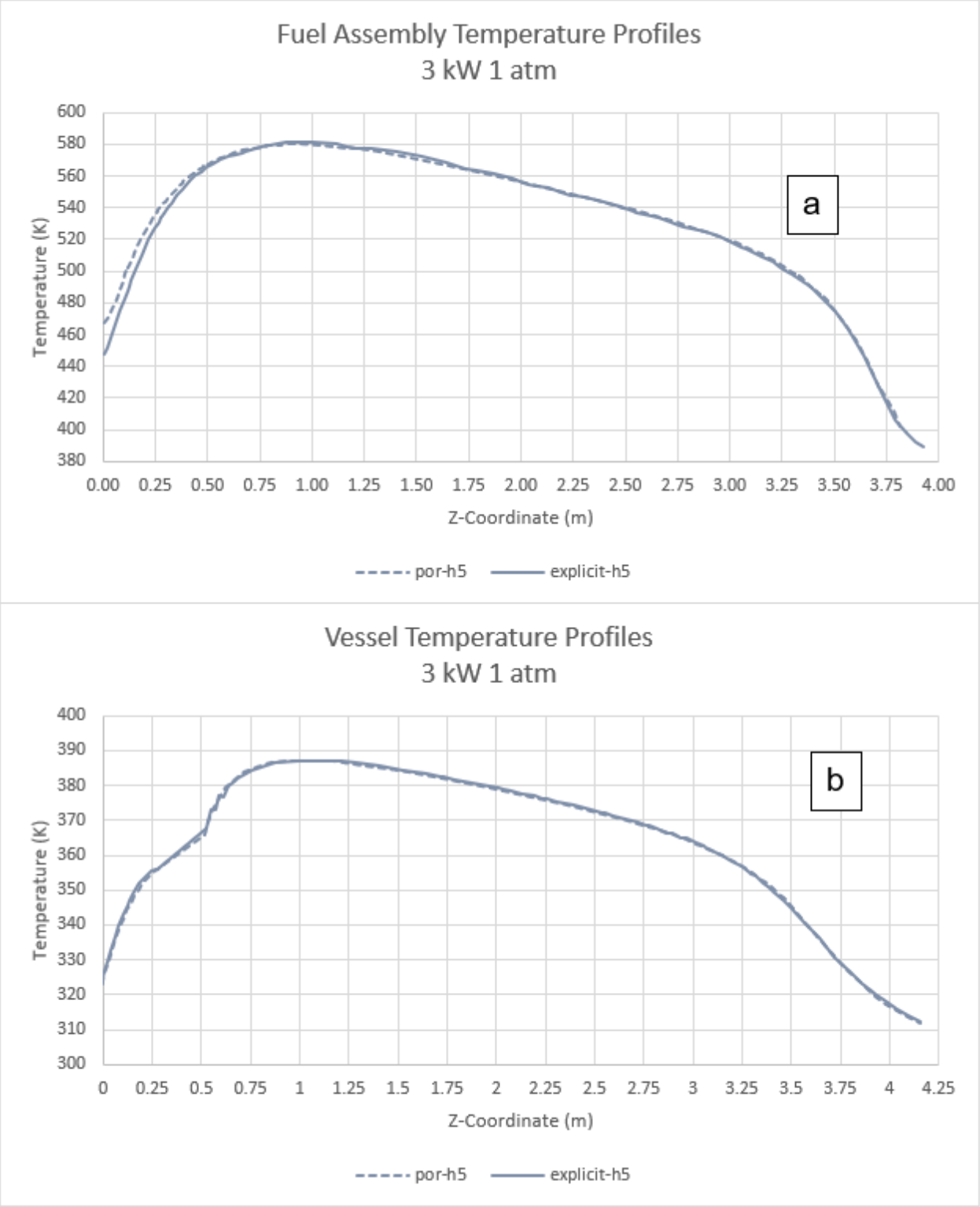


Figure 2-11 Maximum (a) Fuel and (b) Pressure Vessel External Wall Temperature Profiles Comparison Using the Explicit Geometry and Porous CFD Models for 3 kW and 1 atm Steady-State Case

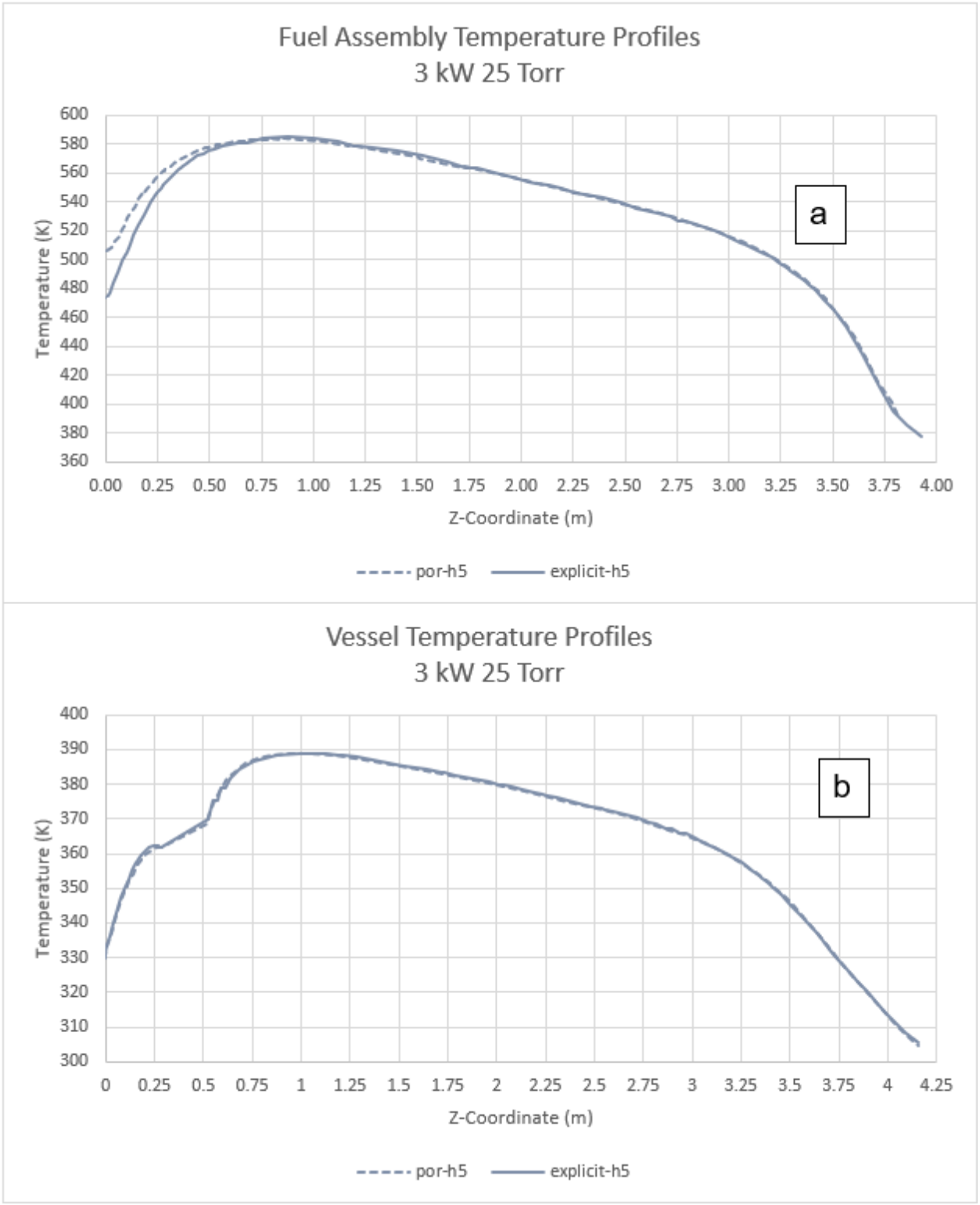


Figure 2-12 Maximum (a) Fuel and (b) Pressure Vessel External Wall Temperature Profiles Comparison Using the Explicit Geometry and Porous CFD Models for 3 kW and 25 Torr Steady-State Case

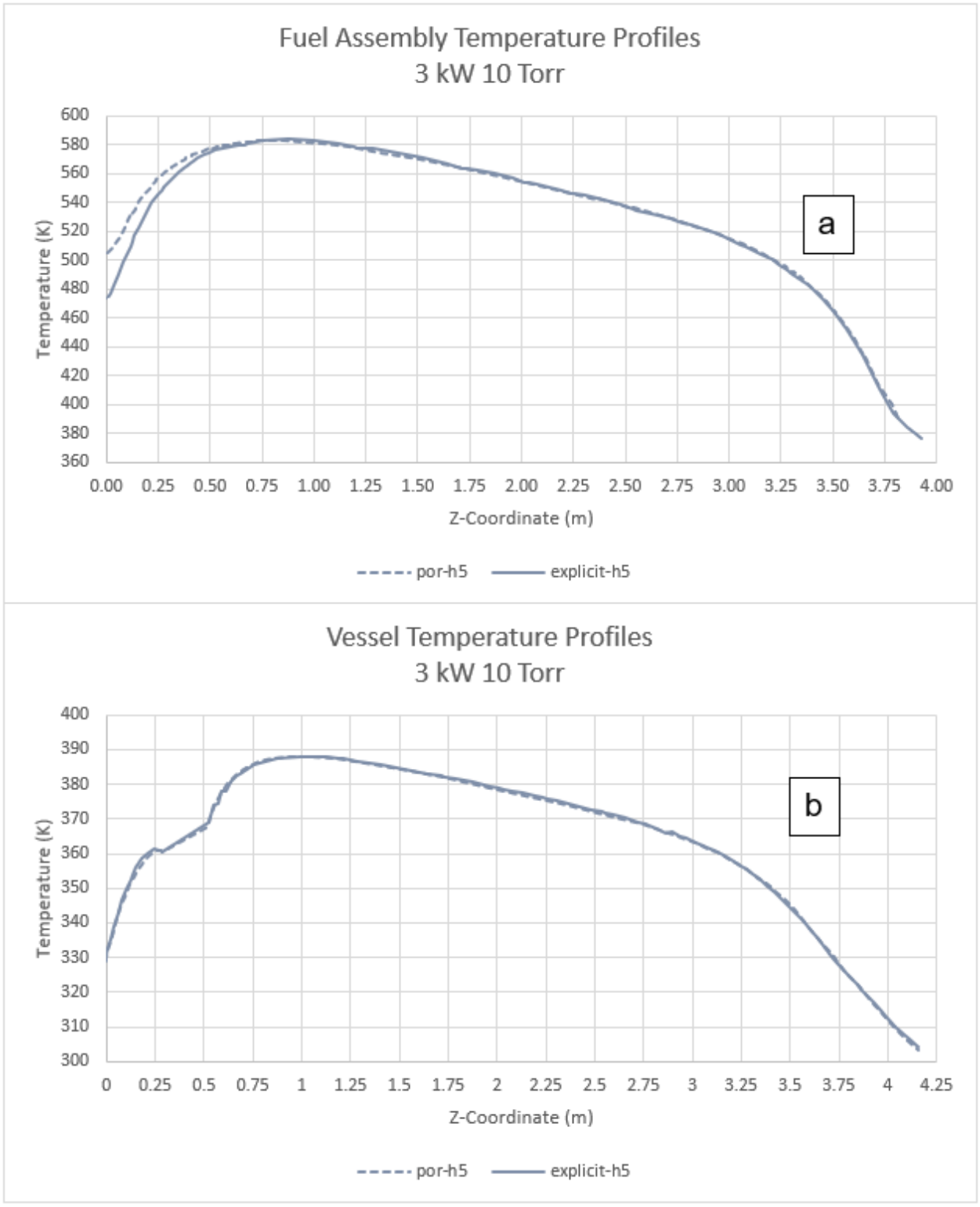


Figure 2-13 Maximum (a) Fuel and (b) Pressure Vessel External Wall Temperature Profiles Comparison Using the Explicit Geometry and Porous CFD Models for 3 kW and 10 Torr Steady-State Case

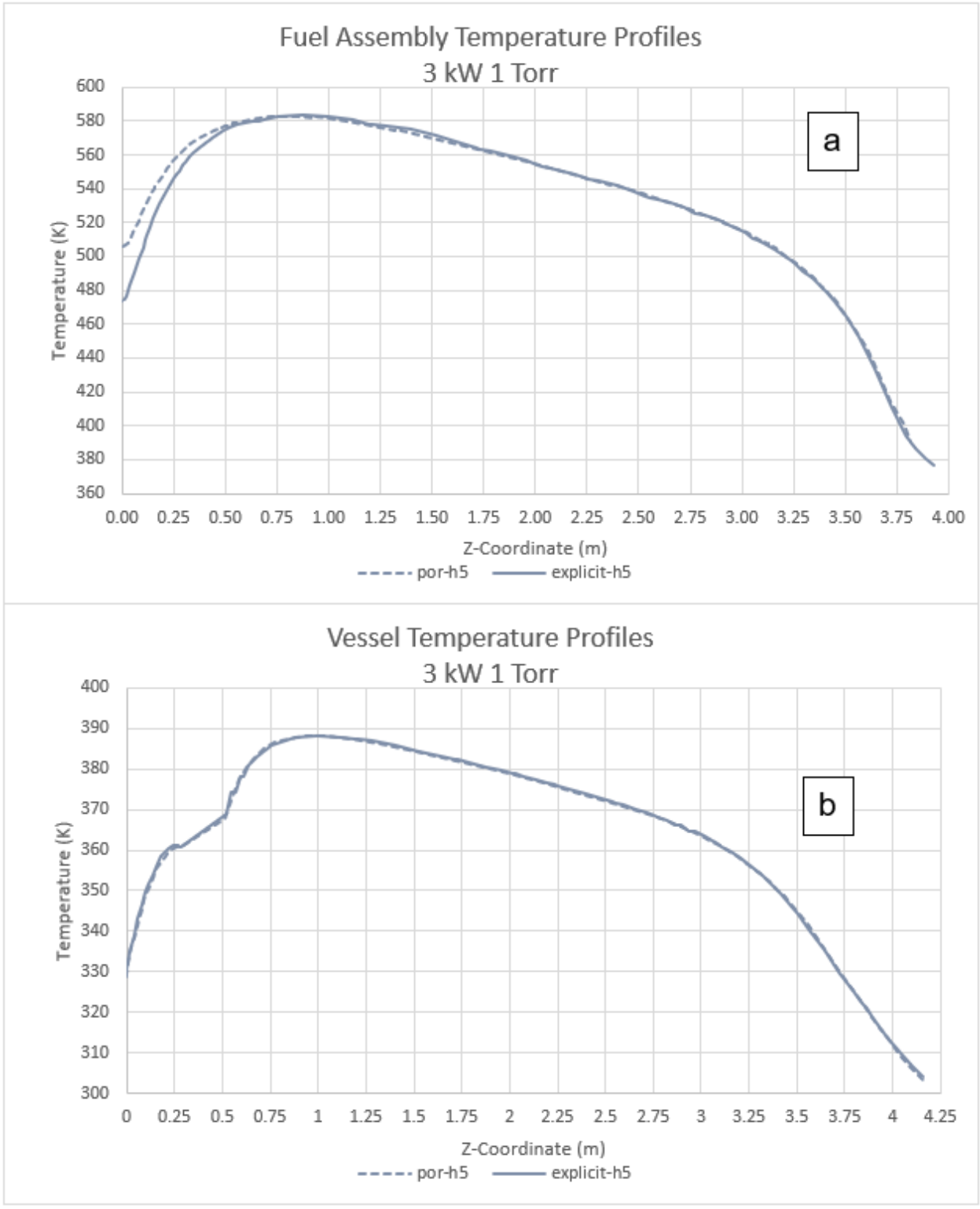


Figure 2-14 Maximum (a) Fuel and (b) Pressure Vessel External Wall Temperature Profiles Comparison Using the Explicit Geometry and Porous CFD Models for 3 kW and 1 Torr Steady-State Case

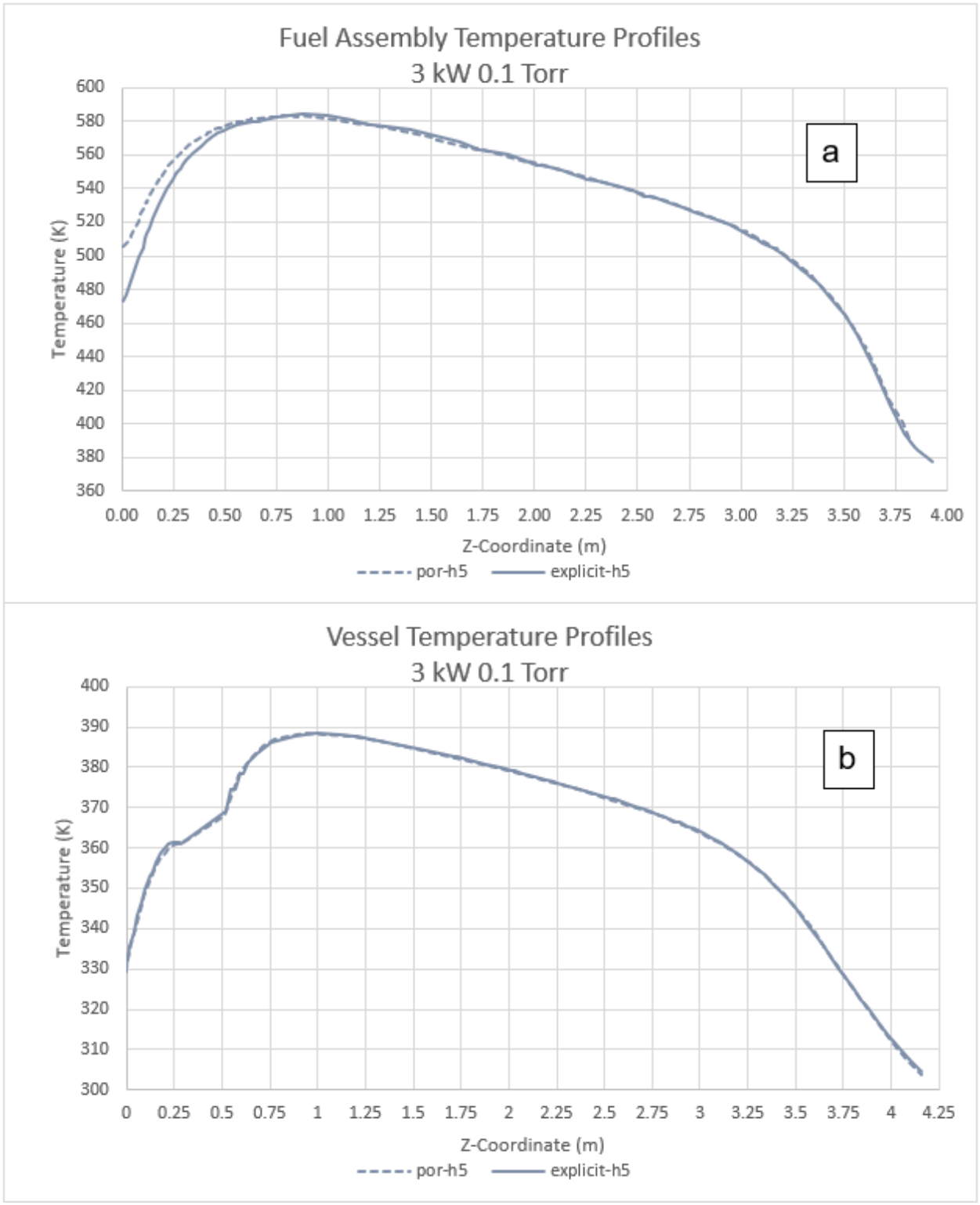


Figure 2-15 Maximum (a) Fuel and (b) Pressure Vessel External Wall Temperature Profiles Comparison Using the Explicit Geometry and Porous CFD Models for 3 kW and 0.1 Torr Steady-State Case

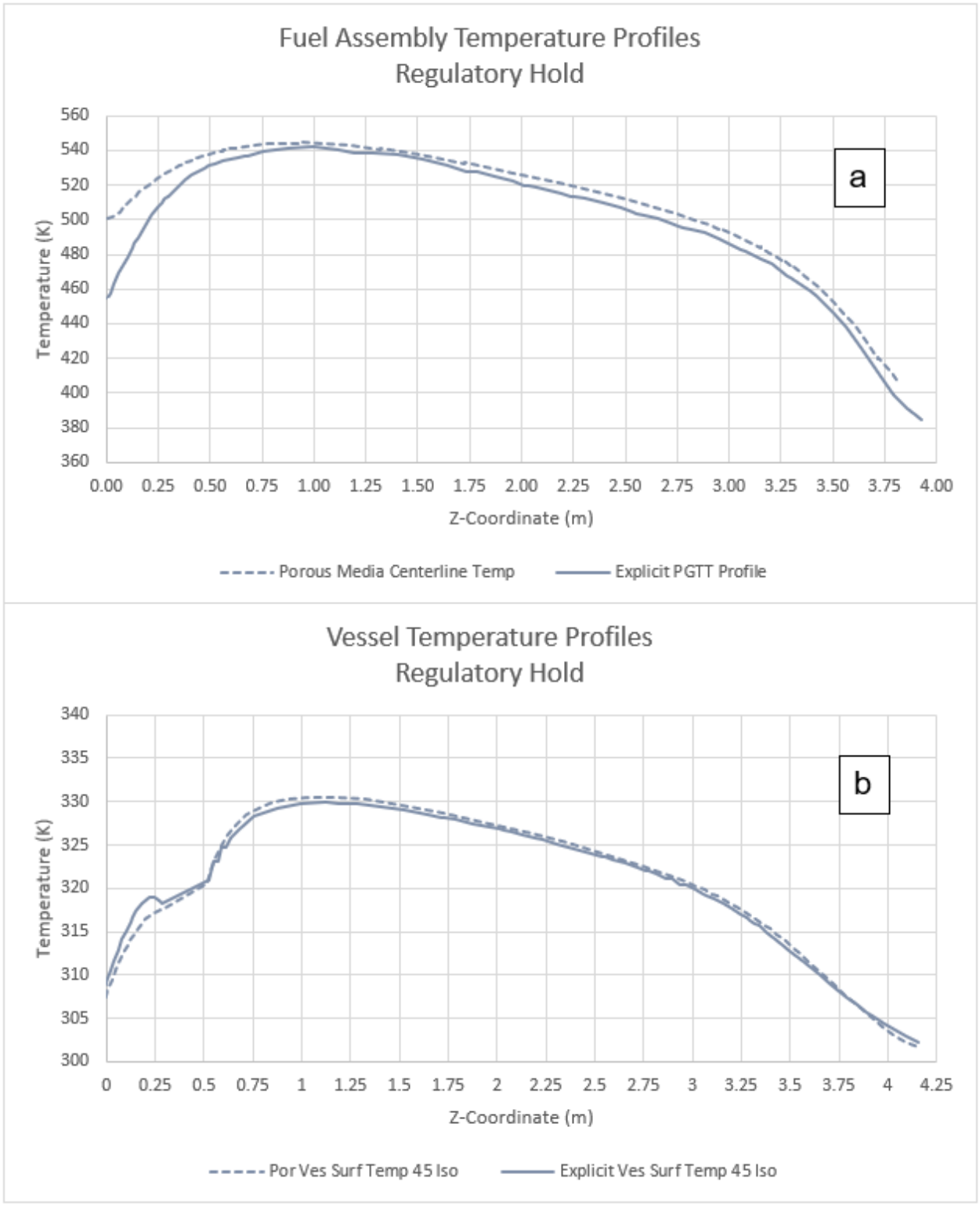


Figure 2-16 Maximum (a) Fuel and (b) Pressure Vessel External Wall Temperature Profiles Comparison Using the Explicit Geometry and Porous CFD Models for the Transient Vacuum Drying Case for 1.483 kW at Regulatory Hold Point

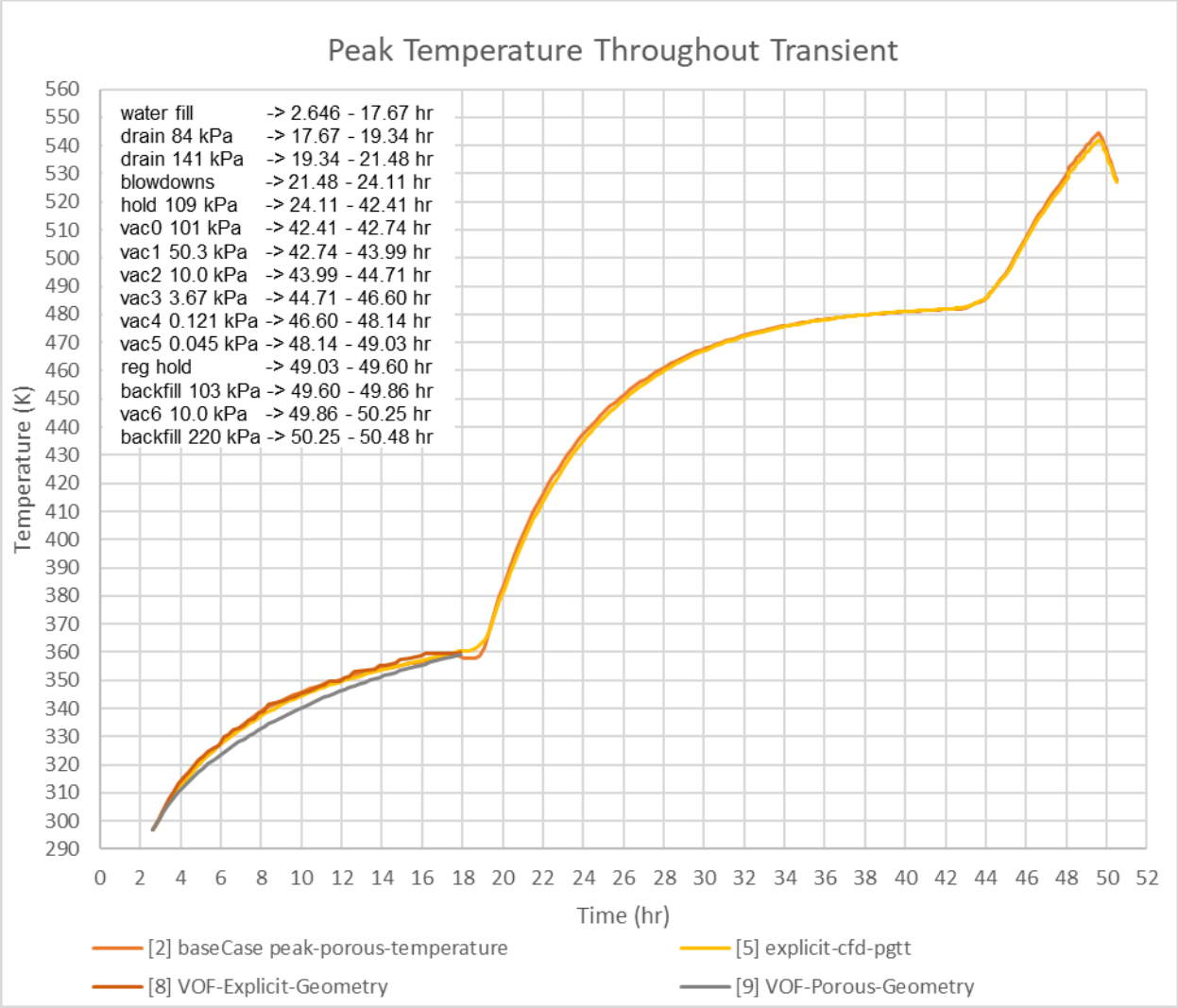


Figure 2-17 Maximum Fuel Temperature Profile Comparison Using the Explicit Geometry and Porous CFD Models for the Vacuum Drying Transient Wet Case; Base Case Plotted for All Transient Steps and VOF Multiphase Model Plotted Only for the Hold After Water-Fill Step

The axial temperature profiles for the maximum fuel temperature inside the assembly and along the external wall of the pressure vessel are plotted for the porous and explicit geometry CFD simulations in Figure 2-10(a) and (b) through Figure 2-15(a) and (b) for six steady-state cases, corresponding to pressures of 12 bar, 1 atm, 25 Torr, 10 Torr, 1 Torr and 0.1 Torr, respectively. For each case, the maximum fuel temperature profile (a) and the pressure vessel external wall temperature profile (b) are both plotted as function of height. These figures clearly show that the porous media model agrees very well with the realistically represented geometry model. This comparison demonstrates that the equivalent radial and axial thermal conductivities and the equivalent thermophysical properties of the PWR 17x17 assembly used to represent the porous model are rooted in good bases and assumptions. Thus, the porous media was a very reasonable representation of the real geometry and produced good predictions of temperature values throughout the ADCS system.

Figure 2-16 and Figure 2-17 present the transient vacuum drying case porous and explicit geometry models. Figure 2-16(a) compares the maximum fuel temperature profile as function of height, while Figure 2-16(b) shows the pressure vessel external wall temperature profile as a function of height. Figure 2-16(a) and (b) represent the ADCS temperature profiles at the regulatory hold step, just after the minimum pressure vacuum step. Figure 2-17 represents the maximum temperature that occurs in the fuel region during the vacuum drying process; these two figures offer further evidence of how well the porous media model can predict the ADCS thermal response.

For the water-filling step and the hold-time after the water fill, two fluids were in the dry cask. The bottom fluid was liquid water topped by saturated air. The proper way to simulate this phenomenon is to use a multiphase model that can appropriately represent heat and mass transfer between the phases. Multiphase modeling also involves tracking the variable interfaces between phases. Interface tracking is handled mainly by the solution of the volumetric fraction equation for the secondary phase. Dry cask applicants do not prefer this approach, because it involves more analysis and could cause difficulties obtaining a well-converged solution.

Thus, the CFD base case used in this report does not involve multiphase modeling. The CFD base case uses a simpler approach, in which the bottom liquid water is physically separated from the top saturated air by a thin wall that allows heat transfer, but not mass transfer, between the two separated fluids. Nevertheless, CFD base case assumptions were compared to the multiphase model in this report. The VOF multiphase model was used to simulate the hold-time after the water fill. The Ansys Fluent manual contains detailed information about the VOF model. Figure 2-17 shows the VOF model predictions used for the water fill hold step, using the explicit geometry model and the porous model. As the figure illustrates, VOF simulations using the porous and explicit geometry models have similar thermal responses. In addition, the CFD base case and the VOF multiphase case show similar behavior and agree favorably.

NUREG-2208 validated the use of porous media and showed that such an approach gave comparable results to the explicit geometry model (which included fuel rods and grid spacers). Furthermore, SAND2019-6079R, and SAND2020-10344R, “Blind Modeling Validation Exercises Using the Horizontal Dry Cask Simulator” confirm that the porous media representation compares very favorably with the experimental data from the aboveground dry cask simulator. SAND2019-6079R stated that the NRC porous model offered results that best fit the experimental data overall, when compared with other participants’ CFD models (including CFD models that used an explicit fuel representation).

Furthermore, in the CFD models submitted to the NRC for review, all dry cask applicants currently favor the use of porous media representations of the fuel assemblies, because it simplifies the configuration and saves on processing time.

2.7 Baseline Simulation Results

In the porous geometry model, the decay heat is conducted through the porous media based on the local temperature-dependent k_{eff} value, which represents the combined radiation and conduction heat transfer in the actual fuel assembly. Additionally, the fill gas is allowed to flow because of natural convection within the porous media, but the effective hydraulic resistance due to the fuel rods, guide tubes and spacer grids, in both the axial and transverse directions, somewhat restricts the flow of the gas. In the explicit geometry model, decay heat conducts through the fuel cladding and is then able to conduct, convect, and radiate through the fill gas to the steel basket. In both models, fill gas is also allowed to convect through the upper and lower

ends of the assembly, which is open at the top and partially restricted by the nozzle and standoff at the bottom. However, the heat transfer from this gas movement is small in comparison to the heat transfer outward from the basket to the fill gas in the downcomer region.

From the basket, heat can conduct, convect, or radiate through the fill gas to the painted steel pressure vessel. From the pressure vessel, heat is allowed to conduct, convect, and radiate to the surrounding ambient air. Figure 2-8 presents the cross-sectional views of the temperature in the 3D simulation for the 10 Torr steady-state case with helium fill for both the porous media model and the realistically represented (explicit) geometry model. Figure 2-8 shows the temperature cross section at 0.91 m, where the PCT occurs at the bottom of the fuel region for low-pressure cases, and 3.66 m at the top of the fuel region where the PCT can occur for high-pressure (e.g., 12 bar) fill gas cases.

2.7.1 Validation Metrics

The metrics provided for simulation validation were fuel maximum temperature profile at J9 (Figure 2-18) in separate axial locations along the fuel region including the peak guide tube temperature (PGTT, analogous and effectively identical to peak cladding temperature (PCT)) and the axial location of the PGTT/PCT (Figure 1-6), and the temperature profile along the external wall of the pressure vessel (Figure 1-10). A coordinate system was defined with an origin (z = 0) at the top of the bottom nozzle on the assembly, where the rectilinear z-coordinate runs along the axial length of the pressure vessel toward the upper flange (Figure 1-6).

The following are the temperature measurement axial locations along the cask used for validation of the maximum fuel temperature inside the assembly:

Axial measurement at J9 @ z (m) = (0.36, 0.91, 1.83, 2.44, 3.01, 3.66, 3.78)

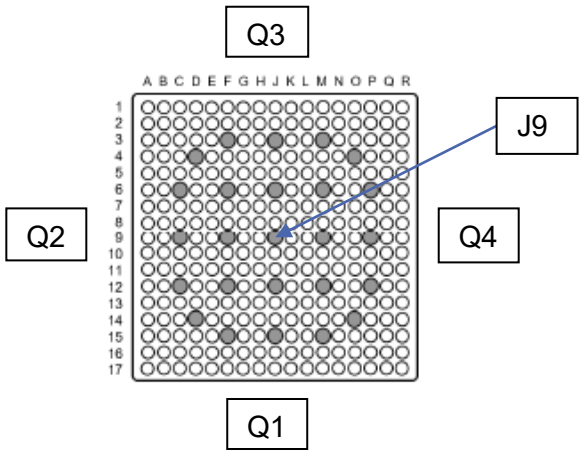


Figure 2-18 Fuel Rod Layout—Axial Measurements at Guide Tube J9

The following are the temperature measurement axial locations along the cask used for validation of the pressure vessel external wall bounding the cask:

Axial measurement z (m) = (0.56, 0.91, 1.83, 2.44, 3.01, 3.66, 4.01)

2.8 Consistency Checks

The first step in validating the simulation and quantifying the uncertainty is to ensure that the simulation is internally consistent. Some consistency checks that are available to demonstrate this are mass conservation, energy conservation across the boundaries of the model, the convergence of numerical equation residuals, and monitoring of target variables as numerical iteration proceeds. As the boundary of the ADCS is not open to the outside to exchange mass, the mass conservation is not part of the consistency checks.

In this validation, two consistency checks were performed. The first involved the conservation of energy obtained from the fuel heat source and the heat loss through the external walls of the casks. For the steady-state simulation, the net heat flux obtained from the heat source, the existing structures, and walls should tend toward zero. For the transient simulation, however, the heat balance will converge to one steady value, due to an additional transient term in the energy equation. The second check involved monitoring of the PGTT/PCT target variable. The target variable should asymptotically converge to a steady value without any major oscillations for the overall steady-state solution, or for every time step of a transient simulation as the numerical solution proceeds from one iteration to another.

To illustrate how consistency checks were performed, the steady-state dry test case using the porous media CFD model with a supplied heat of 3 kW and a helium fill pressure of 10 Torr is used as example. The total heat of 3 kW was applied to the simulation as a volumetric heat source, varying linearly (as explained in earlier sections) and escaped from the model boundaries, including the top and bottom of the cask, vertical surface of the pressure vessel, and external surfaces of flanges. The heat escaped from the cask boundaries to the surroundings through convection and radiation.

The heated section had a volume of 0.1785 m^3 and a heat generation source term of 16,812 W/m^3, for a total heat input of 3,001 W (i.e., the average value reported in SNL's 3 kW steady test at 10 Torr). This yielded a total heat input to the simulation of 375.125 W for the eighth-symmetry model. Table 2-25 reports the heat gain or loss through the peripheral walls bounding the simulated dry cask through convection and radiation to the surroundings at ambient temperature of 297 K.

The total imbalance in heat across the entire model is 0 W, or 0 percent of the total heat input. The heat balance and target variable monitoring (such as PCT) demonstrates model consistency and indicates that it will not introduce significant additional uncertainty into the VVUQ analysis.

Table 2-25 Energy Balance Consistency Check for 10 Torr Steady-State Case

Walls/Volumes	Units:	Heat:
Fuel Assembly Heat Source	Watts	3,001.00
Top Flange	Watts	-14.35
Middle Flange	Watts	-249.21
Pressure Vessel Vertical External Walls	Watts	-2,623.84
Bottom Flange	Watts	-99.50
Bottom Sight Glass	Watts	-14.10
TOTAL	**Watts**	**0.0**

In addition to the heat balance, the peak porous media fuel assembly temperature (porous model) or PGTT/PCT (explicit geometry model) in the fuel region was monitored as function of iteration number. The PCT value should converge to a steady value for at least 2,000 iterations or more for the iterative solution to be stopped.

2.9 Heat Profile Sensitivity

This section compares the base case heat profile to a sensitivity case with the uniform heat profile used in NUREG 2238. PCT and PCT location were used to compare the two heat profiles' predictions, as shown in Table 2-26. The comparisons of CFD predictions were made using a total heat of 3 kW for 12 bar, 1 atm, and 25 Torr steady-state cases and are shown in Figure 2-18, Figure 2-19, and Figure 2-20, respectively. The main observable difference is that more heat is supplied in the bottom half of the fuel assembly than at the top of the assembly when the base case heat profile was used.

As shown in all three figures, temperatures in the bottom half of the fuel assembly are higher for the base case heat profile than for the uniform heat profile for corresponding locations in the fuel. The PCT was higher for the 1 atm and 25 Torr case when using the base case heat profile, as shown in Table 2-26, because in these two cases with low pressures, the PCT occurred in the bottom half of the assembly, where the greater decay heat was applied. The 12 bar case showed that the PCT was higher when the uniform heat profile was used, as the PCT for high-pressure cases occurred in the top half of the fuel and a greater heat was provided in the top of the assembly when a uniform heat profile was used. The PCT location for the low-pressure cases of 1 atm and 25 Torr moved slightly lower for the base case heat profile because the heat source increased inversely with height, as shown in Figure 2-8.

Table 2-26 PCT and PCT Location Using Base Case and Uniform Heat Profile

Case	PCT (Kelvin)		PCT location (m)	
	Base Case Heat Profile	Uniform Heat Profile	Base Case Heat Profile	Uniform Heat Profile
3 kW, 12 bar	467.8	475.7	3.66	3.66
3 kW, 1 atm	580.4	558.6	0.94	2.18
3 kW, 25 Torr	583.7	559.6	0.78	1.96

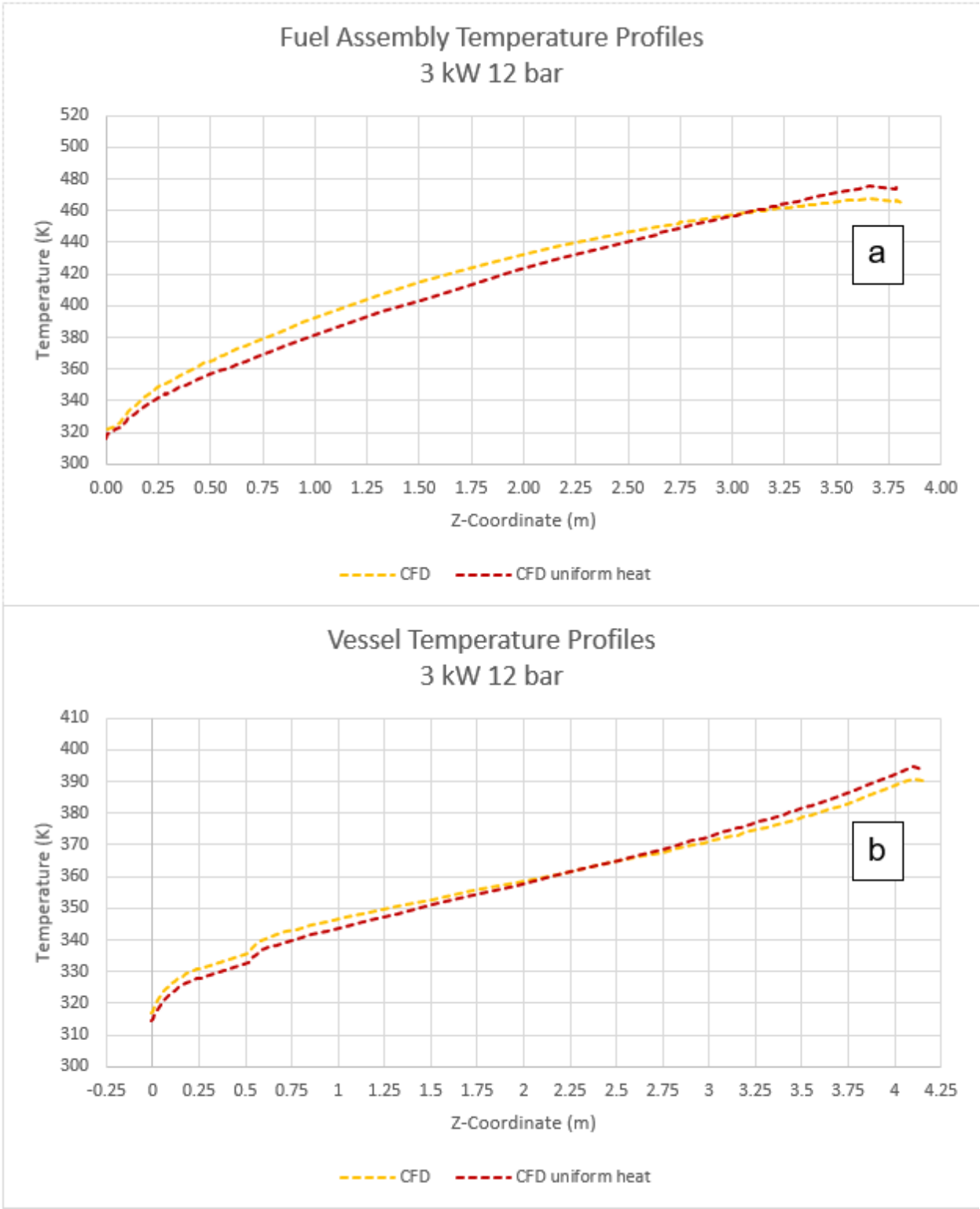


Figure 2-19 Maximum (a) Fuel and (b) Pressure Vessel External Wall Temperature Profiles Comparison Using Base Case with the Base Linear and Uniform Heat Profiles for 3 kW and 12 bar Steady-State Case

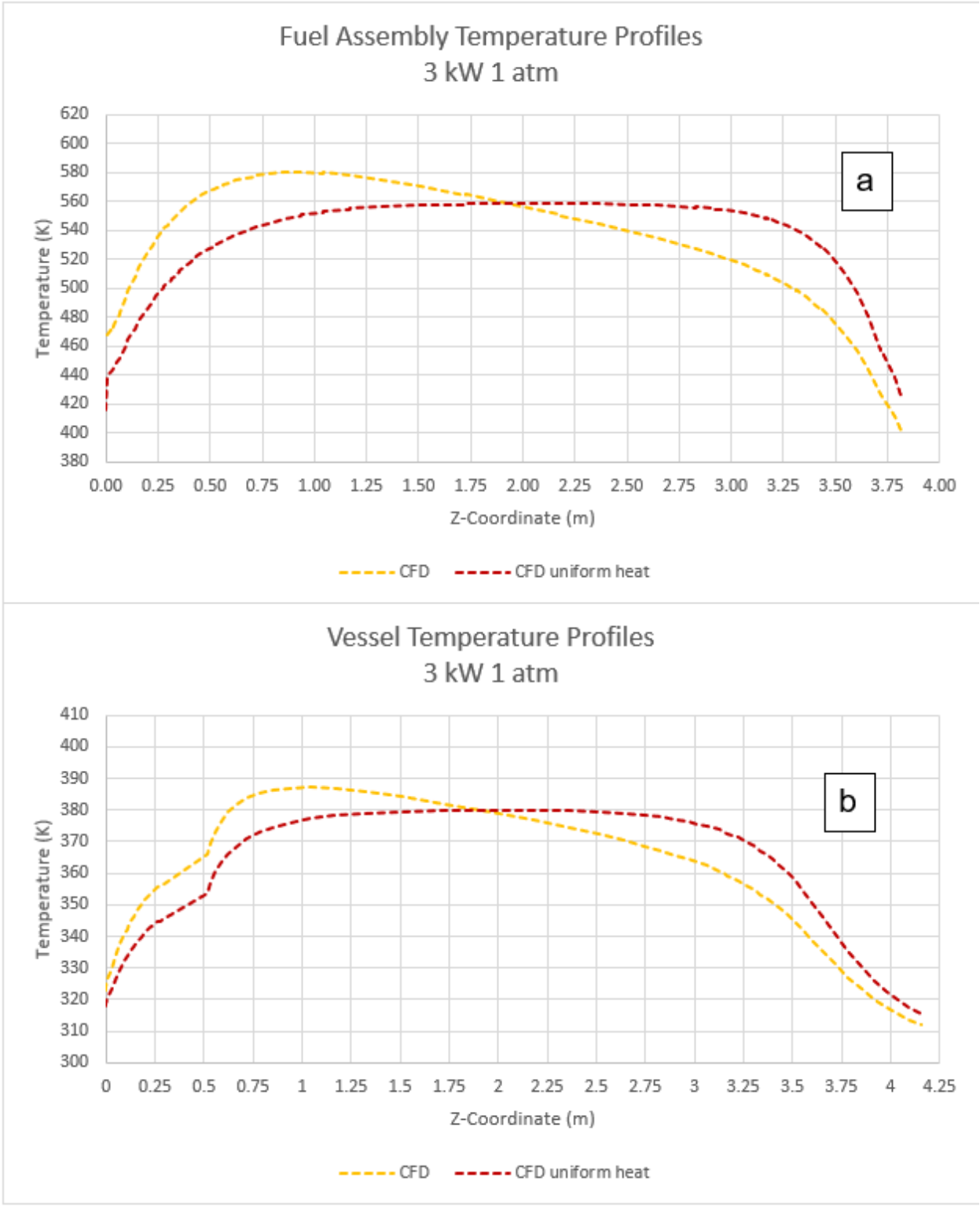


Figure 2-20 Maximum (a) Fuel and (b) Pressure Vessel External Wall Temperature Profiles Comparison Using Base Case with the Base Linear and Uniform Heat Profile for 3 kW and 1 atm Steady-State Case

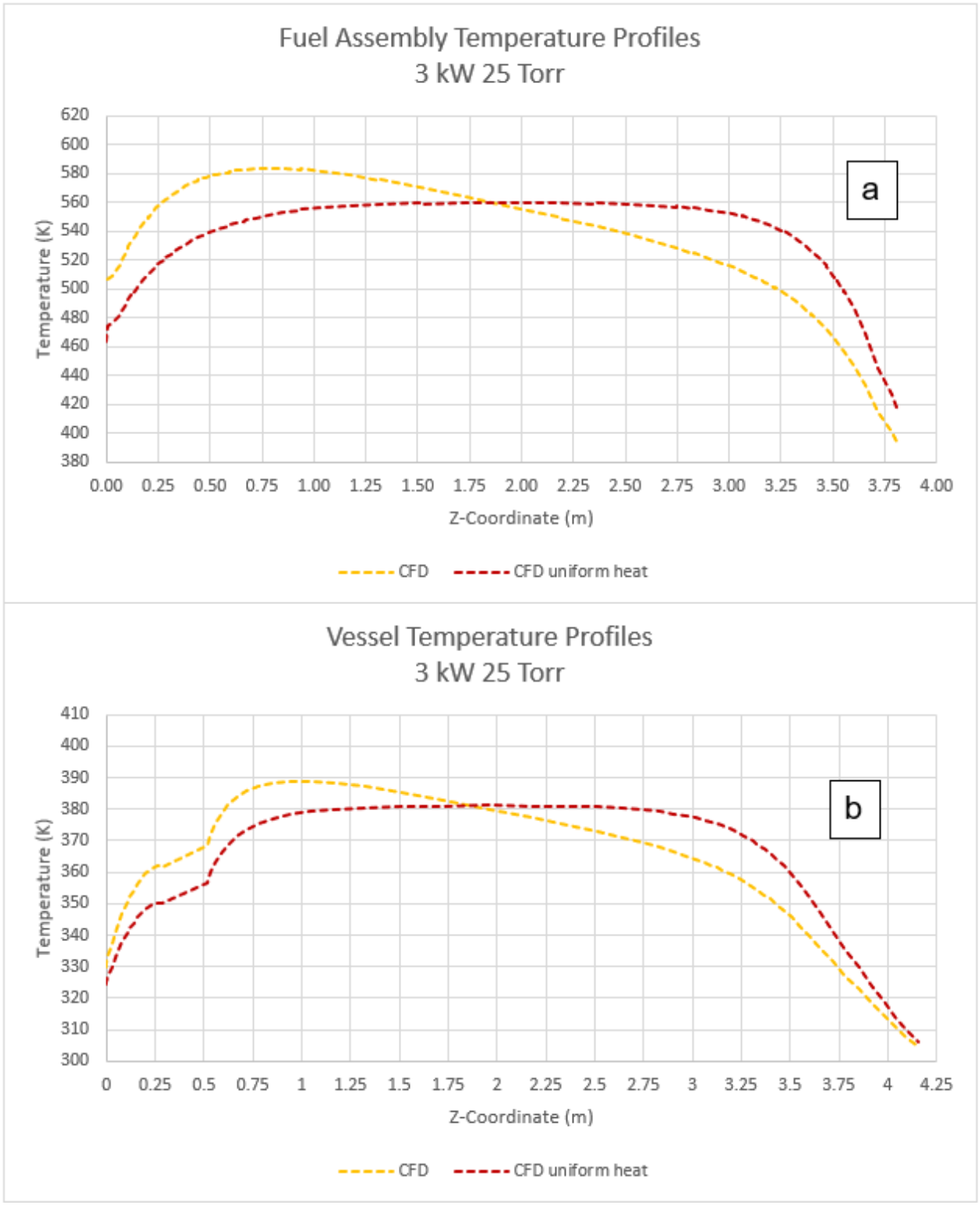


Figure 2-21 Maximum (a) Fuel and (b) Pressure Vessel External Wall Temperature Profiles Comparison Using Base Case with the Base Linear and Uniform Heat Profile for 3 kW and 25 Torr Steady-State Case

3 VERIFICATION, VALIDATION, AND UNCERTAINTY QUANTIFICATION

UQ for the CFD models was obtained using ASME V&V 20-2009 for the target variables of interest: PCT, PCT location, and temperature values at selected locations along the fuel region and the pressure vessel external wall. The analysis examined sources of uncertainty such as simulation inputs, numerical errors (i.e., iterative, discretization, and round-off), and experimental errors. ASME V&V 20-2009 details the method used in this calculation. NUREG-2238 and NUREG/CR-7260 undertake similar work, which this report follows closely.

UQ was performed for PCT, fuel region max temperatures at selected heights, and pressure vessel outer wall temperatures at selected heights for seven cases. The steady-state cases include (1,200 kPa, 3.0 kW), (1 atm, 3.0 kW), (25 Torr, 3.0 kW), (10 Torr, 3.0 kW), (1 Torr, 3.0 kW), and (0.1 Torr, 3.0 kW). The transient vacuum drying case used a constant power of 1.483 kW, with varying pressure (Figure ES-1); during the regulatory hold, the pressure was 0.045 kPa. The results in chapter 4 and appendix A provide detailed UQ results for all cases.

3.1 Numerical Uncertainty

Numerical uncertainty has three major sources: computer round-off error, iterative convergence uncertainty, and discretization uncertainty. Discretization uncertainty can be spatial or temporal, but because most simulations considered in this work are steady state, temporal uncertainty is not of concern. For transient simulations, a limited time-step sensitivity comparison was performed; because the peak temperatures predicted by the base case and reduced-time-step case during the regulatory hold step differed by less than 0.02 K, temporal uncertainty was deemed to be inconsequential. Because computer round-off error is extremely small compared to other sources, it is not considered here.

3.1.1 Iterative Uncertainty

CFD practitioners generally agree that CFD models need to run until they are properly converged. A solution is converged when residuals and target variable monitors no longer vary with additional iterations. However, some solutions are stable and converge better and more easily than others, depending on the physics and the selected solver settings. Some solutions converge as they are supposed to and change very little with each iteration. Others are much “noisier,” with solutions that can vary significantly within a range of values. This variation can be due to numerical instability in the solution or physically based unsteady flow patterns in a steady-state solution.

Once the solution reaches something resembling convergence, the output in question should be recorded for the last 2,000 to 3,000 iterations to determine the range of values over which the output changes. This range represents the iterative convergence uncertainty of a solution.

The PCT values for the baseline solution were recorded in each case for at least 2,000 iterations. Figure 3-1 represents the PCT iteration error of the (3 kW, 12 bar) steady-state case, which was found to have the most iteration error. The average PCT value was found to be 467.9443 ± 0.3889 K (382.6297 ± 0.7000 degrees Fahrenheit (°F)) within a 95 percent confidence level, or within two standard deviations of the average value.

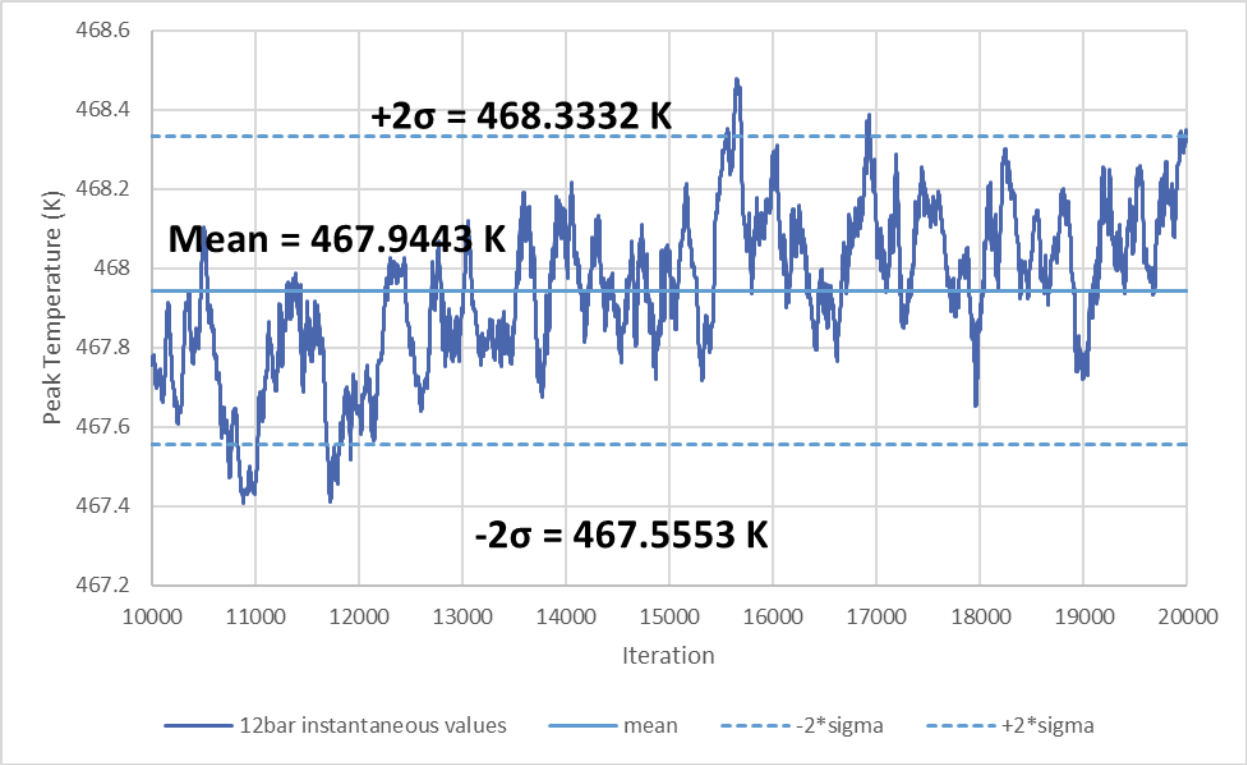


Figure 3-1 Iterative Convergence of PCT for the 12 bar, 3 kW Steady-State Case

The distribution of values gathered during the iterative convergence testing was plotted against a normal distribution to determine whether two standard deviations could safely be used as the 95 percent confidence level for the iterative convergence uncertainty. The data closely follow a normal distribution, as Figure 3-2 illustrates, so this is a valid assumption.

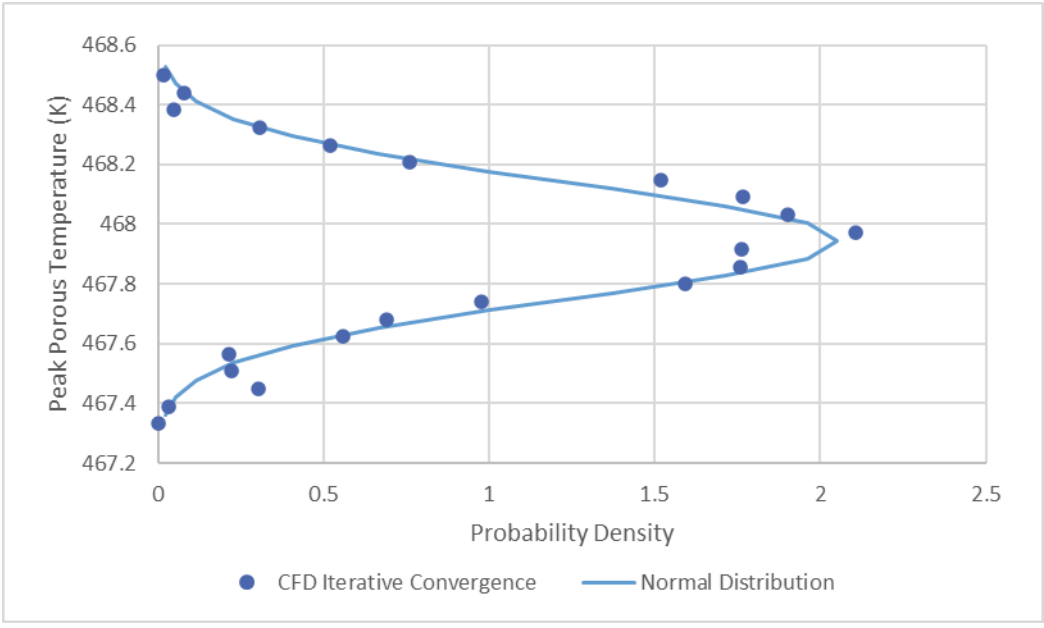


Figure 3-2 Normal Distribution and PCT Iterative Convergence for the 12 bar, 3 kW Steady-State Case

3.1.2 Discretization Uncertainty

The grid convergence index (GCI), as outlined in ASME V&V 20-2009 recommends using at least three grids to determine the uncertainty of a solution with respect to the mesh. This case uses a fine mesh, a medium mesh, and a coarse mesh, where each level of refinement is accomplished by refinement ratio (r_{21}, r_{32}) of 1.33 – 1.36 as shown in Table 3-1.

Table 3-1 GCI Mesh Sizes

Mesh #	GCI Mesh Size	Three-Dimensional Cells
1	Fine	445,192
2	Medium	176,567
3	Coarse	74,502

The GCI, which is the 95 percent confidence level uncertainty in the solution due to the mesh, can be calculated for the finest of three meshes as follows:

$$GCI_{fine} = \frac{F_s * |\varphi_2 - \varphi_1|}{r_{21}^p - 1}$$

Where ϕ is the solution result, and 1, 2, and 3 represent the fine, medium, and coarse meshes, respectively. F_s is an empirically derived factor of safety, which is 1.25 for an asymptotically converging set of three or more meshes, r_{21} is the refinement ratio of fine mesh cells to medium mesh cells, and r_{32} is the refinement ratio of medium mesh cells to coarse mesh cells. The order of accuracy, *p*, can be calculated as follows:

$$p = \frac{\ln\left(\frac{\varphi_3 - \varphi_2}{\varphi_2 - \varphi_1}\right) + q(p)}{\ln(r_{21})}$$

Where *q*(*p*) is defined as:

$$q(p) = ln\ \frac{r_{21}^p - s}{r_{32}^p - s}$$

And *s* is defined as:

$$s = 1 * sign \frac{\varphi_3 - \varphi_2}{\varphi_2 - \varphi_1}$$

Because the coarse mesh is used for all evaluations outside of the grid refinement study, it is also useful to calculate the GCI of the coarse mesh, as follows:

$$GCI_{coarse} = GCI_{fine} * r_{31}^p$$

Calculating the GCI using this Richardson Extrapolation method only works when the successive refinement results in a solution that asymptotically converges towards a fixed value at a cell size of zero.

To achieve a meaningful GCI, ASME V&V 20-2009 highly recommends using a systematic grid refinement (i.e., constant refinement ratio throughout the computational volume), geometrically similar cells in each refinement level, and structured cells where possible. This was a challenge, as it is for many problems. A grid refinement ratio greater than 1.3 was used, as recommended by ASME V&V 20-2009. A systematic grid refinement was achieved for a majority of the refinements but not for all. Additionally, to apply the GCI method, the grid refinement should be in the asymptotic region. It should also be noted that the calculated value of the order of accuracy, *p*, should not differ significantly from the formal value of *p* (i.e., the order of the method). If any of these conditions are not met, an F_s of 3 should be used.

If the solutions do not demonstrate asymptotic convergence with three meshes, particularly in areas of strong temperature gradients, then ASME V&V 20-2009 suggests that four or more mesh resolutions should be used to convincingly demonstrate asymptotic response in difficult problems. However, the computational resources necessary to perform another refinement of mesh resolution were prohibitive.

Since asymptotic convergence was not observed in some cases and at some measurement locations considered in this work, GCI was always calculated from just two mesh resolutions for consistency: the fine mesh and the coarse mesh. In this situation, ASME V&V 20-2009 suggests using a factor of safety of 3 to account for the greater uncertainty associated with using only two mesh refinement levels, and an order of convergence $p = 1$. This allows the GCI to be calculated everywhere in the mesh so that the discretization uncertainty can be included in the overall uncertainty when comparing simulation results to experimental measurements at all the temperature measurement locations for all cases examined.

Table 3-2 illustrates the GCI calculations for the PCT for the steady-state (10 Torr, 3.0 kW) case. In this case, an F_s equal to 3 was used, as the calculated order of accuracy (*p*) differed significantly from the formal order of accuracy.

Table 3-2 GCI Values for PCT for the (10 Torr, 3 kW) Steady-State Case

GCI 3 kW, 10 Torr	PCT
Refinement Ratio, r	1.81
Factor of Safety, F_s	3.0
Coarse (Base) Mesh	583.0 K
Medium Mesh	582.5 K
Fine Mesh	582.5 K
Order of Convergence, p	1
GCI (Fine – Coarse)	3.0 K

3.1.3 Overall Numerical Uncertainty

Table 3-3 presents the overall numerical uncertainty from all sources for the (10 Torr, 3 kW) steady-state case. When computing the total numerical uncertainty, it is not sufficient to use the root mean square addition of iterative convergence error and discretization error because the

two errors are correlated (ASME V&V 20-2009). Instead, they must be combined using simple addition. Appendix A tabulates the results for other scenarios.

Table 3-3 Overall Numerical Uncertainty for PCT for the (10 Torr, 3 kW) Steady-State Case

Overall Numerical Uncertainty	PCT
Computer Round-Off	± 0.0 K
Iterative Convergence	± 0.0 K
Spatial Discretization	± 3.0 K
Total Numerical Uncertainty:	**± 3.0 K**

3.2 Input Uncertainty

The input uncertainty method used was the finite difference method (also variously called the sensitivity coefficient method, perturbation method, mean value method, and possibly others). This is a local approach to determining the input uncertainty, whereby an independent input variable (e.g., total decay heat) is changed by a small amount and the effect that this variable has on the solution is recorded. If the uncertainty of the input is known, then the resulting uncertainty on the solution due to the uncertainty of the input can be calculated using the following equation:

$$u_{input}{}^2 = \sum_{i=1}^{n} \left(\frac{\partial S}{\partial X_i} u_{X_i} \right)^2$$

Where:

u_{input}	=	Total input uncertainty
S	=	Simulation result
u_{X_i}	=	Corresponding standard uncertainty in input parameter X_i
X_i	=	Input parameter
n	=	Number of inputs in the sensitivity study
$\partial S/\partial X_i$	=	Sensitivity coefficient

Depending on how $\partial S/\partial X_i$ and u_{X_i} are defined, it is possible to calculate either one-sided uncertainty (i.e., negative uncertainty and positive uncertainty) or symmetric uncertainty if taking both sides of the standard uncertainty. Signed and symmetric uncertainty were both used in this work.

Each input variable was perturbed both up and down by its uncertainty value, so two separate cases were run for each input variable, in addition to the baseline case. In this analysis, no uncertainty was used for gaps as in NUREG/CR-7260 between cask materials.

This method only works in the local neighborhood around the baseline solution and only as long as the solution is fairly linear with respect to the inputs in that neighborhood. There are more complex global methods of determining uncertainty (e.g., Monte Carlo, Latin Hypercube), but

they typically require more knowledge of the probability distribution of the input variables than are generally available and, with a large number of input variables, require hundreds or perhaps thousands of cases to achieve statistical significance.

Fourteen input variables were used to quantify the uncertainty for the PCT, location of the PCT, and temperature values for at least seven locations in the fuel region and at least seven locations on the pressure vessel external wall. The geometry in this validation was well described and controlled, and as such, fluid gaps were not among the input variables used to quantify the uncertainty. This simulation has a large number of inputs, so several other variables could also have been evaluated, but the uncertainty in those input values was deemed to be of minor importance to the overall simulation uncertainty. Table 3-4 lists the input variables that were evaluated, along with their associated contribution to the uncertainty on PCT.

The input variables were assumed to be uncorrelated, so the total input uncertainty was calculated as the root mean square of all the individual input uncertainties in each column. Table 3-4 describes each input variable, its baseline value, and its associated uncertainty for the PCT, location of the PCT, temperatures in at least seven locations in the fuel region and at least seven locations on the pressure vessel external wall. The following input variables were used to quantify the uncertainty:

- heating power
- external heat transfer coefficient
- effective radial thermal conductivity used for porous media
- effective axial thermal conductivity used for porous media
- fuel hydraulic resistance used for porous media
- axial power profile shape
- air ingress
- fill gas pressure inside the canister
- water vapor molar fraction (transient case)
- ambient temperature
- emissivity values for basket, flange, pressure vessel, stand-off

For all cases, the inputs were perturbed both higher and lower by the amount of uncertainty in the input.

For the heat input and the ambient temperature, the uncertainties in the input values were provided with the BCs for each case. For many of the other inputs, measurement uncertainty was not provided, and in some cases, the input values were not provided. When simulation inputs are not provided, the modeler must make a calculation or an educated guess to obtain the input value, which introduces uncertainty into the simulation. In these cases, a conservative but reasonable estimate of the uncertainty in these input values was assumed.

The external heat transfer coefficient of 5 W/(m^2.K), obtained from correlations that were calculated based on Nusselt number correlations using the wall temperature and geometric configuration of the canister, were assumed to be accurate to within ± 2 W/(m^2.K). The viscous resistance coefficient used in the fuel region for the porous media model, provided as a simulation input, was assumed to have an uncertainty of ± 10 percent. Additionally, the fuel region effective thermal conductivity in the radial and axial directions—both inputs to the porous media properties in the simulation—were assumed to have an uncertainty of ± 10 percent and ± 20 percent, respectively.

The fuel power profile shape uncertainty was obtained from the experimental data involving the weight of nichrome wire as a function of height along the fuel. The uncertainty in the profile shape obtained experimentally was quantified using the standard deviation and confidence interval from statistical methods. The base case power profile and the other two profiles (i.e., skewed steep and skewed shallow) were used to obtain the input uncertainty on the power profile shape as shown in Figure 3-3.

Table 3-4 lists the emissivity values used for all materials in the input sensitivity study. All values were measured with the same type of instrument. When evaluating the uncertainty due to emissivity values, all emissivity values were perturbed higher and lower by 10 percent.

The uncertainties due to each of these input variables are shown in Table 3-4 for the steady-state (3 kW, 10 Torr) case. The dominant input uncertainties for temperature predictions in all cases were found to be the uncertainty in power profile skewness, air ingress molar fraction and external heat transfer coefficient.

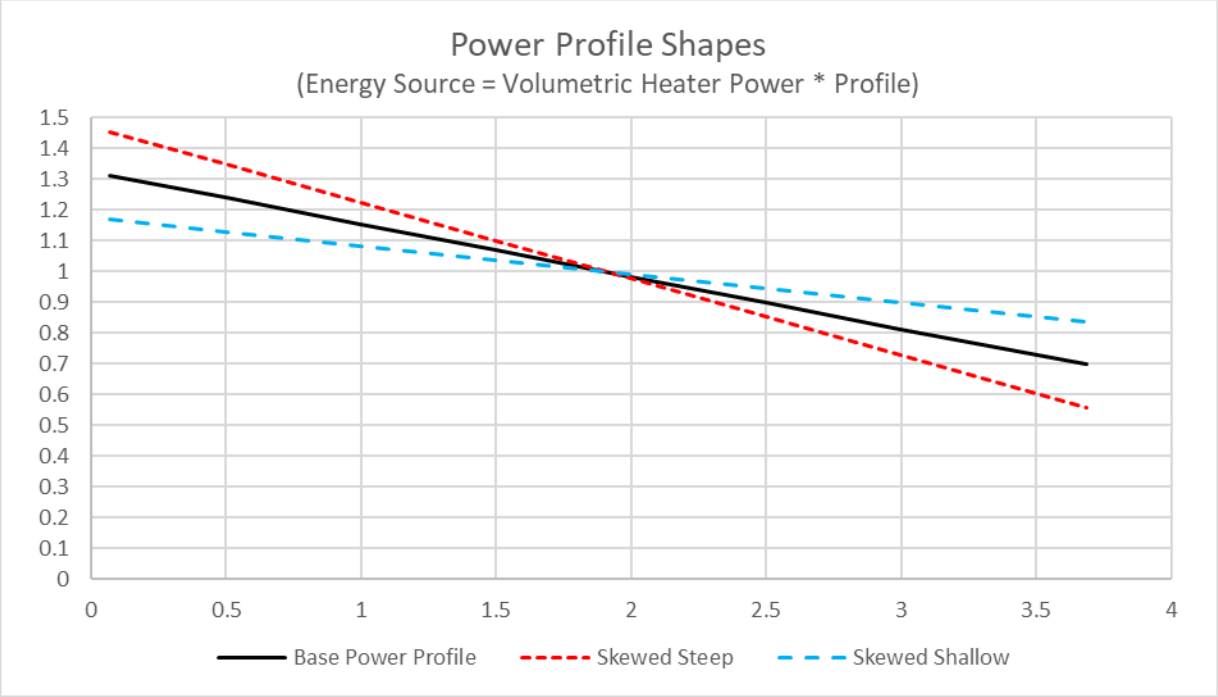


Figure 3-3 Power Profile Shapes Used for Input Uncertainties

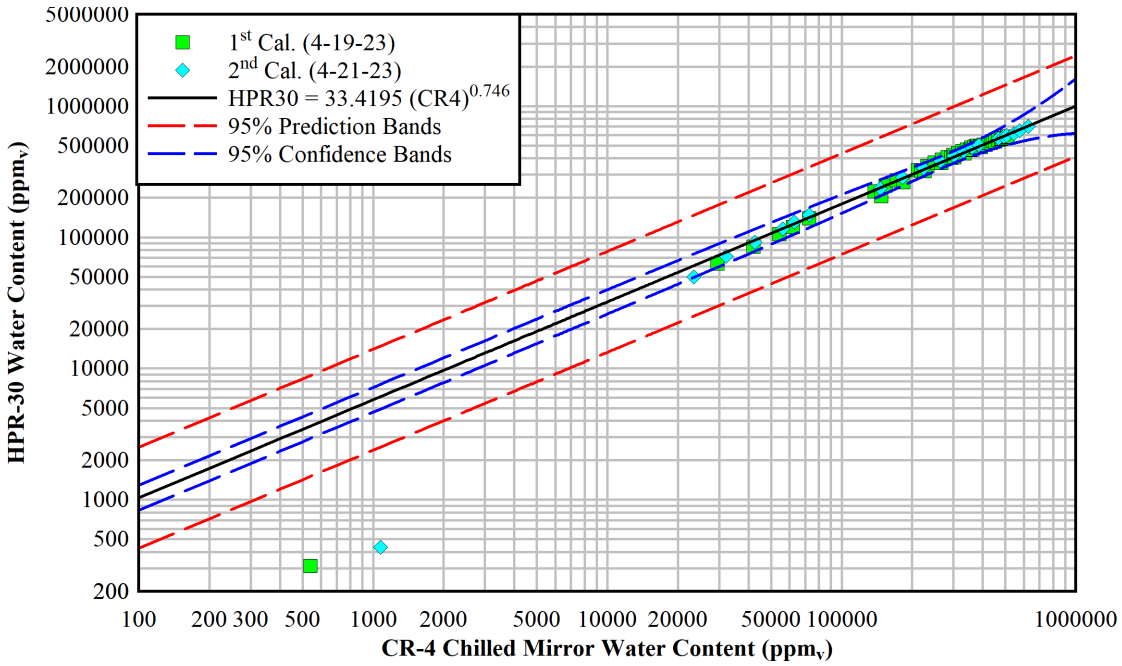


Figure 3-4 Log-Log Plot of the Power Law Fit of the Raw Water Content Measurements, along with the 95 Percent Confidence and Prediction Intervals (SAND2023-0976R)

For the transient vacuum drying case, uncertainty in the water molar fraction measurement is shown Figure 3-4 in SAND2023-0976R. At a water vapor molar fraction of 50 percent, the expanded uncertainty in molar fraction was more than 10 percent. At a water vapor molar fraction of 100 percent, the expanded uncertainty was more than 30 percent. These two values were used to assess the validation uncertainty at regulatory hold: 10 percent uncertainty was used for the vac2 step, as the water vapor molar fraction was measured at close to 50 percent, and 30 percent uncertainty was used for the vac3 step and the steps that followed, including the regulatory hold step, as the water vapor molar fraction was measured at 100 percent.

In the last SNL report (SAND2024) about the ADCS experiment, air ingress was an issue in the low subatmospheric pressure cases, such as 1 Torr and 0.1 Torr helium fill. No assessment was carried out to evaluate the amount of air ingress at these low pressures. Sensitivity CFD predictions were performed for different air leakage molar fractions for the helium-air mixture fill inside the canister. Among the sensitivities performed, 10 percent air molar fraction in the helium-air mixture inside the canister was assessed to be a viable and representative value of the air ingress molar fraction inside the canister. Consequently, the 10 percent air molar fraction was used as an input uncertainty to assess the validation uncertainty on the predicted temperature.

Table 3-4 Input Uncertainty for the (10 Torr, 3 kW) Steady-State Case

Input Variable	Units	Base Value	Input Uncertainty	PCT
External Heat Transfer Coefficient	W/(m^2 K)	5	± 2	+11.8 / -8.0 K
Decay Heat	W	3,001	± 24	+1.6 / -1.6 K
Vessel Pressure	kPa	1.333	± 1	+0.0 / -0.0 K
Ambient Temperature	K	297	± 3	+1.3 / -1.3 K
Fuel Viscous Resistance	1/m^2	1,000,000	± 100,000	+0.0 / -0.0 K
K_eff Radial	W/(m K)	Function of Temperature	± 10%	+10.2 / -8.5 K
K_eff Axial	W/(m K)	Function of Temperature	± 20%	+1.1 / -0.9 K
Pressure Vessel Emissivity	Unitless	0.43	± 10%	+2.7 / -2.3 K
Flange Emissivity	Unitless	0.115	± 10%	+0.1 / -0.1 K
Basket Emissivity	Unitless	0.3151	± 10%	+1.7 / -1.5 K
Power Profile	Unitless (Y-intercept)	1.3117	± 0.142	+14.1 / -13.2 K
			Total Input Uncertainty	**+21.4 / -17.9 K**
			Symmetric Uncertainty	**19.6 K**

3.3 Simulation Uncertainty Quantification

The total simulation uncertainty in Table 3-5 is a combination of the numerical uncertainty (Table 3-3) and the input uncertainty (Table 3-4). These simulation uncertainty calculations were repeated for all the cases for PCT, PCT location, the seven temperature values in the fuel region, and the seven temperature values along the pressure vessel external wall. These simulation uncertainties are the basis for the errors calculated on the baseline simulation results, which are compared to experimental results with associated experimental uncertainties.

Table 3-5 Simulation Uncertainty for PCT for the (10 Torr, 3 kW) Steady-State Case

	Positive (K)	Negative (K)	Symmetric (K)
Numerical Uncertainty	3.0	3.0	± 3.0
Input Uncertainty	21.4	17.9	± 19.6
Simulation Uncertainty	21.6	18.1	± 19.8

3.4 Experimental Uncertainty

The uncertainty and error inherent in an experimental result are critical for accurately interpreting the data. Therefore, this section provides estimates of the uncertainties in the experimental measurements. The general description of the method used and an explanation of the source of each reported measurement uncertainty are described in SNL reports SAND2023-01454R and SANDR-09746R, as follows:

The overall standard uncertainty of an indirect measurement *y*, dependent on *N* indirect measurements x_i, is defined below. The standard uncertainty associated with an indirect measurement is analogous to the standard deviation of a statistical population.

$$u^2 = \sum_{i=1}^{N} \left(\frac{\partial y}{\partial x_i} u_i \right)^2$$

Here, *u* is used to define the standard uncertainty of a measurement. The expanded uncertainty, *U*, is reported in SAND2023-01454R and SAND2023-09746R and defines the bounds that include 95 percent of the possible data. The expanded uncertainty is assumed to be defined as the product of the standard uncertainty and the Student's *t*-value. All uncertainty measurements are assumed to be based on a Student's *t*-distribution with no fewer than 30 measurements. The associated *t*-value for 95 percent intervals is 2.0 for 29 degrees of freedom. Therefore, the equation below shows the definition of the expanded uncertainty as used in the following sections for a 95 percent confidence interval:

$$U = t\text{-}value * u$$

Table 3-6 summarizes the expanded uncertainty for each measurement used in this report. SNL reports (SAND2022-12078R, SAND2023-01454R, SAND2023-09746R, and SAND2024) include further details.

Table 3-6 Summary of the Expanded Uncertainty Determined for Each Measurement

Measurement, x	Units	Expanded Uncertainty, U_x
Peak Cladding Temperature	K	6
Ambient Temperature	K	3
Ambient Pressure	kPa, abs	0.11
Helium Pressure	kPa, abs	1.6
Vacuum	kPa, abs	0.3
Voltage	V	0.02%
Current	A	0.02%
Power	kW	0.024

3.5 Validation Uncertainty Quantification

The total validation uncertainty is a combination of numerical uncertainty, the input uncertainty, and the experimental uncertainty, presented in Table 3-7. These calculations of validation uncertainty were repeated for all the cases for PCT, PCT location, temperature values for at least seven locations along the fuel region, and at least seven temperature values along the pressure vessel external wall.

Table 3-7 Total Validation Uncertainty for PCT for the (10 Torr, 3 kW) Steady-State Case

	Positive (K)	Negative (K)	Symmetric (K)
Numerical Uncertainty	3.0	3.0	± 3.0
Input Uncertainty	21.4	17.9	± 19.6
Experimental Uncertainty	6.0	6.0	± 6.0
Validation Uncertainty	22.4	19.1	± 20.7

For the PCT location uncertainty, only the experimental uncertainty of temperature measurement (i.e., 6 K, as shown in Table 3-6) was considered instead of the total validation uncertainty of the PCT shown in Table 3-7. To obtain the PCT location uncertainty, the axial profile of maximum fuel temperatures was examined to determine where along the profile the temperature fell below predicted PCT by at least the experimental temperature uncertainty. Table 3-8 shows the details of the calculations for the (3 kW, 10 Torr) steady-state case.

Table 3-8 Validation Uncertainty for PCT Location for the (10 Torr, 3 kW) Steady-State Case

	Information	Value	Information Source
1	CFD PCT (K)	583.0	From CFD
2	Experimental uncertainty (K)	6.0	From Table 3-6
3	CFD PCT lower bound temperature (K)	577.0	1 – 2
4	Experiment PCT height (m)	0.91	From experiment
5	CFD PCT height (m)	0.78	From CFD
6	Bottom height of lower bound temperature (m)	0.50	From CFD
7	Top height of lower bound temperature (m)	1.23	From CFD
8	Delta (m) (experiment – CFD)	0.13	4 – 5
9	Negative uncertainty (m)	-0.28	6 – 5
10	Positive uncertainty (m)	0.46	7 – 5
11	Symmetric uncertainty (m)	0.37	(10 + |9|)/2
12	Is CFD PCT location valid?	Yes	Delta ≤ Positive uncertainty

4 RESULTS AND DISCUSSIONS

4.1 Steady-State Computational Fluid Dynamics Model Validation Results

CFD analyses were performed for six steady-state cases in which the ADCS achieved steady conditions for 3.0 kW power and various canister pressures using helium as a fill gas. The canister pressures examined include 12 bar, 1 atm, 25 Torr (3.33 kPa), 10 Torr (1.333 kPa), 1 Torr (133.33 Pa), and 0.1 Torr (13.33 Pa). Additionally, the validation uncertainty (a combination of numerical, input, and experimental uncertainties; detailed in section 3.5) was evaluated for PCT, temperature in at least seven locations along the fuel region, and temperature in at least seven locations along the pressure vessel external wall, for all six cases.

Table 4-1 and Table 4-2 summarize all the steady-state cases' PCT and PCT location, including the validation uncertainty and whether the CFD predictions were able to validate the PCT and its location. Figure 4-1 and Figure 4-2 are grouped bar chart depictions of the information presented in Table 4-1 and Table 4-2. Table 4-3 shows the detailed calculations for the validation uncertainty for the 10 Torr steady-state case for the PCT, PCT location, temperature value at seven locations along the fuel region, and temperature value at seven locations along the pressure vessel external wall.

The tables and figures in this chapter are for cases with uninsulated flanges and no heat trace unless mentioned differently.

Appendix A provides detailed information about the validation uncertainty for all the steady-state cases and the transient vacuum drying case at the regulatory hold step.

Table 4-1 PCT for Steady-State Cases

Test Description	Test Data (K)	CFD Data (K)	Compare Error, E (K)	Negative Uncert. (K)	Positive Uncert. (K)	Valid?
Steady, 3 kW, 1200 kPa, Helium	456.2	467.8	-11.6	-19.5	24.8	**YES**
Steady, 3 kW, 1 atm, Helium	575.5	580.4	-4.9	-18.9	22.1	**YES**
Steady, 3 kW, 25 Torr, Helium	584.8	583.7	1.1	-19.1	22.4	**YES**
Steady, 3 kW, 10 Torr, Helium	590.4	583.0	7.4	-19.1	22.4	**YES**
Steady, 3 kW, 1 Torr, Helium	622.7	583.0	39.7	-19.1	51.6	**YES**
Steady, 3 kW, 0.1 Torr, Helium	597.2	583.1	14.1	-19.1	22.4	**YES**

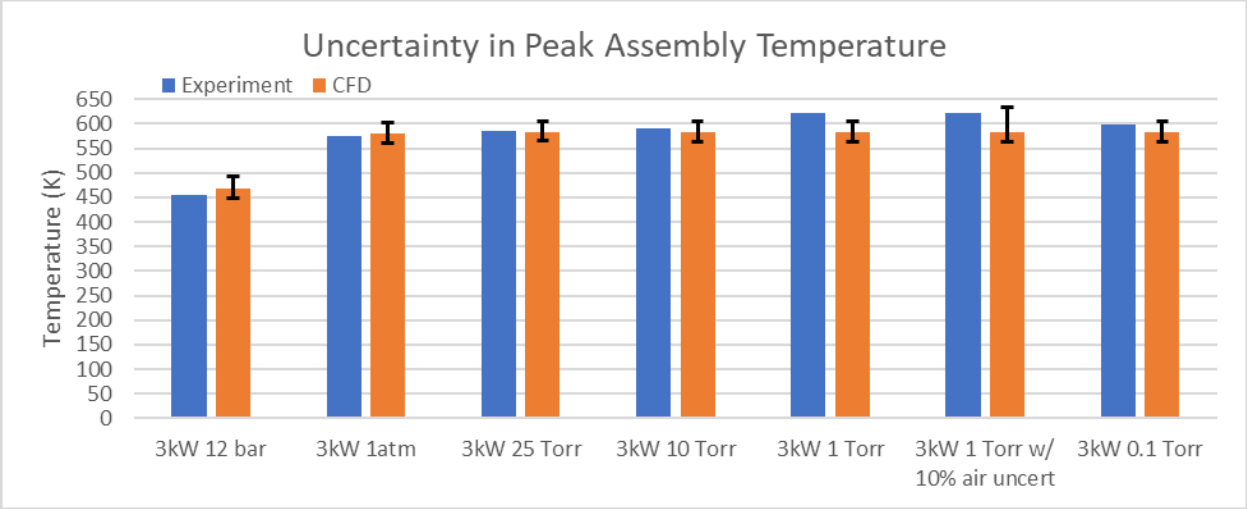


Figure 4-1 PCT Prediction (K) for Steady-State Cases

Table 4-2 PCT Location Prediction (m)

The calculation of uncertainty in PCT location used only the experimental temperature uncertainty and not the total PCT validation uncertainty, as section 3.5 explains.

Test Description	Test Data (m)	CFD Data (m)	Compare Error, E (m)	Negative Uncert. (m)	Positive Uncert. (m)	Valid?
Steady,3 kW, 1200 kPa, Helium	3.66	3.66	0.00	-0.43	0.16	YES
Steady,3 kW, 1 atm, Helium	0.91	0.94	-0.03	-0.32	0.28	YES
Steady, 3 kW, 25 Torr, Helium	0.91	0.78	0.13	-0.28	0.46	YES
Steady, 3 kW, 10 Torr, Helium	0.91	0.78	0.13	-0.28	0.46	YES
Steady, 3 kW, 1 Torr, Helium	0.91	0.78	0.13	-0.28	0.46	YES
Steady, 3 kW, 0.1 Torr, Helium	0.91	0.78	0.13	-0.28	0.46	YES

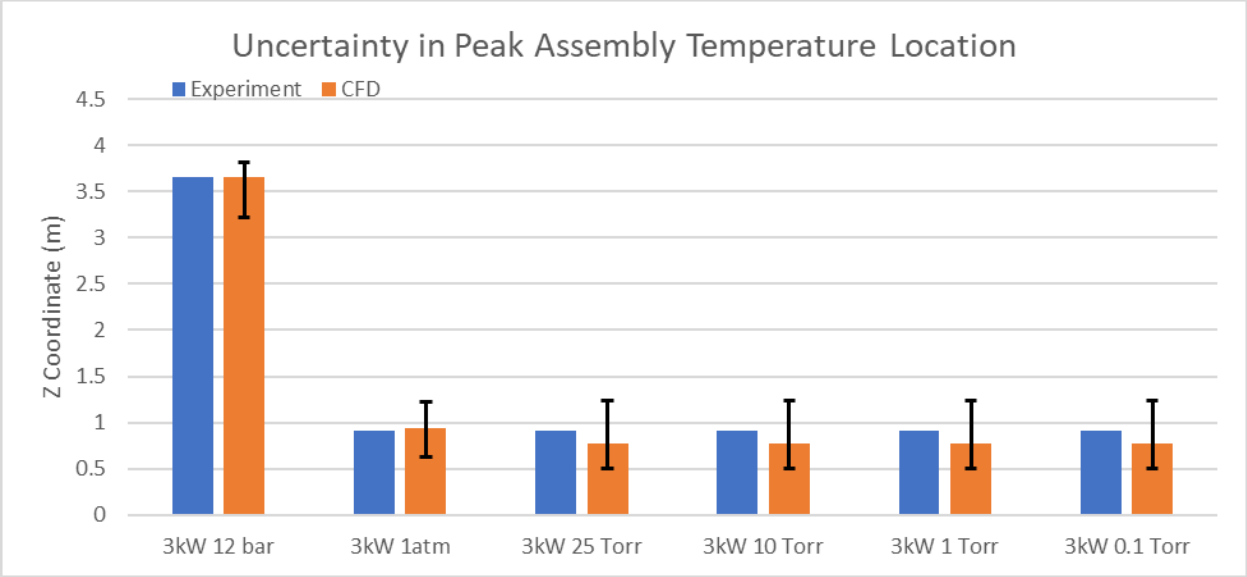


Figure 4-2 PCT Location Prediction (m) for Steady-State Cases

Table 4-1 and Figure 4-1 clearly show that PCT values for all the steady-state cases using the porous media base case are predicted within the validation uncertainty. Table 4-2 and Figure 4-2 also demonstrate that the PCT locations for all the steady-state cases were predicted within the experimental uncertainty.

Figure 4-3 through Figure 4-8 show temperature profiles as function of height for the maximum fuel temperature (i.e., temperature along the assembly centerline) and the pressure vessel external wall for all six steady-state cases. Included in these figures are the validation uncertainty bars calculated at seven or more points along the axial profiles. For the maximum fuel temperature profiles, the PCT and its location uncertainty bar are also shown.

Table 4-3 shows the detailed uncertainty quantifications for the PCT, PCT location, the temperature at seven locations (0.36 m, 0.91 m, 1.83 m, 2.44 m, 3.01 m, 3.66 m, 3.78 m) along the centerline of the fuel region, and the temperature at seven locations (0.56 m, 0.91 m, 1.83 m, 2.44 m, 3.01 m, 3.66 m, 4.01 m) along the pressure vessel external wall for the (10 Torr, 3 kW) steady-state case. These heights along the fuel region and the pressure vessel external wall were chosen to correspond with the locations of temperature measurements in the experiment, as shown in Figure 1-6 and Figure 1-10.

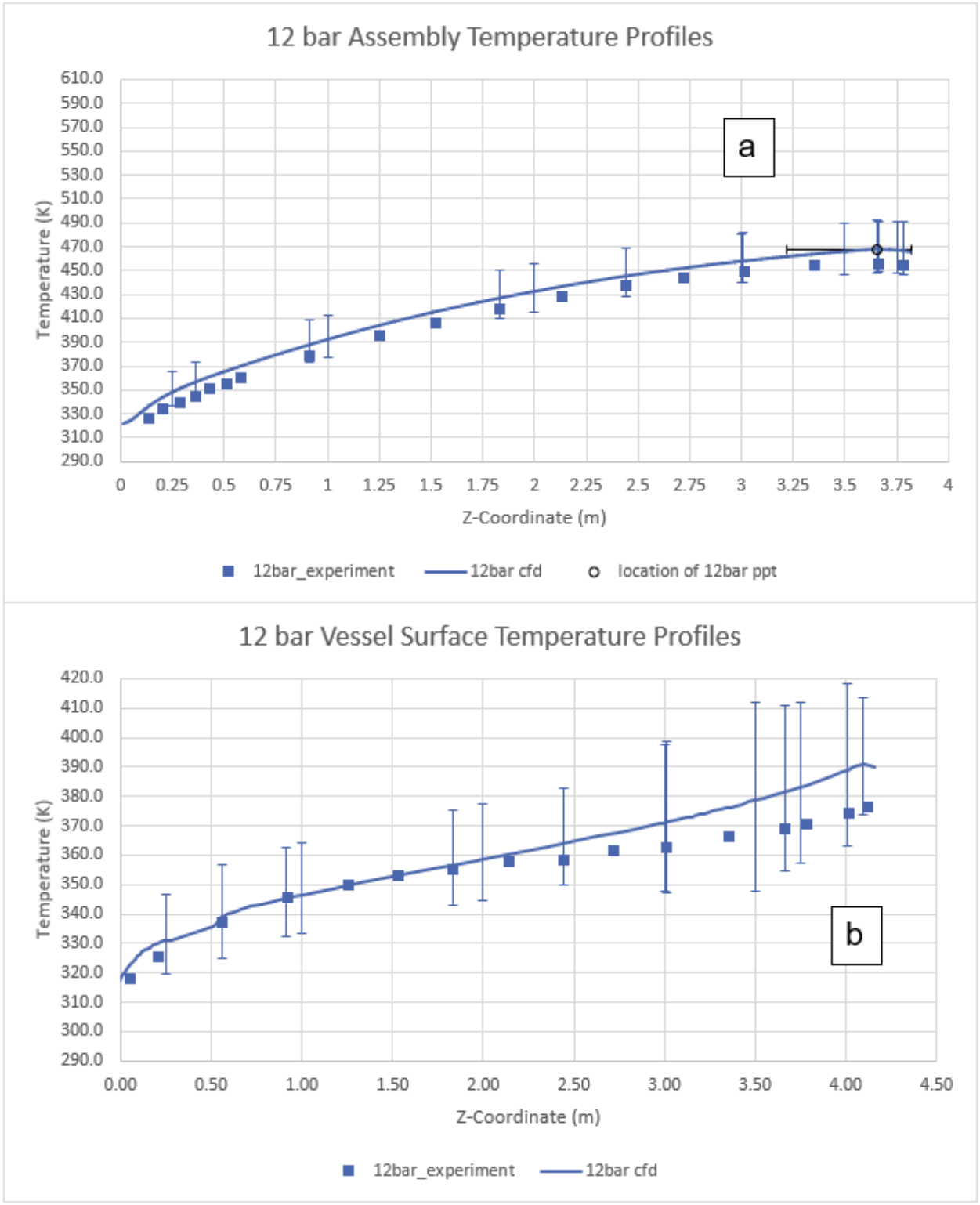


Figure 4-3 3 kW, 12 bar, Helium, Steady-State Case Profiles of (a) Maximum (i.e., Centerline) Fuel Temperature and (b) Pressure Vessel Temperature, with Validation Uncertainty Bars at Selected Locations

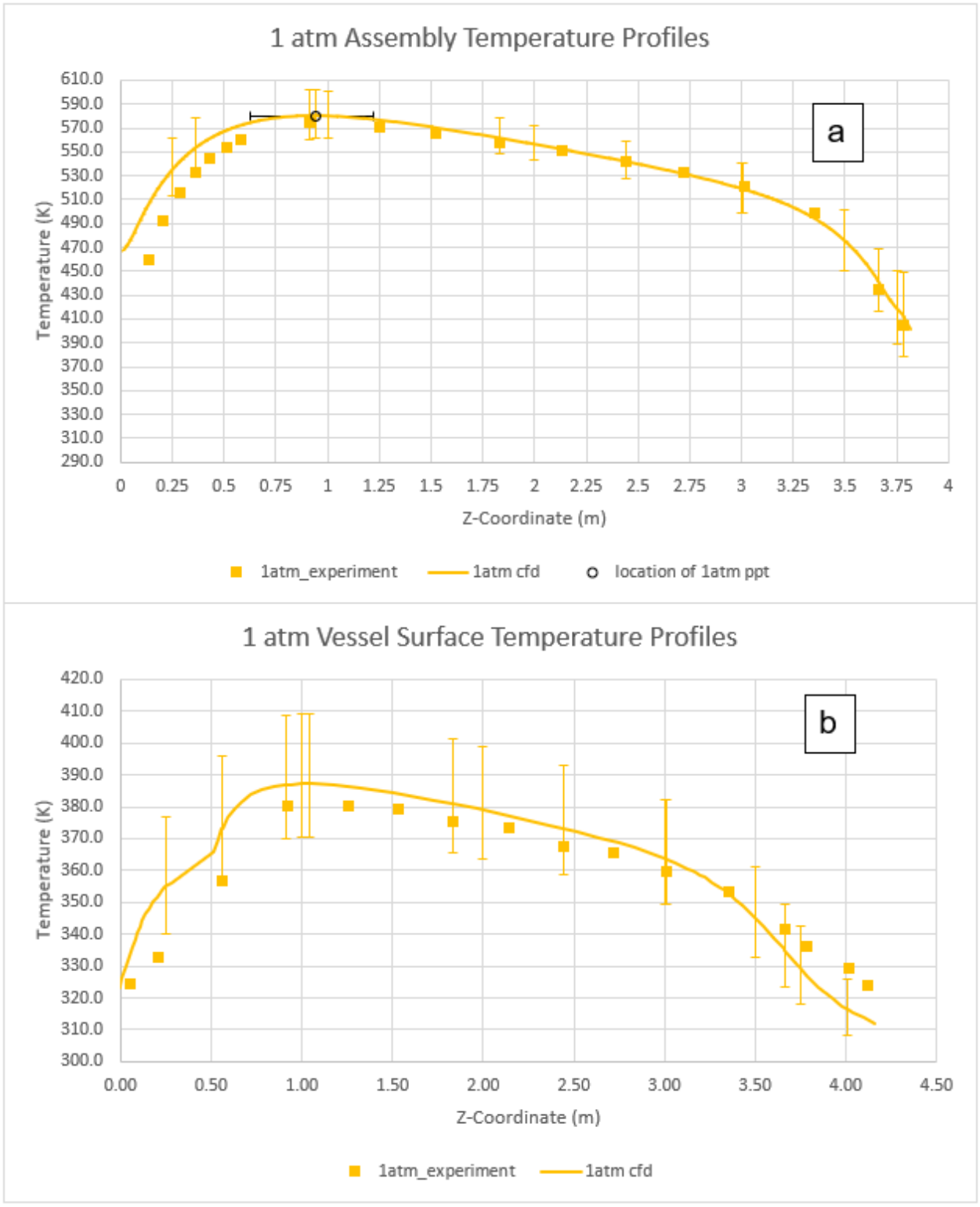


Figure 4-4 **3 kW, 1 atm, Helium, Steady-State Case Profiles of (a) Maximum (i.e., Centerline) Fuel Temperature and (b) Pressure Vessel Temperature, with Validation Uncertainty Bars at Selected Locations**

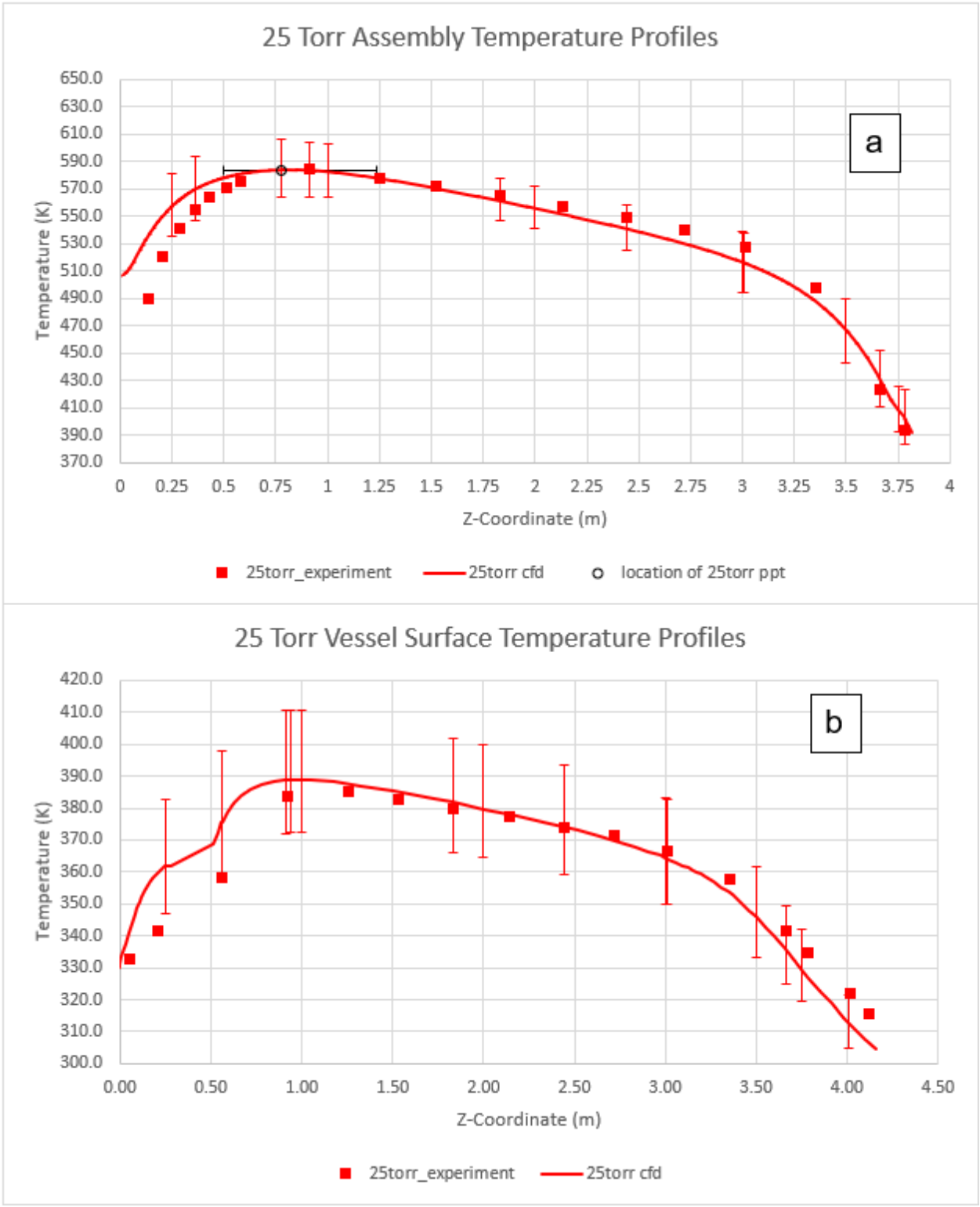


Figure 4-5 **3 kW, 25 Torr, Helium, Steady-State Case Profiles of (a) Maximum (i.e., Centerline) Fuel Temperature and (b) Pressure Vessel Temperature, with Validation Uncertainty Bars at Selected Locations**

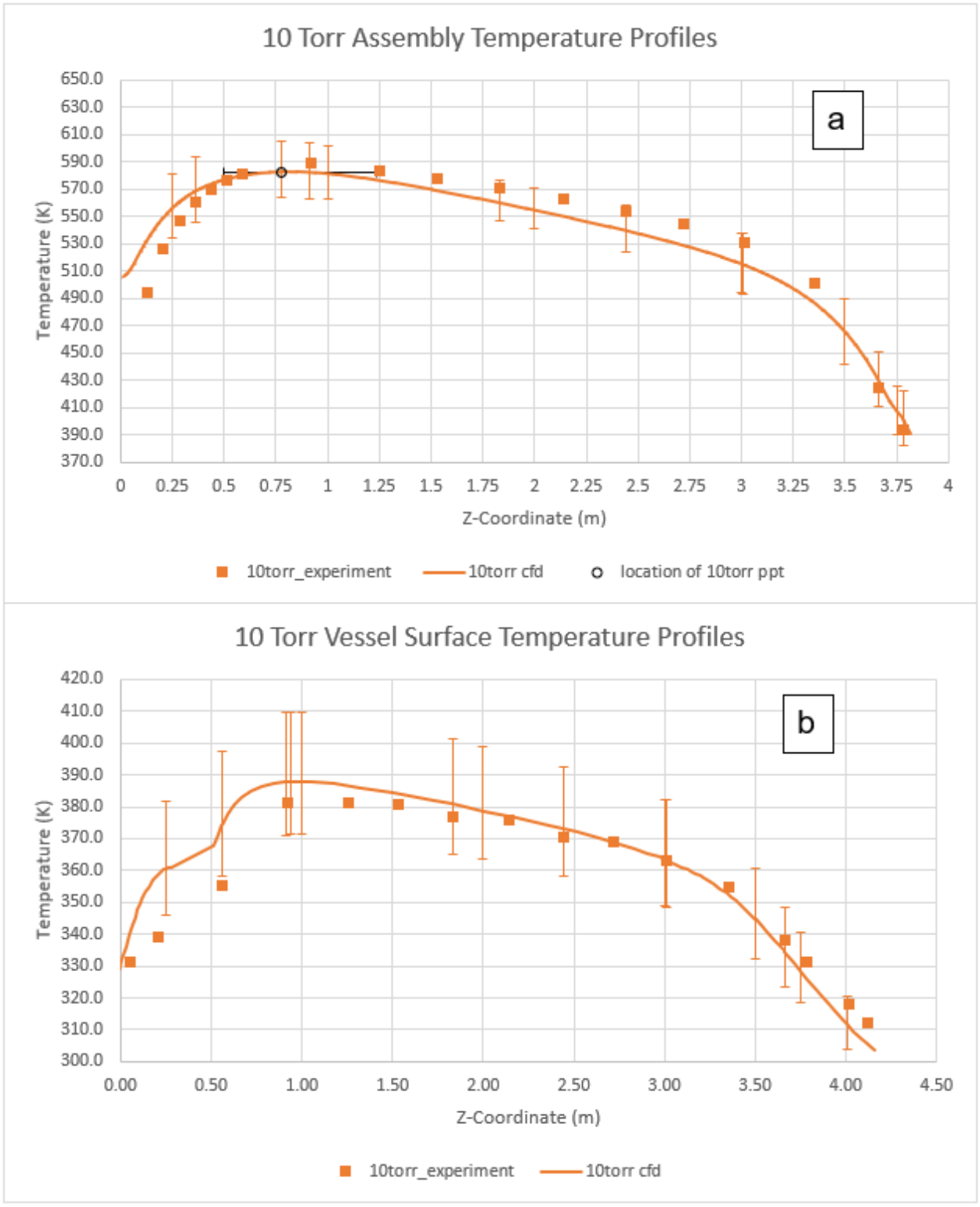


Figure 4-6 **3 kW, 10 Torr, Helium, Steady-State Case Profiles of (a) Maximum Fuel Temperature and (b) Pressure Vessel Temperature, with Validation Uncertainty Bars at Selected Locations**

Table 4-3 Test Results for 3 kW, 10 Torr, Helium, Steady-State Case

Parameter		Exp. Data	CFD Results	Exp – CFD	Negative Uncert.	Positive Uncert.	Sym Uncert.	Valid ?
PCT Location	Units							
Z value	m	0.91	0.78	0.13	-0.28	0.46	0.37	**YES**
PCT Value	K	590.4	583.0	7.4	-19.1	22.4	20.7	**YES**
Fuel Region	**Fuel Maximum Temperature as Function of Height**							
J9 Location								
z = 0.36 m	K	561.6	568.9	-7.3	-22.6	24.5	23.4	**YES**
z = 0.91 m	K	590.4	582.5	7.9	-18.9	21.2	20.0	**YES**
z = 1.83 m	K	571.2	560.1	11.1	-13.5	16.7	15.1	**YES**
z = 2.44 m	K	554.9	539.8	15.1	-15.6	18.1	16.8	**YES**
z = 3.01 m	K	531.9	514.8	17.1	-21.5	22.8	22.1	**YES**
z = 3.66 m	K	425.0	430.6	-5.6	-20.1	20.7	20.3	**YES**
z = 3.78 m	K	394.1	402.3	-8.2	-19.7	20.1	19.8	**YES**
Pressure Vessel	**Pressure Vessel External Temperature as Function of Height**							
z = 0.56 m	K	355.3	374.4	-19.1	-16.3	22.8	19.5	**YES**
z = 0.91 m	K	381.6	387.9	-6.3	-16.9	21.7	19.3	**YES**
z = 1.83 m	K	376.9	380.8	-3.9	-15.6	20.4	18.0	**YES**
z = 2.44 m	K	370.8	373.1	-2.3	-15.0	19.6	17.3	**YES**
z = 3.01 m	K	363.5	363.3	0.2	-14.7	18.7	16.6	**YES**
z = 3.66 m	K	338.2	334.6	3.6	-11.1	13.7	12.3	**YES**
z = 4.01 m	K	318.4	311.4	7.0	-7.8	9.1	8.3	**YES**

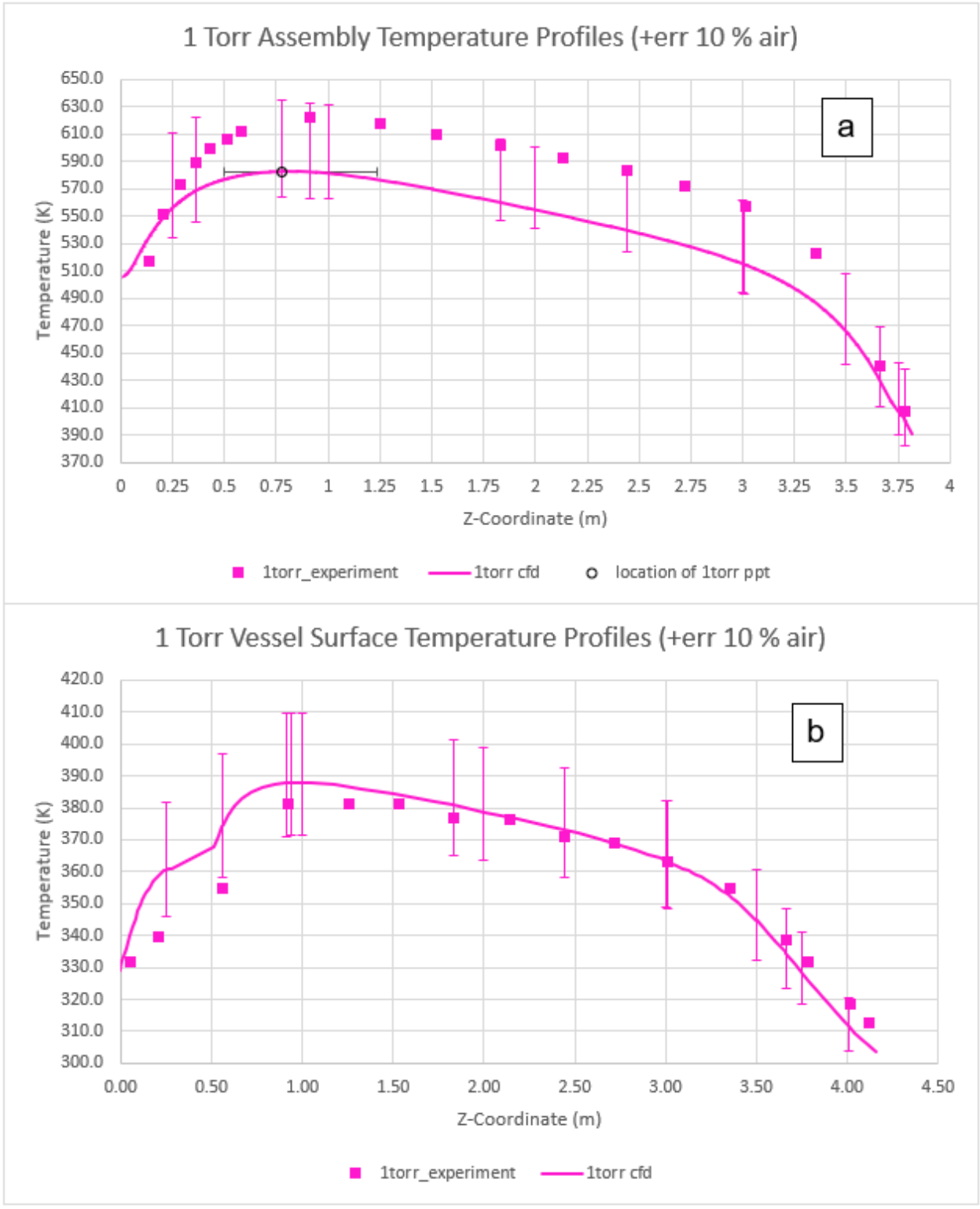


Figure 4-7 **3 kW, 1 Torr, Helium, Steady-State Case Profiles of (a) Maximum Fuel Temperature and (b) Pressure Vessel Temperature, with Validation Uncertainty Bars (Using Air Ingress Molar Fraction of 10 Percent as an Input Uncertainty)**

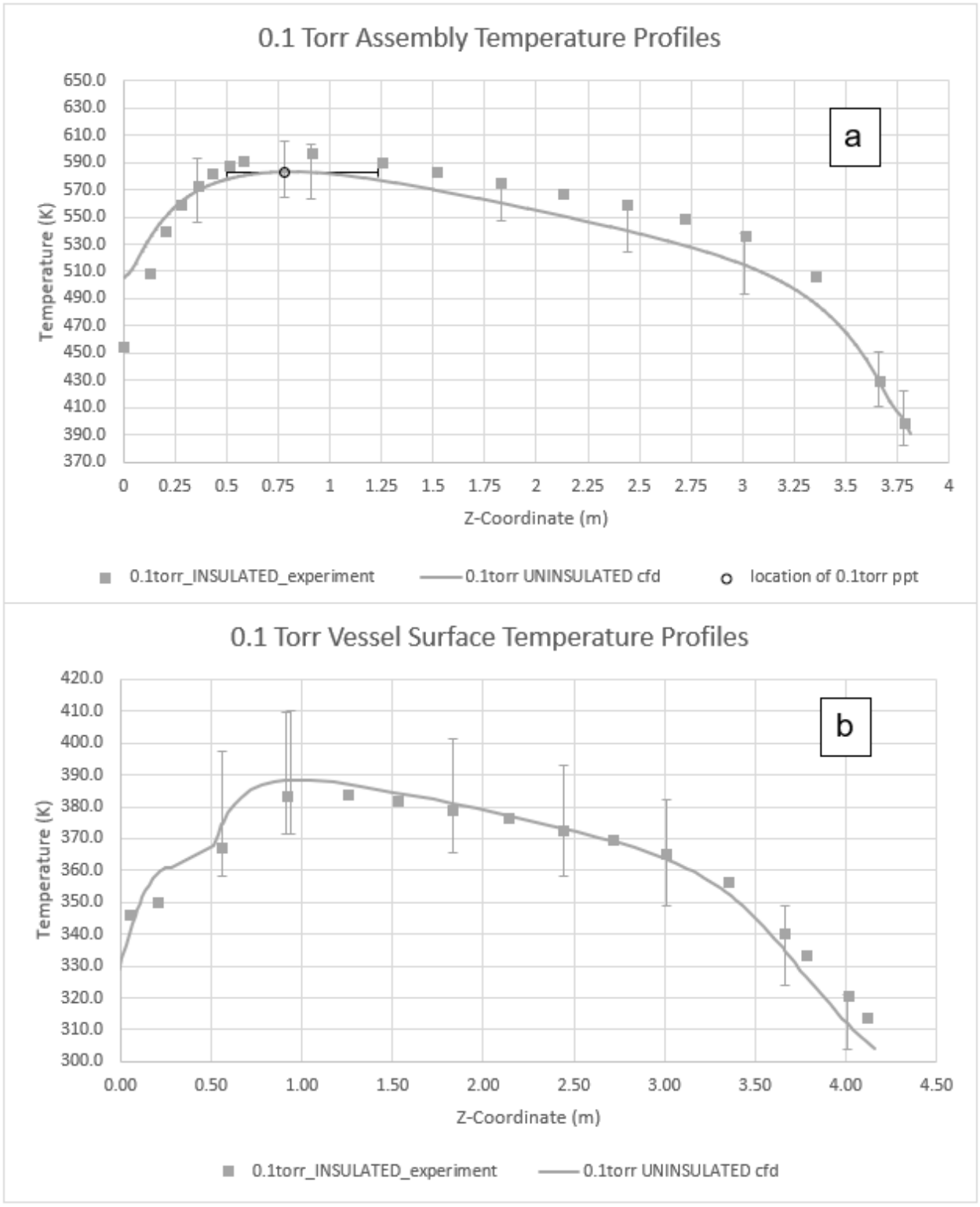


Figure 4-8 3 kW, 0.1 Torr, Helium, Steady-State Case Profiles of (a) Maximum Fuel Temperature and (b) Pressure Vessel Temperature, with Validation Uncertainty Bars (Experimental Data from the Insulated, Heat-Traced Flanges Case)

As shown in Figure 4-3 through Figure 4-8, the base case CFD model using porous media (as in commercial dry cask applications) predicted all the PCT values and the PCT location within the validation uncertainty. In addition, the CFD model predictions for most of the temperatures along the fuel region and the pressure vessel external wall were quite favorable. Table 4-3 shows the details of the CFD model predictions and the uncertainty quantifications at prescribed locations along the fuel region and the pressure vessel external wall (exchanging heat through convection and radiation to the surroundings), along with the PCT and PCT location. Table 4-3 clearly demonstrates that all the predictions were 100 percent favorable and validated within the quantified uncertainties shown in the table.

Concerning the steady-state predictions with a helium fill of 1 Torr, air ingress was included as an additional input uncertainty to evaluate the validation uncertainty as shown in Figure 4-7. This additional input uncertainty considered a helium-air mixture with an air molar fraction of 10 percent as the canister fill gas. This is the only case where the air ingress molar fraction was considered among the input variables used to quantify the uncertainty. When an air molar fraction of 10 percent was considered for the helium-air mixture inside the canister, the PCT, PCT location, and most of the targeted locations in the fuel region and vessel external wall temperature profiles agreed favorably with the experimental data within the quantified validation. Air ingress was an issue for the subatmospheric pressure tests that SNL mentioned in SAND2023-09746R.

When air ingress was not considered in the uncertainty quantification for 1 Torr steady-state case, the quantified uncertainties are shown in Figure 4-9. As the figure shows, the PCT location was well predicted but the values of the PCT and most of the fuel region temperature values were not. However, the predicted pressure vessel external wall temperature agreed favorably with the experimental data within the validation uncertainties calculated at discrete points along the profile, as shown in Figure 4-9. For the rest of this investigation concerning air leakage at these low subatmospheric pressures, only the fuel region was used, as the temperature values on the pressure vessel external wall were not affected (Figure 4-9).

To deepen this investigation of air ingress, we asked whether the underprediction shown in Figure 4-9 was due to air leakage inside the canister or other reasons. One possible reason could be that helium at low subatmospheric pressure (below 10 Torr) exhibits a low thermal conductivity, as shown in Figure 4-17 in Ganta et al. As Figure 4-17 illustrates, the thermal conductivity of helium can be as low as 0.025 W/(m*K) at a pressure of 1 Torr—as low as the thermal conductivity of air at atmospheric conditions. According to Ganta et al., 2011 (the source for Figure 4-17), when gas flow reaches very high Knudsen (Kn) number, it will reach a rarefied state and the continuum assumption will no longer be valid. The Knudsen number is the ratio of mean free path of the gas molecules to the system characteristic length, and it is usually used to classify whether the gas flow is rarefied. If $Kn < 0.01$, then the flow can be considered as a continuum, and if $0.01 < Kn < 10$, then the flow is considered transitional (slip flow). Otherwise, when $Kn > 10$, it will be in a rarefied state (free molecular flow).

To check whether this was a valid issue to consider, the thermal conductivity for helium from Figure 4-17 was used without considering any air leakage into the canister. Figure 4-11 shows the CFD run using this assumption, illustrating the fuel region's maximum temperature profile as a function of height. The PCT from this assumption is 717 K, overpredicting the PCT from the experiment by almost 94 K. This assumption cannot be acceptable due to the large discrepancy and shift between the experimental data and the CFD predictions in the PCT value, as well as the entire fuel region maximum temperature profile as function of height. The postulation that helium has a lower thermal conductivity and is behaving in rarefied state (Ganta et al.) in this case is not a plausible explanation for the discrepancy.

Data from the National Institute of Standards and Technology (NIST) Chemistry WebBook, SRD 69, "Thermophysical Properties of Fluid Systems", shows that the thermal conductivity of helium is independent of pressure at least down to 0.1 Torr. The helium thermal conductivity values for low subatmospheric pressures of 1 Torr and 0.1 Torr are equal to the values at atmospheric conditions for temperatures relevant to vacuum drying conditions. This reference completely negates the thermal conductivity values in Figure 4-17 (Ganta et al.). The NIST Chemistry WebBook was used for all fluid thermophysical properties in this report.

Additional sensitivity predictions were made for the air ingress issue referenced in SAND2024 report. First, the CFD base case was run without the momentum equations, and identical results to the base case predictions were obtained (Figure 4-11). In hindsight, this outcome was predictable, as velocity values (momentum) at 1 Torr pressure are very low and have no effect on the heat exchange of the dry cask system. At this low pressure, the mass of helium inside the canister is very low, and thus the convection is low or negligible. The only modes of heat transfer at 1 Torr will be conduction and radiation heat transfer.

To see the effect of the quantity or the rate of air ingress/leakage into the canister on the thermal performance of the dry cask, four CFD runs using helium-air mixtures with air molar fractions of 5 percent, 10 percent, 40 percent, and 100 percent (i.e., air only) were run. Figure 4-11 shows the predictions of these cases. As the air molar fraction increased, the PCT and the entire profile of maximum temperature in the fuel region shifted upward. The higher temperature in the fuel region is attributed to the lower thermal conductivity of the helium-air mixture inside the cask; the higher the air molar fraction, the lower the mixture thermal conductivity will be. As the thermal conductivity of the gas fill is lower, less heat is conducted out, leading to higher temperatures in the fuel region inside the canister. The simulation results suggest that the plausible air ingress that occurred in the experiment caused an air molar fraction close to 10 percent. The air leakage equivalent to 10 percent air molar fraction predicted a higher PCT much closer to the experimental data.

The discrepancy between the predicted PCT and the measured is 6 K as shown in Figure 4-7(a) and Figure 4-11. As such, air ingress equivalent to an air molar fraction of 10 percent in the helium-air mixture was used to obtain the validation uncertainty shown in Figure 4-7. For reference, the thermal conductivity of this mixture is roughly 33 percent less than that of pure helium, far less severe than the 80 percent reduction seen in Figure 4-17. Uncertainty bands due to air ingress equivalent to 5 percent and 40 percent air molar fraction in the helium-air mixture are shown in Figure 4-10(a) and Figure 4-10(b). The air ingress equivalent to 40 percent air molar fraction in the helium-air mixture predicted a substantially higher PCT. The discrepancy between this case's predicted PCT and the measured is 66 K as shown in Figure 4-10(b) and Figure 4-11, which is excessive and difficult to accept. The air ingress equivalent to 5 percent air molar fraction in the helium-air mixture predicted a lower PCT than that seen in the experiment. Figure 4-10(a) and Figure 4-11 show the 13 K discrepancy between the predicted PCT and the measured PCT.

To make the point about air ingress, experimental data and CFD predictions for the cases that used heat-trace cables on the flanges were also considered. There was no discernable difference between the results of the two case types, as shown in Table 4-4 and Figure 4-12 through Figure 4-16. CFD predictions clearly show that there is no major difference in predictions when the pressure is at 1 atm or below. The main difference between data at higher and lower pressures is that convection heat transfer is greater at higher pressure, leading to a lower PCT and temperature profile. As the pressure reaches 1 atm, momentum equations will not play a major role; most of the heat transfer out of the cask will be done through conduction and radiation. Thus, we can reasonably assume that the PCT and fuel temperature profile will be almost

unchanged, which is supported by CFD predictions in Table 4-4 and in Figure 4-12 through Figure 4-16.

However, the experimentally measured PCT increased almost linearly and without showing asymptotic behavior as pressure decreased. The reason for this thermal response was air leakage into the canister, which changed the composition within, lowering its thermal conductivity, as discussed before. In Figure 4-12, Figure 4-13, and Figure 4-14 for pressures of 12 bar, 1 atm, and 10 Torr, the two types of BCs on the flanges (i.e., isothermal flange external walls when heat-trace cable is used and heat exchange from the flange external walls by convection and radiation to surroundings when heat-trace cable is not used on the flanges) do not make significant differences in the CFD predictions or the experimental data. For the 1 Torr helium pressure (Figure 4-15), CFD predictions for both types of BCs are quite similar. The experimental data without heat-trace cable shows a greater discrepancy. The experimental data using the heat-trace cable BCs showed a closer agreement through the temperature profile. As such, it is concluded that more air ingress occurred for the case not using the heat-trace cable. The experimental data from the heat-trace cable case had less air leakage, but still some, as the PCT should be closer to that measured in the 10 Torr case. The PCT for all the subatmospheric pressure cases should not be beyond 586 ± 6 K. The 1 Torr pressure case without heat-trace cable had a PCT of 622.7 K, exceeding the expected value due to air ingress.

Figure 4-16 shows CFD sensitivity predictions at 0.1 Torr with heat-trace cable to obtain isothermal BCs at the external flange walls. One sensitivity involved the use of helium thermal conductivity from Ganta et al., 2011, shown in Figure 4-17. This sensitivity showed a major overprediction of the temperature profile. The PCT was overpredicted by 178 K. This is further evidence that the helium is not in a rarefied state at these vacuum pressures and that the findings in Ganta et al. are overly conservative for cask vacuum drying applications, even down to vacuums of 0.1 Torr. The next sensitivity shown in Figure 4-16 is for the air fill (i.e., 100 percent air) CFD case, which overpredicted PCT by 125 K. The experimental data is close to the CFD prediction for both types of BCs when using the helium thermal conductivity from the NIST Chemistry WebBook.

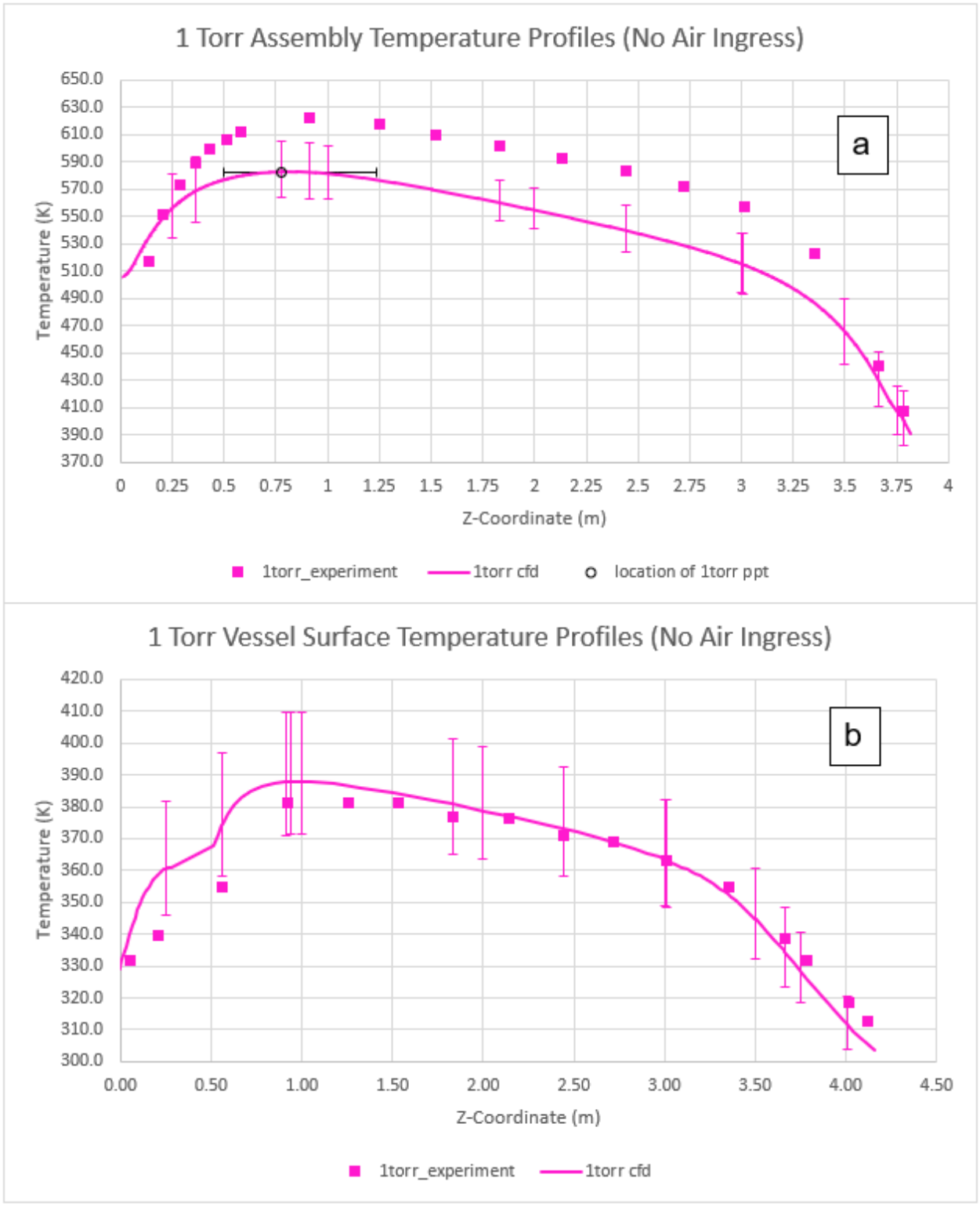


Figure 4-9 **3 kW, 1 Torr, Helium without Air Ingress, Steady-State Case Profiles of (a) Maximum Fuel Temperature and (b) Pressure Vessel Temperature, with Validation Uncertainty Bars**

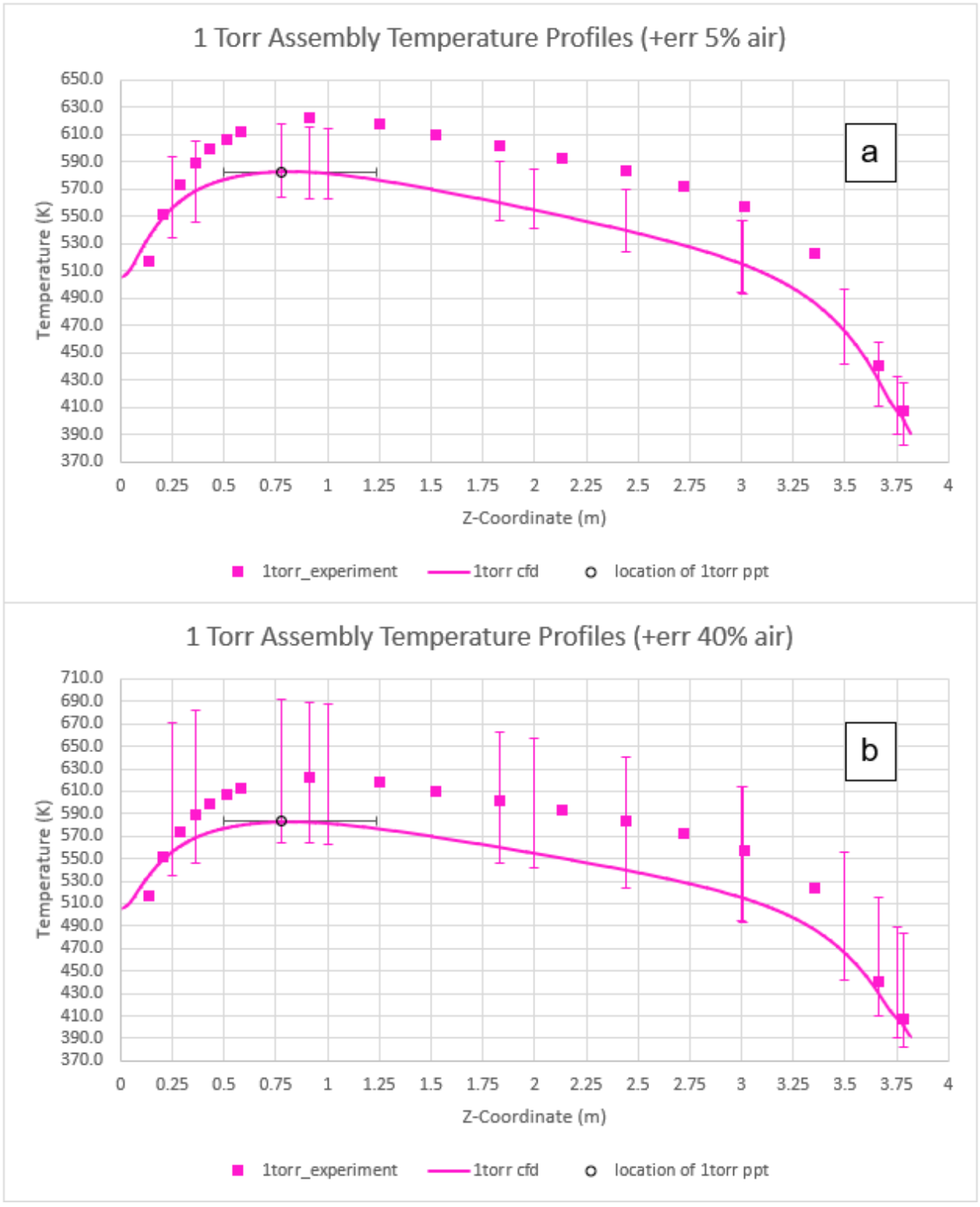


Figure 4-10 Fuel Max Temperature Profiles (a) With Air Ingress Molar Fraction of 5 Percent and (b) With Air Ingress Molar Fraction of 40 Percent for the 3 kW, 1 Torr, Helium, Steady-State Case, with Validation Uncertainty Bars

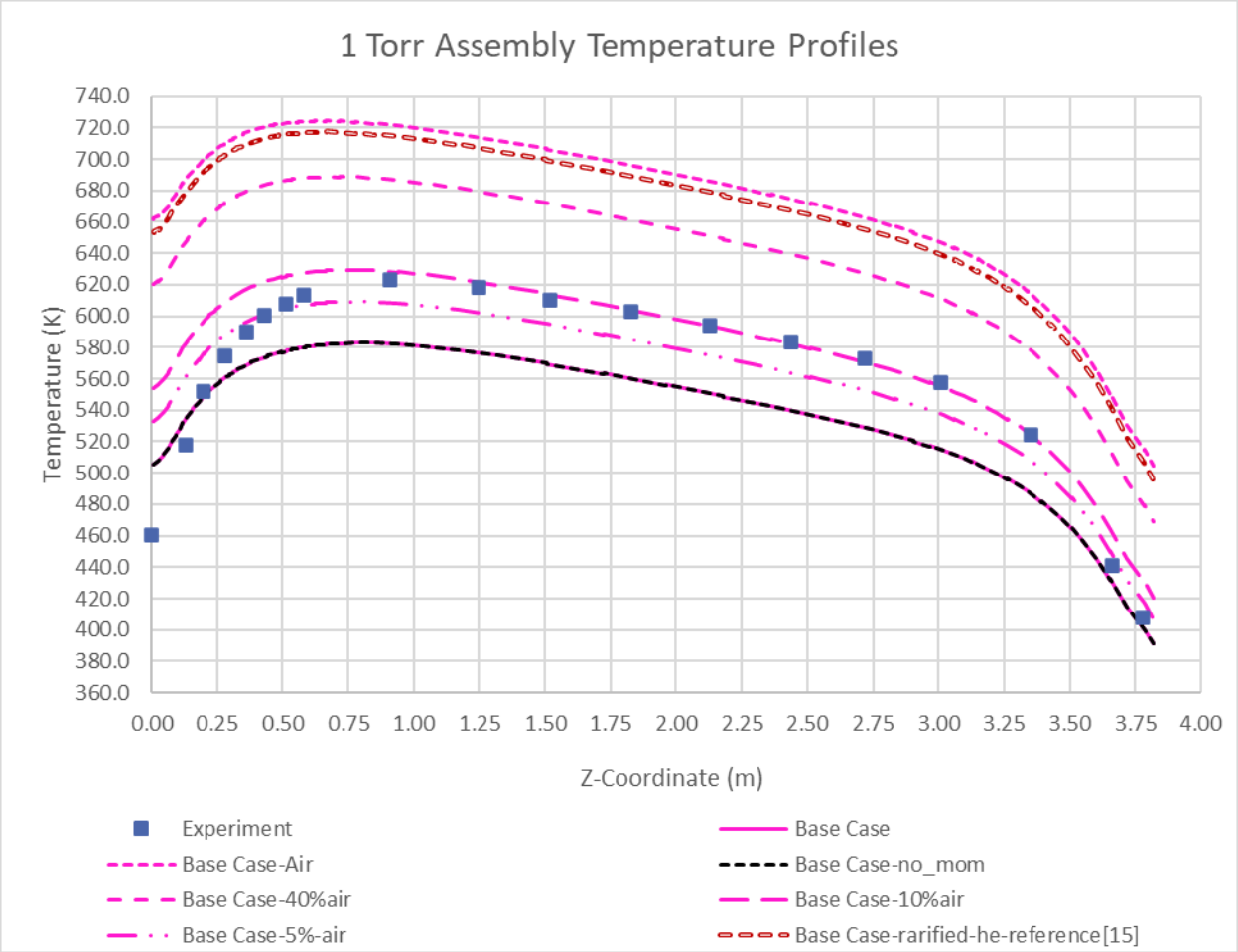


Figure 4-11 3 kW, 1 Torr Sensitivity Predictions for Fuel Max Temperature Profiles Using Porous Media Base Case

Table 4-4 Experimental Data and CFD PCT for Steady-State Cases Using Two Types of Boundary Conditions at the Flanges

BC at Flanges		12 bar	1 atm	25 Torr	10 Torr	1 Torr	0.1 Torr
Uninsulated flanges	Experiment	456.2	575.5	584.8	590.4	622.7	
Uninsulated flanges	CFD	467.8	580.4	583.7	583.0	583.0	583.1
Insulated flanges with heat-traced cable	Experiment	459.6	576.4		586.2	593.4	597.2
Insulated flanges with heat-traced cable	CFD	468.9	578.5	580.9	580.2	580.2	580.4

Note that the actual heat provided in the CFD simulations matched the average reported by SAND2022-12078R, SAND2023-01454R, SAND-2023-09746R, and SAND2024. The 25 Torr simulations therefore use slightly greater heater power than the other cases, leading to marginally greater PCT compared to the lower-pressure simulations.

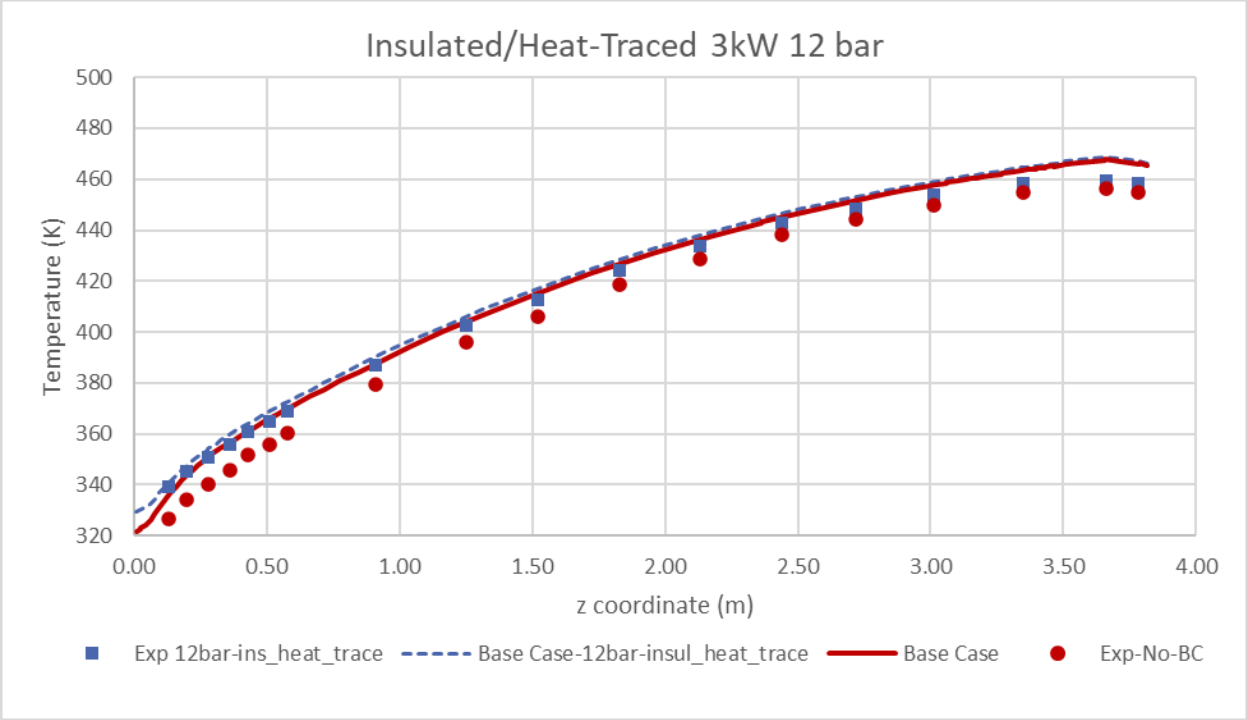


Figure 4-12 Comparison Between CFD and Experiment for Insulated, Heat-Traced Flanges and without (3 kW, 12 bar)

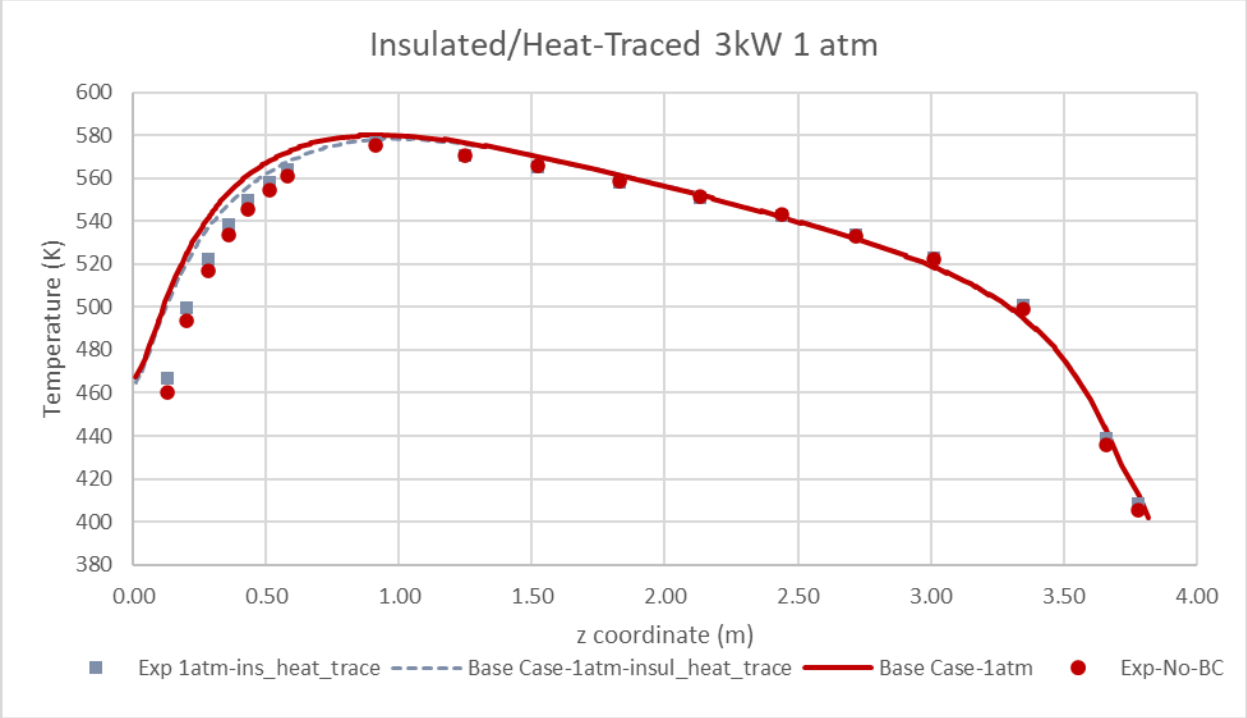


Figure 4-13 Comparison Between CFD and Experiment for Insulated, Heat-Traced Flanges and without (3 kW, 1 atm)

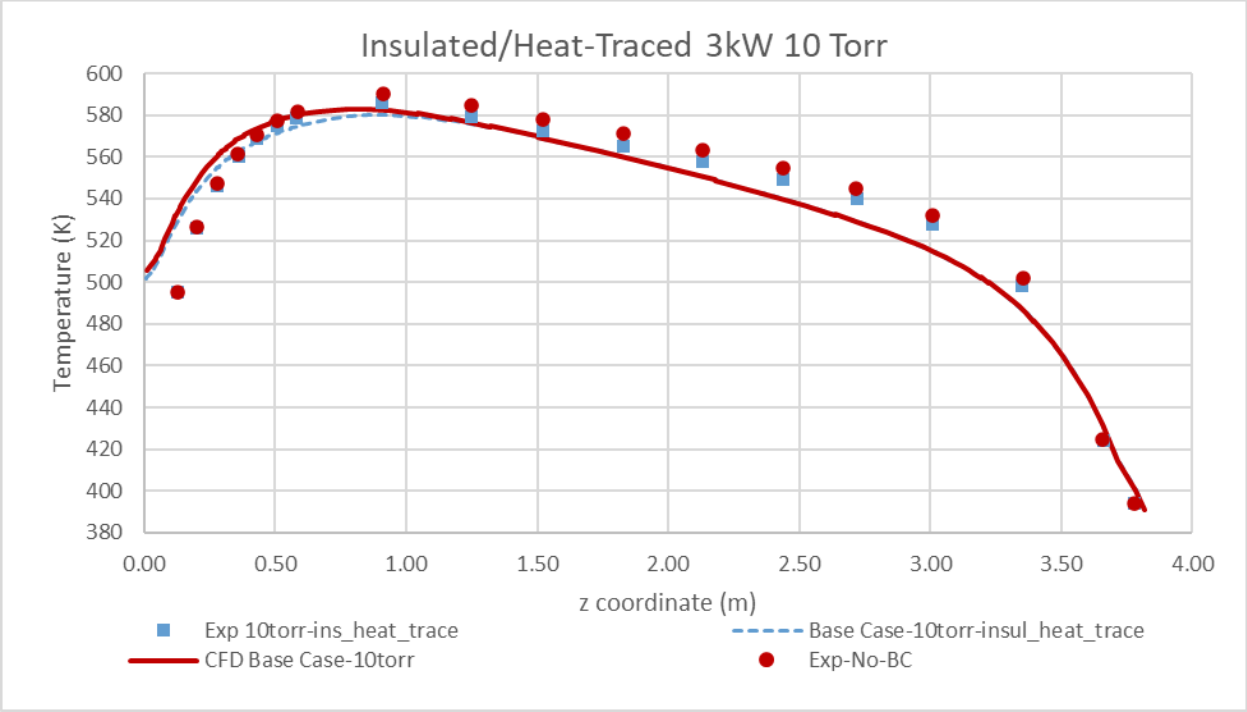


Figure 4-14 Comparison Between CFD and Experiment for Insulated, Heat-Traced Flanges and without (3 kW, 10 Torr)

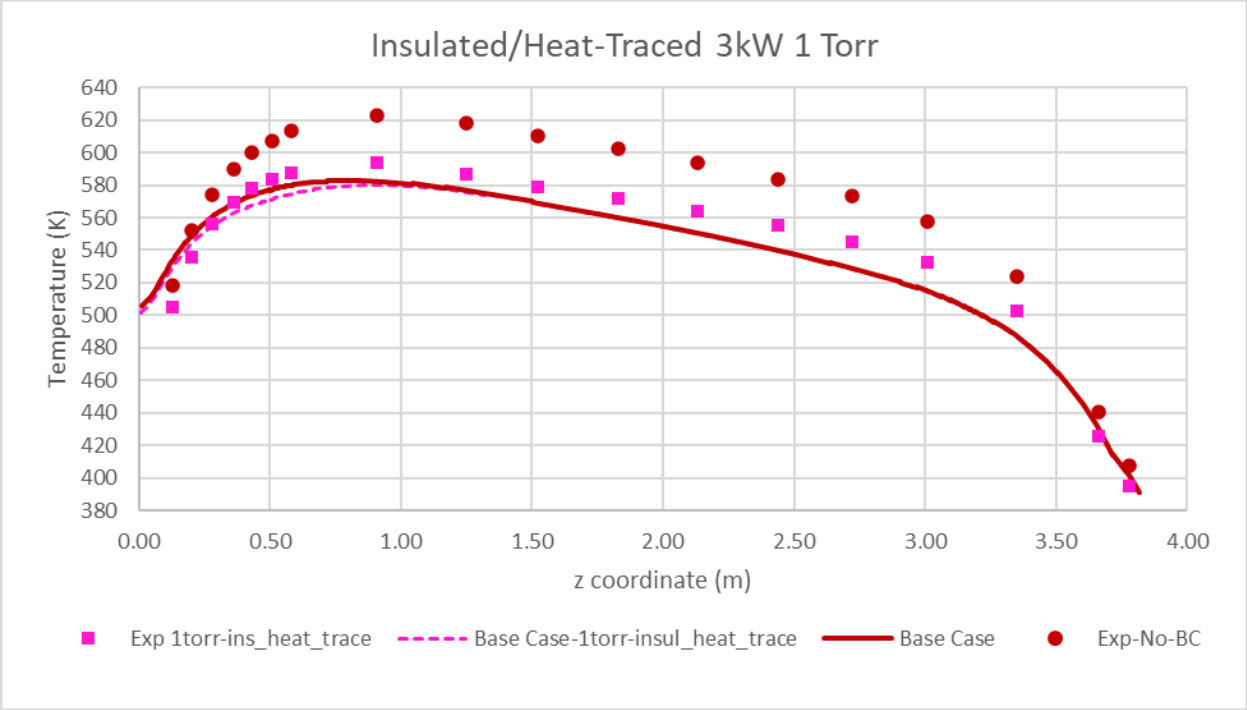


Figure 4-15 Comparison Between CFD and Experiment for Insulated, Heat-Traced Flanges and without (3 kW, 1 Torr)

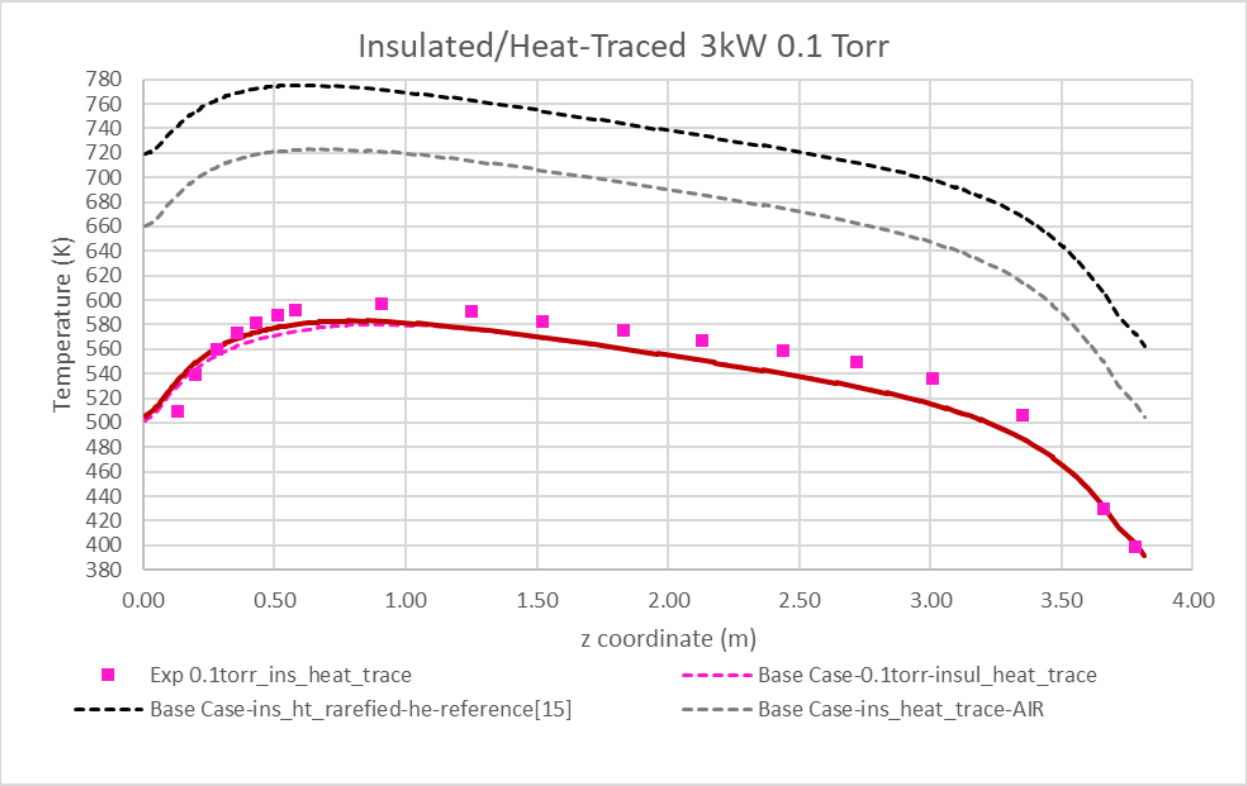


Figure 4-16 Comparison Between CFD and Experiment for Insulated, Heat-Traced Flanges and without (3 kW, 0.1 Torr)

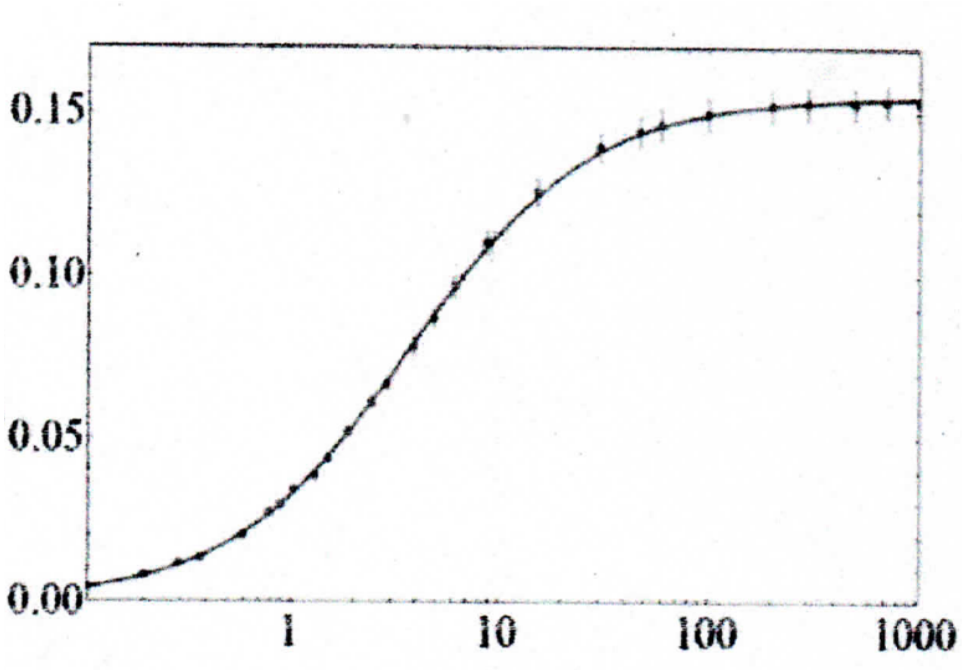


Figure 4-17 Thermal Conductivity (W/(m.k) of Helium Versus Pressure (Torr) from Figure 7 in Ganta et al., 2011

4.2 Transient Vacuum Drying Validation

This section validates the transient vacuum drying steps described in Table ES-1 and Figure ES-1. Validation uncertainties were calculated for the PCT at the regulatory hold step, with and without including a water vapor molar fraction uncertainty of 30 % as shown in Figure 4-18 and Figure 4-19, respectively. Validation uncertainties were also calculated for the fuel region maximum/centerline temperature and pressure vessel external temperature profiles versus height, as shown in Figure 4-20(a) and Figure 4-20(b). Table 4-5 shows the detailed calculations for the validation uncertainties for the PCT, PCT location, maximum temperature values in fuel region at seven discrete locations, and temperature values on the pressure vessel external wall at seven discrete locations.

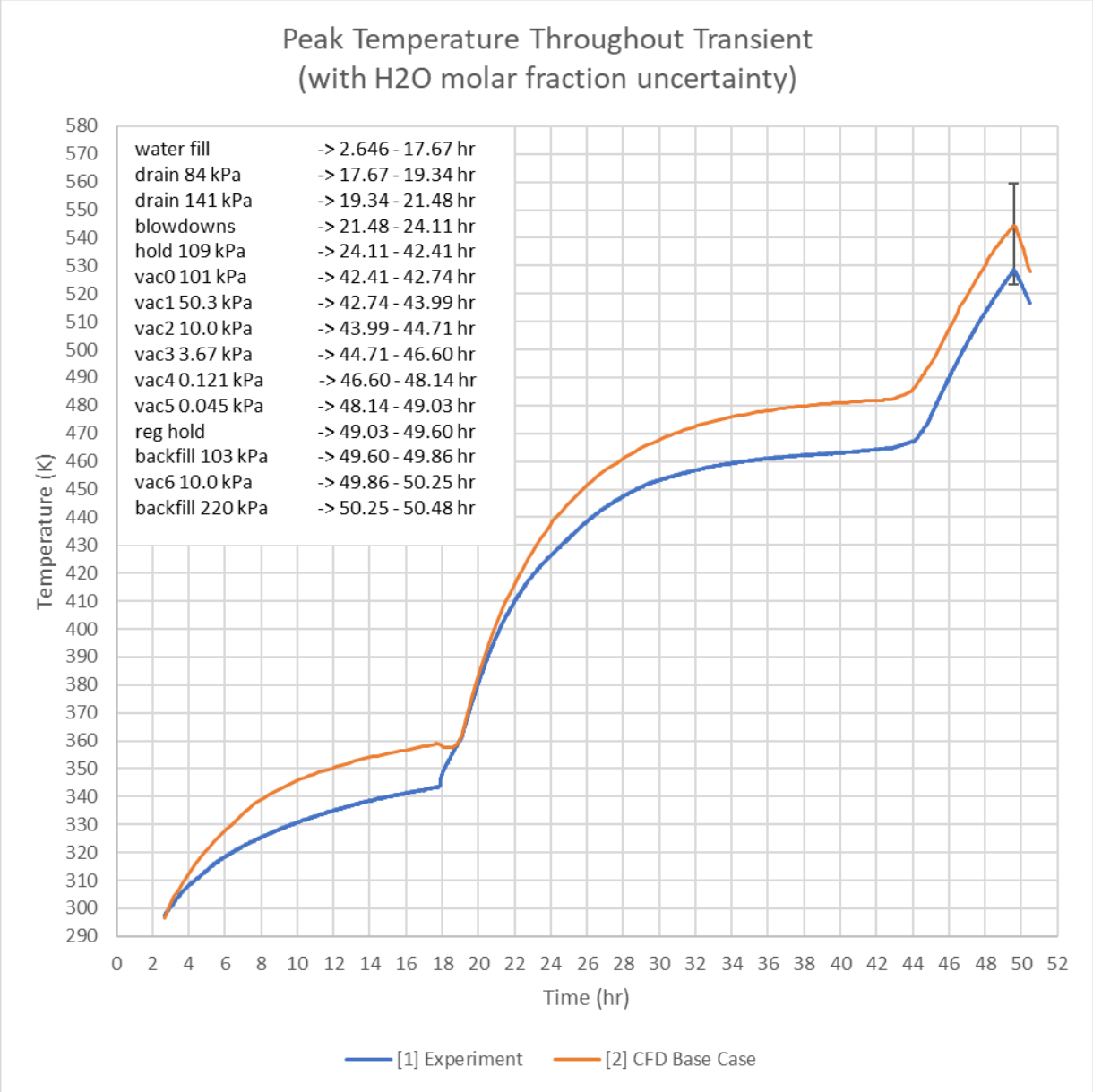


Figure 4-18 PCT as a Function of Time for the 1.483 kW Transient Vacuum Drying Case, Including 30 Percent Water Vapor Molar Fraction Input Uncertainty

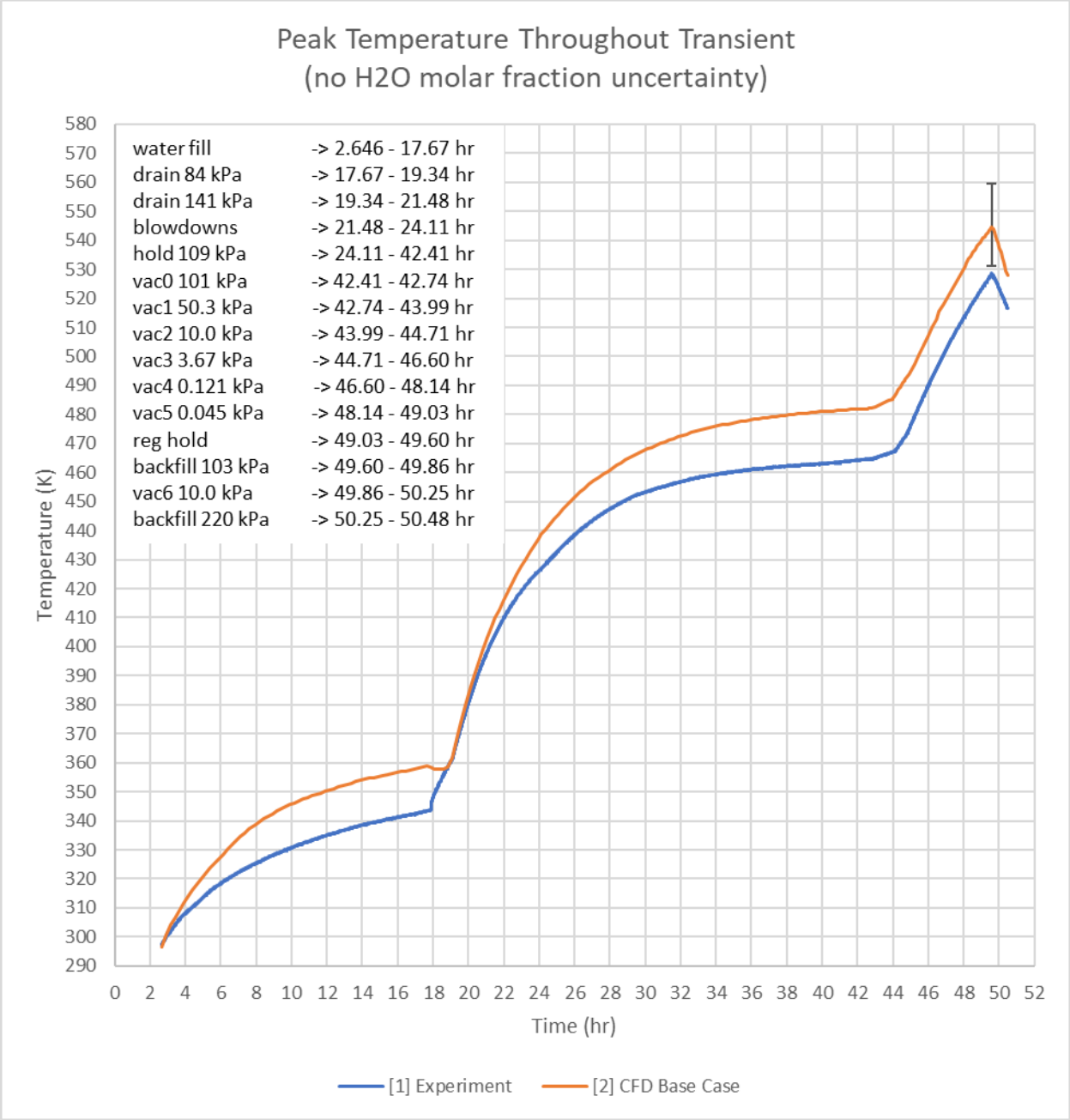


Figure 4-19 PCT as a Function of Time for the 1.483 kW Transient Vacuum Drying Case, without Including Any Uncertainty on the Water Vapor Molar Fraction

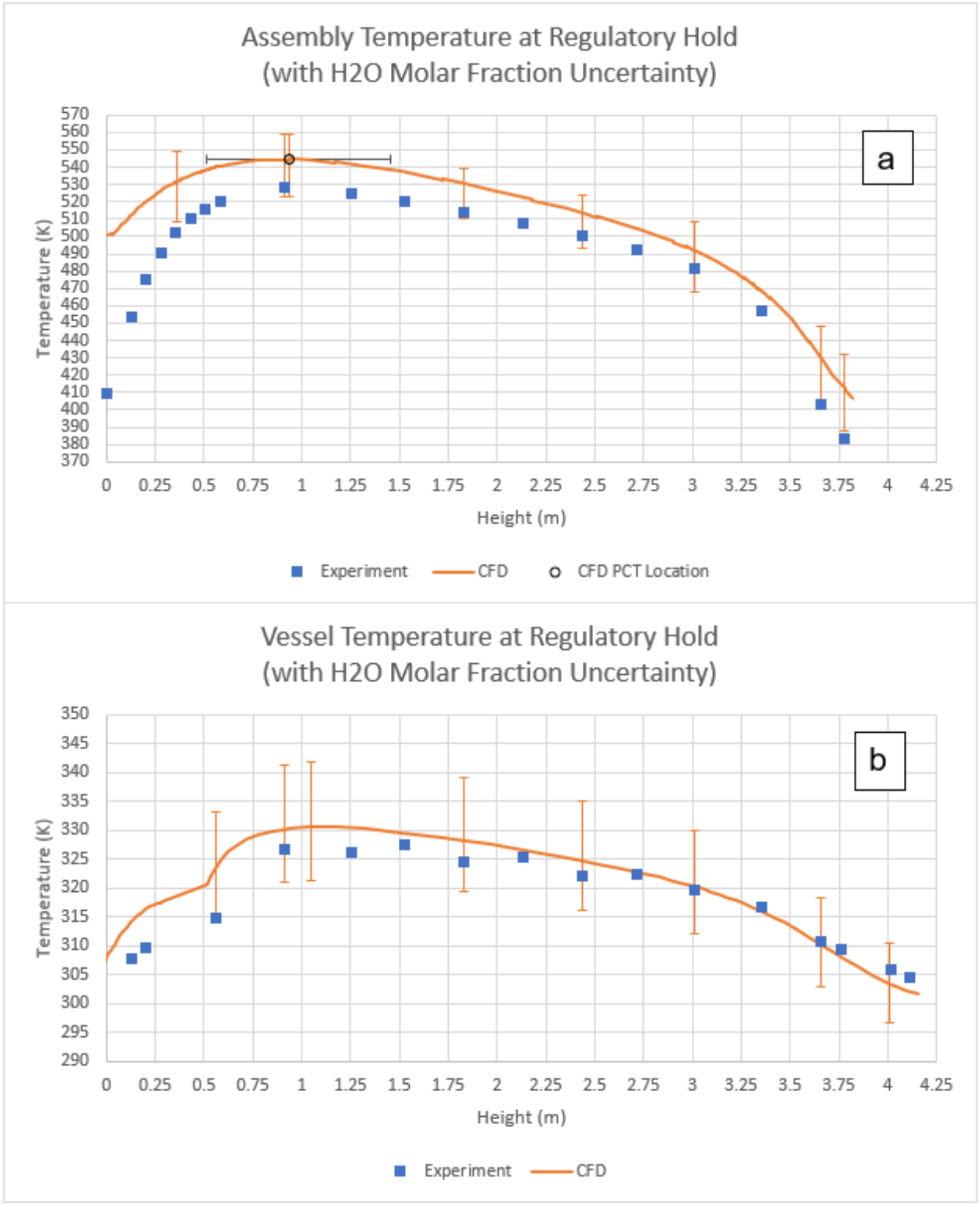


Figure 4-20 (a) Fuel Maximum Axial Temperature and (b) Pressure Vessel Axial Temperature Profile for the 1.483 kW Transient, at Regulatory Hold Point, with Validation Uncertainty Bars Including 30 Percent Water Vapor Molar Fraction Input Uncertainty

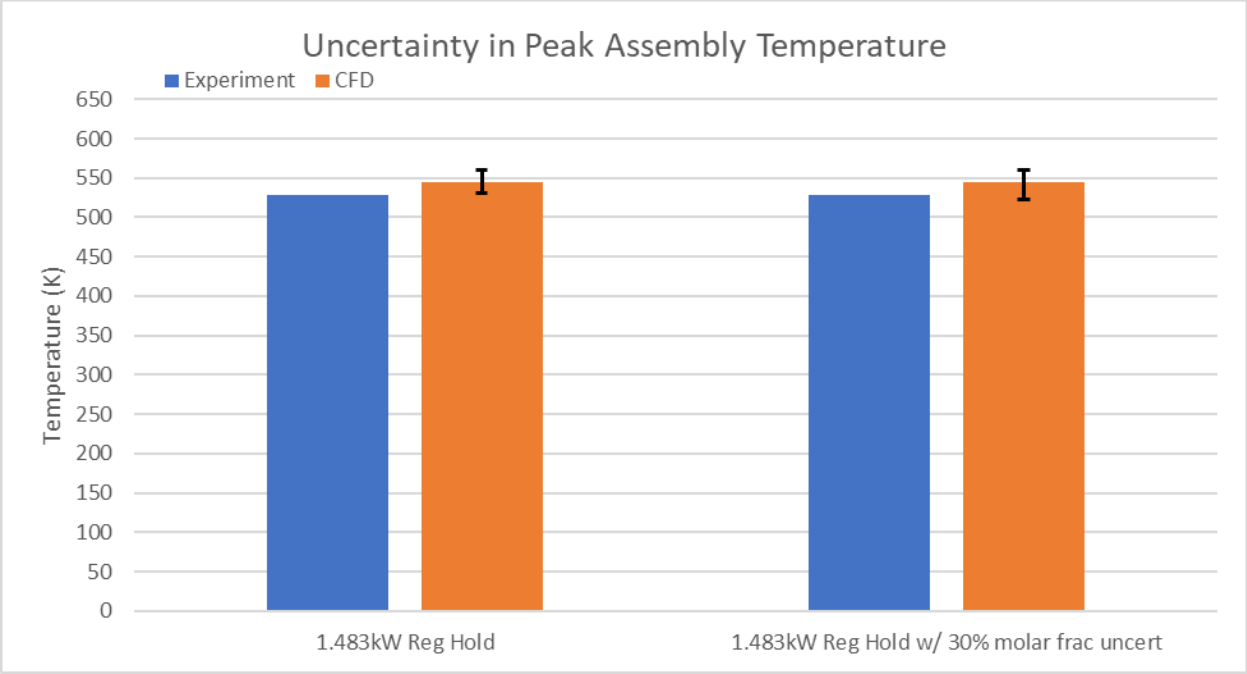


Figure 4-21 PCT Prediction (K) for Transient Vacuum Drying Case at Regulatory Hold Step

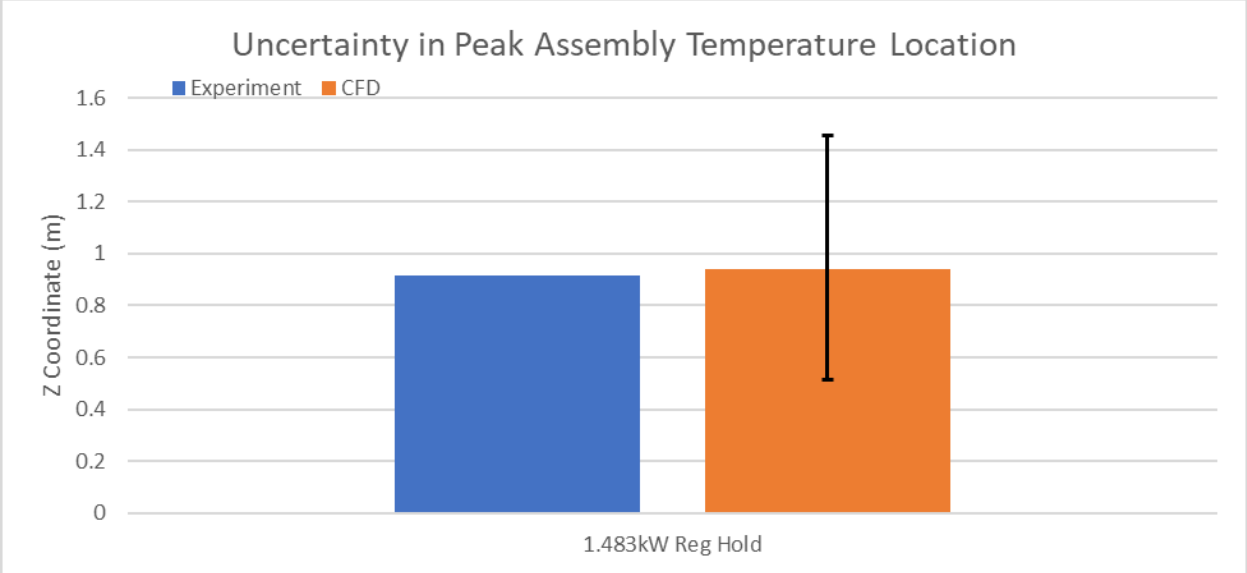


Figure 4-22 PCT Location Prediction (m) for the Transient Vacuum Drying Case at the Regulatory Hold Step

Table 4-5 Transient Test Results at Regulatory Hold Point (1.483 kW, 0.045 kPa, Steam)

Parameter		Exp Data	CFD Results	Data – CFD	Negative Uncert.	Positive Uncert.	Sym Uncert.	Valid?
PCT Location	Units							
Z value	m	0.91	0.94	-0.03	-0.42	0.52	0.47	YES
PCT Value	K	528.7	544.5	-15.8	-21.2	14.8	21.6	YES
Fuel Region	**Fuel Maximum Temperature as Function of Height**							
J9 Location								
z = 0.36 m	K	502.5	531.8	-29.3	-23.0	17.3	22.9	NO
z = 0.91 m	K	528.7	544.5	-15.8	-21.8	14.3	21.8	YES
z = 1.83 m	K	513.7	530.3	-16.6	-19.6	8.7	19.7	YES
z = 2.44 m	K	500.1	513.7	-13.6	-20.6	10.5	20.7	YES
z = 3.01 m	K	481.7	492.0	-10.3	-24.1	16.2	23.9	YES
z = 3.66 m	K	402.8	429.9	-27.1	-24.8	18.5	24.6	NO
z = 3.78 m	K	383.3	412.9	-29.6	-25.2	19.4	25.1	NO
Pressure Vessel	**Pressure Vessel External Temperature as Function of Height**							
z = 0.56 m	K	314.9	323.4	-8.5	-8.5	9.7	9.1	NO
z = 0.91 m	K	326.8	330.2	-3.4	-9.2	11.2	10.2	YES
z = 1.83 m	K	324.4	328.2	-3.8	-8.8	10.9	9.8	YES
z = 2.44 m	K	322.1	324.7	-2.6	-8.5	10.3	9.4	YES
z = 3.01 m	K	319.6	320.3	-0.7	-8.3	9.7	9.0	YES
z = 3.66 m	K	310.8	310.2	0.6	-7.4	8.0	7.7	YES
z = 4.01 m	K	305.8	303.4	2.4	-6.7	7.0	6.9	YES

The base case used in this analysis used porous media, as discussed in section 2.3. As shown in Figure 4-18 and Figure 4-19, the base case model predicts conservative results without uncertainty quantification. The highest temperature occurs at the regulatory hold step, when all the fluid inside the canister is 100 percent water vapor. The maximum temperature at regulatory hold was determined to be 544.5 K, about 16 K higher than the measured value. As the PCT was overpredicted, the focus is on the calculated negative validation uncertainty, which was determined to be 13.5 K when no water vapor molar fraction measurement uncertainty was included, as shown in Figure 4-19 and Figure 4-21. When the water vapor molar fraction

uncertainty of 30 percent (Figure 3-4) was included, the negative validation uncertainty was determined to be 21.2 K, as shown in Figure 4-18, Figure 4-20(a), Figure 4-21, and Table 4-5. The detailed validation uncertainty quantification in Table 4-5, Figure 4-20(a), and Figure 4-20(b), including the PCT, PCT location, the maximum fuel temperature at seven discrete points along the fuel region, and temperature values at seven discrete points along the pressure vessel external wall, shows that most temperature predictions were validated. Figure 4-22 shows the prediction of the PCT location at the regulatory hold step.

4.3 Transient Vacuum Drying Sensitivity Results

This section discusses sensitivity predictions using different models and different gas compositions at various steps of the vacuum drying process (Table 4-6). The thermal response of the dry cask was compared to evaluate the effect of the changes from each sensitivity. Sensitivity predictions included the use of CFD applicants' vacuum drying modeling routine to determine whether the method is conservative. Also, the appropriate technique to simulate the hold step after water fill was to use multiphase modeling; thus, one sensitivity involved multiphase modeling of that step. The CFD base model, despite omitting multiphase modeling, still used two fluids; the liquid and gas phases were separated by a thin wall allowing heat exchange between the two fluids but no mass transfer. To understand the bases of all the sensitivities, a brief description of the CFD base case is needed.

In the CFD base case, the hold step after the water fill used a separating thin wall to model the interface between liquid water in the bottom and saturated air on the top. The thin wall separating the two fluids was modeled to allow heat transfer between the two phases. The heat source throughout the vacuum drying processes was 1,483 W. Table 4-6 lists the transient steps; all of the mixture compositions in the table are obtained from measurements in SAND2024 and given on a molar basis. The hold after the water fill lasted 15.02 hours. The separating thin wall was used for the hold after water fill step only; the thin wall was removed for the other steps in the vacuum drying processes. Following the water fill hold step, water was removed from the vessel in two drain steps. The first drain used a pressure of 84 kPa and lasted 1.67 hours, while the second drain used a pressure of 140.9 kPa and lasted 2.14 hours. Both draining steps used a uniform mixture, "mix0," that consisted of 90 percent helium and 10 percent water vapor.

The next step was a blowdown at a pressure 128.1 kPa using "mix0," which lasted 2.62 hours. After the blowdown, there was a hold for 18.29 hours at a pressure of 109.3 kPa with the same mixture ("mix0"), followed by six vacuum steps ("vac0," "vac1," "vac2," "vac3," "vac4," and "vac 5" in Table 4-6). These vacuum steps lasted 0.33 hours (100.7 kPa), 1.25 hours (50.3 kPa), 0.72 hours (10.0 kPa), 1.89 hours (3.67 kPa), 1.53 hours (0.12 kPa), and 0.89 hours (0.045 kPa), respectively. The fill gas mixtures for each step were named to match the corresponding vacuum step ("mix0," "mix1," "mix2," "mix3," "mix4," and "mix5," respectively). Mix1 consisted of 16.8 percent water vapor and 83.2 percent helium. Mix2 consisted of 47.4 percent water vapor and 52.6 percent helium. The remaining mixtures (mix3, mix4, and mix5) were 100 percent water vapor. After these six vacuum steps, a regulatory hold was observed, lasting 0.57 hours and using mix5 (100 percent water vapor at 0.045 kPa).

The next step was the first backfill ("Backfill 1") at a pressure of 102.7 kPa, with a gas mixture consisting of 99 percent helium and 1 percent water vapor and lasting 0.26 hours. Then, the final vacuum, which lasted 0.36 hours, used a pressure of 10.0 kPa and a mixture consisting of 99 percent helium and 1 percent water vapor. The last step in the vacuum drying transient was the final backfill, lasting 0.23 hours, using a pressure of 219.6 kPa and a 100 percent helium fill.

All of the sensitivity predictions that were performed are shown in Figure 4-23 through Figure 4-29 and explained in Table 4-6 through Table 4-21. The tables describe the 12 steps that each sensitivity used, including initial conditions, pressure, and what fluid existed inside the canister. When multiphase modeling was used for the hold after the water fill (as in sensitivity 7, 8, and 9), the thin wall separating the liquid water and the cover gas was not present. Each figure showing sensitivities includes sensitivity 1 (experimental data) and sensitivity 2 (the CFD base case scenario using porous media, as described above and in Table 4-6) for comparison purposes.

Sensitivities 3 and 4 were like the base case scenario but used successively finer meshes, as described in section 3.1.2, with refinement ratios of 1.33 and 1.82 when compared to the base coarse mesh, respectively. Figure 4-23 illustrates these sensitivities, along with sensitivities 1 and 2. As this figure shows, the thermal response from all three meshes compare favorably. It was thus concluded that the base coarse mesh was sufficient to capture all aspects of flow and heat transfer. Table 4-7 through Table 4-11 present the details of conditions for sensitivities 1, 2, 3, and 4.

Figure 4-24 shows sensitivities 5 and 6, along with sensitivities 1 and 2. Sensitivity 5 used the same assumptions on the fill gas and other conditions as the base case, but instead used the explicitly represented geometry, including fuel rods, guide tubes, and grid spacers. Sensitivity 6 was like sensitivity 5, with one minor difference in the modeling of air in the hold step after the water fill; sensitivity 5 used saturated air while sensitivity 6 used dry air. This minor difference did not have any effect on the CFD predictions, as seen in Figure 4-24. Table 4-7 through Table 4-11 present the details of conditions for sensitivities 5 and 6.

Sensitivities 7, 8, and 9 (in addition to sensitivities 1 and 2), shown in Figure 4-25,use the VOF multiphase flow model as described in sections 1.2.1 and 2.6. Sensitivities 7 and 8 used the explicitly represented geometry while sensitivity 9 used the porous media model. The difference between sensitivities 7 and 8 is that the momentum equations were not solved/included in sensitivity 7. In sensitivities 8 and 9, momentum was solved as usual. The multiphase model is only needed in the hold step after the water fill, where two distinct phases exist. Figure 4-25 shows that when momentum equations were not used, a higher temperature was obtained at the end of the hold step after water fill. The figure also shows that the multiphase model using either porous media or explicitly represented geometry predicted same thermal response as the base case (i.e., sensitivity 2). Due to the difficulties involved in setting up the multiphase flow model for both geometries, and the convergence issues that can result from the additional secondary phase volumetric fraction equation and the interface tracking, it will be preferable for the CFD modeler to use the CFD base case. Table 4-7 through Table 4-16 present the details of conditions for sensitivities 7, 8, and 9.

Figure 4-26 shows sensitivities 10, 11, the base case (i.e., sensitivity 2), and experimental data (i.e., sensitivity 1). Sensitivities 10 and 11 are similar to the approach dry cask applicants use to perform vacuum drying analysis. Sensitivities 10 and 11 completely ignore the water fill and start the simulation from drain step. Sensitivity 10 started the simulation at the beginning of the first drain step at a pressure of 84 kPa at t = 17.67 hours (as shown in Table 4-6) and initialized the temperature field throughout the cask with the water saturation temperature at the pressure of 84 kPa (T sat = 368.0 K). Sensitivity 11 ignored the hold step after the water fill and the first drain step and started the simulation at the second drain step (i.e., at a pressure of 140.9 kPa at t = 19.34 hours and initialized the temperature field throughout the cask with the water saturation temperature at 140.9 kPa (i.e., T sat = 382.6 K).

Sensitivities 10 and 11 both used 100 percent helium as the fill gas throughout the draining steps, blowdown, and hold before vacuum. Following that, 100 percent water vapor was used as a fill gas throughout the vacuum steps and regulatory hold. In the last three steps (i.e., first backfill, final vacuum, and final backfill), 100 percent helium was used as the fill gas. Table 4-12 through Table 4-16 present the details of conditions for sensitivities 10 and 11. Figure 4-26 clearly shows that both sensitivities predicted conservative results at the regulatory hold step where the maximum temperature for the entire transient occurred. Additionally, as both sensitivities used 100 percent helium before vacuum steps, both sensitivity curves move closer to the experimental data. This shift toward experimental data occurred because 100 percent helium has a higher thermal conductivity than mix0 (used in the base case). Because 100 percent steam was used for vacuum steps, including the regulatory hold, conservative temperatures will be obtained as they were in the base case. After the regulatory hold, the PCT followed the same descent as the base case because 100 percent helium was used, as in the base case. Due to the simplified modeling approach (i.e., the use of pure helium before vacuum stages, steam in the vacuum stages, and finally pure helium in the last three steps of the transient) and the resultant conservative PCT predictions, these two sensitivities are attractive alternatives to the base case.

Figure 4-27 shows the predictions from sensitivities 12, 13, 14, and 15, along with sensitivities 1 and 2. Sensitivities 12 and 13 read the initial conditions at two separate points from the base case (i.e., sensitivity 2). Sensitivity 12 reads the temperature field at the end of the hold step after the water fill of sensitivity 2 at t = 17.67 hours as initial conditions, while sensitivity 13 uses temperature values from the end of the first drain step of sensitivity 2 at t = 19.34 hours, as explained in Table 4-12 through Table 4-16. The steps after that follow sensitivity 10 or 11, respectively. After the initial conditions were read, 100 percent helium was used for draining, blowdown, and the hold before vacuum steps. Then,100 percent water vapor was used for all the vacuum steps, including the regulatory hold. The final three steps used 100 percent helium.

Sensitivity 14 modeled an extreme scenario, assuming 100 percent helium for all steps of the transient. In this sensitivity, the hold step after the water fill used helium above the liquid water (instead of saturated air used in the base case), and the other steps used pure helium as the fill gas. Sensitivity 15 was run using the temperature field from the end of sensitivity 14's hold step before vacuum as the initial condition. Then, mix2 (52.6 percent helium and 47.4 percent water vapor) was used through all the vacuum steps, including the regulatory hold. The last three steps after the regulatory hold used 100 percent helium.

Comparisons of sensitivity 12, 13, 14, and 15 predictions with each other and with sensitivities 1 and 2 (Figure 4-27) show that the higher the volume fraction of helium used in the mixtures, the closer the predictions get to the experimental data in the stages before the vacuum steps. Figure 4-27 also indicates that not all steps through vacuum are 100 percent steam. In sensitivity 15, even with 47.4 percent steam, the PCT at the regulatory hold step and the shape of the PCT response through the vacuum steps were favorably predicted and matched the experimental data well. Table 4-12 through Table 4-21 present the details of conditions for sensitivities 12, 13, 14, and 15.

Figure 4-28 shows sensitivities 16 and 17 (in addition to sensitivities 1 and 2). The peak temperature in the hold step after the water fill occurred on the top of the assembly, due to the poor heat transfer of the cover gas compared to the liquid water beneath it. After bulk water drain, there was no longer a drastic difference in fluid thermal conductivity between the top and bottom portions of the vessel (since there was only one fluid in the vessel), and thus the assembly temperature adjusted quickly to reflect the shape of the power profile. That is to say, the PCT location tended to move down in the assembly below a height of 1 m. When the steeper-sloped

power profile was used, more heat was delivered to the bottom of the assembly than the top, relative to the base case power profile. Alternatively, when the less steep slope was used, more heat was delivered to the top of the assembly relative to the base case power profile. As expected, when the less steep (i.e., shallower) power profile was used, the PCT profile showed higher values during the water fill hold, compared to the base case and the steeper power profile. After the water fill hold, the PCT location moved to the bottom of the assembly, and since the steeper profile delivered more heat to the bottom of the assembly, the steeper profile resulted in a greater PCT than the base case or shallow profile. Figure 4-28 illustrates these trends. Table 4-17 through Table 4-21 present the details of conditions for sensitivities 16 and 17. Section 3.2, including Figure 3-3, gives detailed information about the heat profiles used for the base case and the uncertainty quantification cases (i.e., steep power profile and shallow power profile).

Figure 4-29 shows the predictions of sensitivities 18, 19, and 20 (as well as sensitivities 1 and 2), which investigate the effect of the uncertainty in water vapor fraction measurement. Sensitivity 18 used the results from the beginning of the vacuum steps of sensitivity 14 (i.e., beginning of sensitivity 14's vac0). From there, the first and second vacuum steps continued as in the base case (i.e., mix0 for vac0, mix1 for vac1). For the third vacuum step (i.e., vac2), an uncertainty in water vapor molar fraction of about 10 percent (obtained from Figure 3-4 in SAND2023-09746R) was used to create a mixture of 63 percent helium and 37 percent water vapor (i.e., ~10 percent less water vapor than the base case mix2), and that new 63 percent helium mixture filled the vessel. For the rest of the vacuum steps in sensitivity 18, including the regulatory hold, a 30 percent uncertainty (obtained from Figure 3-4 in SAND2023-09746R) was used to create a mixture of 30 percent helium and 70 percent water vapor, and that new 30 percent helium mixture was used as the vessel fill instead of 100 percent water vapor used in the base case (i.e., sensitivity 2). For the rest of the steps after the regulatory hold, 100 percent helium was used.

Sensitivity 19 used the results obtained from the end of the second vacuum step of sensitivity 18 as initial conditions. For the third vacuum step, 20 percent uncertainty (obtained from Figure 3-4 in SAND2023-09746R) was used for the water vapor molar fraction uncertainty to create a mixture of 20 percent helium and 80 percent water vapor. This mixture was the vessel fill for the remaining vacuum steps, including the regulatory hold. After the regulatory hold, 100 percent helium was used.

Sensitivity 20 used the results obtained from the end of the second vacuum step of sensitivity 18 as initial conditions, similar to the procedure for sensitivity 19. For the third vacuum step, 10 percent uncertainty (obtained from Figure 3-4 in SAND2023-09746R) was used for the water vapor molar fraction uncertainty to create a mixture of 10 percent helium and 90 percent water vapor. This mixture was the vessel fill for the remaining vacuum steps, including the regulatory hold. After the regulatory hold, 100 percent helium was used.

As Figure 4-29 illustrates, closer thermal response was obtained when an uncertainty on water vapor molar fraction of 30 percent was used. When compared to the experimental data, fuel maximum temperature plots for sensitivities 18, 19, and 20 (Figure 4-29) show better agreement than the base case, indicating that helium was present in the canister and the fluid was not 100 percent water vapor in vac3, vac4, vac5, and the regulatory hold steps. However, as Figure 4-29 shows, the 100 percent water vapor in vac3, vac4, vac5, and the regulatory hold steps—as measured and used in the base case—predicted conservative results. Table 4-17 through Table 4-21 present the details of conditions for sensitivities 18, 19, and 20.

Table 4-6 Transient Vacuum Drying Case Steps, Fill Fluid, and Characteristics for Base Case

Process	Time (hr)	Pressure (kPa)	Power (W)	Elapsed Time (hr)	Materials	H2O mol Fraction	Helium mol Fraction
Hold After Water Fill	2.65	84.0	1,483		h2o_liq + sat_air	h2o_liq + sat_air	h2o_liq + sat_air
	17.67	84.0	1,483	15.02			
Drain	17.67	84.0	1,483		mix0	0.1	0.9
	19.34	84.0	1,483	1.67			
Drain	19.34	140.9	1,483		mix0	0.1	0.9
	21.48	140.9	1,483	2.14			
Blowdown	21.48	128.1	1,483		mix0	0.1	0.9
	24.11	128.1	1,483	2.63			
Hold Before Vacuum	24.11	109.3	1,483		mix0	0.1	0.9
	42.41	109.3	1,483	18.30			
Vac 0	42.41	100.7	1,483		mix0	0.1	0.9
	42.74	100.7	1,483	0.33			
Vac 1	42.74	50.3	1,483		mix1	0.168	0.832
	43.99	50.3	1,483	1.25			
Vac 2	43.99	10.0	1,483		mix2	0.474	0.526
	44.71	10.0	1,483	0.72			
Vac 3	44.71	3.67	1,483		mix3	1	0
	46.60	3.67	1,483	1.89			
Vac 4	46.60	0.12	1,483		mix4	1	0
	48.14	0.12	1,483	1.54			
Vac 5	48.14	0.045	1,483		mix5	1	0
	49.03	0.045	1,483	0.89			
Regulatory Hold	49.03	0.045	1,483		mix5	1	0
	49.60	0.045	1,483	0.57			
Backfill 1	49.60	102.7	1,483		mix6	0.01	0.99
	49.86	102.7	1,483	0.26			
Final Vacuum	49.86	10.0	1,483		mix6	0.01	0.99
	50.25	10.0	1,483	0.39			
Final Backfill	50.25	219.6	1,483		He	0	1
	50.48	219.6	1,483	0.23			

Table 4-7 Description of Transient Vacuum Drying Case Sensitivities 1–7 for Steps 1–3

Sensitivity	Water fill (1)	Drain_84kPa (2)	Drain_140.9kPa (3)
1	Experiment, H2O_liq filled to 3.35m, air_sat, 1483.3W avg, 84kPa, T_amb = 296.7 K, t = 2.65-17.67 hr	Experiment, 84kPa, no mass spec data (assumed ~90% He from 42.7 hr), t = 17.67-19.34 hr	Experiment, 140.9kPa, no mass spec data (assumed ~90% He from 42.7 hr), t = 19.34-21.48 hr
2	Single-Phase, liquid-gas separation present, porous media, air_sat, H2O_liq, initialize at T_amb, base case	mix0 = 90% He, 10% H2O vapor, no separation from here onward (in all sensitivity cases)	mix0 = 90% He, 10% H2O vapor
3	Single-Phase, liquid-gas separation present, porous media, air_sat, H2O_liq, initialize at T_amb, mesh refined	mix0 = 90% He, 10% H2O vapor, no separation from here onward	mix0 = 90% He, 10% H2O vapor
4	Single-Phase, liquid-gas separation present, porous media, air_sat, H2O_liq, initialize at T_amb, mesh further refined	mix0 = 90% He, 10% H2O vapor, no separation from here onward	mix0 = 90% He, 10% H2O vapor
5	Single-Phase, liquid-gas separation present, explicit geometry, air_sat, H2O_liq, initialize at T_amb	mix0 = 90% He, 10% H2O vapor, no separation from here onward	mix0 = 90% He, 10% H2O vapor
6	Single-Phase, liquid-gas separation present, explicit geometry, dry_air, H2O_liq, initialize at T_amb	mix0 = 90% He, 10% H2O vapor, no separation from here onward	mix0 = 90% He, 10% H2O vapor
7	Multi-Phase, VOF, interface, air_sat, H2O_liq, explicit geometry, momentum equation disabled	n/a	n/a

Table 4-8 Description of Transient Vacuum Drying Case Sensitivities 1–7 for Steps 4–6

Sensitivity	Blowdown (4)	Hold_Before_Vac (5)	Vac0 (6)
1	Experiment, 95-160kPa (128.1kPa avg), no mass spec data (assumed ~90% He from 42.7 hr), t = 21.48-24.11 hr	Experiment, 109.3kPa, no mass spec data (assumed 104563 ppmv H2O @ 42.7 hr -> ~90% He), t = 24.11-42.41hr	Experiment, 100.7kPa, 104563 ppmv H2O -> ~90% He, t = 42.41-42.74 hr
2	mix0 = 90% He, 10% H2O vapor	mix0 = 90% He, 10% H2O vapor	mix0 = 90% He, 10% H2O vapor
3	mix0 = 90% He, 10% H2O vapor	mix0 = 90% He, 10% H2O vapor	mix0 = 90% He, 10% H2O vapor
4	mix0 = 90% He, 10% H2O vapor	mix0 = 90% He, 10% H2O vapor	mix0 = 90% He, 10% H2O vapor
5	mix0 = 90% He, 10% H2O vapor	mix0 = 90% He, 10% H2O vapor	mix0 = 90% He, 10% H2O vapor
6	mix0 = 90% He, 10% H2O vapor	mix0 = 90% He, 10% H2O vapor	mix0 = 90% He, 10% H2O vapor
7	n/a	n/a	n/a

Table 4-9 Description of Transient Vacuum Drying Case Sensitivities 1–7 for Steps 7–9

Sensitivity	Vac1 (7)	Vac2 (8)	Vac3 (9)
1	Experiment, 50.3kPa, 168163 ppmv H2O -> ~83% He, t = 42.74-43.99 hr	Experiment, 10.0kPa, 474264 ppmv H2O -> ~53% He, t = 43.99-44.71 hr	Experiment, 3.67kPa, no mass spec data (flooded, assumed 0% He), t = 44.71-46.60 hr
2	mix1 = 83.2% He, 16.8% H2O vapor	mix2 = 52.6% He, 47.4% H2O vapor	mix3 = 0% He, 100% H2O vapor
3	mix1 = 83.2% He, 16.8% H2O vapor	mix2 = 52.6% He, 47.4% H2O vapor	mix3 = 0% He, 100% H2O vapor
4	mix1 = 83.2% He, 16.8% H2O vapor	mix2 = 52.6% He, 47.4% H2O vapor	mix3 = 0% He, 100% H2O vapor
5	mix1 = 83.2% He, 16.8% H2O vapor	mix2 = 52.6% He, 47.4% H2O vapor	mix3 = 0% He, 100% H2O vapor
6	mix1 = 83.2% He, 16.8% H2O vapor	mix2 = 52.6% He, 47.4% H2O vapor	mix3 = 0% He, 100% H2O vapor
7	n/a	n/a	n/a

Table 4-10 Description of Transient Vacuum Drying Case Sensitivities 1–7 for Steps 10–12

Sensitivity	Vac4 (10)	Vac5 (11)	Reg_hold (12)
1	Experiment, 0.12kPa, no mass spec data (flooded, assumed -> 0% He), t = 46.60-48.14 hr	Experiment, 0.045kPa, no mass spec data (flooded, assumed -> 0% He), t = 48.14-49.03 hr	Experiment, 0.045kPa, no mass spec data (flooded, assumed -> 0% He), t = 49.03-49.60 hr
2	mix4 = 0% He, 100% H2O vapor	mix5 = 0% He, 100% H2O vapor	mix5 = 0% He, 100% H2O vapor
3	mix4 = 0% He, 100% H2O vapor	mix5 = 0% He, 100% H2O vapor	mix5 = 0% He, 100% H2O vapor
4	mix4 = 0% He, 100% H2O vapor	mix5 = 0% He, 100% H2O vapor	mix5 = 0% He, 100% H2O vapor
5	mix4 = 0% He, 100% H2O vapor	mix5 = 0% He, 100% H2O vapor	mix5 = 0% He, 100% H2O vapor
6	mix4 = 0% He, 100% H2O vapor	mix5 = 0% He, 100% H2O vapor	mix5 = 0% He, 100% H2O vapor
7	n/a	n/a	n/a

Table 4-11 Description of Transient Vacuum Drying Case Sensitivities 1–7 for Steps 13–15

Sensitivity	Backfill_1 (13)	Final vacuum (14)	Final backfill (15)
1	Experiment, 102.7kPa, 4698 ppmv H2O -> ~99% He, t = 49.60-49.86 hr	Experiment, 10.0kPa, 6921 ppmv H2O -> ~99% He, t = 49.86-50.25 hr	Experiment, 219.6kPa, 586 ppmv H2O -> ~100% He, t = 50.25-50.48 hr
2	mix6 = 99% He, 1% H2O vapor	mix6 = 99% He, 1% H2O vapor	100% He
3	mix6 = 99% He, 1% H2O vapor	mix6 = 99% He, 1% H2O vapor	100% He
4	mix6 = 99% He, 1% H2O vapor	mix6 = 99% He, 1% H2O vapor	100% He
5	mix6 = 99% He, 1% H2O vapor	mix6 = 99% He, 1% H2O vapor	100% He
6	mix6 = 99% He, 1% H2O vapor	mix6 = 99% He, 1% H2O vapor	100% He
7	n/a	n/a	n/a

Table 4-12 Description of Transient Vacuum Drying Case Sensitivities 8–14 for Steps 1–3

Sensitivity	Water fill (1)	Drain_84kPa (2)	Drain_140.9kPa (3)
8	Multi-Phase, VOF, interface, air_sat, H2O_liq, explicit geometry	n/a	n/a
9	Multi-Phase, VOF, interface, air_sat, H2O_liq, porous media	n/a	n/a
10	n/a	initialize at H2O Tsat = 368.0K 100% He, no separation from here onward	100% He
11	n/a	n/a	initialize at H2O Tsat = 382.6K, 100% He
12	n/a	read temperature from case #2's end-of-water-fill data file, 100% He, no separation from here onward	100% He
13	n/a	n/a	read temperature from case #2's end-of-drain_84kPa data file, 100% He
14	Single-Phase, liquid-gas separation present, porous media, He, H2O_liq, initialize at T_amb	100% He, no separation from here onward	100% He

Table 4-13 Description of Transient Vacuum Drying Case Sensitivities 8–14 for Steps 4–6

Sensitivity	Blowdown (4)	Hold_Before_Vac (5)	Vac0 (6)
8	n/a	n/a	n/a
9	n/a	n/a	n/a
10	100% He	100% He	100% water vapor at 100.7 kPa
11	100% He	100% He	100% water vapor at 100.7 kPa
12	100% He	100% He	100% water vapor at 100.7 kPa
13	100% He	100% He	100% water vapor at 100.7 kPa
14	100% He	100% He	100% He

Table 4-14 Description of Transient Vacuum Drying Case Sensitivities 8–14 for Steps 7–9

Sensitivity	Vac1 (7)	Vac2 (8)	Vac3 (9)
8	n/a	n/a	n/a
9	n/a	n/a	n/a
10	100% water vapor at 50.3 kPa	100% water vapor at 10.0 kPa	100% water vapor at 3.67 kPa
11	100% water vapor at 50.3 kPa	100% water vapor at 10.0 kPa	100% water vapor at 3.67 kPa
12	100% water vapor at 50.3 kPa	100% water vapor at 10.0 kPa	100% water vapor at 3.67 kPa
13	100% water vapor at 50.3 kPa	100% water vapor at 10.0 kPa	100% water vapor at 3.67 kPa
14	100% He	100% He	100% He

Table 4-15 Description of Transient Vacuum Drying Case Sensitivities 8–14 for Steps 10–12

Sensitivity	Vac4 (10)	Vac5 (11)	Reg_hold (12)
8	n/a	n/a	n/a
9	n/a	n/a	n/a
10	100% water vapor at 0.120 kPa	100% water vapor at 0.045 kPa	100% water vapor at 0.045 kPa
11	100% water vapor at 0.120 kPa	100% water vapor at 0.045 kPa	100% water vapor at 0.045 kPa
12	100% water vapor at 0.120 kPa	100% water vapor at 0.045 kPa	100% water vapor at 0.045 kPa
13	100% water vapor at 0.120 kPa	100% water vapor at 0.045 kPa	100% water vapor at 0.045 kPa
14	100% He	100% He	100% He

Table 4-16 Description of Transient Vacuum Drying Case Sensitivities 8–14 for Steps 12–15

Sensitivity	Backfill_1 (13)	Final vacuum (14)	Final backfill (15)
8	n/a	n/a	n/a
9	n/a	n/a	n/a
10	100% He	100% He	100% He
11	100% He	100% He	100% He
12	100% He	100% He	100% He
13	100% He	100% He	100% He
14	100% He	100% He	100% He

Table 4-17 Description of Transient Vacuum Drying Case Sensitivities 15–20 for Steps 1–3

Sensitivity	Water fill (1)	Drain_84kPa (2)	Drain_140.9kPa (3)
15	n/a	n/a	n/a
16	Single-Phase, liquid-gas separation present, porous, air_sat, H2O_liq, init at T_amb, pwr profile more uniform axially (skewed shallow)	mix0 = 90% He, 10% H2O vapor, no separation from here onward	mix0 = 90% He, 10% H2O vapor
17	Single-Phase, liquid-gas separation present, porous, air_sat, H2O_liq, init at T_amb, pwr prof more bottom-peaked axially (skewed steep)	mix0 = 90% He, 10% H2O vapor, no separation from here onward	mix0 = 90% He, 10% H2O vapor
18	n/a	n/a	n/a
19	n/a	n/a	n/a
20	n/a	n/a	n/a

Table 4-18 Description of Transient Vacuum Drying Case Sensitivities 15–20 for Steps 4–6

Sensitivity	Blowdown (4)	Hold_Before_Vac (5)	Vac0 (6)
15	n/a	n/a	Read temperature from case #14's end-of-Hold_Before_Vac data file, mix2 = 52.6% He, 47.4% H2O vapor
16	mix0 = 90% He, 10% H2O vapor	mix0 = 90% He, 10% H2O vapor	mix0 = 90% He, 10% H2O vapor
17	mix0 = 90% He, 10% H2O vapor	mix0 = 90% He, 10% H2O vapor	mix0 = 90% He, 10% H2O vapor
18	n/a	n/a	Read temperature from case #14's end-of-Hold_Before_Vac data file, mix0 = 90% He, 10% H2O vapor
19	n/a	n/a	n/a
20	n/a	n/a	n/a

Table 4-19 Description of Transient Vacuum Drying Case Sensitivities 15–20 for Steps 7–9

Sensitivity	Vac1 (7)	Vac2 (8)	Vac3 (9)
15	mix2 = 52.6% He, 47.4% H2O vapor	mix2 = 52.6% He, 47.4% H2O vapor	mix2 = 52.6% He, 47.4% H2O vapor
16	mix1 = 83.2% He, 16.8% H2O vapor	mix2 = 52.6% He, 47.4% H2O vapor	mix3 = 0% He, 100% H2O vapor
17	mix1 = 83.2% He, 16.8% H2O vapor	mix2 = 52.6% He, 47.4% H2O vapor	mix3 = 0% He, 100% H2O vapor
18	mix1 = 83.2% He, 16.8% H2O vapor	mix2-sensitivty = 63% He, 37% H2O vapor	mix3-sensitivty = 30% He, 70% H2O vapor
19	n/a	n/a	read temperature data from case #18's end-of-Vac2 data file, mix3-sensitivty = 20% He, 80% H2O vapor
20	n/a	n/a	read temperature data from case #18's end-of-Vac2 data file, mix3-sensitivty = 10% He, 90% H2O vapor

Table 4-20 Description of Transient Vacuum Drying Case Sensitivities 15–20 for Steps 10–12

Sensitivity	Vac4 (10)	Vac5 (11)	Reg_hold (12)
15	mix2 = 52.6% He, 47.4% H2O vapor	mix2 = 52.6% He, 47.4% H2O vapor	mix2 = 52.6% He, 47.4% H2O vapor
16	mix4 = 0% He, 100% H2O vapor	mix5 = 0% He, 100% H2O vapor	mix5 = 0% He, 100% H2O vapor
17	mix4 = 0% He, 100% H2O vapor	mix5 = 0% He, 100% H2O vapor	mix5 = 0% He, 100% H2O vapor
18	mix4-sensitivty = 30% He, 70% H2O vapor	mix5-sensitivty = 30% He, 70% H2O vapor	mix5-sensitivty = 30% He, 70% H2O vapor
19	mix4-sensitivty = 20% He, 80% H2O vapor	mix5-sensitivty = 20% He, 80% H2O vapor	mix5-sensitivty = 20% He, 80% H2O vapor
20	mix4-sensitivty = 10% He, 90% H2O vapor	mix5-sensitivty = 10% He, 90% H2O vapor	mix5-sensitivty = 10% He, 90% H2O vapor

Table 4-21 Description of Transient Vacuum Drying Case Sensitivities 15–20 for Steps 13–15

Sensitivity	Backfill_1 (13)	Final vacuum (14)	Final backfill (15)
15	100% He	100% He	100% He
16	mix6 = 99% He, 1% H2O vapor	mix6 = 99% He, 1% H2O vapor	100% He
17	mix6 = 99% He, 1% H2O vapor	mix6 = 99% He, 1% H2O vapor	100% He
18	100% He	100% He	100% He
19	100% He	100% He	100% He
20	100% He	100% He	100% He

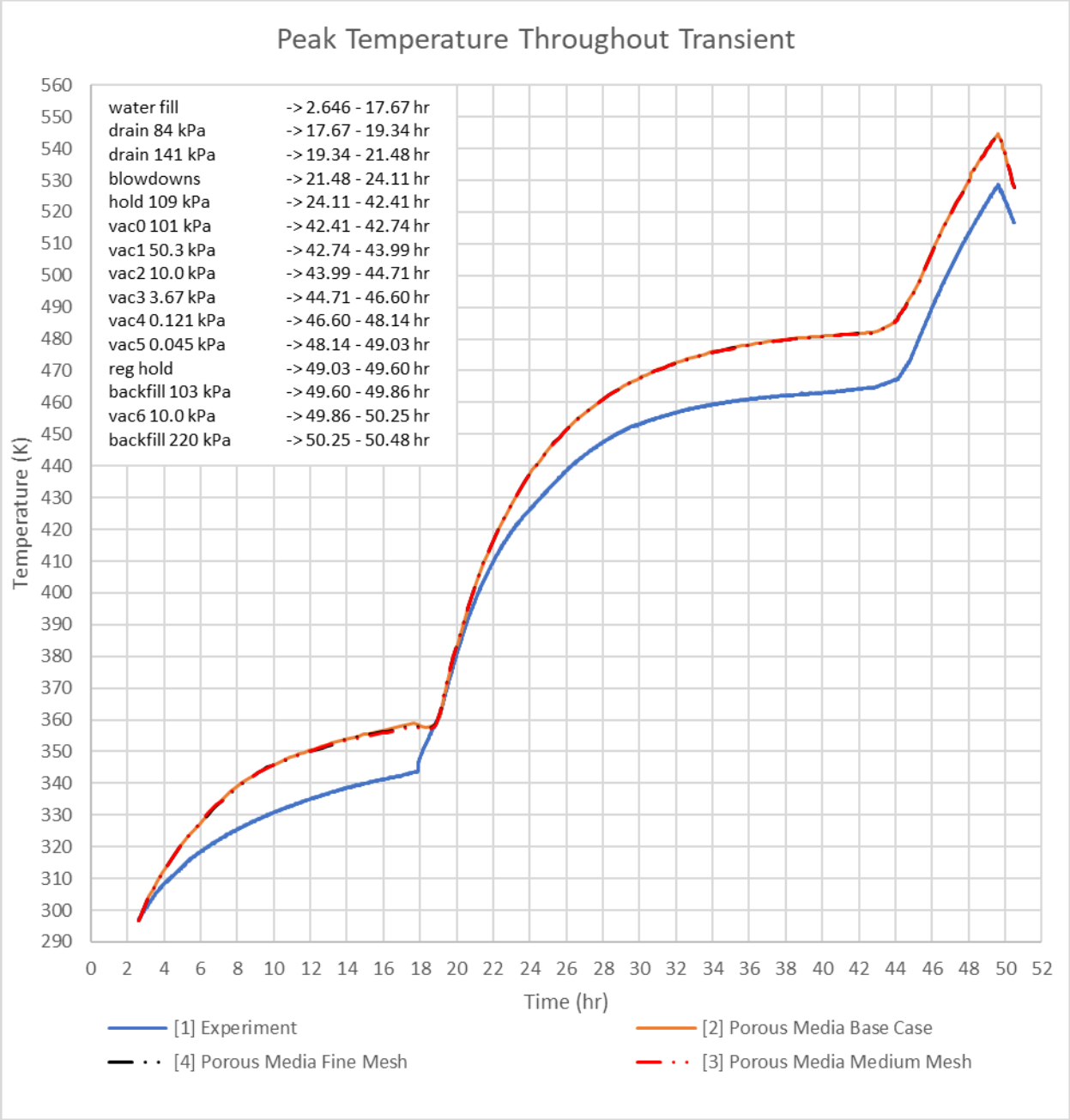


Figure 4-23 Transient Fuel Axial Max Temperature Profile for the 1.483 kW for Sensitivities 1, 2, 3, and 4

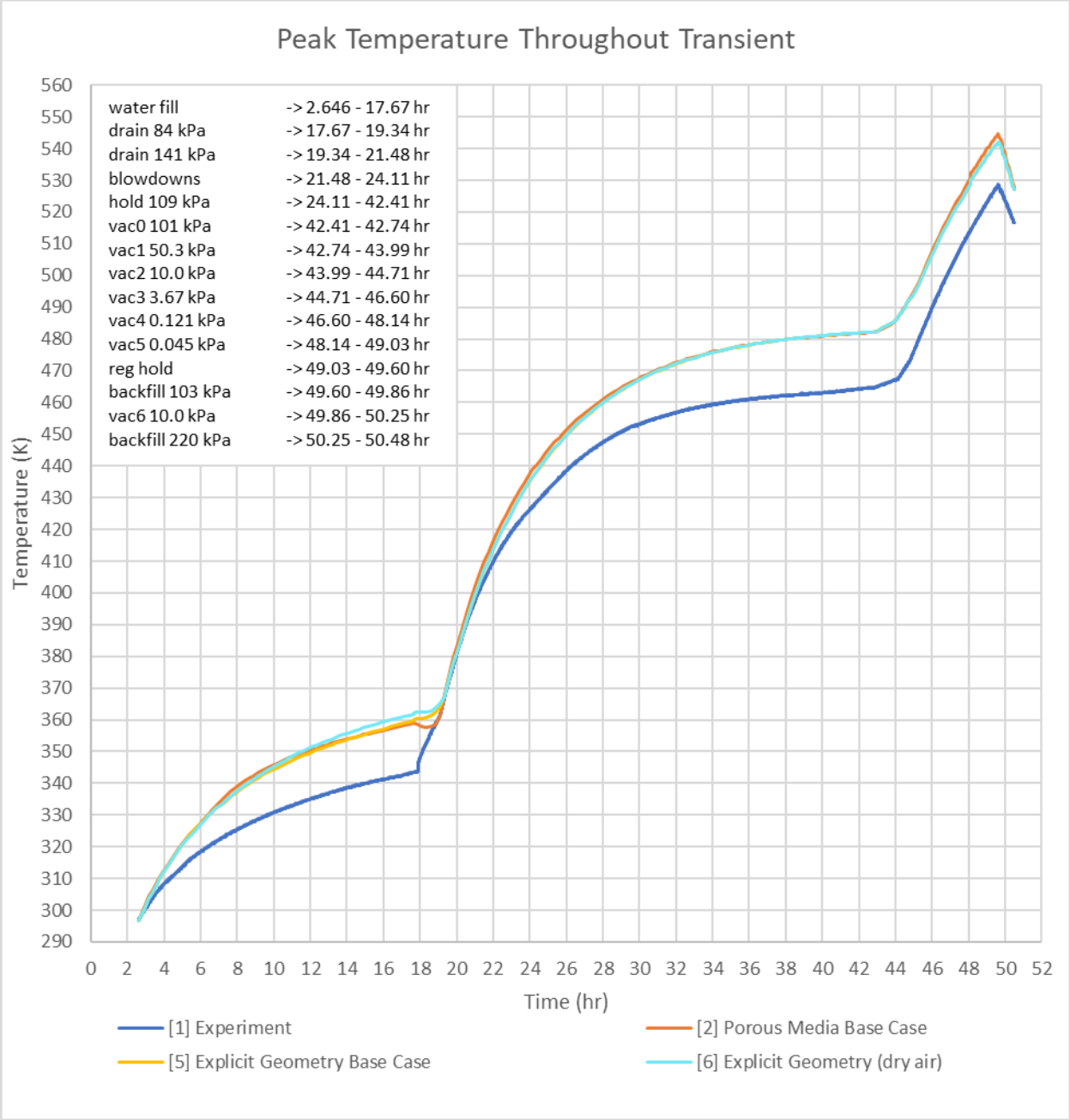


Figure 4-24 Transient Fuel Axial Max Temperature Profile for the 1.483 kW for Sensitivities 1, 2, 5, and 6

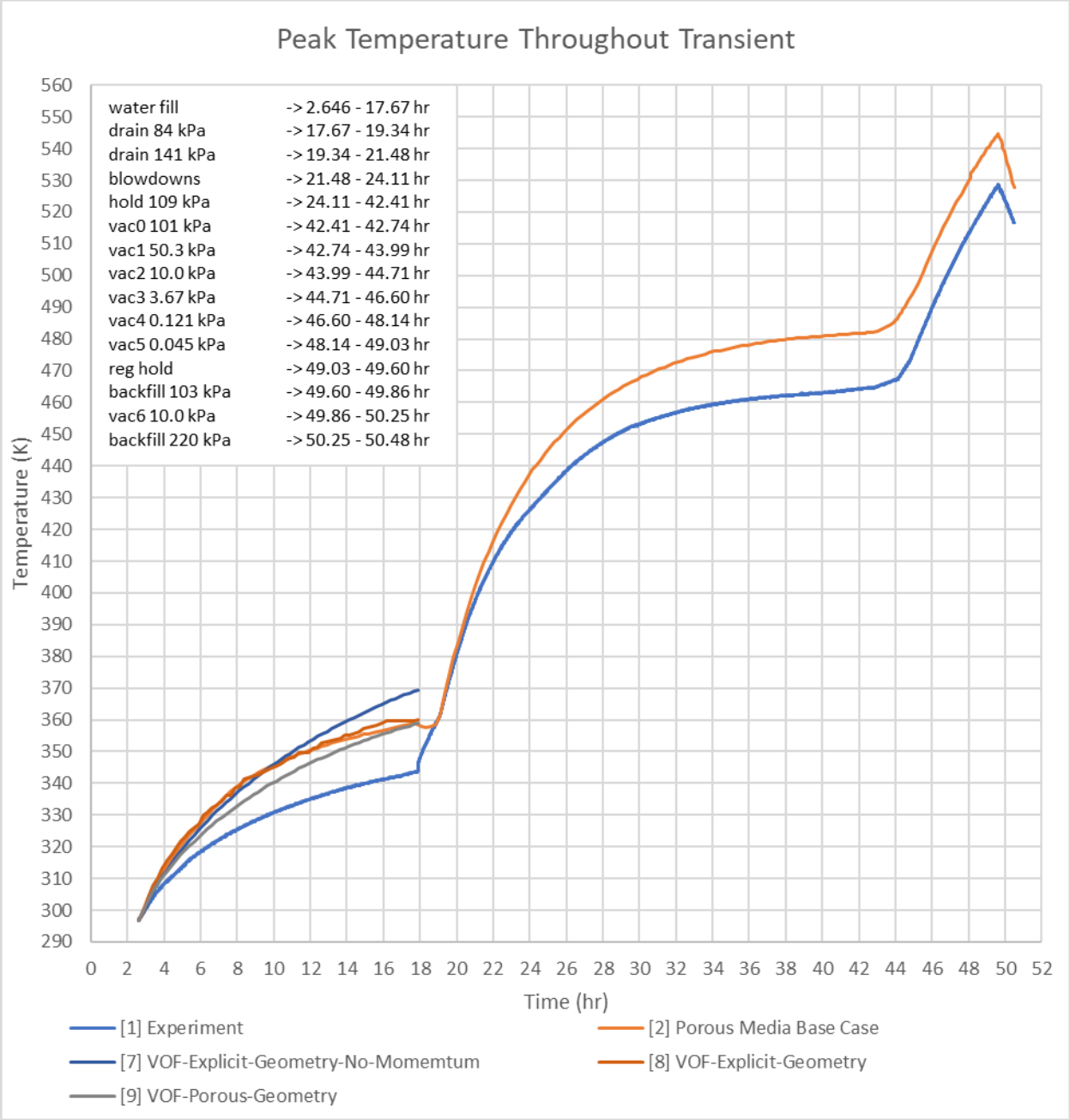


Figure 4-25 Transient Fuel Axial Max Temperature Profile for the 1.483 kW for Sensitivities 1, 2, 7, 8, and 9

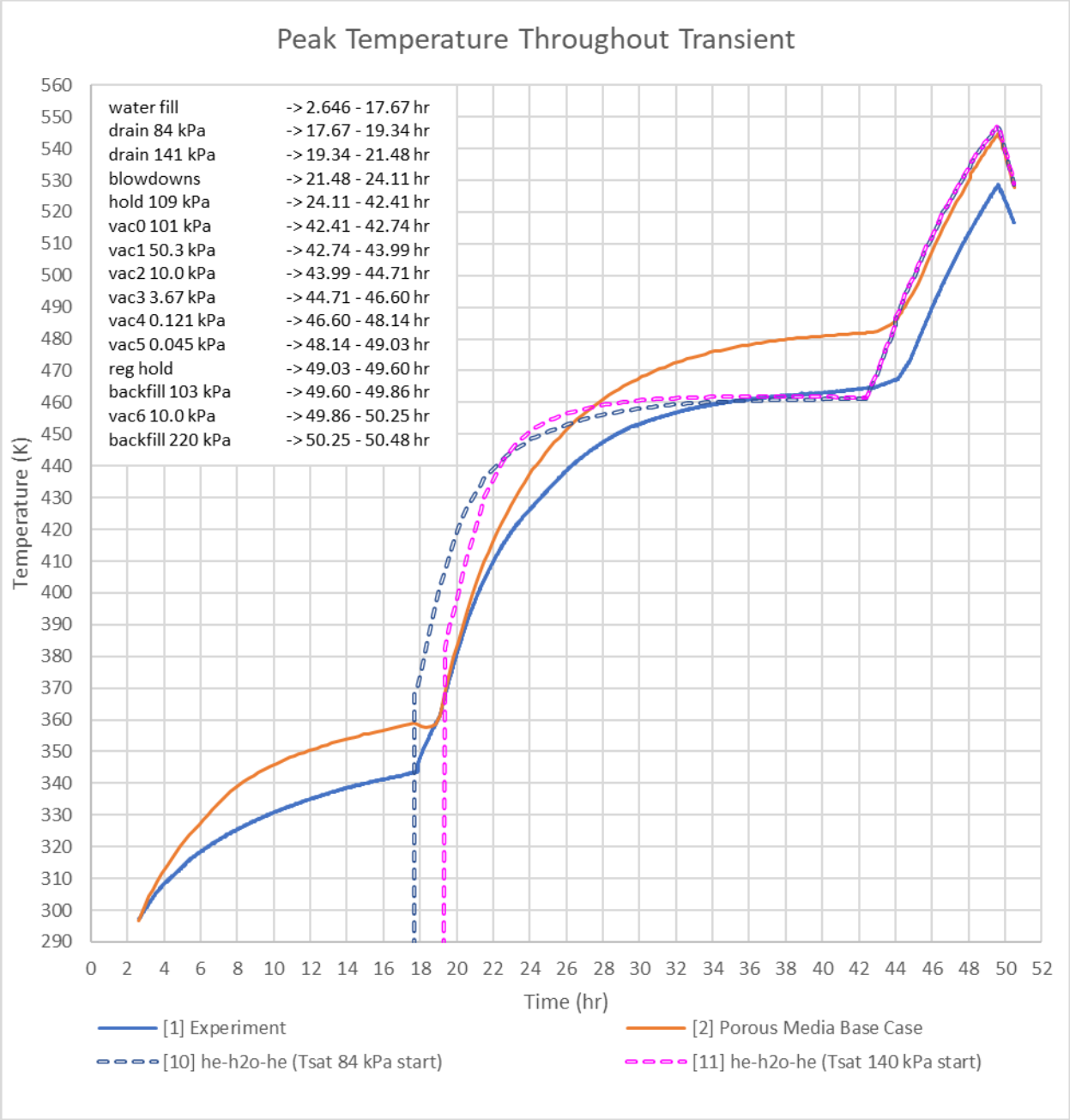


Figure 4-26 Transient Fuel Axial Max Temperature Profile for the 1.483 kW for Sensitivities 1, 2, 10, and 11

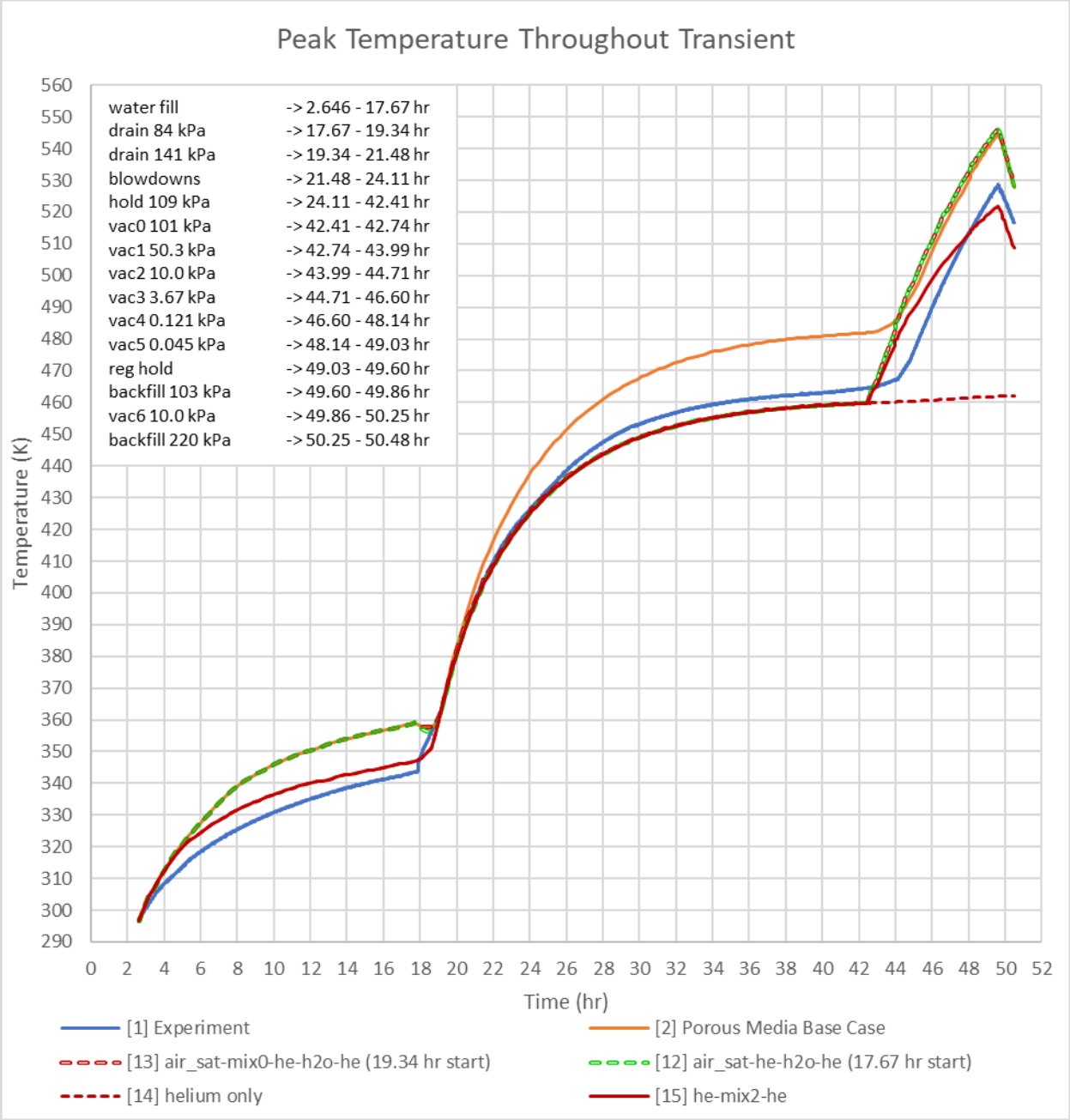


Figure 4-27 Transient Fuel Axial Max Temperature Profile for the 1.483 kW for Sensitivities 1, 2, 12, 13, 14, and 15

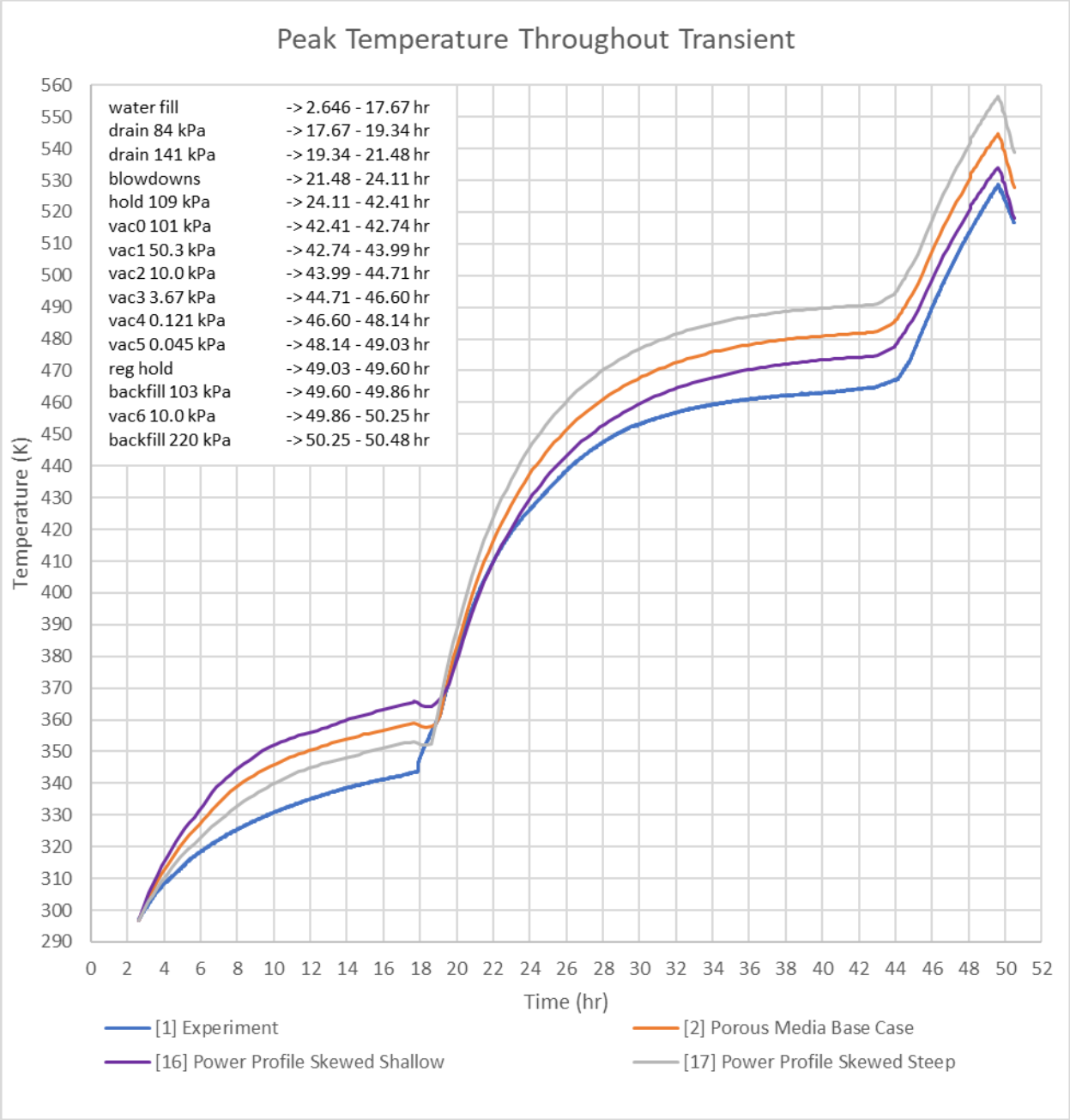


Figure 4-28 Transient Fuel Axial Max Temperature Profile for the 1.483 kW for Sensitivities 1, 2, 16, and 17

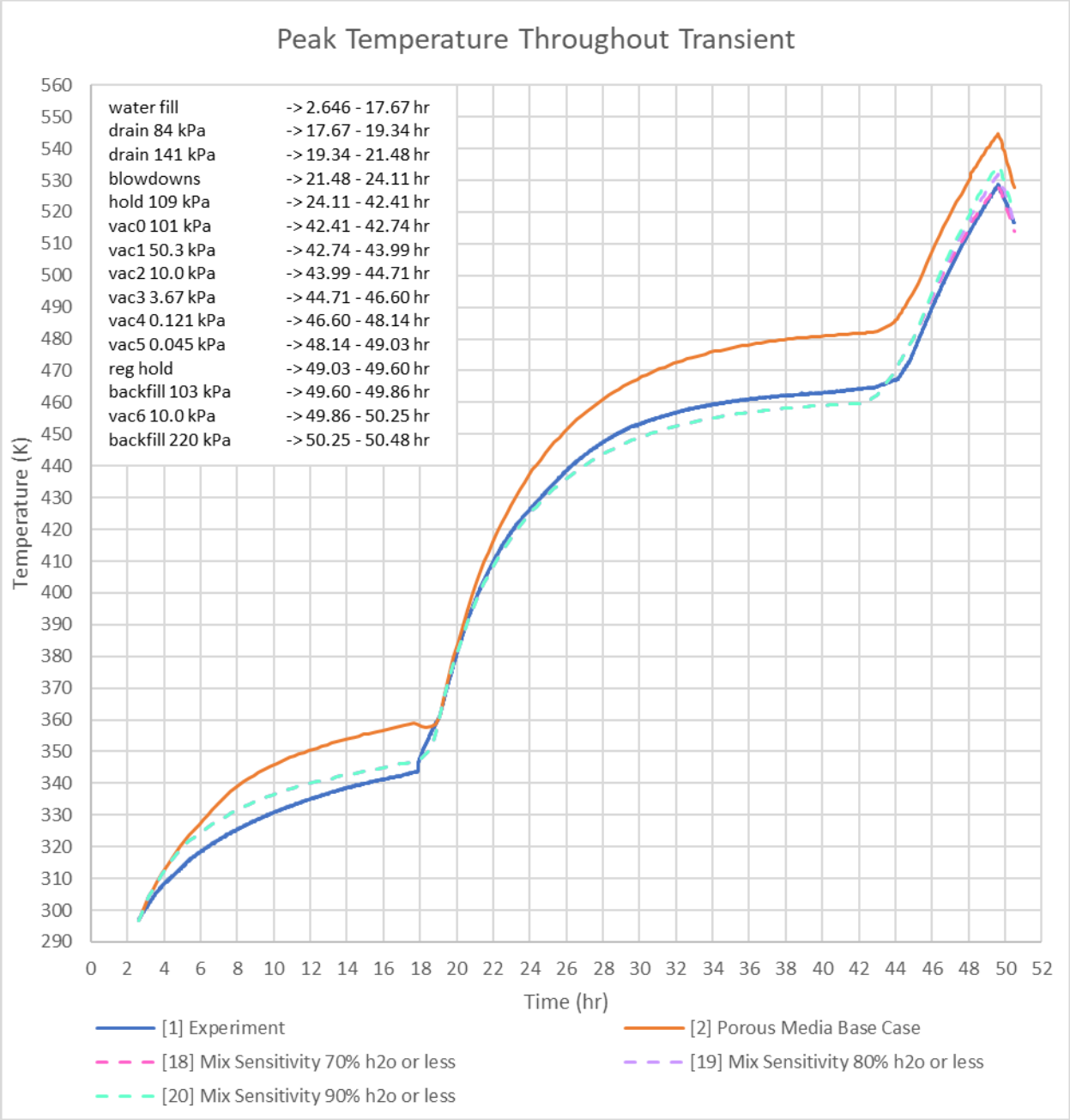


Figure 4-29 Transient Fuel Axial Max Temperature Profile for the 1.483 kW for Sensitivities 1, 2, 18, 19, and 20

5 CONCLUSIONS

A CFD validation based on data collected from the Sandia National Laboratories (SNL) Advanced Drying Cycle Simulator (ADCS) was performed following guidelines from NUREG-2152 and ASME V&V 20-2009. The ADCS, a test apparatus simulating the fuel compartment of a dry cask, was constructed and operated to produce first of a kind, high-fidelity transient and steady-state thermal-hydraulic data sets suitable for CFD model validation.

Two types of measurements were obtained in this experimental work. The first comprised steady-state case data involving helium fill gas at different storage pressures and decay heats. In this phase, cases involving 3 kW decay heat with canister pressures of 12 bar, 1 atm, 25 Torr, 10 Torr, 1 Torr and 0.1 Torr were used to validate the CFD base case model. The second type of measurement involved transient (time-dependent) data of the dry cask vacuum drying processes. In this phase, a case using decay heat of 1.483 kW was used to validate the CFD base case model. The steady-state and transient CFD models were both successfully validated using the ADCS experimental data.

The dry cask base case CFD modeling technique using porous media to simulate the fuel assembly internals was first compared with a fully explicit representation of the geometry including all the fuel assembly components. The favorable comparison between the two models (detailed in section 2.6) proved that the CFD porous model used for dry cask applications is very suitable, yet simpler and easier to create than the explicit geometry model. This comparison was made for the steady-state tests and the transient vacuum drying processes, including use of the multiphase Volume of Fluid (VOF) model.

Following the porous media versus explicit geometry comparisons, the CFD base case predictions for steady-state and transient vacuum drying cases were compared and validated using experimental data. The validation used a full and detailed uncertainty quantification (UQ) approach. The UQ included numerical uncertainty, CFD model input uncertainty, and experimental uncertainties. The numerical uncertainty included computer round-off error, iterative convergence error, and discretization error using the grid convergence index (GCI). The input uncertainty included errors due to the likely uncertainty of the inputs used to create the CFD case model. The details of all input errors considered are shown and explained in chapter 3. Among the input errors that contributed the most uncertainty were the external canister wall heat transfer coefficient, power profile skewness, ambient temperature, porous media fuel assembly viscous resistance, air ingress molar fraction in subatmospheric vacuum pressure conditions for steady-state cases, and the water vapor molar fraction measurement uncertainty for the transient vacuum drying case at the regulatory hold step.

The validation used comparison metrics including the PCT, the PCT location, the fuel region maximum (i.e., centerline) temperature for at least seven axial locations, and the pressure vessel external wall temperature in at least seven axial locations. The CFD predictions were found to match experimental data within the simulation uncertainty for most of the comparison metrics used for the PCT, PCT location, maximum fuel temperature in the fuel region in at least seven locations, and the temperature values on the pressure vessel external wall for at least seven locations. The PCT and the PCT location for all the steady-state cases as well as the transient were fully validated.

This report, along with NUREG-2238, “Validation of a Computational Fluid Dynamics Method Using Vertical Dry Cask Simulator Data”, NUREG/CR-7260, “CFD Validation of Vertical Dry Cask Storage System”, and NUREG/CR-7274, “Validation of Computational Fluid Dynamics Method

Using Horizontal Dry Cask Simulator Data" demonstrates how to implement ASME V&V 20-2009 to quantify the uncertainty of a spent fuel storage cask CFD model.

It is demonstrated that the porous media approach is an accurate method (i.e., has the correct physical models) to predict the PCT value, given accurate simulation inputs. This enables applicants to take a conservative approach in demonstrating the thermal compliance of their cask thermal design by using conservative boundary conditions and geometric assumptions, while using an accurate modeling process, as documented in NUREG-2152. Numerical uncertainty exists in all simulations, and it should be demonstrated to be less than the margin. However, the use of conservative input values makes the need for the rigorous input sensitivity (UQ for input parameters) demonstrated here unnecessary.

The PCT validation uncertainty for all helium fill steady-state cases, for the pressure varying from 0.1 Torr to 12 bar and excluding the 1 Torr case, varied between 22–25 degrees Celsius (°C) (40–45 degrees Fahrenheit (°F)). For the 1 Torr case, excessive air ingress into the canister increased the validation uncertainty to 52°C (94°F), which was evaluated for an air ingress molar fraction of 10 percent. The air ingress for the 1 Torr steady-state case is discussed in depth in section 4.1. Beside the air ingress that occurred only in the 1 Torr case, the main contributor to uncertainty for the steady-state cases was the external convection coefficient and power profile. For the transient vacuum drying case at the regulatory hold step, the validation uncertainty was evaluated to be 15°C (27°F) without the inclusion of the water vapor measurement error. When 30 percent of water vapor molar fraction uncertainty was included, an uncertainty of 21°C (38°F) was obtained. The main contributor to validation uncertainty for the transient drying case was the uncertainty from the power profile and the water vapor molar fraction.

The water vapor molar fraction uncertainty is discussed in detail in sections 4.2 and 4.3. The validation uncertainty for the 1 Torr steady-state case would be greatly reduced if the air ingress observed during that test did not occur. Similarly, the validation uncertainty for the transient vacuum drying case would be substantially reduced if the uncertainty in water vapor molar fraction measurement were smaller. All cases other than the 12 bar steady-state case would have noticeably reduced validation uncertainty if the power profile shape were more certain. These uncertainties (air ingress, water vapor molar fraction, and power profile shape) could be feasibly reduced, or perhaps eliminated, and doing so would generally cut validation uncertainties by 40 percent or more (except for the 12 bar case, which is governed by the vessel external surface heat transfer coefficient).

In sensitivity section 4.3, the primary concern was to compare different options to model the ADCS experiment for the transient vacuum drying case. These options included types of physical models and conditions of the gas mixture in the canister. Some of these routines were amenable and easy to apply and produced conservative predictions without any difficulties in creating the case or obtaining converged solutions. The sensitivity included 18 cases, concluding the following:

- Multiphase flow is not needed for the first step (i.e., the hold step after the water fills the canister). Using multiphase models will complicate the simulation and create difficulties in obtaining a converged solution. The difficulties stem from the additional secondary phase volumetric fraction conservation equation and an interface tracking mechanism between the phases.

- The hold step after the water fill step is not needed to get safe, conservative thermal predictions. Other safe and easier-to-model options exist, such as initializing the entire

solution field with the water vapor saturation temperature at the draining and/or blowdown pressure.

- It is not necessary to use different mixtures of gases during the steps of the vacuum drying process. The optimal method is to use 100 percent helium before the vacuum steps, 100 percent water vapor during the vacuum steps, and then 100 percent helium after the regulatory hold step. Using these steps will enable easier model creation and convergence while providing conservative results.

- The predicted CFD data approached and matched the vacuum drying experimental data when 100 percent helium was used before the vacuum steps, then 50–70 percent water vapor molar fraction and 50–30 percent helium molar fraction were used for the vacuum steps, including the regulatory hold, and 100 percent helium was used for the final steps after the regulatory hold.

The option most often used by dry cask applicants ignores the water fill and post-water-fill hold step, as in sensitivity 10 or 11 (explained in section 4.3). The solution is initialized after water drain/blowdown with the water vapor saturation temperature at the existing pressure. Then, 100 percent helium is used before vacuum steps, followed by 100 percent water vapor during the vacuum steps, including the regulatory hold step. In the final steps following the regulatory hold, 100 percent helium is used. The CFD model in this approach used single-phase physical modeling with either 100 percent helium or 100 percent water vapor. The temperature predictions from this choice are acceptable and result in a safe, conservative method.

Applicants' PCT predictions are generally within a margin of 10–20°C (18–36°F), especially for cask designs with a high heat load. For this reason, a thermal model with a validation uncertainty of 21–52°C (38–94°F), as obtained in this report using the best estimate analysis (i.e., the most likely scenario supplemented by a complete UQ analysis), will not be useful to justify predictions with a margin of 10–20°C. Conversely, if a thermal model with conservative input parameters is used, UQ for input parameters is not necessary. Only numerical uncertainty consisting of discretization errors (i.e., GCI), round-off errors, and iteration errors are recommended. In this validation exercise, the PCT numerical uncertainty varied from 2–10°C (4–18°F) for the steady-state cases and 2°C for the transient vacuum drying case. Consequently, thermal models that have conservative input parameters (as is usually the case when applicants follow CFD modeling guidelines as documented in NUREG-2152) would generally be deemed acceptable with adequately demonstrated thermal margins.

When the cask is designed for higher decay heat, the PCT values approach the allowable limit, and the obtained margin is questionable. The method presented in this report to evaluate the UQ can be used to show certainty and confidence in the obtained margins. The method presented here, when used properly, will inform the applicant and the thermal reviewer about the confidence and certainty of the margin for any cask design. Often, the cask applicant uses the worst-case scenario to perform dry cask thermal analyses, especially when there is enough margin from the allowable PCT limit. The worst-case scenario model should be based on proven conservative input values using a phenomena identification and ranking table (PIRT). The right PIRT should include all the possible input variables and modeling settings with possible uncertainties. As such, the worst-case scenario model will consist of input choices that negatively impact the dry cask thermal performance (i.e., each input variable will lead to a higher PCT). The modeling uncertainty for this type of thermal model should include only numerical uncertainties. In this case, the safety margin would generally be acceptable if it is demonstrated that it adequately covers the numerical uncertainty and any other additional unknown modeling uncertainties, given that the thermal

model for the worst-case scenario followed CFD best practice guidelines, as documented in NUREG-2152.

The validation exercise contained in this report, NUREG-2238, NUREG/CR-7260, NUREG/CR-7274, and the SNL validation synthesis reports SAND2019 and SAND2020 showed that the CFD thermal model (as described in this report) using CFD best practice guidelines documented in NUREG-2152 resulted in PCT predictions that agreed very favorably with the experimental data, within the calculated validation uncertainty.

This report has demonstrated that the CFD simulation results of the ADCS thermal model are within the calculated validation uncertainties of the experimental data measured at SNL. Moreover, the process outlined here demonstrates the process by which simulation uncertainty can be quantified, as outlined in ASME V&V 20-2009, and using guidelines in NUREG-2152 for a complex, real-world application.

The typical certification process in 10 CFR Part 72 requires that the applicant demonstrate compliance under worst-case scenarios. For dry cask storage, the PCT must remain below the safe operating limits of the materials under the hottest ambient conditions that are expected to occur at a particular site. Using the same line of thinking, the simulation inputs (e.g., decay heat, ambient temperature, emissivity, etc.) would all be chosen as conservatively bounding values that would yield a PCT value equal to or greater than the actual PCT value. This type of approach provides reasonable assurance of the safe operation of the dry cask system.

Cask vendors have been submitting applications with margins in the range of about 10–20°C of the ISG-11 temperature limit of 400°C (752°F). A validation experiment would be useful and successful if it could improve the model's capabilities. This can be achieved if it is demonstrated that the accuracy of the CFD thermal model using the validation uncertainty is less than or equal to this margin of 10–20°C. Designs that are complex enough to benefit from CFD modeling generally have a great many inputs that influence the simulation result. CFD-grade experiments are those that precisely measure each one of these inputs so that the input uncertainty of the simulation can be minimized. It is a difficult and complicated task to design and conduct such an experiment, even for relatively simple configurations, which is why so few are conducted. However, to gain confidence in the application of CFD as a tool in the certification process, especially with more complex physics, validation exercises such as this are necessary.

The experimental data collected in this program was geared toward obtaining a CFD-grade experiment. The main objective of the CFD-grade experiment is to minimize validation uncertainty and hence to improve the CFD thermal model. When a thermal model is well validated, the dry cask applicants and thermal reviewers will have confidence in the predicted margin, even when it is minimized without exceeding the set limit. This report shows that a well-crafted, best estimate thermal model is one that is implemented using the design basis following CFD best practice guidelines and complemented by UQ. Such a model will provide enough information for dry cask applicants and thermal reviewers on the margins that can be considered safe for applications and certifications.

The method presented here, using a best estimate analysis that consisted of a base case CFD thermal model, complemented by UQ, shows that the PCT, PCT locations, and most of the fuel region centerline temperature predictions for all the cases were predicted within the calculated validation uncertainty bands, as shown in the result sections. Thus, the CFD models and inputs that were used in the ADCS modeling approach, as suggested in CFD best practice guidelines in NUREG-2152, were successfully validated using the data obtained from the ADCS

experiment at SNL. The validation uncertainty in this program consisted of possible variability of the model's input parameters and numerical and experimental uncertainties, as shown in the uncertainty chapter (i.e., chapter 3), results chapter (i.e., chapter 4), and appendix A.

As discussed earlier, among the leading contributors to the validation uncertainty in the ADCS program were measurement uncertainties such as air ingress molar fraction for the steady-state case and water vapor molar fraction for the transient vacuum drying case. These errors are specific to the ADCS program and will not be part of input errors in dry cask applications. Additional reasons for the increased validation uncertainty were the external convection coefficient to ambient, decay heat, and heat profile curve fitting uncertainty. Because the NRC certifies dry casks for a specific heat input and a prescribed peaking factor, the uncertainty input from these variables will not be of concern.

Additionally, dry cask applicants perform CFD analyses using worst-case scenarios with conservative values for the external convection coefficient, emissivity values, and thermophysical properties. The conservative input data should be obtained using rigorous PIRT and optimization to ensure the highest PCT is obtained for each chosen input parameter. Use of the worst-case scenario eliminates the input uncertainty but not the numerical uncertainty. Thus, the validation uncertainty, which also can be considered as margins to be kept from the limiting temperature, will decrease. Consequently, 10–20 K thermal margins can be considered acceptable if the worst-case scenario estimate CFD thermal model is used in addition to numerical uncertainty, including discretization (i.e., GCI), convergence error, and round-off errors. Alternatively, if the dry cask applicant chooses to not use the worst-case scenario with conservative input parameters, then the best estimate case is required, consisting of the base case and UQ using CFD best practice guidelines.

Based on this validation, the NRC has full confidence that the physical models and solver settings used in this thermal model will be able to predict dry cask thermal performance. The UQ method for dry cask analysis should include the following:

- numerical uncertainty
  - discretization error
  - convergence errors
  - round-off errors
- input uncertainty, including wall thermal emissivity, porous media effective thermal conductivity (i.e., radial and axial), thermophysical properties for fluids and solids, BCs (i.e., ambient temperature, heat exchange with ambient, inlet BC if applicable, geometrical uncertainties (e.g., gaps, geometrical approximations))
- experimental uncertainty, in the case of validation

6 REFERENCES

"Ansys Fluent User's Guide," January 2024.

ASME V&V 20-2009, "Standard for Verification and Validation in Computational Fluid Dynamics and Heat Transfer," American Society of Mechanical Engineers, 2009.

Bestion, D. et al., "Requirement for CFD-Grade Experiments for Nuclear Reactor Thermal-Hydraulics," Organisation for Economic Co-operation and Development, Nuclear Energy Agency, Committee on the Safety of Nuclear Installations, Working Group on Analysis and Management of Accidents, CFD Group, 2019.

Bestion, D. et al., "Review of Uncertainty Methods for Computational Fluid Dynamics Application to Nuclear Reactor Thermal Hydraulics," Organisation for Economic Co-operation and Development, Nuclear Energy Agency, Committee on the Safety of Nuclear Installations, Working Group on Analysis and Management of Accidents, CFD Group, 2016.

EPRI 3002013124, "High-Burnup Used Fuel Dry Storage System Thermal Modeling Benchmark," Electric Power Research Institute, April 2020.

Gambit 2.4.6, Fluent Inc, 2007.

Ganta, D., et al., "Optical method for measuring thermal accommodation coefficient using a whispering-gallery microresonator," *The Journal of Chemical Physics* 135, 084313 (2011), August 2011.

Interim Staff Guidance-11, Rev. 3, "Cladding Considerations for the Transportation and Storage of Spent Fuel," U.S. Nuclear Regulatory Commission, November 2003.

National Institute of Standards and Technology, NIST Chemistry WebBook, SRD 69, "Thermophysical Properties of Fluid Systems," https://webbook.nist.gov/chemistry/fluid/.

NUREG/CR-7260, "CFD Validation of Vertical Dry Cask Storage System," K. Hall, A. Zigh, and J. Solis., Alden Research Laboratory, Inc., May 2019.

NUREG/CR-7274, "Validation of Computational Fluid Dynamics Method Using Horizontal Dry Cask Simulator Data," Office of Nuclear Regulatory Research, U.S. Nuclear Regulatory Commission, December 2020.

NUREG-0800, "Standard Review Plan for the Review of Safety Analysis Reports for Nuclear Power Plants: LWR Edition," U.S. Nuclear Regulatory Commission, March 2017.

NUREG-2152, "Computational Fluid Dynamics Best Practice Guidelines for Dry Cask Applications, Final Report," U.S. Nuclear Regulatory Commission, March 2013.

NUREG-2174, "Impact of Variation in Environmental Conditions on the Thermal Performance of Dry Storage Casks," Office of Nuclear Regulatory Research and Office of Nuclear Material Safety and Safeguards, U.S. Nuclear Regulatory Commission, March 2016.

NUREG-2208, "Validation of Computational Fluid Dynamics Methods Using Prototypic Light Water Reactor Spent Fuel Assembly Thermal-Hydraulic Data," Office of Nuclear Regulatory Research, U.S. Nuclear Regulatory Commission, March 2017.

NUREG-2215, "Standard Review Plan for Spent Fuel Dry Storage Systems and Facilities," U.S. Nuclear Regulatory Commission, April 2020.

NUREG-2238, "Validation of a Computational Fluid Dynamics Method Using Vertical Dry Cask Simulator Data," Office of Nuclear Regulatory Research, U.S. Nuclear Regulatory Commission, June 2020.

Regulatory Guide 1.203, “Transient and Accident Analysis Methods,” U.S. Nuclear Regulatory Commission, December 2005.

SAND2017-13058R, “Materials and Dimensional Reference Handbook for the Boiling Water Reactor Dry Cask Simulator,” E.R. Lindgren and S.G. Durbin, Sandia National Laboratories, November 2017.

SAND2019-6079R, “Modeling Validation Exercises Using the Dry Cask Simulator,” R.J.M. Pulido, E.R. Lindgren, S.G. Durbin, A. Zigh, J. Solis, S.R. Suffield, D.J. Richmond, J.A. Fort, L.E. Herranz., F. Feria, J. Penalva, M. Lloret, M. Galban, J. Benavides, and G. Jimenez, Sandia National Laboratories, May 2019.

SAND2020-10344R, “Blind Modeling Validation Exercises Using the Horizontal Dry Cask Simulator,” R.J.M. Pulido, et al., Sandia National Laboratories, September 2020.

SAND2022-12078R, “Update on the Investigation of Commercial Drying Cycles Using the Advanced Drying Cycle Simulator,” R.J.M. Pulido, et al., Sandia National Laboratories, September 2022.

SAND2023-01454R, “Advanced Drying Cycle Simulator Thermal Response to Commercial Drying Conditions,” R.J.M. Pulido, et al., Sandia National Laboratories, March 2023.

SAND2023-09746R, “Preliminary Simulations of Commercial Drying Cycles Using the Advanced Drying Cycle Simulator,” R.J.M. Pulido, et al., Sandia National Laboratories, September 2023.

SAND2024, “Summary of Spent Nuclear Fuel Thermal and Drying Research at Sandia National Laboratories,” R.J.M. Pulido, et al., Sandia National Laboratories, draft, September 2024.

Title 10 of the *Code of Federal Regulations,* U.S. Nuclear Regulatory Commission, Washington, DC.

Title 10 of the *Code of Federal Regulations* Part 72, “Licensing Requirements for the Independent Storage of Spent Nuclear Fuel, High-Level Radioactive Waste, and Reactor-Related Greater than Class C Waste,” U.S. Nuclear Regulatory Commission, 2016.

TRW Environmental Safety Systems, Inc., “Spent Nuclear Fuel Effective Thermal Conductivity Report,” prepared for U.S. Department of Energy, July 11, 1996.

APPENDIX A DETAILED VERIFICATION, VALIDATION, AND UNCERTAINTY QUANTIFICATION FOR ALL CASES

The following tables contain comparisons of computational fluid dynamics (CFD) results with the experimentally measured values for all measurements performed by Sandia National Laboratories (SNL) and used in this validation. Each measurement includes the validation uncertainty and whether the CFD result accurately predicts the experimental measurement within the validation uncertainty.

Additionally, grouped bar charts of the temperature values along the axial direction at discrete points where the measurements were made in the fuel region and the external wall of the pressure vessel are included for each test case. Experimentally measured values and CFD predicted values are shown side by side for each case for the peak cladding temperature (PCT) in the fuel region, the location of the PCT, and the temperature values for specific heights for the fuel region and the external wall of the pressure vessel. Error bars are provided at each experimental measurement location to denote the validation uncertainty at each location. The validation uncertainty includes experimental uncertainty and simulation uncertainty, as explained in chapter 3, so there are no separate error bars for the experimental uncertainty.

The tables and figures in this appendix are for cases with uninsulated flanges and no heat trace unless mentioned differently.

Table A-1 Steady-State Test Results for 3 kW, 1,200 kPa, Helium

Parameter		Test Result	CFD Result	Test – CFD	Neg Uncert.	Pos Uncert.	Sym Uncert.	Valid?
PCT Location	Units							
Z value	m	3.66	3.66	0.00	-0.43	0.16	0.30	YES
PCT Value	K	456.2	467.8	-11.6	-19.5	24.8	22.1	YES
Fuel Region								
J9 Location								
z = 0.36 m	K	345.9	356.6	-10.7	-10.5	16.2	13.3	NO
z = 0.91 m	K	379.2	387.7	-8.5	-13.1	19.1	16.0	YES
z = 1.83 m	K	418.8	426.7	-7.9	-15.4	22.0	18.6	YES
z = 2.44 m	K	438.2	445.1	-6.9	-15.7	22.4	19.0	YES
z = 3.01 m	K	449.8	457.7	-7.9	-15.6	22.2	18.9	YES
z = 3.66 m	K	456.2	467.4	-11.2	-15.6	21.8	18.7	YES
z = 3.78 m	K	454.8	466.3	-11.5	-15.4	21.4	18.4	YES

Table A-2 Steady-State Test Results for 3 kW, 1 atm, Helium

Parameter		Test Result	CFD Result	Test – CFD	Neg Uncert.	Pos Uncert.	Sym Uncert.	Valid?
PCT Location	Units							
Z value	m	0.91	0.94	-0.03	-0.32	0.28	0.30	YES
PCT Value	K	575.5	580.4	-4.9	-18.9	22.1	20.4	YES
Fuel Region								
J9 Location								
z = 0.36 m	K	533.7	553.7	-20.0	-21.7	24.3	22.9	YES
z = 0.91 m	K	575.5	580.2	-4.7	-18.3	20.8	19.5	YES
z = 1.83 m	K	558.9	561.6	-2.7	-11.7	15.1	13.4	YES
z = 2.44 m	K	542.9	542.1	0.8	-13.3	16.2	14.7	YES
z = 3.01 m	K	522.3	518.9	3.4	-19.3	20.6	19.9	YES
z = 3.66 m	K	435.7	442.3	-6.6	-18.8	19.3	19.0	YES
z = 3.78 m	K	405.7	413.9	-8.2	-15.5	16.1	15.7	YES

Table A-3 Steady-State Test Results for 3 kW, 25 Torr, Helium

Parameter		Test Result	CFD Result	Test – CFD	Neg Uncert.	Pos Uncert.	Sym Uncert.	Valid?
PCT Location	Units							
Z value	m	0.91	0.78	0.13	-0.28	0.46	0.37	YES
PCT Value	K	584.8	583.7	1.1	-19.1	22.4	20.7	YES
Fuel Region								
J9 Location								
z = 0.36 m	K	555.8	569.7	-13.9	-21.4	23.3	22.2	YES
z = 0.91 m	K	584.8	583.2	1.6	-17.8	20.2	18.9	YES
z = 1.83 m	K	565.7	560.9	4.8	-11.9	15.3	13.6	YES
z = 2.44 m	K	549.9	540.6	9.3	-14.2	16.9	15.5	YES
z = 3.01 m	K	528.0	515.6	12.4	-20.5	21.8	21.1	YES
z = 3.66 m	K	424.2	431.5	-7.3	-18.8	19.4	19.0	YES
z = 3.78 m	K	394.0	403.2	-9.2	-15.7	16.3	15.9	YES

Table A-4 Steady-State Test Results for 3 kW, 10 Torr, Helium

Parameter		Test Result	CFD Result	Test – CFD	Neg Uncert.	Pos Uncert.	Sym Uncert.	Valid?
PCT Location	Units							
Z value	m	0.91	0.78	0.13	-0.28	0.46	0.37	YES
PCT Value	K	590.4	583.0	7.4	-19.1	22.4	20.7	YES
Fuel Region								
J9 Location								
z = 0.36 m	K	561.6	568.9	-7.3	-21.4	23.4	22.3	YES
z = 0.91 m	K	590.4	582.5	7.9	-17.8	20.2	18.9	YES
z = 1.83 m	K	571.2	560.1	11.1	-11.9	15.4	13.6	YES
z = 2.44 m	K	554.9	539.8	15.1	-14.3	17.0	15.6	YES
z = 3.01 m	K	531.9	514.8	17.1	-20.5	21.8	21.1	YES
z = 3.66 m	K	425.0	430.6	-5.6	-18.8	19.4	19.1	YES
z = 3.78 m	K	394.1	402.3	-8.2	-15.8	16.3	16.0	YES

Table A-5 Steady-State Test Results for 3 kW, 1 Torr, Helium

Parameter		Test Result	CFD Result	Test – CFD	Neg Uncert.	Pos Uncert.	Sym Uncert.	Valid?
PCT Location	Units							
Z value	m	0.91	0.78	0.13	-0.28	0.46	0.37	YES
PCT Value	K	622.7	583.0	39.7	-19.1	22.4	20.7	NO
Fuel Region								
J9 Location								
z = 0.36 m	K	590.1	568.9	21.2	-21.4	23.4	22.3	YES
z = 0.91 m	K	622.7	582.5	40.2	-17.8	20.2	18.9	NO
z = 1.83 m	K	602.7	560.1	42.6	-11.9	15.4	13.6	NO
z = 2.44 m	K	583.8	539.8	44.0	-14.3	17.0	15.6	NO
z = 3.01 m	K	557.9	514.8	43.1	-20.5	21.8	21.1	NO
z = 3.66 m	K	440.9	430.6	10.3	-18.8	19.4	19.1	YES
z = 3.78 m	K	408.0	402.3	5.7	-15.8	16.3	16.0	YES

Table A-6 Steady-State Test Results for 3 kW, 1 Torr, Helium, Using 10 Percent Molar Fraction Ingress in the Uncertainty Quantification

Parameter		Test Result	CFD Result	Test – CFD	Neg Uncert.	Pos Uncert.	Sym Uncert.	Valid?
PCT Location	Units							
Z value	m	0.91	0.78	0.13	-0.28	0.46	0.37	YES
PCT Value	K	622.7	583.0	39.7	-19.1	51.6	50.9	YES
Fuel Region								
J9 Location								
z = 0.36 m	K	590.1	568.9	21.2	-21.4	53.6	53.2	YES
z = 0.91 m	K	622.7	582.5	40.2	-17.8	50.2	49.7	YES
z = 1.83 m	K	602.7	560.1	42.6	-11.9	46.5	45.9	YES
z = 2.44 m	K	583.8	539.8	44.0	-14.3	45.7	45.2	YES
z = 3.01 m	K	557.9	514.8	43.1	-20.5	45.8	45.5	YES
z = 3.66 m	K	440.9	430.6	10.3	-18.8	37.6	37.4	YES
z = 3.78 m	K	408.0	402.3	5.7	-15.8	34.4	34.2	YES

Table A-7 Steady-State Test Results for 3 kW, 1 Torr, Helium, Using Insulated Heat Traced Flanges Experimental Data and Insulated Flanges CFD Predictions with Uninsulated Uncertainty

Parameter		Test Result	CFD Result	Test – CFD	Neg Uncert.	Pos Uncert.	Sym Uncert.	Valid?
PCT Location	Units							
Z value	m	0.91	0.94	-0.03	-0.28	0.46	0.37	YES
PCT Value	K	593.4	580.2	13.2	-19.1	22.4	20.7	YES
Fuel Region								
J9 Location								
z = 0.36 m	K	569.3	563.2	6.1	-21.4	23.4	22.3	YES
z = 0.91 m	K	593.4	580.1	13.3	-17.8	20.2	18.9	YES
z = 1.83 m	K	572.0	560.0	12.0	-11.9	15.4	13.6	YES
z = 2.44 m	K	555.1	539.8	15.3	-14.3	17.0	15.6	YES
z = 3.01 m	K	532.2	514.8	17.4	-20.5	21.8	21.1	YES
z = 3.66 m	K	425.9	430.5	-4.6	-18.8	19.4	19.1	YES
z = 3.78 m	K	395.3	402.3	-7.0	-15.8	16.3	16.0	YES

Table A-8 Steady-State Test Results for 3 kW, 0.1 Torr, Helium, Using Insulated Heat Traced Flanges Experimental Data and Uninsulated Flanges CFD Predictions and Uncertainty Quantification

Parameter		Test Result	CFD Result	Test – CFD	Neg Uncert.	Pos Uncert.	Sym Uncert.	Valid?
PCT Location	Units							
Z value	m	0.91	0.78	0.13	-0.28	0.46	0.37	YES
PCT Value	K	597.2	583.1	14.1	-19.1	22.4	20.7	YES
Fuel Region								
J9 Location								
z = 0.36 m	K	573.0	569.1	3.9	-21.4	23.3	22.3	YES
z = 0.91 m	K	597.2	582.6	14.6	-17.8	20.2	18.9	YES
z = 1.83 m	K	575.7	560.3	15.4	-11.9	15.4	13.6	YES
z = 2.44 m	K	558.8	540.0	18.8	-14.2	17.0	15.6	NO
z = 3.01 m	K	535.8	515.0	20.8	-20.5	21.8	21.1	YES
z = 3.66 m	K	429.3	430.8	-1.5	-18.8	19.4	19.0	YES
z = 3.78 m	K	398.4	402.6	-4.2	-15.7	16.3	16.0	YES

Table A-9 Steady-State Test Results for 3 kW, 0.1 Torr, Helium, Using Insulated Heat Traced Flanges CFD and Experimental Data but Uncertainty Quantification of Uninsulated Flanges CFD Case

Parameter		Test Result	CFD Result	Test – CFD	Neg Uncert.	Pos Uncert.	Sym Uncert.	Valid?
PCT Location	Units							
Z value	m	0.91	0.94	-0.03	-0.28	0.46	0.37	YES
PCT Value	K	597.2	580.4	16.8	-19.1	22.4	20.7	YES
Fuel Region								
J9 Location								
z = 0.36 m	K	573.0	562.8	10.2	-21.4	23.3	22.3	YES
z = 0.91 m	K	597.2	580.3	16.9	-17.8	20.2	18.9	YES
z = 1.83 m	K	575.7	560.2	15.5	-11.9	15.4	13.6	YES
z = 2.44 m	K	558.8	540.0	18.8	-14.2	17.0	15.6	NO
z = 3.01 m	K	535.8	515.0	20.8	-20.5	21.8	21.1	YES
z = 3.66 m	K	429.3	430.8	-1.5	-18.8	19.4	19.0	YES
z = 3.78 m	K	398.4	402.6	-4.2	-15.7	16.3	16.0	YES

Table A-10 Transient Test Results for 1.483 kW, at Regulatory Hold, Water Vapor

Parameter		Test Result	CFD Result	Test – CFD	Neg Uncert.	Pos Uncert.	Sym Uncert.	Valid?
PCT Location	Units							
Z value	m	0.91	0.94	-0.03	-0.42	0.52	0.47	YES
PCT Value	K	528.7	544.5	-15.8	-21.2	14.8	21.6	YES
Fuel Region								
J9 Location								
z = 0.36 m	K	502.5	531.8	-29.3	-23.0	17.3	22.9	NO
z = 0.91 m	K	528.7	544.5	-15.8	-21.8	14.3	21.8	YES
z = 1.83 m	K	513.7	530.3	-16.6	-19.6	8.7	19.7	YES
z = 2.44 m	K	500.1	513.7	-13.6	-20.6	10.5	20.7	YES
z = 3.01 m	K	481.7	492.0	-10.3	-24.1	16.2	23.9	YES
z = 3.66 m	K	402.8	429.9	-27.1	-24.8	18.5	24.6	NO
z = 3.78 m	K	383.3	412.9	-29.6	-25.2	19.4	25.1	NO

Table A-11 Helium Fill Gas Steady State and Transient Vacuum Drying Case at Regulatory Hold PCT Results

PCT	EXP Data (K)	CFD Data (K)	EXP – CFD (K)	Neg Uncert. (K)	Pos Uncert. (K)	Sym Uncert (K)	Valid?
Steady (3 kW, 12 bar)	456.2	467.8	-11.6	-19.5	24.8	22.1	**YES**
Steady (3 kW, 1 atm)	575.5	580.4	-4.9	-18.9	22.1	20.4	**YES**
Steady (3 kW, 25 Torr)	584.8	583.7	1.1	-19.1	22.4	20.7	**YES**
Steady (3 kW, 10 Torr)	590.4	583.0	7.4	-19.1	22.4	20.7	**YES**
Steady (3 kW, 1 Torr)	622.7	583.0	39.7	-19.1	22.4	20.7	**NO**
Steady (3 kW, 1 Torr) w/ 10% air uncert	622.7	583.0	39.7	-19.1	51.6	50.9	**YES**
Steady (3 kW, 0.1 Torr)	597.2	583.1	14.1	-19.1	22.4	20.7	**YES**
Transient 1.483 kW at Reg Hold	528.7	544.5	-15.8	-13.5	14.8	14.1	**NO**
Transient 1.483 kW at Reg Hold w/ 30% water vapor uncert	528.7	544.5	-15.8	-21.2	14.8	21.6	**YES**

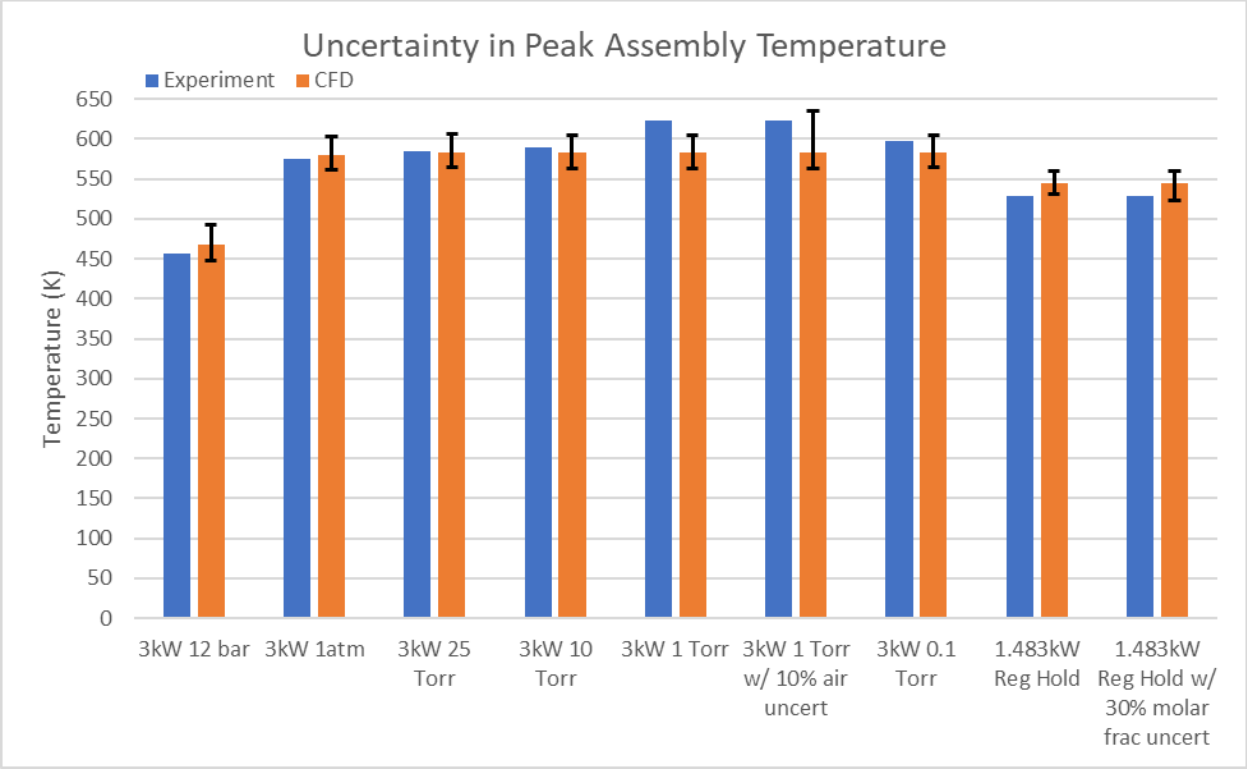


Figure A-1 PCT Results for Steady-State Cases and Transient Vacuum Drying Case at Regulatory Hold

Table A-12 Helium Steady-State and Transient Vacuum Drying Case at Regulatory Hold PCT Location Results

PCT Locations	EXP Data (m)	CFD Data (m)	EXP – CFD (m)	Neg Uncert. (m)	Post Uncert. (m)	Sym Uncert. (m)	Valid?
Steady (3 kW, 12 bar)	3.66	3.66	0.00	-0.43	0.16	0.30	**YES**
Steady (3 kW, 1 atm)	0.91	0.94	-0.03	-0.32	0.28	0.30	**YES**
Steady (3 kW, 25 Torr)	0.91	0.78	0.13	-0.28	0.46	0.37	**YES**
Steady (3 kW, 10 Torr)	0.91	0.78	0.13	-0.28	0.46	0.37	**YES**
Steady (3 kW, 1 Torr)	0.91	0.78	0.13	-0.28	0.46	0.37	**YES**
Steady (3 kW, 1 Torr) w/ 10% air uncert	0.91	0.78	0.13	-0.28	0.46	0.37	**YES**
Steady (3 kW, 0.1Torr)	0.91	0.78	0.13	-0.28	0.46	0.37	**YES**
Transient 1.483 kW at Reg Hold	0.91	0.94	-0.03	-0.42	0.52	0.47	**YES**
Transient 1.483 kW at Reg Hold w/ 30% water vapor uncert	0.91	0.94	-0.03	-0.42	0.52	0.47	**YES**

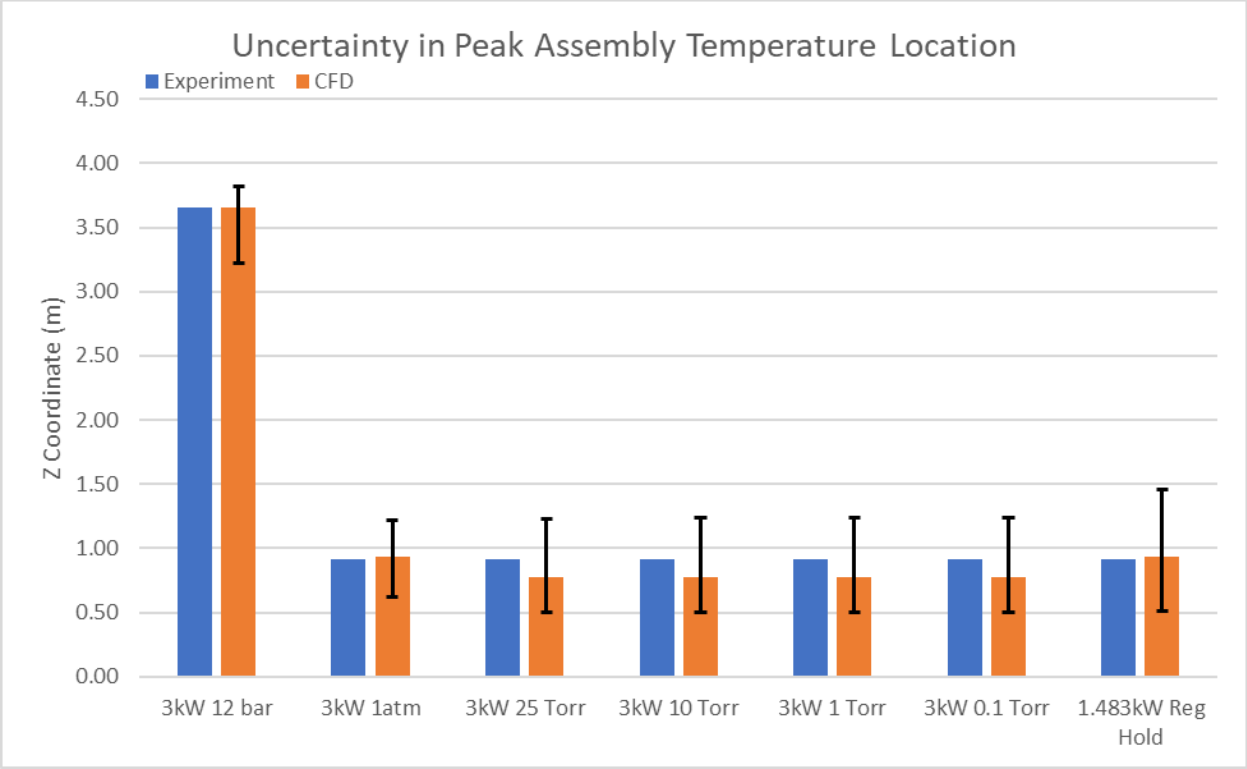


Figure A-2 PCT Locations Results for Steady-State Cases and Transient Vacuum Drying Case at Regulatory Hold

Table A-13 Helium Steady-State and Transient Vacuum Drying Case at Regulatory Hold Fuel Assembly Temperature Results at 0.36 m

Fuel Temp at 0.36 m	EXP Data (K)	CFD Data (K)	EXP – CFD (K)	Neg Uncert. (K)	Pos Uncert. (K)	Sym Uncert (K)	Valid?
Steady (3 kW, 12 bar)	345.9	356.6	-10.7	-10.5	16.2	13.3	**NO**
Steady (3 kW, 1 atm)	533.7	553.7	-20.0	-21.7	24.3	22.9	**YES**
Steady (3 kW, 25 Torr)	555.8	569.7	-13.9	-21.4	23.3	22.2	**YES**
Steady (3 kW, 10 Torr)	561.6	568.9	-7.3	-21.4	23.4	22.3	**YES**
Steady (3 kW, 1 Torr)	590.1	568.9	21.2	-21.3	23.3	22.3	**YES**
Steady (3 kW, 1 Torr) w/ 10% air uncert	590.1	568.9	21.2	-21.3	53.6	53.2	**YES**
Steady (3 kW, 0.1 Torr)	573.0	569.1	3.9	-21.4	23.3	22.3	**YES**
Transient 1.483 kW at Reg Hold	502.5	531.8	-29.3	-17.6	17.3	17.4	**NO**
Transient 1.483 kW at Reg Hold w/ 30% water vapor uncert	502.5	531.8	-29.3	-23.0	17.3	22.9	**NO**

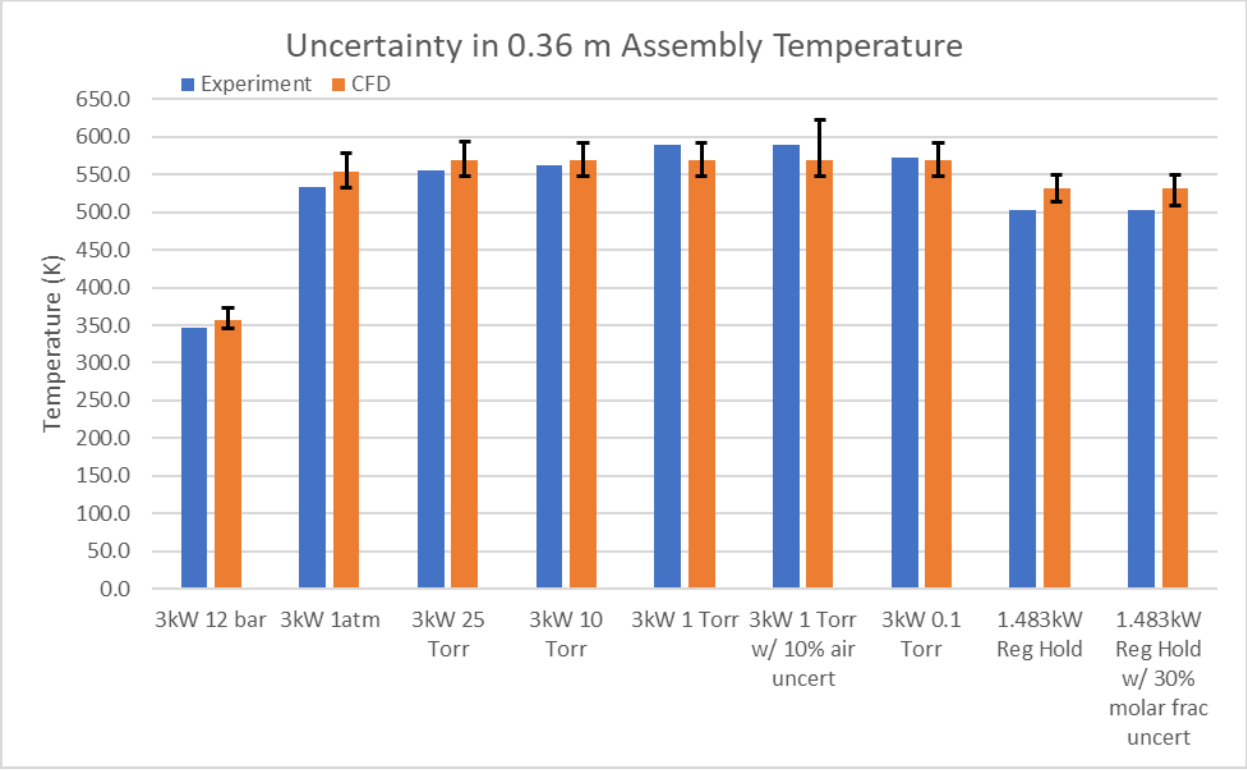


Figure A-3 Fuel Assembly Temperature Results for Steady-State Cases and Transient Vacuum Drying Case at Regulatory Hold at 0.36 m

Table A-14 Helium Steady-State and Transient Vacuum Drying Case at Regulatory Hold Fuel Assembly Temperature Results at 0.91 m

Fuel Temp at 0.91 m	EXP Data (K)	CFD Data (K)	EXP – CFD (K)	Neg Uncert. (K)	Pos Uncert. (K)	Sym Uncert (K)	Valid?
Steady (3 kW, 12 bar)	379.2	387.7	-8.5	-13.1	19.1	16.0	**YES**
Steady (3 kW, 1 atm)	575.5	580.2	-4.7	-18.3	20.8	19.5	**YES**
Steady (3 kW, 25 Torr)	584.8	583.2	1.6	-17.8	20.2	18.9	**YES**
Steady (3 kW, 10 Torr)	590.4	582.5	7.9	-17.8	20.2	18.9	**YES**
Steady (3 kW, 1 Torr)	622.7	582.5	40.2	-17.8	20.2	18.9	**NO**
Steady (3 kW, 1 Torr) w/ 10% air uncert	622.7	582.5	40.2	-17.8	50.2	49.7	**YES**
Steady (3 kW, 0.1 Torr)	597.2	582.6	14.6	-17.8	20.2	18.9	**YES**
Transient 1.483 kW at Reg Hold	528.7	544.5	-15.8	-14.3	14.3	14.3	**NO**
Transient 1.483 kW at Reg Hold w/ 30% water vapor uncert	528.7	544.5	-15.8	-21.8	14.3	21.8	**YES**

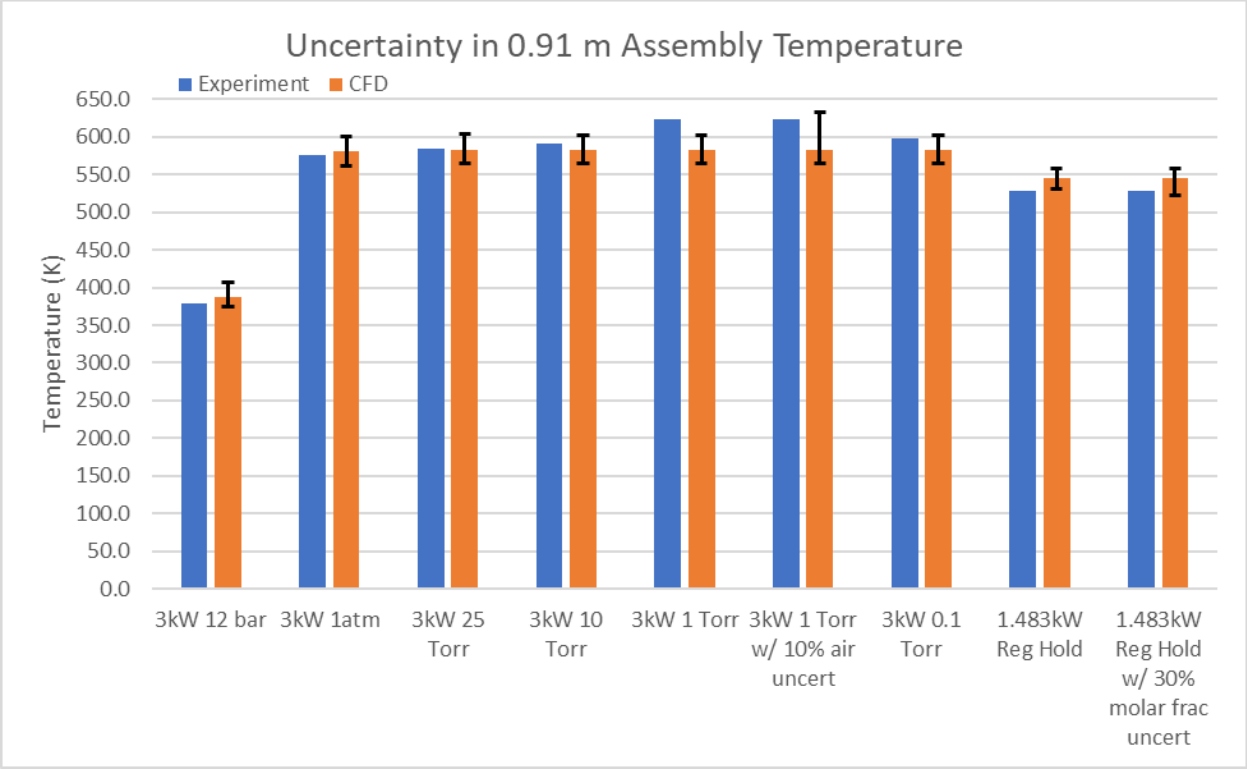


Figure A-4 Fuel Assembly Temperature Results for Steady-State Cases and Transient Vacuum Drying Case at Regulatory Hold at 0.91 m

Table A-15 Helium Steady-State and Transient Vacuum Drying Case at Regulatory Hold Fuel Assembly Temperature Results at 1.83 m

Fuel Temp at 1.83 m	EXP Data (K)	CFD Data (K)	EXP – CFD (K)	Neg Uncert. (K)	Pos Uncert. (K)	Sym Uncert (K)	Valid?
Steady (3 kW, 12 bar)	418.8	426.7	-7.9	-15.4	22.0	18.6	**YES**
Steady (3 kW, 1 atm)	558.9	561.6	-2.7	-11.7	15.1	13.4	**YES**
Steady (3 kW, 25 Torr)	565.7	560.9	4.8	-11.9	15.3	13.6	**YES**
Steady (3 kW, 10 Torr)	571.2	560.1	11.1	-11.9	15.4	13.6	**YES**
Steady (3 kW, 1 Torr)	602.7	560.1	42.6	-11.9	15.4	13.6	**NO**
Steady (3 kW, 1 Torr) w/ 10% air uncert	602.7	560.1	42.6	-11.9	46.5	45.9	**YES**
Steady (3 kW, 0.1 Torr)	575.7	560.3	15.4	-11.9	15.4	13.6	**YES**
Transient 1.483 kW at Reg Hold	513.7	530.3	-16.6	-8.2	8.7	8.5	**NO**
Transient 1.483 kW at Reg Hold w/ 30% water vapor uncert	513.7	530.3	-16.6	-19.6	8.7	19.7	**YES**

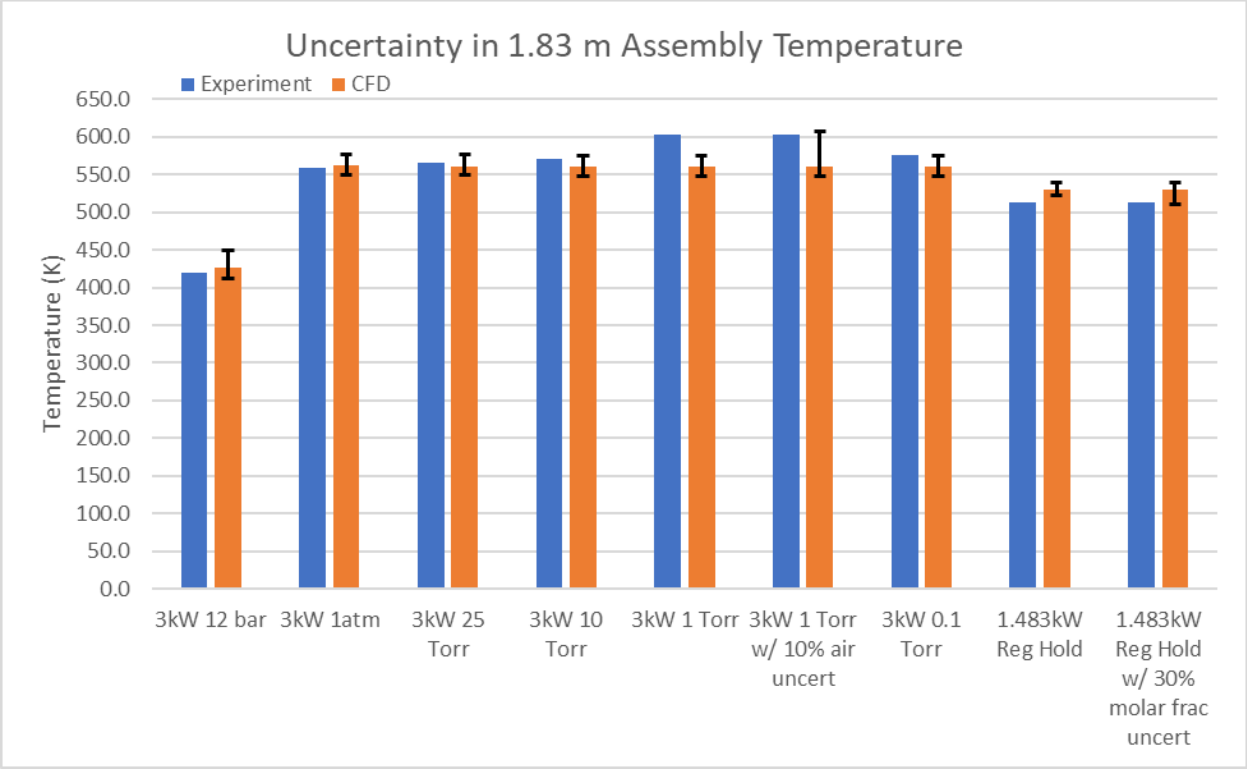


Figure A-5 Fuel Assembly Temperature Results for Steady-State Cases and Transient Vacuum Drying Case at Regulatory Hold at 1.83 m

Table A-16 Helium Steady-State and Transient Vacuum Drying Case at Regulatory Hold Fuel Assembly Temperature Results at 2.44 m

Fuel Temp at 2.44 m	EXP Data (K)	CFD Data (K)	EXP – CFD (K)	Neg Uncert. (K)	Pos Uncert. (K)	Sym Uncert (K)	Valid?
Steady (3 kW, 12 bar)	438.2	445.1	-6.9	-15.7	22.4	19.0	**YES**
Steady (3 kW, 1 atm)	542.9	542.1	0.8	-13.3	16.2	14.7	**YES**
Steady (3 kW, 25 Torr)	549.9	540.6	9.3	-14.2	16.9	15.5	**YES**
Steady (3 kW, 10 Torr)	554.9	539.8	15.1	-14.3	17.0	15.6	**YES**
Steady (3 kW, 1 Torr)	583.8	539.8	44.0	-14.3	17.0	15.6	**NO**
Steady (3 kW, 1 Torr) w/ 10% air uncert	583.8	539.8	44.0	-14.3	45.7	45.2	**YES**
Steady (3 kW, 0.1 Torr)	558.8	540.0	18.8	-14.2	17.0	15.6	**NO**
Transient 1.483 kW at Reg Hold	500.1	513.7	-13.6	-10.4	10.5	10.4	**NO**
Transient 1.483 kW at Reg Hold w/ 30% water vapor uncert	500.1	513.7	-13.6	-20.6	10.5	20.7	**YES**

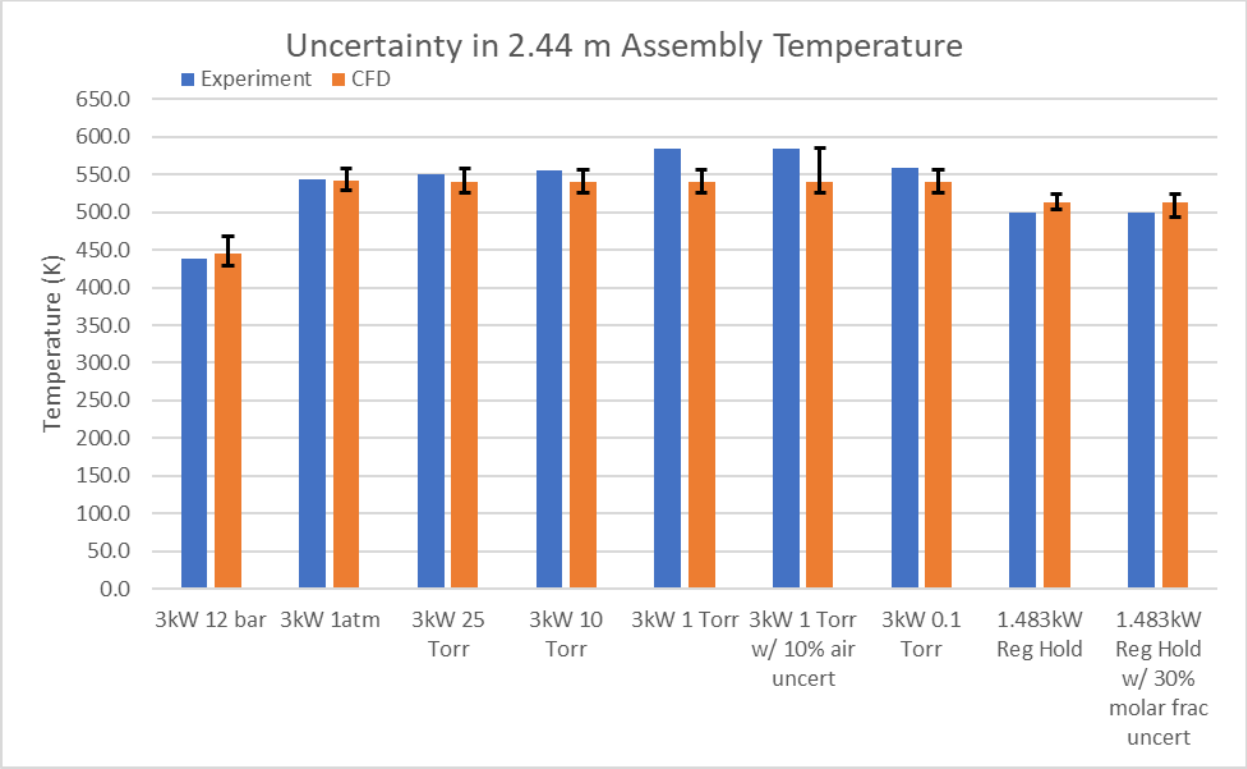


Figure A-6 Fuel Assembly Temperature Results for Steady-State Cases and Transient Vacuum Drying Case at Regulatory Hold at 2.44 m

Table A-17 Helium Steady-State and Transient Vacuum Drying Case at Regulatory Hold Fuel Assembly Temperature Results at 3.01 m

Fuel Temp at 3.01 m	EXP Data (K)	CFD Data (K)	EXP – CFD (K)	Neg Uncert. (K)	Pos Uncert. (K)	Sym Uncert (K)	Valid?
Steady (3 kW, 12 bar)	449.8	457.7	-7.9	15.6	22.2	18.9	**YES**
Steady (3 kW, 1 atm)	522.3	518.9	3.4	19.2	20.6	19.9	**YES**
Steady (3 kW, 25 Torr)	528.0	515.6	12.4	20.5	21.8	21.1	**YES**
Steady (3 kW, 10 Torr)	531.9	514.8	17.1	20.5	21.8	21.1	**YES**
Steady (3 kW, 1 Torr)	557.9	514.8	43.1	20.5	21.8	21.1	**NO**
Steady (3 kW, 1 Torr) w/ 10% air uncert	557.9	514.8	43.1	20.5	45.8	45.4	**YES**
Steady (3 kW, 0.1 Torr)	535.8	515.0	20.8	20.5	21.8	21.1	**YES**
Transient 1.483 kW at Reg Hold	481.7	492.0	-10.3	16.5	16.2	16.4	**YES**
Transient 1.483 kW at Reg Hold w/ 30% water vapor uncert	481.7	492.0	-10.3	24.1	16.2	23.9	**YES**

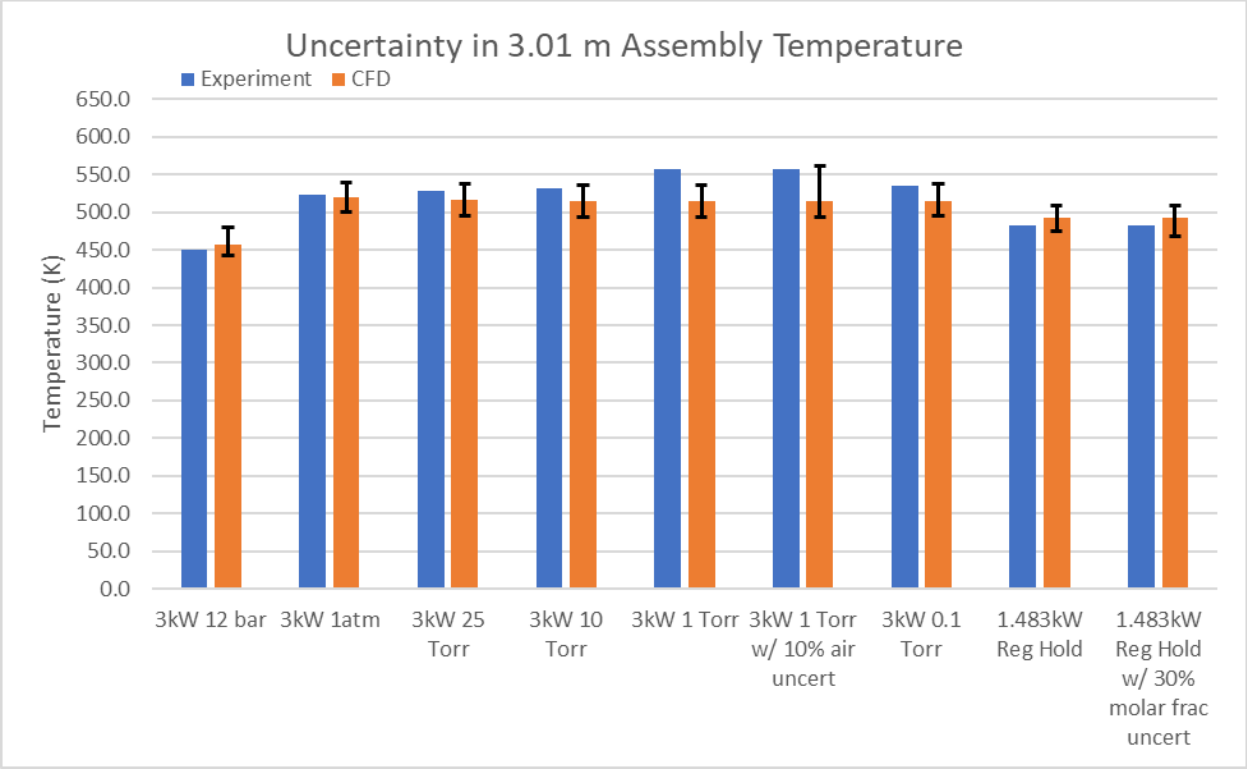


Figure A-7 Fuel Assembly Temperature Results for Steady-State Cases and Transient Vacuum Drying Case at Regulatory Hold at 3.01 m

Table A-18 Helium Steady-State and Transient Vacuum Drying Case at Regulatory Hold Fuel Assembly Temperature Results at 3.66 m

Fuel Temp at 3.66 m	EXP Data (K)	CFD Data (K)	EXP – CFD (K)	Neg Uncert. (K)	Pos Uncert. (K)	Sym Uncert (K)	Valid?
Steady (3 kW, 12 bar)	456.2	467.4	-11.2	-15.6	21.8	18.7	**YES**
Steady (3 kW, 1 atm)	435.7	442.3	-6.6	-18.8	19.3	19.0	**YES**
Steady (3 kW, 25 Torr)	424.2	431.5	-7.3	-18.8	19.4	19.0	**YES**
Steady (3 kW, 10 Torr)	425.0	430.6	-5.6	-18.8	19.4	19.1	**YES**
Steady (3 kW, 1 Torr)	440.9	430.6	10.3	-18.8	19.4	19.1	**YES**
Steady (3 kW, 1 Torr) w/ 10% air uncert	440.9	430.6	10.3	-18.8	37.6	37.4	**YES**
Steady (3 kW, 0.1 Torr)	429.3	430.8	-1.5	-18.8	19.4	19.0	**YES**
Transient 1.483 kW at Reg Hold	402.8	429.9	-27.1	-18.9	18.5	18.7	**NO**
Transient 1.483 kW at Reg Hold w/ 30% water vapor uncert	402.8	429.9	-27.1	-24.8	18.5	24.6	**NO**

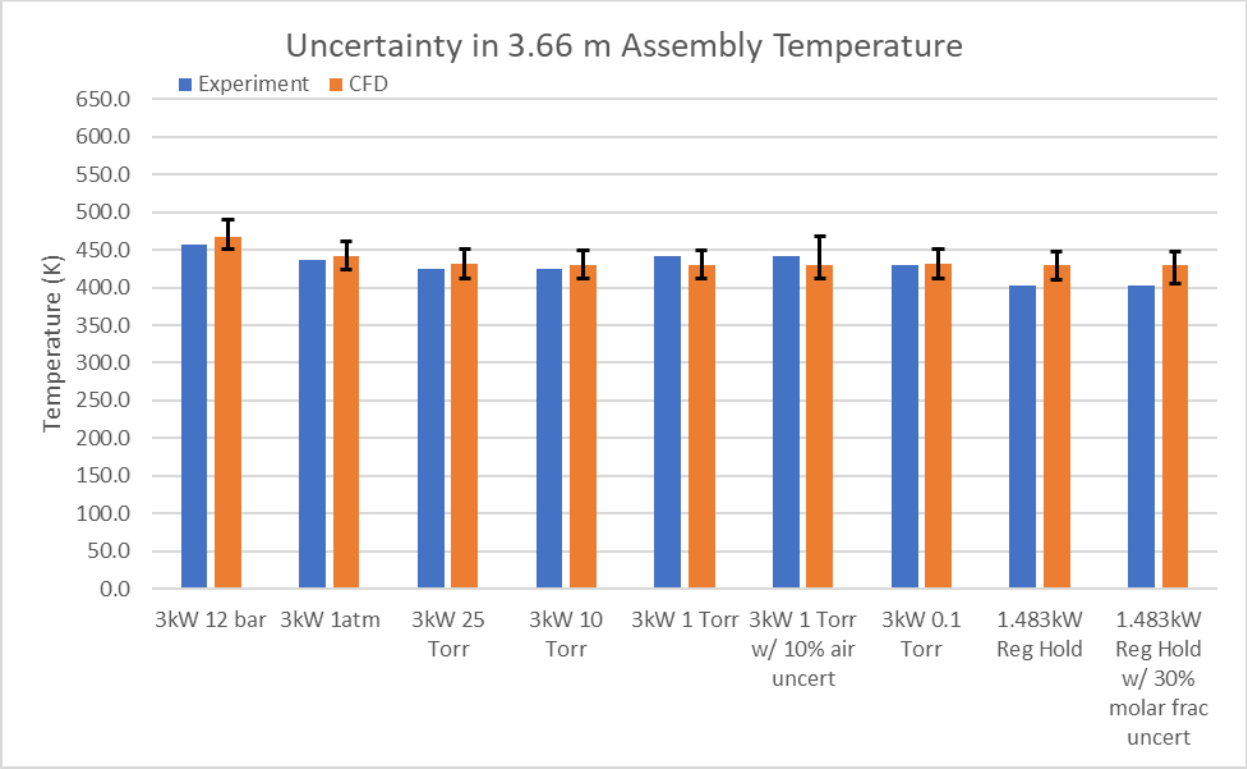


Figure A-8 Fuel Assembly Temperature Results for Steady-State Cases and Transient Vacuum Drying Case at Regulatory Hold at 3.66 m

Table A-19 Helium Steady-State and Transient Vacuum Drying Case at Regulatory Hold Fuel Assembly Temperature Results at 3.78 m

Fuel Temp at 3.78 m	EXP Data (K)	CFD Data (K)	EXP – CFD (K)	Neg Uncert. (K)	Pos Uncert. (K)	Sym Uncert (K)	Valid?
Steady (3 kW, 12 bar)	454.8	466.3	-11.5	-15.4	21.4	18.4	**YES**
Steady (3 kW, 1 atm)	405.7	413.9	-8.2	-15.5	16.1	15.7	**YES**
Steady (3 kW, 25 Torr)	394.0	403.2	-9.2	-15.7	16.3	15.9	**YES**
Steady (3 kW, 10 Torr)	394.1	402.3	-8.2	-15.8	16.3	16.0	**YES**
Steady (3 kW, 1 Torr)	408.0	402.3	5.7	-15.8	16.3	16.0	**YES**
Steady (3 kW, 1 Torr) w/ 10% air uncert	408.0	402.3	5.7	-15.8	34.4	34.2	**YES**
Steady (3 kW, 0.1 Torr)	398.4	402.6	-4.2	-15.7	16.3	16.0	**YES**
Transient 1.483 kW at Reg Hold	383.3	412.9	-29.6	-19.8	19.4	19.6	**NO**
Transient 1.483 kW at Reg Hold w/ 30% water vapor uncert	383.3	412.9	-29.6	-25.2	19.4	25.1	**NO**

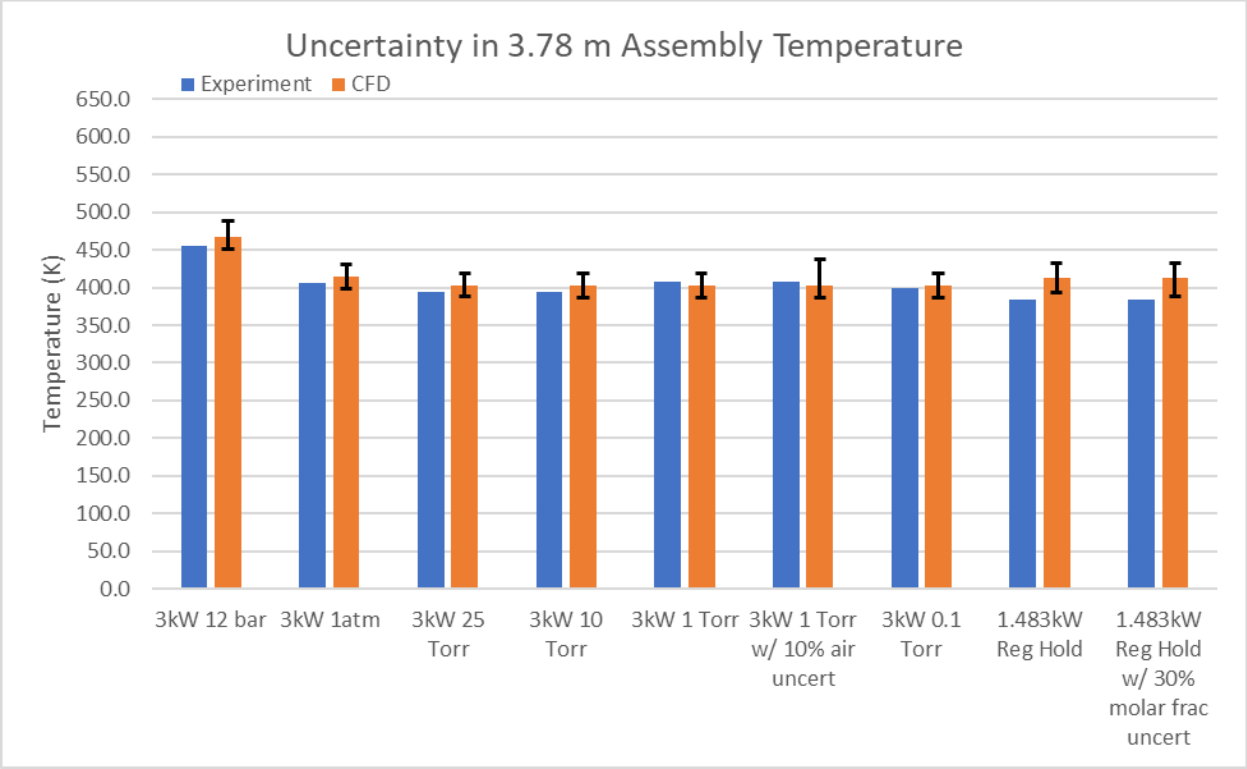


Figure A-9 Fuel Assembly Temperature Results for Steady-State Cases and Transient Vacuum Drying Case at Regulatory Hold at 3.78 m

Table A-20 Helium Fill Gas Steady-State and Transient Vacuum Drying Case at Regulatory Hold Pressure Vessel External Wall Results at 0.56 m

Vessel Temp at 0.56 m	EXP Data (K)	CFD Data (K)	EXP – CFD (K)	Neg Uncert. (K)	Pos Uncert. (K)	Sym Uncert (K)	Valid?
Steady (3 kW, 12 bar)	337.2	338.8	-1.6	-10.2	15.3	12.7	**YES**
Steady (3 kW, 1 atm)	357.0	373.2	-16.2	-15.3	21.8	18.5	**NO**
Steady (3 kW, 25 Torr)	358.4	375.5	-17.1	-15.1	21.8	18.4	**NO**
Steady (3 kW, 10 Torr)	355.3	374.4	-19.1	-15.2	22.0	18.5	**NO**
Steady (3 kW, 1 Torr)	355.2	374.4	-19.2	-15.2	21.9	18.5	**NO**
Steady (3 kW, 1 Torr) w/ 10% air uncert	355.2	374.4	-19.2	-15.2	22.0	18.5	**NO**
Steady (3 kW, 0.1 Torr)	367.3	374.7	-7.4	15.1	21.9	18.5	**YES**
Transient 1.483 kW at Reg Hold	314.9	323.4	-8.5	-8.4	9.7	9.0	**NO**
Transient 1.483 kW at Reg Hold w/ 30% water vapor uncert	314.9	323.4	-8.5	-8.5	9.7	9.1	**YES**

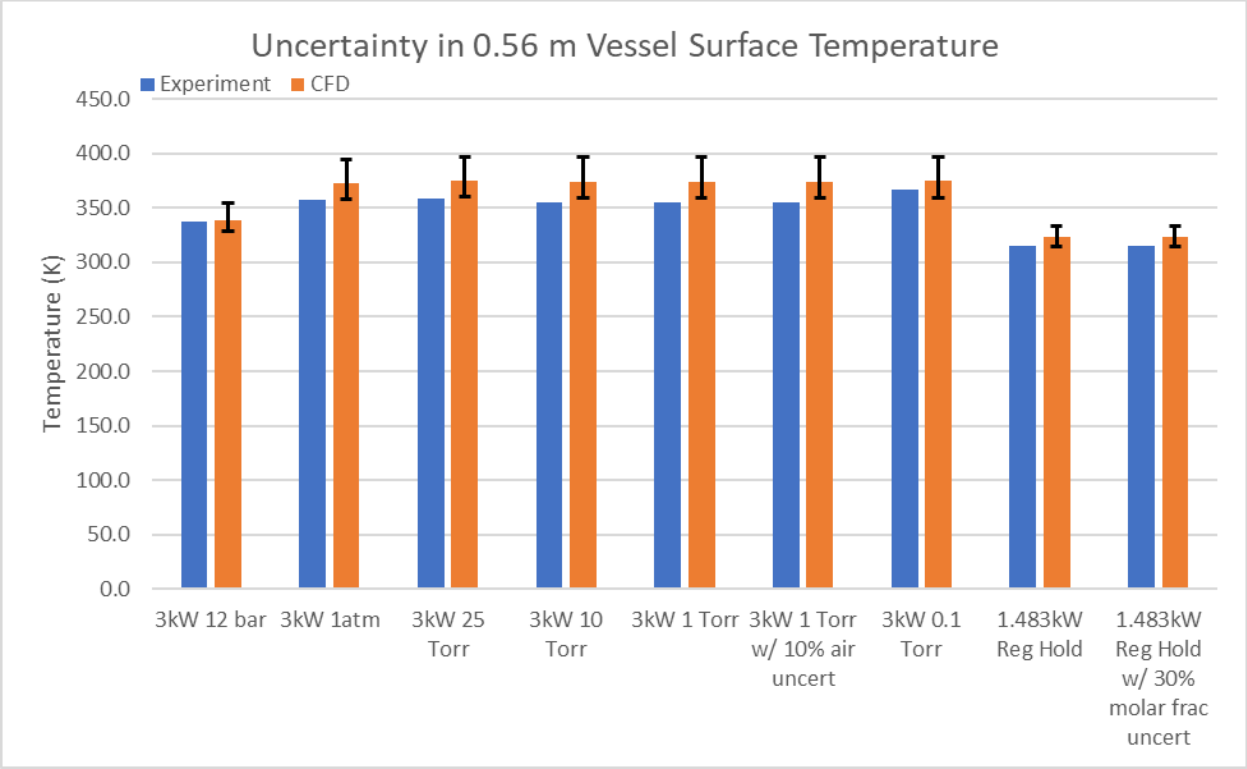


Figure A-10 Pressure Vessel External Wall Temperature Results for Steady-State Cases and Transient Vacuum Drying Case at Regulatory Hold at 0.56 m

Table A-21 Helium Fill Gas Steady-State and Transient Vacuum Drying Case at Regulatory Hold Pressure Vessel External Wall Results at 0.91 m

Vessel Temp at 0.91 m	EXP Data (K)	CFD Data (K)	EXP – CFD (K)	Neg Uncert. (K)	Pos Uncert. (K)	Sym Uncert (K)	Valid?
Steady (3 kW, 12 bar)	346.1	345.3	0.8	-10.9	16.1	13.5	**YES**
Steady (3 kW, 1 atm)	380.7	386.9	-6.2	-16.0	21.1	18.5	**YES**
Steady (3 kW, 25 Torr)	384.0	388.9	-4.9	-15.7	20.8	18.2	**YES**
Steady (3 kW, 10 Torr)	381.6	387.9	-6.3	-15.8	20.9	18.3	**YES**
Steady (3 kW, 1 Torr)	381.7	387.9	-6.2	-15.8	20.9	18.3	**YES**
Steady (3 kW, 1 Torr) w/ 10% air uncert	381.7	387.9	-6.2	-15.8	20.9	18.3	**YES**
Steady (3 kW, 0.1 Torr)	383.5	388.2	-4.7	-15.7	20.8	18.3	**YES**
Transient 1.483 kW at Reg Hold	326.8	330.2	-3.4	-9.2	11.2	10.1	**YES**
Transient 1.483 kW at Reg Hold w/ 30% water vapor uncert	326.8	330.2	-3.4	-9.2	11.2	10.2	**YES**

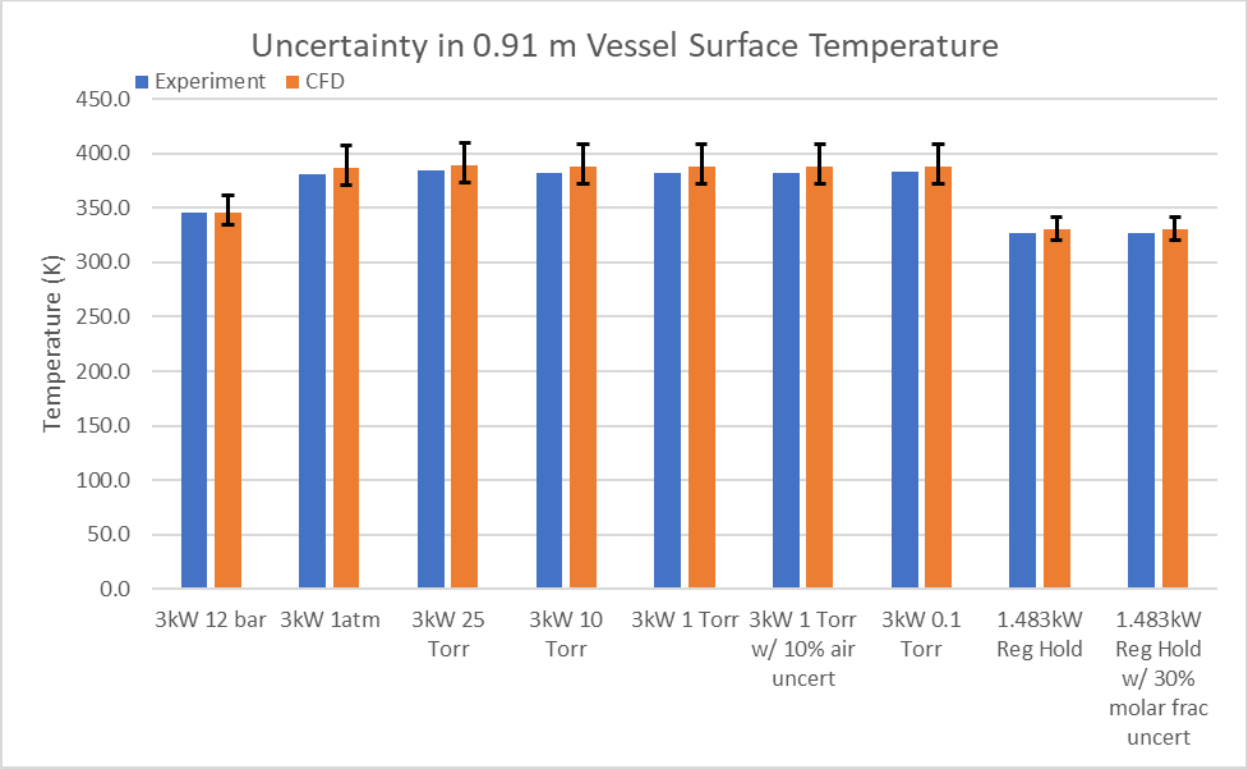


Figure A-11 Pressure Vessel External Wall Temperature Results for Steady-State Cases and Transient Vacuum Drying Case at Regulatory Hold at 0.91 m

Table A-22 Helium Fill Gas Steady-State and Transient Vacuum Drying Case at Regulatory Hold Pressure Vessel External Wall Results at 1.83 m

Vessel Temp at 1.83 m	EXP Data (K)	CFD Data (K)	EXP – CFD (K)	Neg Uncert. (K)	Pos Uncert. (K)	Sym Uncert (K)	Valid?
Steady (3 kW, 12 bar)	355.4	356.6	-1.2	-12.0	17.6	14.8	**YES**
Steady (3 kW, 1 atm)	375.8	381.0	-5.2	-14.3	19.4	16.9	**YES**
Steady (3 kW, 25 Torr)	380.2	381.8	-1.6	-14.3	19.3	16.8	**YES**
Steady (3 kW, 10 Torr)	376.9	380.8	-3.9	-14.4	19.5	16.9	**YES**
Steady (3 kW, 1 Torr)	377.1	380.8	-3.7	-14.4	19.5	16.9	**YES**
Steady (3 kW, 1 Torr) w/ 10% air uncert	377.1	380.8	-3.7	-14.4	19.5	16.9	**YES**
Steady (3 kW, 0.1 Torr)	379.3	381.1	-1.8	-14.3	19.4	16.9	**YES**
Transient 1.483 kW at Reg Hold	324.4	328.2	-3.8	-8.7	10.9	9.8	**YES**
Transient 1.483 kW at Reg Hold w/ 30% water vapor uncert	324.4	328.2	-3.8	-8.8	10.9	9.8	**YES**

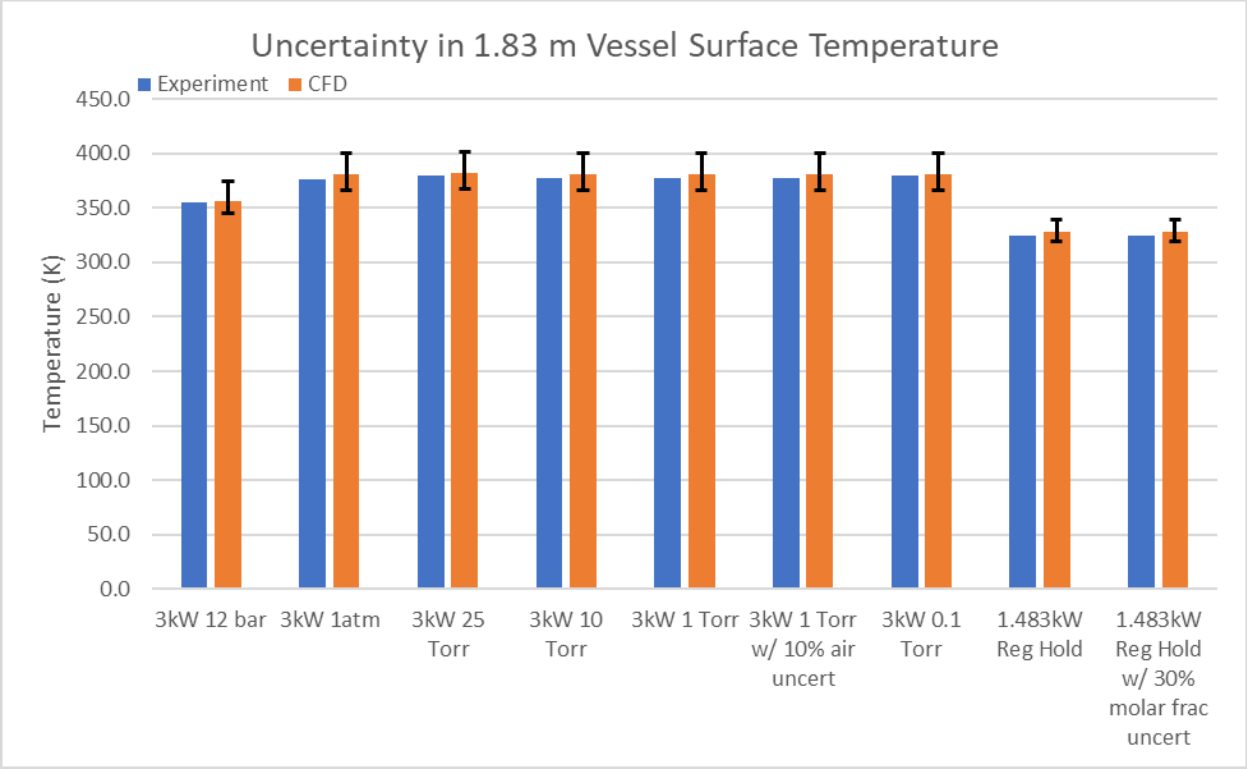


Figure A-12 Pressure Vessel External Wall Temperature Results for Steady-State Cases and Transient Vacuum Drying Case at Regulatory Hold at 1.83 m

Table A-23 Helium Fill Gas Steady-State and Transient Vacuum Drying Case at Regulatory Hold Pressure Vessel External Wall Results at 2.44 m

Vessel Temp at 2.44 m	EXP Data (K)	CFD Data (K)	EXP – CFD (K)	Neg Uncert. (K)	Pos Uncert. (K)	Sym Uncert (K)	Valid?
Steady (3 kW, 12 bar)	358.9	363.9	-5.0	-12.6	18.1	15.3	**YES**
Steady (3 kW, 1 atm)	368.0	373.4	-5.4	-13.6	18.5	16.0	**YES**
Steady (3 kW, 25 Torr)	373.9	374.1	-0.2	-13.7	18.5	16.1	**YES**
Steady (3 kW, 10 Torr)	370.8	373.1	-2.3	-13.8	18.7	16.2	**YES**
Steady (3 kW, 1 Torr)	371.1	373.1	-2.0	-13.7	18.6	16.2	**YES**
Steady (3 kW, 1 Torr) w/ 10% air uncert	371.1	373.1	-2.0	-13.7	18.6	16.2	**YES**
Steady (3 kW, 0.1 Torr)	372.7	373.4	-0.7	-13.7	18.6	16.1	**YES**
Transient 1.483 kW at Reg Hold	322.1	324.7	-2.6	-8.5	10.3	9.3	**YES**
Transient 1.483 kW at Reg Hold w/ 30% water uncert	322.1	324.7	-2.6	-8.5	10.3	9.4	**YES**

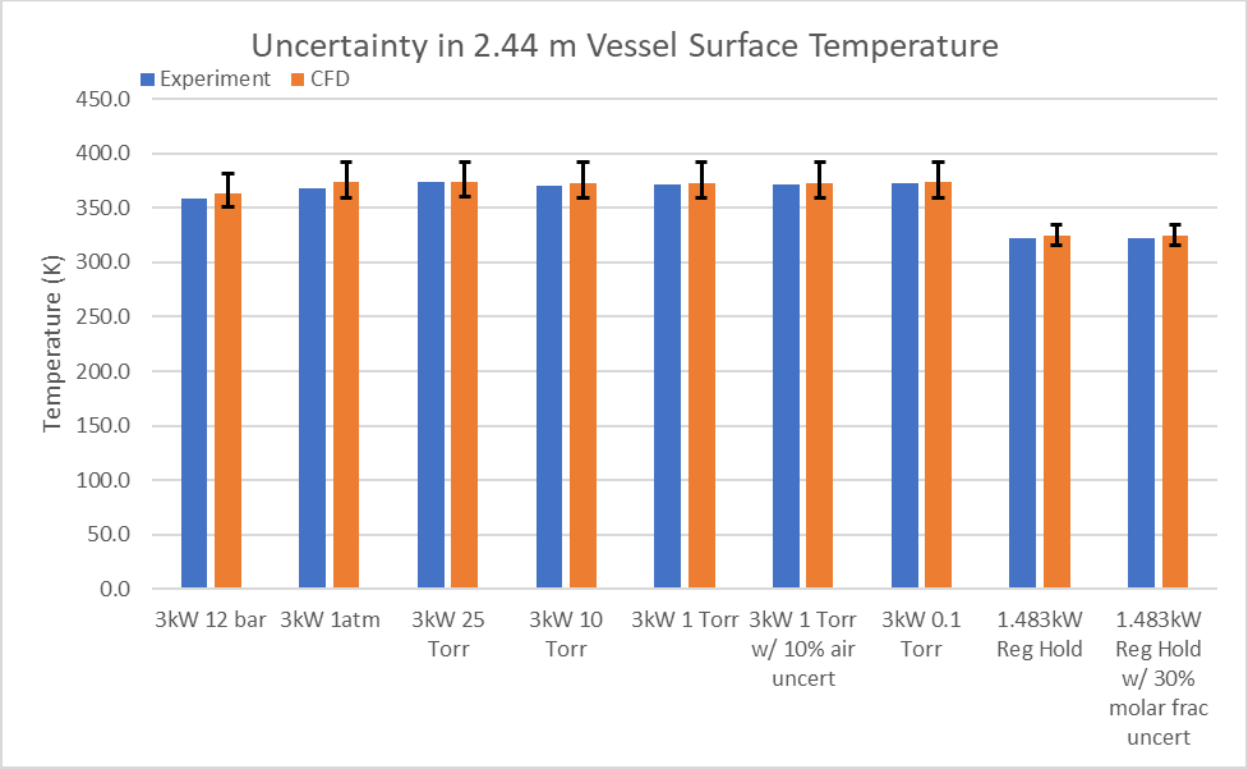


Figure A-13 Pressure Vessel External Wall Temperature Results for Steady-State Cases and Transient Vacuum Drying Case at Regulatory Hold at 2.44 m

Table A-24 Helium Fill Gas Steady-State and Transient Vacuum Drying Case at Regulatory Hold Pressure Vessel External Wall Results at 3.01 m

Vessel Temp at 3.01 m	EXP Data (K)	CFD Data (K)	EXP – CFD (K)	Neg Uncert. (K)	Pos Uncert. (K)	Sym Uncert (K)	Valid?
Steady (3 kW, 12 bar)	363.2	371.2	-8.0	-12.9	18.4	15.7	**YES**
Steady (3 kW, 1 atm)	360.1	363.6	-3.5	-13.0	17.4	15.2	**YES**
Steady (3 kW, 25 Torr)	366.9	364.3	2.6	-13.3	17.6	15.4	**YES**
Steady (3 kW, 10 Torr)	363.5	363.3	0.2	-13.4	17.7	15.5	**YES**
Steady (3 kW, 1 Torr)	363.6	363.3	0.3	-13.4	17.7	15.5	**YES**
Steady (3 kW, 1 Torr) w/ 10% air uncert	363.6	363.3	0.3	-13.4	17.7	15.5	**YES**
Steady (3 kW, 0.1 Torr)	365.3	363.6	1.7	-13.4	17.7	15.5	**YES**
Transient 1.483 kW at Reg Hold	319.6	320.3	-0.7	-8.3	9.7	8.9	**YES**
Transient 1.483 kW at Reg Hold w/ 30% water vapor uncert	319.6	320.3	-0.7	-8.3	9.7	9.0	**YES**

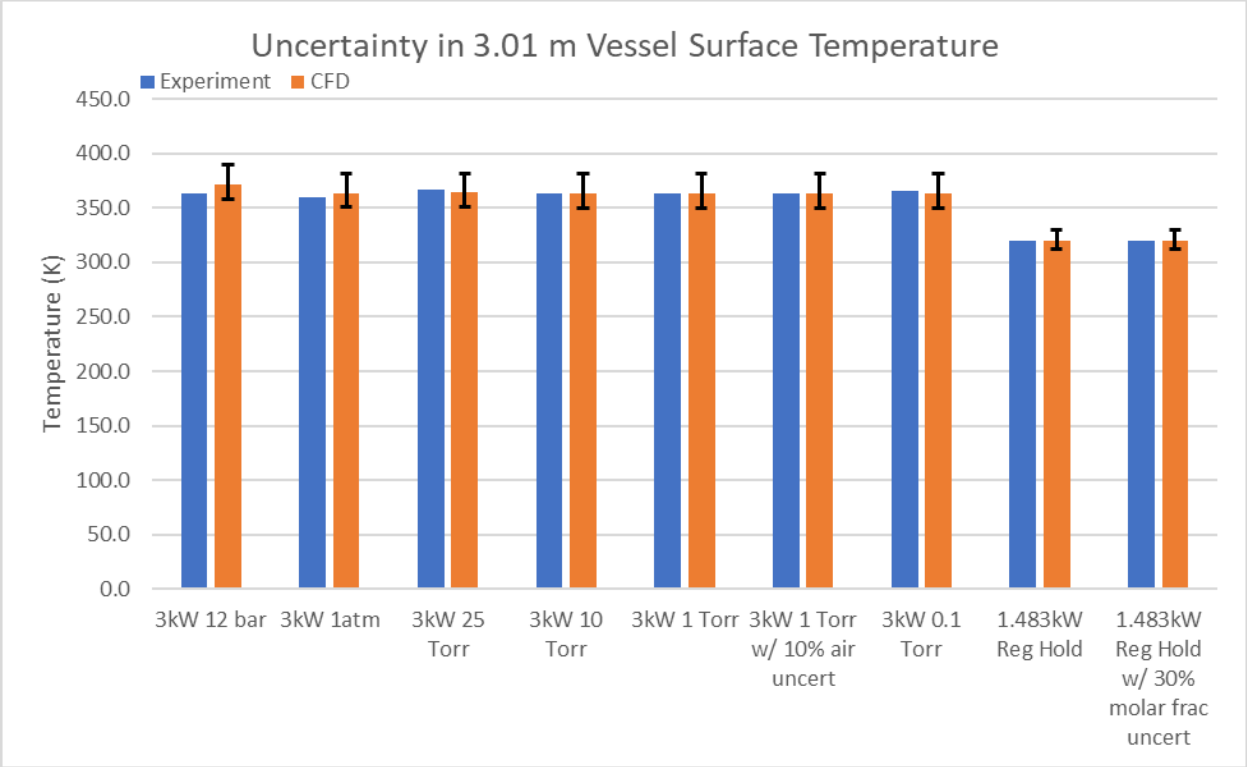


Figure A-14 Pressure Vessel External Wall Temperature Results for Steady-State Cases and Transient Vacuum Drying Case at Regulatory Hold at 3.01 m

Table A-25 Helium Fill Gas Steady-State and Transient Vacuum Drying Case at Regulatory Hold Pressure Vessel External Wall Results at 3.66 m

Vessel Temp at 3.66 m	EXP Data (K)	CFD Data (K)	EXP – CFD (K)	Neg Uncert. (K)	Pos Uncert. (K)	Sym Uncert (K)	Valid?
Steady (3 kW, 12 bar)	369.4	381.4	-12.0	-13.2	18.6	15.9	**YES**
Steady (3 kW, 1 atm)	341.8	335.2	6.6	-8.8	11.8	10.2	**YES**
Steady (3 kW, 25 Torr)	342.0	335.7	6.3	-9.2	12.2	10.7	**YES**
Steady (3 kW, 10 Torr)	338.2	334.6	3.6	-9.3	12.3	10.7	**YES**
Steady (3 kW, 1 Torr)	338.7	334.6	4.1	-9.3	12.3	10.7	**YES**
Steady (3 kW, 1 Torr) w/ 10% air uncert	338.7	334.6	4.1	-9.3	12.3	10.7	**YES**
Steady (3 kW, 0.1 Torr)	340.3	335.0	5.3	-9.2	12.3	10.7	**YES**
Transient 1.483 kW at Reg Hold	310.8	310.2	0.6	-7.3	8.0	7.6	**YES**
Transient 1.483 kW at Reg Hold w/ 30% water vapor uncert	310.8	310.2	0.6	-7.3	8.0	7.6	**YES**

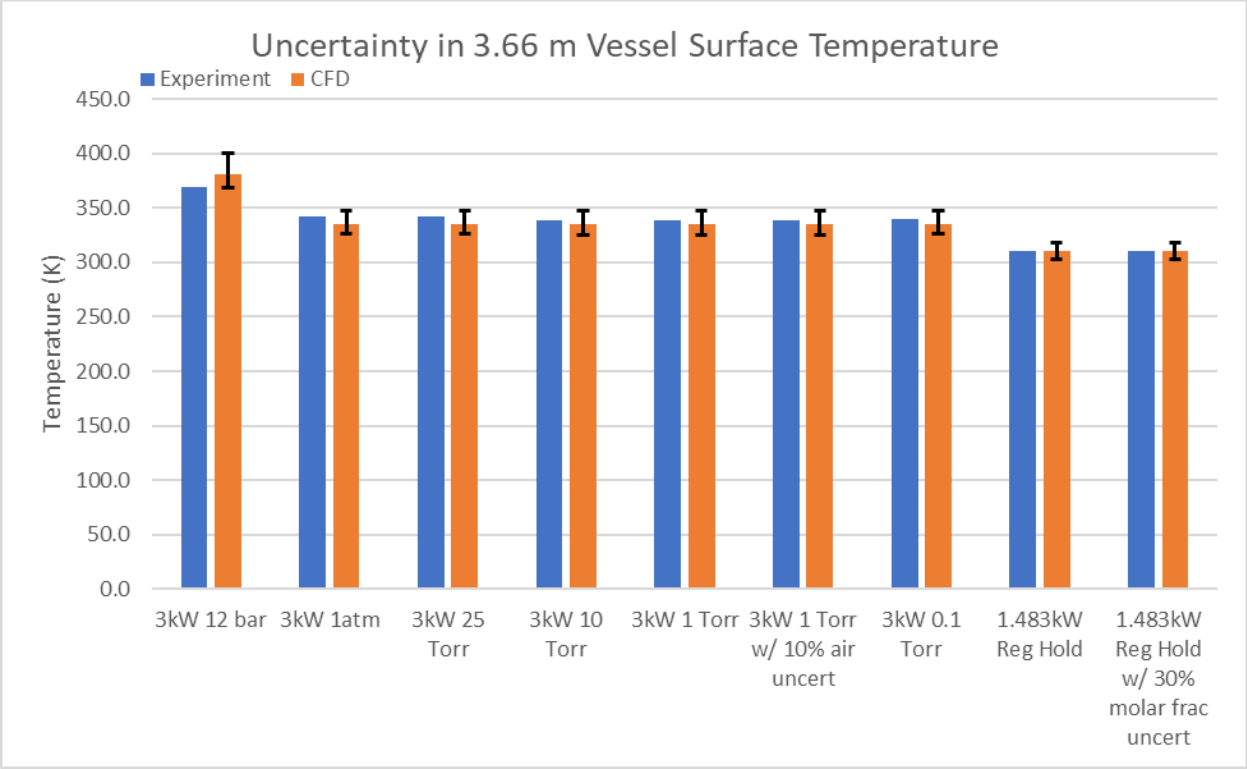


Figure A-15 Pressure Vessel External Wall Temperature Results for Steady-State Cases and Transient Vacuum Drying Case at Regulatory Hold at 3.66 m

Table A-26 Helium Fill Gas Steady-State and Transient Vacuum Drying Case at Regulatory Hold Pressure Vessel External Wall Results at 4.01 m

Vessel Temp at 4.01 m	EXP Data (K)	CFD Data (K)	EXP – CFD (K)	Neg Uncert. (K)	Pos Uncert. (K)	Sym Uncert (K)	Valid?
Steady (3 kW, 12 bar)	374.7	389.2	-14.5	-13.4	18.9	16.1	**NO**
Steady (3 kW, 1 atm)	329.5	316.4	13.1	-5.0	7.1	6.0	**NO**
Steady (3 kW, 25 Torr)	322.2	312.5	9.7	-4.8	6.7	5.7	**NO**
Steady (3 kW, 10 Torr)	318.4	311.4	7.0	-4.9	6.7	5.7	**NO**
Steady (3 kW, 1 Torr)	318.8	311.4	7.4	-4.9	6.7	5.7	**NO**
Steady (3 kW, 1 Torr) w/ 10% air uncert	318.8	311.4	7.4	-4.9	6.8	5.8	**NO**
Steady (3 kW, 0.1 Torr)	320.5	311.8	8.7	-4.8	6.7	5.7	**NO**
Transient 1.483 kW at Reg Hold	305.8	303.4	2.4	-6.7	7.0	6.9	**YES**
Transient 1.483 kW at Reg Hold w/ 30% water vapor uncert	305.8	303.4	2.4	-6.7	7.0	6.9	**YES**

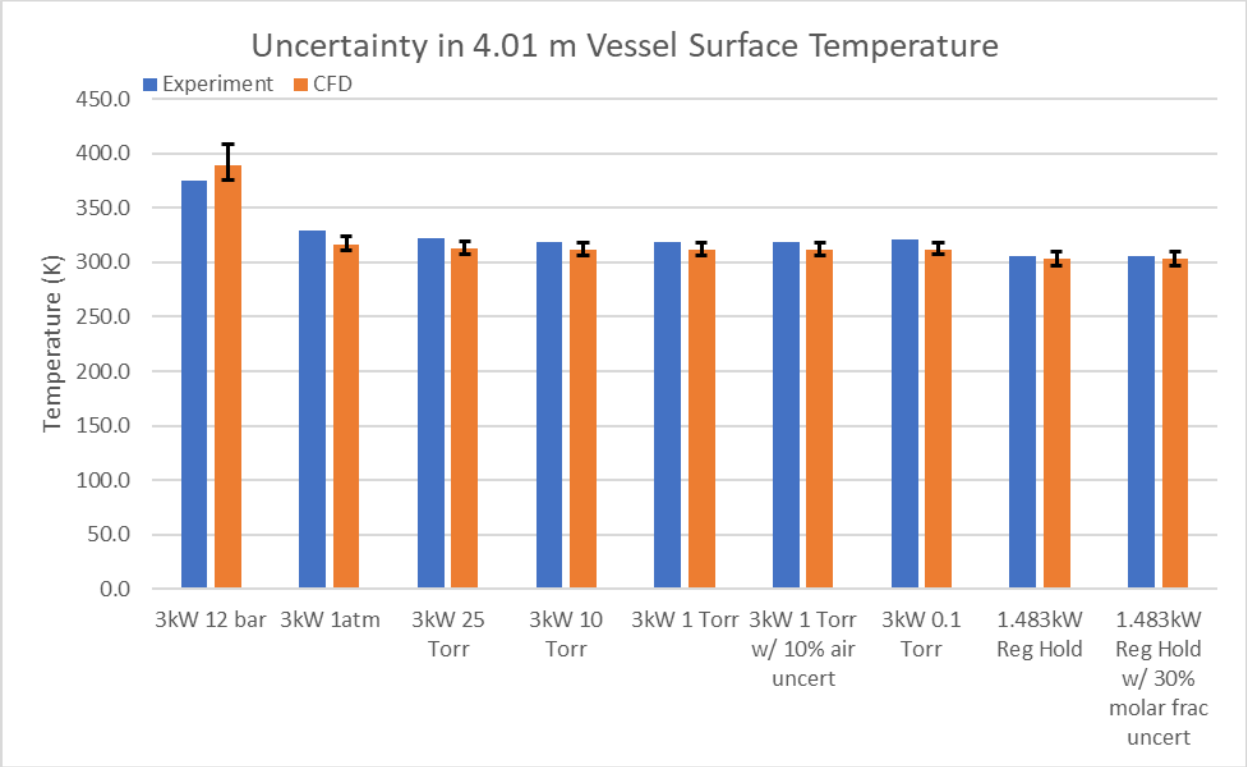


Figure A-16 Pressure Vessel External Wall Temperature Results for Steady-State Cases and Transient Vacuum Drying Case at Regulatory Hold at 4.01 m

NRC FORM 335
(12-2010)
NRCMD 3.7

U.S. NUCLEAR REGULATORY COMMISSION

BIBLIOGRAPHIC DATA SHEET

(See instructions on the reverse)

1. REPORT NUMBER
(Assigned by NRC, Add Vol., Supp., Rev., and Addendum Numbers, if any.)

NUREG-2272

2. TITLE AND SUBTITLE

Validation of a Computational Fluid Dynamics Method Using Advanced Drying Cycle Simulator Data

3. DATE REPORT PUBLISHED

MONTH	YEAR
October	2026

4. FIN OR GRANT NUMBER

5. AUTHOR(S)

Abdelghani Zigh

Justin Coury

6. TYPE OF REPORT

Technical

7. PERIOD COVERED (Inclusive Dates)

8. PERFORMING ORGANIZATION - NAME AND ADDRESS (If NRC, provide Division, Office or Region, U. S. Nuclear Regulatory Commission, and mailing address; if contractor, provide name and mailing address.)

Division of Systems Analysis
Office of Nuclear Regulatory Research
U.S. Nuclear Regulatory Commission
Washington, DC 20555-0001

9. SPONSORING ORGANIZATION - NAME AND ADDRESS (If NRC, type "Same as above", if contractor, provide NRC Division, Office or Region, U. S. Nuclear Regulatory Commission, and mailing address.)

Division of Fuel Management
Office of Nuclear Material Safety and Safeguards
U.S. Nuclear Regulatory Commission
Washington, DC 20555-0001

10. SUPPLEMENTARY NOTES

11. ABSTRACT (200 words or less)

Recent applications have increasingly used thermal-hydraulic analyses using computational fluid dynamics (CFD) codes (e.g., Ansys Fluent) to demonstrate the adequacy of the thermal design. The applicants are also seeking to license casks with decay heat close to 70 kilowatts, resulting in a peak cladding temperature (PCT) close to the NUREG-2215-suggested temperature limit of 400 degrees Celsius (752 degrees Fahrenheit). CFD predictions for the PCT or any other target variable should be supported by an uncertainty quantification to provide assurance and confidence that the obtained margin is adequate. For this reason, and through Office of Nuclear Material Safety and Safeguards (NMSS) user need request NMSS-2019-002, the Office of Nuclear Regulatory Research joined Sandia National Laboratories (SNL) to validate CFD methods used for dry cask applications using data obtained from the SNL Advanced Drying Cycle Simulator (ADCS) sponsored by the U.S. Department of Energy. This validation study will be used to support regulatory decisions ensuring adequate protection for storage and transportation casks. The NRC recognizes that finite volume method CFD is one of the methods for the applicants to show compliance with the regulations for the thermal response of a dry cask storage system. Additionally, when demonstrating compliance, it is valuable to quantify the uncertainty in the simulation result as a function of the computational mesh and simulation inputs. The NRC led this validation effort to include uncertainty quantification and followed the CFD best practice guidelines in NUREG-2152.

12. KEY WORDS/DESCRIPTORS (List words or phrases that will assist researchers in locating the report.)

Advanced Drying Cycle Simulator (ADCS); ADCS; spent nuclear fuel; dry storage cask; computational fluid dynamics; validation; verification; CFD-grade experiment; uncertainty quantification; VVUQ; V&V; UQ; ASME V&V 20-2009

13. AVAILABILITY STATEMENT

unlimited

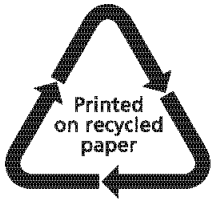
14. SECURITY CLASSIFICATION

(This Page)
unclassified

(This Report)
unclassified

15. NUMBER OF PAGES

16. PRICE



Federal Recycling Program



UNITED STATES
NUCLEAR REGULATORY COMMISSION
WASHINGTON, DC 20555-0001

OFFICIAL BUSINESS

